CELL TYPE-SPECIFIC ROLES OF FOXP TRANSCRIPTION FACTORS IN VOCALIZATION AND COGNITION

APPROVED BY SUPERVISORY COMMITTEE

Peter Tsai, M.D., Ph.D., Chair

Genevieve Konopka, Ph.D., Mentor

Jane Johnson, Ph.D.

Todd Roberts, Ph.D.

DEDICATION

This work is dedicated to family (*Mom, Dad, Franklin, Alex*), friends (*Stephanie, Ashley, DJ, Fatma, The Nasty Eyebrows*), mentors (*Gena, Peter, Todd, Jane, Nancy*), and colleagues who have supported me and my transformation into a full-fledged scientist.

CELL TYPE-SPECIFIC ROLES OF FOXP TRANSCRIPTION FACTORS IN VOCALIZATION AND COGNITION

by

MARISSA CO

DISSERTATION

Presented to the Faculty of the Graduate School of Biomedical Sciences

The University of Texas Southwestern Medical Center at Dallas

In Partial Fulfillment of the Requirements

For the Degree of

DOCTOR OF PHILOSOPHY

The University of Texas Southwestern Medical Center

Dallas, Texas

August, 2019

Copyright

By

Marissa Co, 2019

All Rights Reserved

CELL TYPE-SPECIFIC ROLES OF FOXP TRANSCRIPTION FACTORS IN VOCALIZATION AND COGNITION

Marissa Co, Ph.D.

The University of Texas Southwestern Medical Center at Dallas, 2019

Genevieve Konopka, Ph.D.

ABSTRACT

Mutations of the forkhead domain transcription factors FOXP2 and FOXP1 are highly associated with neurodevelopmental disorders affecting speech and language. Across vertebrate species, their conserved expression patterns in the developing and adult brain predict important functions in neural circuits mediating vocalization and sensorimotor learning. Their known gene targets regulate neuronal development, activity, and plasticity, and animal models of FoxP2 and FoxP1 function have linked some of these molecular functions with neurophysiological and behavioral phenotypes. Still, much

remains unknown about molecular networks in the brain driven by these transcription factors, especially in specific regions and cell types. During my dissertation work, I sought to elucidate FoxP2 and FoxP1 functions in cortical, striatal, and cerebellar neurons in mice and zebra finches. This approach of combining comparative genomics with functional studies of salient genes has proven a powerful method for understanding higher cognitive functions such as language (**Chapter Two**). By characterizing mice lacking cortical *Foxp2*, I identified its roles in dopamine signaling, interneuron development, and cognitive behavior, but surprisingly not in vocalization (**Chapter Three**). I further studied the interaction between FoxP2 and its cortical binding partner TBR1, and I found synergistic gene regulation by these transcription factors in neural cells (**Chapter Four**). I contributed to identification of roles for cortico-hippocampal FoxP1 in cortical development and vocalization (**Chapter Five**), as well as roles for cerebellar FoxP2 in Purkinje cell morphology, vocalization, and gross motor function (**Chapter Six**). Finally, I generated tools and datasets to further our understanding of corticostriatal functions of FoxP2 and FoxP1 in vocal learning zebra finches (**Chapter Seven**). In light of these studies, I discuss their implications for understanding human disorders affecting speech and language, and I impart further hypotheses and recommendations for continuing their study (**Chapter Eight**). Together, these findings contribute to our knowledge of conserved roles for FoxP2 and FoxP1 in vocal behavior and cognition.

TABLE OF CONTENTS

ABSTRACT ..... **V**

TABLE OF CONTENTS ..... **VII**

CHAPTER ONE: BACKGROUND AND INTRODUCTION **1**

ASSOCIATION OF *FOXP* GENES WITH NEURODEVELOPMENTAL DISORDERS 1
FOXP2 mutations predominantly impair speech and language *1*
Structural and functional brain abnormalities upon FOXP2 mutation *3*
Genetic evidence for FOXP2 involvement in other neurodevelopmental disorders *5*
FOXP1 mutations cause a severe global neurodevelopmental disorder *7*
EXPRESSION PATTERNS OF *FOXP2* AND *FOXP1* 8
Neural pathways underlying vocalization *8*
Expression in the cortex *9*
Expression in the basal ganglia *13*
Expression in the thalamus *15*
Expression in the cerebellum *16*
Expression in other brain regions *17*
MOLECULAR AND CELLULAR FUNCTIONS REGULATED BY FOXP2 AND FOXP1 IN THE BRAIN . 19
FoxP transcription factors show distinct structure and evolution *19*
FoxP2 and FoxP1 interact with other transcriptional regulators *20*
FoxP2 regulates neurodevelopmental genes and signaling pathways *22*
FoxP2 regulates corticostriatal synaptic and dopamine signaling genes *24*
FoxP1 regulates neurodevelopmental, neuronal activity, and synaptic genes *26*
ANIMAL MODELS OF FOXP2 FUNCTION 28
Homozygous Foxp2 loss-of-function mice *28*
Heterozygous Foxp2 loss-of-function mice *29*
Cortex-specific Foxp2 manipulations *33*
Striatum-specific FoxP2 manipulations *36*
Thalamus-specific Foxp2 manipulations *38*
Cerebellum-specific Foxp2 manipulations *38*
Humanized Foxp2 mice *40*
ANIMAL MODELS OF FOXP1 FUNCTION 41
Whole-body Foxp1 loss-of-function mouse models *41*
Brain- and region-specific Foxp1 manipulations *42*
INTRODUCTION 44
FIGURES 46
Figure 1.1 *Structural and functional brain abnormalities in affected KE family members.* *46*
Figure 1.2 *FoxP2 and FoxP1 expression patterns in mammalian and zebra finch brain.* *47*
Figure 1.3 *Putative molecular pathways regulated by FoxP2 and FoxP1 in the cortex.* *48*
Figure 1.4 *FoxP2 and FoxP1 protein interactors.* *49*

CHAPTER TWO: DECODING THE MOLECULAR EVOLUTION OF HUMAN COGNITION USING COMPARATIVE GENOMICS **50**

CHAPTER THREE: CORTICAL *FOXP2* SUPPORTS BEHAVIORAL FLEXIBILITY AND DEVELOPMENTAL DOPAMINE D1 RECEPTOR EXPRESSION **51**

ABSTRACT 51
INTRODUCTION 52
RESULTS 54
Cortical Foxp2 deletion impairs reversal learning *54*
Cortical Foxp2 deletion decreases sound pressure of neonatal vocalizations *56*
Foxp2 is dispensable for cortical layering and layer 6 axon targeting *57*
Cortical Foxp2 deletion reduces dopamine signaling gene expression *58*
Identification of D1R-expressing cell types in developing frontal cortex *60*
Foxp2 deletion increases SP9+ interneurons in postnatal cortex *62*
Foxp2 deletion induces non-cell-autonomous effects on cortical gene expression *63*
Putative direct targets of Foxp2 in postnatal cortex *65*
Efforts toward identification of genome-wide direct Foxp2 targets in postnatal cortex *66*
DISCUSSION 67
Foxp2-regulated cortical dopamine signaling and behavioral flexibility *67*
Genetic diversity of dopaminoceptive cell types in developing cortex *68*
Limited roles of cortical Foxp2 in mouse vocalization *69*
Neurodevelopmental disorder gene regulation by Foxp2 in the cortex *71*
MATERIALS AND METHODS 74
Mice *74*
Behavioral analyses *74*
Reversal learning in water Y-maze *75*
Spontaneous alternation in T-maze *75*
Novel object recognition *76*
Cued and contextual fear conditioning with extinction *76*
Three-chamber social interaction *77*
Novel cage activity *78*
Open field *78*
Elevated plus maze *79*
Adult courtship ultrasonic vocalizations *79*
Neonatal isolation ultrasonic vocalizations *80*
Righting reflex *80*
Negative geotaxis *80*
Immunohistochemistry, imaging, and analysis *81*
Protein extractions and Western blotting *84*
Single-cell RNA sequencing *85*
Chromatin immunoprecipitation (ChIP) *90*
Cleavage under targets and release using nuclease (CUT&RUN) *92*
FIGURES 93
Figure 3.1 *Cortex-specific deletion of Foxp2 by Emx1-Cre.* *93*
Figure 3.2 *Foxp2 cKO mice show cognitive deficits specific to behavioral flexibility.* *94*
Figure 3.3 *Foxp2 cKO mice show normal social, locomotor, and anxiety-related behaviors.* *96*
Figure 3.4 *Foxp2 cKO mice show normal adult courtship vocalizations.* *97*
Figure 3.5 *Foxp2 cKO mice show normal postnatal isolation vocalizations, save for decreased loudness.* *99*
Figure 3.6 *Foxp2 cKO mice show normal gross cortical development.* *100*
Figure 3.7 *Foxp2 cKO mice show decreased dopamine D1 receptor expression in postnatal and adult cortex.* *101*

Figure 3.8 *Dopamine D1 receptors are expressed in multiple cell types in postnatal frontal cortex.* *103*
Figure 3.9 *Foxp2 cKO mice show altered composition of dopamine D1 receptor-expressing neuronal subtypes.* *105*
Figure 3.10 *Cortical Foxp2 deletion induces non-cell-autonomous dysregulation of cytoskeletal genes.* *107*
Figure 3.11 *Identification of genes directly regulated by Foxp2 in the cortex.* *109*
Figure 3.12 *Efforts toward identification of genome-wide direct Foxp2 targets in postnatal cortex.* *110*
Figure 3.13 *Summary of behavioral and molecular findings in Foxp2 cKO mice.* *112*
TABLES 113
Table 3.1 *PCR genotyping primers.* *113*
Table 3.2 *Results and statistics for behavioral analyses.* *114*
Table 3.3 *Results and statistics for IHC analyses.* *119*
Table 3.4 *Foxp2, tdTomato, and TLE4 overlaps in P7 mPFC L5 and L6.* *121*
Table 3.5 *Pseudo-bulk RNA-seq DEGs between control and cKO Drd1a-tdTomato neurons.* *122*
Table 3.6 *Pseudo-bulk RNA-seq DEGs by cell type between control and cKO Drd1a-tdTomato neurons.* *123*
Table 3.7 *Pseudo-bulk RNA-seq DEGs between control and cKO golli-τ-eGFP neurons.* *126*

CHAPTER FOUR: MOLECULAR CHARACTERIZATIONS OF FOXP2-TBR1 INTERACTION 127

ABSTRACT 127
INTRODUCTION 127
RESULTS AND DISCUSSION 129
Foxp2 and TBR1 follow similar expression patterns over mouse cortical development *129*
Nuclear colocalization of Foxp2 and TBR1 in cortical layer 6 ..... *129*
Mixed results for endogenous Foxp2-TBR1 interaction by coimmunoprecipitation *130*
Synergistic gene regulation by FoxP2 and TBR1 in neural cells *131*
Reduced pulldown of TBR1 by FOXP2 deletion mutants *133*
Altered subcellular localization of TBR1 by FOXP2 deletion mutants *134*
MATERIALS AND METHODS 136
Mice *136*
Cell cultures and lentivirus production *136*
Constructs *137*
Protein extractions, coimmunoprecipitations, Western blotting *137*
Immunostaining and imaging *140*
Quantitative reverse transcription PCR *141*
Dual-luciferase assays *142*
FIGURES 144
Figure 4.1 *Foxp2 and TBR1 colocalize and interact in cortical layer 6* *144*
Figure 4.2 *Synergistic gene regulation by FoxP2 and TBR1 in neural cells at a non-canonical FoxP2 motif* *146*
Figure 4.3 *Reduced pulldown of TBR1 by FOXP2 deletion mutants* *148*
Figure 4.4 *Altered subcellular localization of TBR1 by FOXP2 deletion mutants* *149*
TABLES 150
Table 4.1 *Candidate Foxp2-TBR1 targets.* *150*

CHAPTER FIVE: FOXP1 REGULATION OF NEONATAL VOCALIZATIONS VIA CORTICAL DEVELOPMENT 154

CHAPTER SIX: SUMOYLATION OF FOXP2 REGULATES MOTOR FUNCTION AND VOCAL COMMUNICATION THROUGH PURKINJE CELL DEVELOPMENT 155

CHAPTER SEVEN: TOOLS AND TECHNIQUES FOR UNDERSTANDING FOXP FUNCTION IN ZEBRA FINCH SONG NUCLEI 156

ABSTRACT 156
INTRODUCTION 156
RESULTS AND DISCUSSION 157
Optimization of Area X tissue processing for single-nucleus RNA-seq 157
Preliminary analysis of FoxP2 expression in juvenile Area X cell types 158
Antibody test for FoxP2 ChIP 159
Viral constructs for FoxP1 knockdown and rescue in HVC 159
MATERIALS AND METHODS 162
Area X single-cell dissociation 162
Area X nuclear extractions and single-nucleus RNA sequencing 162
Area X chromatin immunoprecipitation 164
Constructs 164
Hairpin tests in 293T cells 165
FIGURES 167
Figure 7.1 *Optimization of snRNA-seq for Area X FoxP2 knockdown. 167*
Figure 7.2 *Antibody test for Area X FoxP2 chromatin immunoprecipitation. 169*
Figure 7.3 *In vitro and in vivo tests of a viral FoxP1 knockdown construct. 170*
Figure 7.4 *In vitro tests of hairpin-resistant FoxP1 rescue constructs. 171*
TABLES 172
Table 7.1 *Samples collected for Area X snRNA-seq. 172*
Table 7.2 *Primers used to generate constructs. 173*

CHAPTER EIGHT: DISCUSSION AND FUTURE DIRECTIONS 174

FOXP2 AND *FOXP1* HAVE DISTINCT CORTICAL FUNCTIONS 174
FOXP2 REGULATION OF DOPAMINE SIGNALING IN THE BRAIN 179
RELATING MOUSE BEHAVIORAL PHENOTYPES TO HUMAN *FOXP2* AND *FOXP1* DISORDERS 182

BIBLIOGRAPHY 186

CHAPTER ONE: Background and Introduction

Note on nomenclature: In this thesis, I will use the standard FoxP nomenclature published within the field, with human genes and proteins in uppercase (e.g. FOXP2), mouse in lowercase (e.g. Foxp2), and other species or multi-species in mixed case (e.g. FoxP2).

Scientists have long sought to understand the biological mechanisms underlying language and cognition, which are particularly sophisticated abilities in the human lineage. To this end, recent advances in molecular biology have enabled detailed study of the brain at many levels, from large-scale neuronal networks to single genes with vital functions. *FOXP2* is one of few genes known to play a role in speech and language, and its paralog *FOXP1* is a high-confidence autism risk gene. Conservation of these genes in form and function across species has enabled their use as genetic tools to study neural mechanisms underlying vocalization and cognition.

Association of *FOXP* genes with neurodevelopmental disorders

FOXP2 mutations predominantly impair speech and language

Mutation of the gene encoding the Forkhead Box P2 transcription factor (*FOXP2*) was the first identified monogenic cause of a developmental speech and language disorder (Lai et al., 2001). Clinicians had recognized an autosomal dominant inheritance pattern of this disorder within a large multigenerational family (KE) and hypothesized that a single gene was responsible (Hurst et al., 1990). Subsequent analyses localized this genetic cause to a region on chromosome 7 dubbed *SPCH1* (Fisher et al., 1998). Finally, after discovery of an unrelated patient (CS) with similar phenotypes as the KE family, *FOXP2* was identified as the gene responsible for their speech and language impairments

(Lai et al., 2000; Lai et al., 2001). Further studies of patients with speech and language disorders have identified more than a dozen other pathogenic variants within *FOXP2*, solidifying its role in proper development of these capabilities (Morgan et al., 2017).

Much of our understanding of *FOXP2*-related language impairments comes from extensive characterization of the KE family, comparing affected members to unaffected members. Affected members showed normal neonatal development, including feeding and achievement of early motor milestones, but then presented with severely delayed and nearly unintelligible speech throughout early childhood (Hurst et al., 1990). While their speech and language abilities improved with therapy and age, affected members remained impaired into adulthood (Gopnik and Crago, 1991; Hurst et al., 1990). Core features of their disorder included childhood apraxia of speech and orofacial dyspraxia; in other words, while they could perform simple movements of the tongue and lips, they had difficulty performing sequential orofacial movements, both linguistic (e.g. consonant clusters in “spoon” or “blue”) and nonlinguistic (e.g. “close the lips, then open the mouth, then protrude the tongue”) (Alcock et al., 2000b; Hurst et al., 1990; Vargha-Khadem et al., 1995; Watkins et al., 2002a). Perhaps related to these motor sequencing deficits, they demonstrated impaired perception and production of musical rhythms, but not pitch or melody (Alcock et al., 2000a). Affected members also struggled with aspects of grammar, such as pluralization, derivational morphology (e.g. “There is a lot of sun. It is very *sunny*.”), and tense production (e.g. “Every day he walks eight miles. Yesterday he *walked*.”) (Gopnik and Crago, 1991; Vargha-Khadem et al., 1995; Watkins et al., 2002a). Furthermore, they showed impairment of the phonological loop, a working memory

component specific to speech-based information (Schulze et al., 2017). Altogether these studies demonstrate language-related motor and cognitive impairments in KE family members affected by *FOXP2* mutation.

Investigations of non-verbal intelligence and overall cognition in patients with *FOXP2* mutations have suggested mild impairments. Case histories of seven affected KE members reported intelligence “within the normal range” (Hurst et al., 1990), but formal testing found significant decreases in both verbal and non-verbal intelligence quotients (IQ) of affected members, resulting in full-scale IQ scores in the low average range (Vargha-Khadem et al., 1995; Watkins et al., 2002a). The phonological loop study of affected KE members found normal visuospatial working memory and slightly impaired central executive memory, or the control system integrating phonological and visuospatial working memory (Schulze et al., 2017). Patients unrelated to the KE family with *FOXP2* mutations have demonstrated non-verbal and full-scale IQ scores in the low average to average range (Morgan et al., 2017). Thus, *FOXP2* mutations may produce general cognitive impairments in some patients, but whether these arise separately or stem from their speech and language deficits remains undetermined.

Structural and functional brain abnormalities upon FOXP2 mutation

The discovery of a major role for *FOXP2* in speech and language prompted investigations into brain regions affected by its mutation and thus critical for these abilities. A structural magnetic resonance imaging (MRI) dataset was collected from 10 affected and 7 unaffected KE family members, and then analyzed using several different comparison methods, some involving additional control subjects (Argyropoulos et al.,

2018; Belton et al., 2003; Vargha-Khadem et al., 1998; Watkins et al., 2002b). Across two or more analysis methods, affected KE members showed unilateral or bilateral gray matter decreases in cortical areas (inferior frontal gyrus / Broca's area, precentral gyrus, supplementary motor area, temporal pole), the caudate nucleus of the basal ganglia, and lobules VIIb-VIIIb of the cerebellum; they also showed gray matter increases in other cortical areas (angular gyrus, anterior insula, sensorimotor cortex, superior temporal gyrus) (**Fig. 1.1A**). Brain areas altered within single studies included other basal ganglia structures (lentiform nucleus, putamen) and the posterior thalamus (Vargha-Khadem et al., 1998; Watkins et al., 2002b). A recent analysis including two additional structural MRI datasets found decreased gray matter in cerebellar lobule VIIa Crus I of affected KE members, and their caudate nucleus volumes correlated with Crus I and supplementary motor area volumes (Argyropoulos et al., 2018). Outside of the KE family, an eight-year-old patient (A-II) with a de novo intragenic *FOXP2* deletion showed volume reductions in the basal ganglia (globus pallidus, caudate nucleus), thalamus, and hippocampus compared with 26 controls; inability to detect cortical or cerebellar changes was likely a technical artifact of the single-case study design (Liegeois et al., 2016). Altogether these studies indicate that *FOXP2* mutation mainly affects structures within the cortex, basal ganglia, and cerebellum, with possible effects on the hippocampus and thalamus.

Functional brain imaging has also offered insights into how *FOXP2* mutation affects brain activity during various language tasks. Positron emission tomography (PET) and functional MRI (fMRI) studies of the KE family have shown differential activation of cortical, basal ganglia, and cerebellar regions during word repetition, non-word repetition,

silent verb generation, and spoken verb generation (Argyropoulos et al., 2018; Liegeois et al., 2003; Liegeois et al., 2011; Vargha-Khadem et al., 1998) (**Fig. 1.1B**). Many of the under- or overactive brain regions in affected KE members also showed altered gray matter volumes in the structural MRI studies, including the inferior frontal gyrus, sensory and motor cortices, temporal gyri and pole, the caudate nucleus, and cerebellar lobule VIIa Crus I (Argyropoulos et al., 2018; Belton et al., 2003; Vargha-Khadem et al., 1998; Watkins et al., 2002b). In addition, fMRI of patient A-II during non-word repetition showed underactivation of the inferior frontal gyrus at similar coordinates as affected KE members during silent verb generation; however, no differences between A-II and controls survived multiple comparisons correction (Liegeois et al., 2016).

In summary, brain imaging studies indicate that *FOXP2* mutation most prominently alters the structure and function of the cortex, basal ganglia, and cerebellum. Thus, the studies within this thesis have especially focused on *FoxP2* function within these regions to elucidate neural mechanisms underlying speech and language disorders.

Genetic evidence for FOXP2 involvement in other neurodevelopmental disorders

Given that many neurodevelopmental disorders involve language and communication deficits, *FOXP2* variation may contribute to the etiology of these disorders. Early studies with small cohort sizes, up to ~1100 total individuals, directly queried the involvement of *FOXP2* variants in autism spectrum disorder (ASD), and some found association while others did not (Chien et al., 2011; Gauthier et al., 2003; Gong et al., 2004; Laroche et al., 2008; Li et al., 2005; Marui et al., 2005; Newbury et al., 2002; Richler et al., 2006; Toma et al., 2013; Wassink et al., 2002). A larger study involving over

2500 trios, comprised of an affected proband and two parents, identified *FOXP2* among ASD risk loci in a homozygous haplotype mapping approach (Casey et al., 2012). Recent trio exome sequencing identified de novo *FOXP2* variants in two individuals with ASD and speech and language disorder (Deciphering Developmental Disorders, 2015; Reuter et al., 2017). Additionally, unpublished data from the largest ASD exome sequencing cohort to date (>35,000 total individuals) place *FOXP2* among the 78 most significant ASD-associated risk genes (Satterstrom et al., 2019). Additionally, a recent large (>50,000 total individuals) genome-wide association study of attention deficit / hyperactivity disorder (ADHD) identified an intron of *FOXP2* among 12 loci associated with this disorder (Demontis et al., 2019). ASD and ADHD show genetic overlap, as they frequently co-occur in individuals and within families (Ghirardi et al., 2017), so *FOXP2* may function upstream of biological pathways pertinent to both neurodevelopmental disorders.

Some studies have investigated whether *FOXP2* variants are associated with schizophrenia, a language-disrupting cognitive disorder with molecular underpinnings similar to those of ASD (Gandal et al., 2018). Like ASD studies with small cohorts, studies involving cohorts of up to ~2500 total individuals have found mixed results regarding *FOXP2* variation and susceptibility to schizophrenia (Laroche et al., 2008; Li et al., 2013; Sanjuan et al., 2005; Yin et al., 2018). Small studies have also investigated the contribution of *FOXP2* variants to symptom severity among patients with this disorder, to varying conclusions (Jamadar et al., 2011; McCarthy et al., 2018; Rao et al., 2017; Sanjuan et al., 2006; Tolosa et al., 2010). The most recent schizophrenia genome-wide

association studies to date (>100,000 total individuals) have not implicated *FOXP2* in risk for developing this disorder (Li et al., 2017; Schizophrenia Working Group of the Psychiatric Genomics et al., 2014). Thus, increasing evidence implicates *FOXP2* in the etiology of ASD and ADHD, but not in vulnerability to the related disorder schizophrenia. However, the molecular mechanisms by which *FOXP2* variation confers increased risk for ASD and ADHD have yet to be elucidated.

FOXP1 mutations cause a severe global neurodevelopmental disorder

The association of *FOXP2* with developmental speech and language disorder spurred research on potential roles for its close paralog *FOXP1* (64% total protein sequence similarity, 89% in the forkhead domain) in neurodevelopmental disorders. Specific investigation of this gene in patients with ASD and/or intellectual disability (ID) identified de novo *FOXP1* mutations in two patients, both of whom also showed severe language impairment (Hamdan et al., 2010). Subsequent ASD genetics studies have identified many additional mutations in this gene, and to date, >40 pathogenic variants have been documented and reviewed in (Siper et al., 2017). Comprehensive phenotyping of 9 children and adolescents with *FOXP1* mutations revealed core features of motor and language delays, language impairment, ASD behaviors, visuomotor integration difficulties, and psychiatric symptoms (Siper et al., 2017). Other medical features included endocrine, gastrointestinal, sleep, and sinopulmonary problems, as well as brain structural abnormalities (enlarged ventricles in 3/9 patients) and dysmorphic features (Siper et al., 2017). Notably, patients with a *FOXP1* mutation equivalent to the *FOXP2* KE mutation also presented with these broad developmental delays and deficits, as

opposed to primarily a speech and language disorder (Sollis et al., 2017). Thus, despite the high degree of similarity between FOXP2 and FOXP1, mutations in their genes typically result in distinct neurodevelopmental disorders, with *FOXP1* mutations conferring risk for more global impairments. How these phenotypic differences arise at the cellular and molecular level is a subject of current explorations into *FoxP2* and *FoxP1* function in the brain, including those within this thesis.

Expression patterns of *FoxP2* and *FoxP1*

In the developing and adult mouse, *Foxp2* and *Foxp1* are expressed in multiple tissues throughout the body, including heart, lung, kidney, skeletal muscle, cartilage, spleen, small intestine, spinal cord, and brain; *Foxp1* is also expressed in the liver (Morikawa et al., 2009; Shu et al., 2001; Tamura et al., 2003; Zhao et al., 2015). Given the focus of this thesis on neurodevelopmental roles of these transcription factors, I will detail their shared and distinct expression patterns in neural tissues, particularly those relevant to language and vocalization (**Fig. 1.2**).

Neural pathways underlying vocalization

The aforementioned KE family brain imaging studies, combined with human lesion studies and experiments in mice and avian vocal learners, have elucidated the conserved neural pathways underlying vocalization. While mice differ from humans and avian vocal learners in that their vocalizations are largely innate (Hammerschmidt et al., 2012; Mahrt et al., 2013), they share similar vocal production and sensorimotor learning circuits with these species, as well as some limited ability for vocal modification (Arriaga et al., 2012). While mammalian and avian brains differ in their structural organization, their homologous

vocalization circuits all involve connections between the cortex/pallium, basal ganglia, thalamus, and cerebellum (**Fig. 1.2**). Specifically, output neurons in the cortex/pallium project to the basal ganglia, thalamus, and brainstem; the basal ganglia and cerebellum project to the thalamus; and the thalamus projects back to cortex/pallium (Konopka and Roberts, 2016a; Pidoux et al., 2018). In songbirds, a class of avian vocal learners, the pallial song nuclei consist of HVC (proper name), robustus arcopallii (RA), and lateralis magnocellularis (lMAN), and the striatal target of HVC and lMAN projections is Area X (Konopka and Roberts, 2016a).

Expression in the cortex

The mammalian neocortex (referred to as cortex throughout this thesis) is a dorsal telencephalon-derived brain structure with six architecturally defined layers, with some layers absent or subdivided based on cortical area. These layers contain diverse subtypes of projection neurons (~80%) and interneurons (~20%); the former typically form long-range excitatory connections within and outside of the cortex, and the latter form local inhibitory connections. The cortex also contains astrocytes, oligodendrocytes, and microglia.

Cortical development follows a generally similar trajectory across mammals, with some evolutionary differences in early cortical features driving primate- and human-specific specializations (Hoerder-Suabedissen and Molnar, 2015; Lui et al., 2011). In mice, radial glia in the ventricular zone (VZ) of the dorsal pallium produce an initial wave of newborn neurons forming the preplate (PP) above the VZ. As radial glia proliferate within the VZ, they produce intermediate progenitors and migrating neurons which form

a subventricular zone (SVZ) under the PP. Neurons migrating through the SVZ enter the PP and split it into an inner subplate (SP) and an outer marginal zone (MZ), and they continue to populate this new in-between zone termed the cortical plate (CP). The earliest CP neurons eventually become layer (L) 6 of the mature cortex, and neurons continue to fill the CP in an “inside-out” fashion until L2 is formed and the VZ and SVZ are depleted. The outermost MZ becomes L1, and the innermost SP remains as part of L6b in mice. During this process of projection neuron generation and radial migration, interneurons are generated in the subpallium, specifically the medial and caudal ganglionic eminences (MGE and CGE) and the preoptic area, and migrate tangentially into the cortex through streams in the MZ, SVZ, and SP (Lim et al., 2018).

Foxp2 and *Foxp1* are expressed in the mouse cortex during embryonic development and maintained into adulthood (Ferland et al., 2003). In situ hybridization (ISH) has shown their mRNA expression by embryonic day (E) 14.5 in lateral aspects of the CP, and immunohistochemistry (IHC) has shown protein expression here by E16.5 (Ferland et al., 2003). Very faint ISH signals for *Foxp2* and *Foxp1* appear in the VZ at E12.5 (Ferland et al., 2003), but expression of their proteins in proliferative zones remains controversial. IHC at E12.5 has suggested low Foxp2 expression in PAX6+ radial glia and TBR2+ intermediate progenitors (Tsui et al., 2013), but other IHC studies report no Foxp2 protein expression in the VZ (Ferland et al., 2003; Kast et al., 2019). Similarly, some IHC studies indicate Foxp1 expression at E12.5 in the VZ (Braccioli et al., 2017; Pearson et al., 2018), but Foxp1 was not detectable in the VZ in another study (Ferland et al., 2003). A possible contributor to these discrepancies across studies is the use of different mouse

strains, including Swiss Webster (Ferland et al., 2003), CD1 (Tsui et al., 2013), and C57BL/6 (Kast et al., 2019; Pearson et al., 2018). No studies to date have investigated coexpression of *Foxp2* and *Foxp1* within the same neurons during embryonic cortical development.

In the postnatal and mature mouse cortex, Foxp2 and Foxp1 are expressed in excitatory projection neurons but not interneurons (Hisaoka et al., 2010). To summarize marker colocalization and tracing studies to date, Foxp2 is expressed in DARPP-32+/TBR1+/NTSR1+/PCP4+ corticothalamic L6 neurons in all cortical areas examined (motor, somatosensory, auditory, visual), as well as a subpopulation of CTIP2+ L5 neurons in motor and somatosensory areas (Hisaoka et al., 2010; Kast et al., 2019; Sorensen et al., 2015) (**Fig. 1.3A**). Early postnatal cortex also contains a small population of Foxp2+/MET+/CCK+ L6 corticocortical neurons in somatosensory cortex (Kast et al., 2019). In contrast, Foxp1 is mainly expressed in SATB2+ projection neurons in L3-5 and some DARPP-32+/TBR1+ neurons in L6a throughout motor, somatosensory, auditory, and visual cortical areas (Hisaoka et al., 2010) (**Fig. 1.3A**). While published studies have not delineated projection neuron subtypes expressing Foxp1, its coexpression with SATB2 and retrograde tracing from our laboratory suggest that it is expressed in intratelencephalic neurons, both corticocortical and corticostriatal, of L3-5 (Alcamo et al., 2008; Anderson et al., unpublished; Britanova et al., 2008; Sohur et al., 2014). Coexpression of Foxp2 and Foxp1 in L6a increases over development, with few Foxp1+ neurons colabeled with Foxp2 in early postnatal cortex and 31-64% of L6a Foxp1+ neurons colabeled with Foxp2 in adult motor, somatosensory, and auditory cortical areas

(Hisaoka et al., 2010). This suggests that some L6a corticothalamic neurons express Foxp1. Foxp2 and Foxp1 are also coexpressed in early postnatal L5 of motor and somatosensory cortex (Hisaoka et al., 2010), but their coexpression pattern in adult L5 is unknown. Also undescribed are the expression patterns of Foxp2 and Foxp1 in the frontal cortex, which mediates cognitive functions commonly disrupted in neurodevelopmental disorders (Schubert et al., 2015).

Cortical expression patterns of *FoxP2* show some variation across mammalian species. Muroid rodents show consistent FoxP2 expression in L6 and some variability in L5 expression (Campbell et al., 2009). In contrast, two vocal learning bat species show L2-4 FoxP2 expression in addition to L5-6 expression (Rodenas-Cuadrado et al., 2018). In postnatal monkey and human fetal cortex, *FoxP2* expression more closely follows that of mouse cortex, with highest expression in lower cortical layers (Takahashi et al., 2008; Teramitsu et al., 2004). Cortical *FoxP1* expression patterns are more consistent across mammalian species, with broad distribution throughout the cortex and enrichment in upper layers compared to lower layers (Rodenas-Cuadrado et al., 2018; Takahashi et al., 2008; Teramitsu et al., 2004).

FoxP2 and *FoxP1* are also expressed in avian pallial regions. A study of avian vocal learners and non-learners found that, like in mammals, *FoxP2* expression was more limited within the pallium while *FoxP1* was more widely expressed (Haesler et al., 2004). This pattern holds true for the zebra finch, a common experimental model of vocal learning, where *FoxP2* is expressed at very low levels in the hyperpallium, mesopallium, nidopallium, and lMAN, while *FoxP1* is highly expressed in the hyperpallium,

mesopallium, nidopallium, HVC, and RA (Haesler et al., 2004; Mendoza et al., 2015; Teramitsu et al., 2004). In terms of mammalian homology, the significance of avian pallial *FoxP2* is unclear, as no studies to date in nonmammalian amniotes have formally identified neurons homologous to L6 corticothalamic neurons (Briscoe and Ragsdale, 2018). On the other hand, *FoxP1*+ intratelencephalic neurons of the mesopallium share some gene expression homology with mammalian L2-6 intratelencephalic neurons (Briscoe et al., 2018), suggesting evolutionarily conserved cortical functions for *FoxP1*. Conserved cell types and *FoxP1* functions in song nuclei such as HVC are currently being elucidated, with some contributions included in this thesis.

In summary, within cortical or pallial brain regions across species, *FoxP2* shows more restricted expression patterns while *FoxP1* is more widely expressed. In mice, and presumably most mammals, *Foxp2* is limited to L6 corticothalamic neurons and a subpopulation of L5 neurons, and *Foxp1* is expressed in L3-6a intratelencephalic neurons and some L6a corticothalamic neurons (**Fig. 1.3A**).

Expression in the basal ganglia

The basal ganglia are a diverse group of nuclei derived from multiple embryonic origins. Forebrain regions arise from the MGE, lateral GE (LGE), and preoptic domain (Medina et al., 2014), and consist of the striatum (subdivided into dorsal and ventral), globus pallidus (subdivided into internal and external), ventral pallidum, and subthalamic nucleus. The dorsal striatum is comprised of inhibitory spiny projection neurons (SPNs), interneurons, and glia, and it is organized by both neurochemical zones (striosome and matrix) and projection pathways (direct and indirect). The midbrain-derived component of

the basal ganglia is the substantia nigra, and it consists of the pars compacta (SNc), the major source of striatal dopamine, and the pars reticulata (SNr).

The developing and adult basal ganglia are among sites with the highest *FoxP2* and *FoxP1* expression in the mammalian brain. In rodents, *FoxP2* and *FoxP1* mRNA appear in the LGE around E12.5 and remain in the developing and adult striatum (Ferland et al., 2003; Lai et al., 2003; Precious et al., 2016; Takahashi et al., 2003). Within the dorsal striatum of mice and monkeys, *FoxP2* is enriched in the striosome compartment, while *FoxP1* is equally expressed in striosomes and matrix (Takahashi et al., 2003; Takahashi et al., 2008). Similarly, mouse Foxp2 is enriched in direct pathway SPNs, which express the dopamine D1 receptor (D1R), while Foxp1 is equally expressed in direct and indirect pathway SPNs, which express the dopamine D2 receptor (D2R) (Fong et al., 2018; Vernes et al., 2011). Within the ventral striatum of mice and monkeys, *FoxP2* is restricted to the nucleus accumbens shell, while *FoxP1* is expressed in both the shell and the core (Takahashi et al., 2003; Takahashi et al., 2008). In contrast with the high striatal expression of these proteins, in the mouse globus pallidus, *Foxp2* is low and *Foxp1* is absent (Ferland et al., 2003; Lai et al., 2003). Similar to mice and monkeys, human *FOXP2 and FOXP1* are expressed in the developing striatum, while *FOXP2* alone is expressed in the internal globus pallidus (Lai et al., 2003; Teramitsu et al., 2004). In the mouse substantia nigra, *Foxp2* is expressed embryonically and enriched in adulthood compared with *Foxp1* (Ferland et al., 2003; Lai et al., 2003).

Developing and adult zebra finches show similar *FoxP2* and *FoxP1* expression patterns in the basal ganglia as mammals, with high expression of both in the striatum,

little *FoxP2* and no *FoxP1* in the globus pallidus, and enriched *FoxP2* in the SNc (Haesler et al., 2004; Teramitsu et al., 2004). In the striatal song nucleus Area X, *FoxP1* shows consistent enrichment compared with the surrounding striatum, whereas *FoxP2* expression varies over development (increased during sensorimotor song learning period) and with singing (decreased during adult undirected singing) (Haesler et al., 2004; Mendoza et al., 2015; Miller et al., 2008; Teramitsu et al., 2004; Teramitsu and White, 2006). In both juvenile and adult Area X, a subpopulation of neurons expressing the SPN marker DARPP-32 also express FoxP2, similar to mouse Foxp2 enrichment in a subset of striatal SPNs (Adam et al., 2016; Rochefort et al., 2007). Genetic dissection of cell types within Area X, particularly D1R- and D2R-expressing neurons, will enhance our understanding of *FoxP2* and *FoxP1* function within this song nucleus, and experimental work toward that goal is included within this thesis.

In summary, vertebrates show conserved *FoxP2* and *FoxP1* expression patterns within the basal ganglia: restricted *FoxP2* and broad *FoxP1* within the striatum, low *FoxP2* and no *FoxP1* within the globus pallidus, expression of both within the subthalamic nucleus, and enriched *FoxP2* within the SNc.

Expression in the thalamus

The thalamus is a diencephalon-derived subcortical structure with a complex organization of nuclei relaying information between various brain structures. As early as E12, mouse Foxp2 shows a graded expression pattern in the thalamic primordium, with highest expression in the posterior region, and by E16 this gradient is lost and Foxp2 remains in some thalamic nuclei (Ebisu et al., 2016). By adulthood, nuclei expressing

Foxp2 include paraventricular, lateral posterior, habenular, medial and lateral geniculate, and some dorsal nuclei (Ferland et al., 2003; Lai et al., 2003). Thalamic *Foxp1* expression is more restricted, with structures including paraventricular and various posterior nuclei (Ferland et al., 2003). In perinatal monkey, *FoxP2* and *FoxP1* are expressed in centromedial and -lateral, ventral posteromedial and -lateral, and lateral geniculate nuclei, and *FoxP2* was additionally expressed in mediodorsal and medial habenular nuclei (Takahashi et al., 2008). Similarly, in developing human and developing and adult zebra finch, *FoxP2* and *FoxP1* are both expressed in the thalamus, but *FOXP2* is expressed in additional sensorimotor nuclei and more strongly expressed overall (Lai et al., 2003; Teramitsu et al., 2004). Thus, in the thalamus, *FoxP2* and *FoxP1* show a conserved expression pattern of stronger and more extensive *FoxP2* expression among nuclei than *FoxP1*.

Expression in the cerebellum

The cerebellum is a major hindbrain structure consisting of a tightly folded cerebellar cortex, which contains molecular, Purkinje, and granular layers, and deep cerebellar nuclei embedded in the white matter underneath. The cerebellum is divided into three lobes which are further divided into lobules. In rodents, *FoxP2* is expressed in the cerebellar primordium at E13.5, in all Purkinje cells and some deep cerebellar nuclei neurons by E17.5, and in a fraction of Purkinje cells and some deep cerebellar nuclei neurons by adulthood (Ferland et al., 2003; Fujita and Sugihara, 2012; Lai et al., 2003; Takahashi et al., 2003). In adult mouse, there are Foxp2+, Foxp2-, and mixed Purkinje cell regions following a transverse striping pattern along the cerebellum (Fujita and

Sugihara, 2012). *Foxp1* expression is limited to deep cerebellar nuclei (Ferland et al., 2003), and zebra finch cerebellum shows the same pattern of *FoxP2* presence and *FoxP1* absence in Purkinje cells (Haesler et al., 2004; Teramitsu et al., 2004). In human fetal brain, *FOXP2* is expressed in the alar plate of the cerebellar primordium and later in more developed cerebellum (Lai et al., 2003). While not located within the cerebellum, the inferior olive of the brainstem provides excitatory synaptic inputs onto Purkinje cell dendrites and also shows high *FoxP2* expression across vertebrate species (Ferland et al., 2003; Fujita and Sugihara, 2012; Haesler et al., 2004; Lai et al., 2003). Thus, these conserved expression patterns in cerebellum-related structures indicate more extensive roles for *FoxP2* in the development and function of this brain region than *FoxP1*.

Expression in other brain regions

The hippocampus, while not classically involved in vocalization circuitry, is nonetheless important for other forms of learning and memory and a crucial site of *Foxp1* function in the brain (Araujo et al., 2017). In the rodent hippocampus, *FoxP2* is not detected at the mRNA or protein level at any developmental stage, while *FoxP1* appears at E17.5 and is enriched in the CA1 subfield from birth onward (Ferland et al., 2003; Takahashi et al., 2003). Vocal learning bats show variable expression levels of FoxP2 and consistent expression of FoxP1 in CA1 (Rodenas-Cuadrado et al., 2018). In postnatal monkey and human fetal hippocampus, *FoxP2* was not detected by ISH (Lai et al., 2003; Takahashi et al., 2008), but one study claimed to detect *FOXP2* by microarray in hippocampi from epileptic patients of various ages (Wilcke et al., 2011). In postnatal monkey, *FoxP1* is expressed in the CA1 and CA3 hippocampal subfields (Takahashi et

al., 2008). Curiously, in the zebra finch hippocampal formation, neither *FoxP2* nor *FoxP1* appear to be expressed (Mendoza et al., 2015). In summary, mammals show variable *FoxP2* expression and consistent *FoxP1* expression in CA1 of the hippocampus.

FoxP2 and *FoxP1* are expressed in other sites throughout the developing and adult brain. A notable site of *FoxP2* expression in mouse and zebra finch is the ventral tegmental area (VTA), a midbrain region supplying dopamine to numerous areas of the brain including the frontal cortex (Campbell et al., 2009; Haesler et al., 2004; Teramitsu et al., 2004). Regions expressing both *Foxp2* and *Foxp1* in the mouse are the anterior olfactory nucleus, olfactory tubercle, amygdala, hypothalamus, and superior colliculus (Ferland et al., 2003; Lai et al., 2003). Additional *Foxp2* sites include the olfactory bulbs, septal nucleus, inferior colliculus, lateral lemniscus nucleus, and zona incerta, and *Foxp1* is additionally expressed in the pontine nuclei and septum (Ferland et al., 2003; Lai et al., 2003). In fetal human brain, *FOXP2* is expressed in the medullary raphe, medulla oblongata, hypothalamus, and red nucleus (Lai et al., 2003; Teramitsu et al., 2004). Zebra finch *FoxP2* is expressed in similar regions as mammalian, such as the hypothalamus, and is generally more enriched in midbrain and hindbrain nuclei than *FoxP1* (Haesler et al., 2004; Teramitsu et al., 2004). Thus, *FoxP2* and *FoxP1* expression in these additional brain regions appear to be fairly conserved across vertebrates.

To broadly summarize patterns of *FoxP2* and *FoxP1* expression throughout the vertebrate brain, the cortex, hippocampus, and striatum have restricted or absent *FoxP2* expression and broader *FoxP1* expression, while the inverse is true for thalamus, cerebellum, and mid- and hindbrain structures. Some neuronal subtypes, such as L6a

corticothalamic projection neurons and striatal direct pathway SPNs, show overlapping expression of these transcription factors, while many other cell types express one or the other. These shared and distinct sites of expression may underlie the similarities (e.g. language deficits) and differences (e.g. gross motor delays) between patients with *FOXP2* mutations and those with *FOXP1* mutations. Furthermore, sites of *FoxP2* expression in the embryonic brain coincide with the cortical, basal ganglia, and cerebellar structural and functional abnormalities seen in patients with *FOXP2* mutations, lending further evidence for direct roles of this transcription factor in the development of these regions.

Molecular and cellular functions regulated by FoxP2 and FoxP1 in the brain

FoxP transcription factors show distinct structure and evolution

FoxP2 and FoxP1 belong to the large Fox family of transcription factors, which share a common DNA binding domain called winged helix or forkhead after the *fork head* gene in *Drosophila*. Their forkhead domains are highly similar to the *Drosophila* FoxP forkhead domain, suggesting an evolutionarily ancient origin for this transcription factor subfamily (Shu et al., 2001). Thus, many pathological *FOXP2* and *FOXP1* variants, including the KE family mutation, impact this highly conserved DNA binding domain (Lai et al., 2001; Morgan et al., 2017; Siper et al., 2017). Unlike other Fox transcription factors, FoxP family members can homo- and heterodimerize through a leucine zipper domain to bind DNA (Li et al., 2004; Wang et al., 2003). This involves a unique ability to form domain-swapped dimers, as shown by the crystal structure of FOXP2 bound to DNA (Stroud et al., 2006). Gene expression and luciferase assays in cultured cells have suggested that homotypic and heterotypic FoxP interactions can differentially regulate

downstream target genes (Mendoza and Scharff, 2017; Sin et al., 2015). In vivo studies supporting gene coregulation by FoxP2 and FoxP1 are coimmunoprecipitation of the two proteins in zebra finch Area X, as well as the significant overlap between dysregulated striatal genes in mice heterozygous for *Foxp2* or *Foxp1* (Araujo et al., 2015; Mendoza and Scharff, 2017).

Human FOXP2 shows additional distinct evolutionary features. It differs at three amino acid positions from mouse Foxp2 and two positions from chimpanzee, gorilla, and rhesus macaque FoxP2 (Enard et al., 2002). These human-specific variants are not located in a known functional domain of the protein, nor do they affect its ability to interact with other FoxP family members (Konopka et al., 2009). Nonetheless, they confer differential ability to regulate neurodevelopment-related genes in human SH-SY5Y and neural progenitor cells compared with non-human primate forms of FoxP2 (Konopka et al., 2009; Oswald et al., 2017). While evidence for recent positive selection of *FOXP2* is currently debated (Atkinson et al., 2018; Coop et al., 2008; Enard et al., 2002; Krause et al., 2007), there are clearly functional consequences of the two human-specific FOXP2 mutations on gene regulation in human cells.

FoxP2 and FoxP1 interact with other transcriptional regulators

In addition to forming homo- and heterodimers, FoxP2 and FoxP1 interact with numerous other proteins involved in transcription (**Fig. 1.4**). Initial studies utilized biochemical methods such as yeast two-hybrid screens, coimmunoprecipitations, and luciferase assays in cultured cells to identify FoxP2 and FoxP1 interactors. FoxP2 and FoxP1 can interact with CTBP1 via sites near their leucine zipper domains to repress

transcription (Li et al., 2004). NKX2-1 transcriptional activity is inhibited by its direct interaction with Foxp2 (Zhou et al., 2008). Foxp2 and Foxp1 also bind with components of the nucleosome remodeling and deacetylase (NuRD) chromatin-remodeling complex, including p66β/GATAD2B, HDAC1, and HDAC2 (Chokas et al., 2010). Yeast two-hybrid screening confirmed the FOXP2-CTBP1 interaction and also found interaction with the related protein CTBP2, the E3-type small ubiquitin-like modifier (SUMO) ligase PIAS3, and the transcription factor TBR1 (Sakai et al., 2011). FOXP2 also binds POT1 through its forkhead domain to promote nuclear localization of this telomere maintenance protein (Tanabe et al., 2011). Mass spectrometry combined with bioluminescence resonance energy transfer (BRET) assays have identified several binding partners of FOXP2 and/or FOXP1 in cultured cells, including NR2F1, NR2F2, SATB1, SATB2, SOX5, TBR1, YY1, and ZMYM2 (Deriziotis et al., 2014; Estruch et al., 2018). Recent work from our laboratory utilized chromatin accessibility and proximity ligation assays in human neuronal cultures to identify the transcription factors NFIA and NFIB as FOXP2 interactors (Hickey et al., 2019). Altogether these studies demonstrate the variety of proteins interacting with FoxP2 and FoxP1 in vitro, and further work is needed to verify these interactions and determine their biological significance in vivo.

Of particular interest for this thesis is the interaction between FoxP2 and TBR1, although it is also noteworthy that FoxP1 and TBR1 also interact (Deriziotis et al., 2014). *TBR1* is among the most significant recurrently mutated genes in ASD (De Rubeis et al., 2014; Iossifov et al., 2014; O'Roak et al., 2012; Sanders et al., 2015; Satterstrom et al., 2019), and Foxp2, Foxp1, and/or TBR1 colocalize in L6 corticothalamic projection

neurons (Hisaoka et al., 2010). Foxp1 and TBR1 are also broadly expressed in other cortical layers, but their coexpression patterns here remain to be described (Bulfone et al., 1995; Hisaoka et al., 2010). Given the associations of *FOXP2* and *FOXP1* with ASD, interactions among FOXP2, FOXP1, and TBR1 in the cortex may be vital for proper regulation of gene networks involved in language-disrupting neurodevelopmental disorders. In this thesis I describe molecular characterizations of FoxP2-TBR1 interaction, including gene coregulation in neural cells.

FoxP2 regulates neurodevelopmental genes and signaling pathways

As transcription factors, FoxP2 and FoxP1 bind DNA to regulate gene expression, which influences numerous downstream signaling pathways and cellular functions (**Fig. 1.3B**). Initial studies identified neurodevelopment-related FOXP2 targets in human fetal cortex, fetal basal ganglia, and SH-SY5Y cells through chromatin immunoprecipitation followed by hybridization of DNA fragments to promoter microarrays (ChIP-chip) (Spiteri et al., 2007; Vernes et al., 2007). Among these targets are modulators of the Notch and Wnt signaling pathways, which regulate proliferation, differentiation, and migration of neuronal cells (Bray, 2016; Noelanders and Vleminckx, 2016). Later functional studies indicated that FOXP2 directly represses *DISC1*, a Wnt modulator implicated in neuropsychiatric disorders (De Rienzo et al., 2011; Walker et al., 2012). FoxP2 may also influence cell migration by directly activating *VLDLR*, which encodes a core receptor for Reelin signaling, and directly repressing *CNTNAP2*, which encodes a transmembrane protein mediating cell-cell adhesion (Adam et al., 2016; Mendoza and Scharff, 2017; Spiteri et al., 2007; Vernes et al., 2008; Vernes et al., 2007). One study found activation

of *CNTNAP2* by FoxP2 in a zebra finch cell line, suggesting an effect of cellular context on gene regulation by FoxP2 (Adam et al., 2017). Genetic disruptions of *RELN*, which encodes Reelin, and *CNTNAP2* are causative for neurodevelopmental disorders, further implicating FOXP2-mediated gene networks in these conditions (De Rubeis et al., 2014; Rodenas-Cuadrado et al., 2013).

FOXP2 also regulates signaling pathways to promote neuronal maturation in mouse and human cell cultures. Forced Foxp2 expression in E14.5 mouse cortical progenitors increases the number of TUJ1+ neurons, while knockdown in E14.5 GE progenitors reduces neuron number and attenuates retinoic acid-mediated differentiation (Chiu et al., 2014). This effect was mediated through activation of the growth factor gene *Pdgfra* and repression of the Sonic hedgehog pathway, including the gene *Ptch1* (Chiu et al., 2014). Human SH-SY5Y cells stably expressing FOXP2 show higher expression of retinoic acid signaling genes, as well as enhanced differentiation-related gene expression responses to retinoic acid (Devanna et al., 2014). Likewise, in human neuronal cultures, forced FOXP2 expression results in repression of proliferation-related gene networks and activation of neuronal maturation gene networks (Hickey et al., 2019).

Another facet of neurodevelopment regulated by FoxP2 is the outgrowth of neuronal projections. The human tissue and cell line ChIP-chip studies described above also found targets involved in neurite outgrowth, axonal morphology, and axon guidance (Spiteri et al., 2007; Vernes et al., 2007). ChIP-chip and expression microarrays in whole brain and ganglionic eminences, respectively, identified similar themes in embryonic mouse brain (Vernes et al., 2011). In addition, mouse Neuro2a and human SH-SY5Y cell

lines stably expressing FoxP2 grow longer and more complex neurites during retinoic acid-mediated differentiation, while cultured ganglionic eminence neurons from mice with the *Foxp2* KE mutation grow shorter neurites (Devanna et al., 2014; Vernes et al., 2011).

FoxP2 targets also implicate this transcription factor in cortical patterning and projection neuron identity. Consistent with FoxP2 repression of *CNTNAP2*, these genes show inverse laminar expression patterns in developing and mature cortex (Rodenas-Cuadrado et al., 2018; Vernes et al., 2008). Experiments in human neural progenitors found that FOXP2 also represses *MET*, a receptor tyrosine kinase highly associated with ASD (Mukamel et al., 2011). *Met* is expressed throughout the postnatal mouse cortex, but within L6 *Met* is enriched in corticocortical projection neurons whereas *Foxp2* is enriched in corticothalamic neurons (Kast et al., 2017). Thus, FoxP2 may repress *CNTNAP2* and *MET* in the cortex to establish layer and projection neuron identities, respectively. Altogether these studies elucidate the various signaling pathways by which FoxP2 may influence proliferation, migration, differentiation, neurite outgrowth, and cell identity during brain development.

FoxP2 regulates corticostriatal synaptic and dopamine signaling genes

Many of the neurodevelopmental FoxP2-regulated genes and signaling pathways described above may also play roles in neuronal activity and plasticity. Reelin and Wnt pathways have been shown to modulate dendritic spine formation and synaptic plasticity, and *CNTNAP2* knockdown in mouse cortical neurons impairs spine growth and neuronal network activity (Anderson et al., 2012; Lee and D'Arcangelo, 2016; Oliva et al., 2013). Additional targets also implicate FoxP2 in regulation of synapses. Experiments in HEK-

293T cells, cultured rat hippocampal neurons, and postnatal mouse cortex identified the language disorder-associated gene *SRPX2* as a directly repressed target of FoxP2 (Roll et al., 2010; Sia et al., 2013). *FoxP2* overexpression reduces excitatory synapses in cultured rat hippocampal neurons, while cotransfection of *FoxP2* and *SRPX2* rescues this depletion of synapses (Sia et al., 2013). In mouse striatal SPNs, Foxp2 directly represses the ASD risk gene *Mef2c*, and reduction of *Mef2c* rescues the loss of excitatory synapses onto SPNs in *Foxp2* heterozygotes (Chen et al., 2016). *Foxp2* heterozygotes also show increased presynaptic content and release of GABA from striatal D1R+ SPNs, presumably through derepression of the GABA enzyme gene *Gad1* (van Rhijn et al., 2018; Vernes et al., 2011). Thus, FoxP2 may regulate synaptic density and function through direct repression of *CNTNAP2*, *SRPX2*, *MEF2C*, and *GAD1*.

FoxP2 may also modulate neuronal activity and plasticity through regulation of dopamine signaling genes. Its repressed target DISC1 interacts with many proteins involved in dopamine signaling, and animal models of *DISC1* disruption commonly show dopaminergic dysfunction (Dahoun et al., 2017). In embryonic mouse brain, Foxp2 binds the promoter of *Ppp1r1b*, which encodes the D1R effector DARPP-32 (Vernes et al., 2011). In zebra finch Area X, *FoxP2* knockdown reduces DARPP-32 and D1R levels and slows cortico-striato-thalamo-cortical signal propagation in a manner similar to D1R antagonism in Area X (Murugan et al., 2013). These studies, combined with the enriched Foxp2 expression in DARPP-32+ cortical neurons and D1R+ SPNs, indicate that FoxP2 directly activates DARPP-32 and directly or indirectly activates D1R (Hisaoka et al., 2010; Vernes et al., 2011). This dopaminergic regulation may be especially important for proper

corticostriatal signaling. Explorations of the role of cortical *Foxp2* in D1R expression during development and adulthood are a major component of this thesis.

In summary, the FoxP2 targets identified thus far mediate both neurodevelopment and neuronal function through multiple signaling pathways. While the importance of these molecular functions has been demonstrated for corticostriatal signaling, less is known about FoxP2 targets mediating the development and activity of corticothalamic, thalamocortical, and cerebellar circuits. Moreover, direct FoxP2 targets have been identified using ChIP-chip, ChIP with shotgun sequencing, or motif searches near a putative target, but genome-wide direct targets remain unknown. Thus, studies within this thesis have been conducted to elucidate these aspects of FoxP2 molecular function within the brain.

FoxP1 regulates neurodevelopmental, neuronal activity, and synaptic genes

FoxP1 regulates similar neurodevelopmental signaling pathways as its paralog FoxP2. FoxP1 binds and activates *VLDLR*, indicating a role in Reelin signaling, and it also influences expression of Wnt signaling genes in HEK-293T cells (Mendoza and Scharff, 2017; Sin et al., 2015). ChIP followed by sequencing (ChIP-seq) combined with RNA sequencing (RNA-seq) in mouse neural stem cells found that Foxp1 regulates Notch signaling genes through direct repression of *Jag1* (Braccioli et al., 2017). This study, as well as an RNA-seq study of human neural progenitors with forced *FOXP1* expression, identified other neurodevelopmental gene ontology categories associated with FoxP1, such as neurogenesis, neuronal development/differentiation, and axon guidance (Araujo et al., 2015; Braccioli et al., 2017). Also, like FoxP2, FoxP1 directly binds *CNTNAP2*, but

luciferase assays show activation at the zebra finch promoter while FOXP1 overexpression in HEK-293T cells suggests repression of *CNTNAP2* (Mendoza and Scharff, 2017; O'Roak et al., 2011). Nevertheless, these studies combined show an important role for FoxP1 in neurodevelopment through its regulation of multiple signaling pathways.

Foxp1 also modulates expression of genes involved in neuronal activity. RNA-seq in *Foxp1* heterozygous mice followed by weighted gene coexpression network analysis (WGCNA) identified a striatum-specific module enriched for voltage-gated channel activity genes, such as the Kv4.2 potassium channel regulator *Dpp10* (Araujo et al., 2015). This study also found that striatal Foxp1 targets specific to D2R+ SPNs include many cation transport genes, which may underlie the increased excitability of D2R+ SPNs in *Foxp1* heterozygous mice (Araujo et al., 2015). RNA-seq in adult mice lacking cortical and hippocampal *Foxp1* found that dysregulated genes common to both of these brain regions are involved in potassium channel activity and calcium ion transmembrane transport (Araujo et al., 2017). Moreover, downregulated hippocampal targets are associated with reduced long-term potentiation (LTP) and abnormal synaptic transmission gene ontology categories, in agreement with the impaired LTP maintenance occurring in the hippocampus of these mice (Araujo et al., 2017). Altogether these studies indicate brain-wide roles for FoxP1 in neurodevelopment, neuronal excitability, and synaptic function through its gene targets. However, given that FoxP1 cofactors vary in expression by brain region, cell type-specific targets of FoxP1 in both mouse and zebra finch are currently being elucidated by our laboratory.

Animal models of FoxP2 function

Clinical phenotyping of *FOXP2* and *FOXP1* patients, combined with examination of expression patterns of these genes, have indicated key brain regions and cell types for the various molecular actions of these transcription factors. A crucial approach for linking molecular functions to behavioral phenotypes is the manipulation of gene expression and function in animal models, which can be conducted in a brain region- or cell type-specific manner. Here I will describe animal models of *FoxP2* function, and later *FoxP1* function, with regards to neurophysiological, brain morphological, and behavioral phenotypes mediated by these genes.

Homozygous Foxp2 loss-of-function mice

Several whole-body loss-of-function *Foxp2* mouse lines have been generated and characterized. The first line was generated by replacement of exons 12-13 with a neomycin cassette via homologous recombination, thus deleting part of the forkhead domain and causing absence of Foxp2 protein in homozygotes (*Foxp2-ex12/13-KO*) (Shu et al., 2005). Then two mouse lines were generated to model the KE family mutation, one of which resulted from a knockin strategy via homologous recombination (*Foxp2-R552H-KI*) (Fujita et al., 2008) and the other from an N-ethyl-N-nitrosourea (ENU) mutagenesis screen (*Foxp2-R552H*) (Groszer et al., 2008). Two additional mutations were generated from the ENU screen, one near the KE mutation (*Foxp2-N549K*) and the other similar to the R328X mutation in a family with speech and language disorder (*Foxp2-S321X*) (Groszer et al., 2008). The R552H and N549K mutations do not affect Foxp2 expression levels, but S321X causes absence of protein and reduction of mRNA, presumably due to

nonsense-mediated decay (Fujita et al., 2008; Groszer et al., 2008). Last, another *Foxp2* knockout line was generated by Cre-loxP deletion of exon 7, resulting in a similar reduction of mRNA and absence of protein (*Foxp2-ex7-KO*) (Enard et al., 2009).

Severe developmental abnormalities appear in mice homozygous for the above mutations, including delayed weight gain, gross motor impairments, reduced isolation ultrasonic vocalizations (USVs), reduced cerebellum size, and death by 3-4 weeks after birth (Fujita et al., 2008; Gaub et al., 2010; Groszer et al., 2008; Shu et al., 2005). *Foxp2-N549K* homozygotes show comparable but milder developmental and cerebellar volume deficits, and they survive for 3-5 months (Groszer et al., 2008). Other than volume, cerebellar phenotypes vary by mouse line, with *Foxp2-ex12/13-KO* and *Foxp2-R552H-KI* mice showing disorganized Purkinje cells and reduced dendritic arborization, and *Foxp2-R552H* mice showing normal Purkinje histoarchitecture (Fujita et al., 2008; Groszer et al., 2008; Shu et al., 2005). *Foxp2-ex7-KO* mice show normal striosome-matrix formation in the striatum but fewer excitatory synapses and postsynaptic currents in SPNs (Chen et al., 2016). Other brain morphological phenotypes reported in homozygous *Foxp2* mutants are impaired survival of amygdalar intercalated cells, abnormal thalamic patterning, reduced posterior thalamocortical projections, and altered cortical barrel formation (Ebisu et al., 2016; Kuerbitz et al., 2017). These studies reveal the requirement for *Foxp2* for normal development and survival and are consistent with the lack of homozygous *FOXP2* patients in the literature.

Heterozygous Foxp2 loss-of-function mice

Mice heterozygous for *Foxp2* mutations, on the other hand, develop mostly normally and survive into adulthood. Different mutant lines show slight variations in motor development and USVs, presumably due to differences in mutant generation methods and/or genetic background strains. For example, mice created through homologous recombination (*Foxp2-ex12/13-KO, Foxp2-R552H-KI*) show small decreases in postnatal weight gain and motor ability, while mice from the ENU screen (*Foxp2-R552H, Foxp2-S321X*) do not (Fujita et al., 2008; Groszer et al., 2008; Shu et al., 2005). Most *Foxp2* heterozygote lines show neonatal USV reductions (*Foxp2-ex7-KO, Foxp2-ex12/13-KO, Foxp2-R552H-KI, Foxp2-S321X*), although one study of *Foxp2-R552H* heterozygotes did not find differences (Chen et al., 2016; Fujita et al., 2008; Gaub et al., 2010; Groszer et al., 2008; Shu et al., 2005). *Foxp2-ex12/13-KO* heterozygotes continue to show USV abnormalities from juvenile development into adulthood, with fewer courtship calls and altered bouts (Castellucci et al., 2016). Adult *Foxp2-R552H* and *Foxp2-S321X* heterozygotes also exhibit courtship USV alterations in either acoustic structure or social modulation of syntax, depending on the study (Chabout et al., 2016; Gaub et al., 2016). These results generally implicate *Foxp2* heterozygosity in vocalization deficits, consistent with the speech impairments found in patients heterozygous for *FOXP2* mutations.

Additional behavioral assessments have been carried out in adult *Foxp2* heterozygous mice. The most consistent finding among heterozygote studies (*Foxp2-ex7-KO, Foxp2-R552H, Foxp2-S321X*) is impairment on the rotarod assay, a motor-skill task where mice learn to stay atop an accelerating rotating rod over several days (Enard et al., 2009; French et al., 2012; Groszer et al., 2008). *Foxp2-R552H* heterozygotes also

show difficulties with a tilted running-wheel assay, another assessment of motor-skill learning (Groszer et al., 2008). In addition to impaired motor-skill learning, *Foxp2-R552H* and *Foxp2-S321X* mice exhibit impaired auditory-motor association learning, which is assessed in a task where mice learn to jump over a hurdle in response to a 12 kHz tone and to refrain from jumping when hearing a 7 kHz tone (Kurt et al., 2012). Interestingly, these mutations have differential effects on performance in this task: whereas R552H delays the rate at which mice reach wild-type levels of performance, S321X slows learning more severely and prevents mice from reaching wild-type levels (Kurt et al., 2012). Given that these mouse lines were backcrossed to the same genetic background, this result suggests that the non-DNA-binding form of Foxp2 in the R552H mutant still performs molecular functions allowing for some learning, while the reduced *Foxp2* dosage in the S321X mutant causes stronger impairments. In contrast, *Foxp2-ex12/13-KO* heterozygotes did not have spatial learning deficits as tested in the Morris water maze, nor did *Foxp2-R552H* mice show working memory deficits or perseverative behaviors via spontaneous alternation in a T-maze (Groszer et al., 2008; Shu et al., 2005). *Foxp2-ex7-KO* heterozygotes did show increased exploration in a modified hole board assay, while *Foxp2-R552H* mice showed normal locomotion, anxiety, and grooming behaviors (Enard et al., 2009; Groszer et al., 2008). In summary, mice heterozygous for *Foxp2* mutations commonly show alterations in motor-skill and motor-auditory association learning, while other forms of learning and baseline motor behaviors appear normal.

Accompanying the motor learning changes in *Foxp2* heterozygotes are neurophysiological and neurochemical alterations. The brain region most implicated in

these deficits is the striatum, which shows increased baseline firing rates in awake *Foxp2-R552H* mice and abnormally modulated firing and entrainment during the rotarod assay (French et al., 2012). In addition, slice electrophysiology studies indicate absence of striatal long-term depression (LTD) in *Foxp2-R552H* mice, as well as decreased excitatory and increased inhibitory currents in D1R+ SPNs of *Foxp2-S321X* mice (Groszer et al., 2008; van Rhijn et al., 2018). Other brain regions also show abnormal physiology in *Foxp2* heterozygotes. Cerebellar slices from *Foxp2-R552H* mice show increased paired-pulse facilitation of parallel-fiber-Purkinje cell synapses, indicating changes in short-term plasticity (Groszer et al., 2008). However, Purkinje cell LTD was normal in these mice (Groszer et al., 2008). *Foxp2-R552H* mice also show altered brainstem responses to auditory tones while *Foxp2-S321X* do not, another instance of *Foxp2* mutations differentially affecting phenotypes (Kurt et al., 2009). A study of neurotransmitter levels in *Foxp2-ex7-KO* heterozygotes found increased dopamine in the globus pallidus and nucleus accumbens, increased serotonin in the nucleus accumbens, and decreased GABA in the frontal cortex, suggesting altered chemical modulation of neurons in these brain regions (Enard et al., 2009). Altogether these studies indicate a requirement for Foxp2 for normal striatal, cerebellar, and auditory brainstem physiology and corticostriatal neurotransmitter levels.

In summary, studies of heterozygous *Foxp2* mutant mice have offered important insights into the etiology of speech and language disorders. They highlight motor-skill learning, auditory-motor association learning, and innate vocalization as key abilities regulated by Foxp2. They also reveal some of the neurophysiological and neurochemical

abnormalities potentially underlying these disorders. Strongly implicated brain regions include the striatum and cerebellum, which agrees with the altered morphology and function of these regions in the KE family. However, despite the cortical abnormalities found in these brain imaging studies, cortical morphology and physiology of any *Foxp2* mutant mouse line has yet to be described in the literature. Furthermore, whole-body *Foxp2* mutation obscures the contributions of individual brain regions and cell types to behavioral phenotypes. To this end, brain region-specific manipulations of *Foxp2* have been conducted in this thesis and provide additional insights into neurodevelopmental disorder etiology.

To allow for tissue- and/or temporal-specific deletions of *Foxp2*, a mutant mouse line was generated with loxP sites flanking exons 12-14, allowing for Cre-mediated deletion of the forkhead domain and subsequent loss of Foxp2 protein expression (French et al., 2007). These *Foxp2*$^{flox/flox}$ mice were validated through crosses with mice expressing *Sox2*-Cre, which is expressed throughout the early embryo, resulting in offspring with the severe developmental abnormalities, reduced cerebellar size, and early death seen in other homozygous *Foxp2* mutants (French et al., 2007). These mice have proven useful for brain region-specific conditional knockout (cKO) of *Foxp2*, as have molecular tools allowing for spatially controlled reductions or overexpression of *Foxp2*.

Cortex-specific Foxp2 manipulations

Developmental manipulations of cortical *Foxp2* expression have been performed to ascertain the role of cortical *Foxp2* in neurogenesis, neuronal migration, cortical morphology, and behavior. In one study, *Foxp2* knockdown by in utero electroporation

(IUE) of a short hairpin RNA (shRNA) at E13/14 impaired the transition of PAX6+ radial glia into TBR2+ intermediate progenitors and SATB2+ neurons (Tsui et al., 2013). This knockdown also impaired the migration of NeuN+ neurons into upper layers of the cortex (Tsui et al., 2013). While these results support the predicted molecular functions of *Foxp2* in neuronal differentiation and migration, crosses of *Foxp2*$^{flox/flox}$ mice with cortical Cre-driver mice have resulted in cortical *Foxp2* cKO mice with grossly normal cortical size, neuronal density, layering, and projections (French et al., 2018; Kast et al., 2019; Medvedeva et al., 2018). These major discrepancies could result from molecular compensations occurring after degradation of *Foxp2* mutant mRNA from the floxed allele, but not after *Foxp2* knockdown, a recently proposed mechanism for the phenomenon of knockdowns causing more severe phenotypes than genetic knockouts (El-Brolosy et al., 2019). An alternative mechanism involving altered interneuron migration is proposed later in this thesis.

Despite grossly normal cortical development, cortical *Foxp2* cKO mice show some behavioral deficits. To assess motor-skill learning, cortical *Foxp2* cKO mice were generated using *Emx1*-Cre, which induces recombination at E10.5 in progenitors and projection neurons derived from the dorsal telencephalon (French et al., 2018; Gorski et al., 2002). These mice gained weight normally over postnatal development and into adulthood, indicating grossly normal development (French et al., 2018). They performed normally on the rotarod, during operant lever-pressing, and during unperturbed sessions on the ErasmusLadder, another motor-skill learning test where mice walk across a horizontal ladder with movable rungs (French et al., 2018). However, during perturbed

sessions of the ErasmusLadder, where a rung is randomly raised to create an obstacle, cortical *Foxp2* cKO mice made more missteps than control littermates (French et al., 2018). While these results indicate some contribution of cortical *Foxp2* to motor-skill learning, deficits in these cKO mice were much less severe than striatal or cerebellar cKO mice described below.

Given the association of FOXP2-dependent molecular networks with ASD, social behaviors were measured in cortical *Foxp2* cKO mice generated using *Neurod6*-Cre (*Nex*-Cre), which causes recombination around E11.5 in postmitotic projection neurons of the dorsal telencephalon (Goebbels et al., 2006; Medvedeva et al., 2018). In a paradigm where control or cKO “hosts” are introduced to an unfamiliar wild-type “visitor” in an arena, cKO hosts spent less time with the visitor overall and engaged in less following, chasing, and close contact (Medvedeva et al., 2018). They also exhibited fewer paw control events, a social dominance behavior (Medvedeva et al., 2018). Additionally, they showed subtle alterations in USVs depending on social context, where call acoustic structure was abnormal during courtship and both acoustic structure and syntax were abnormal during male same-sex interactions (Medvedeva et al., 2018). These behavioral changes were not due to generalized anxiety, as cKO mice spent equal amounts of time in the open arms of an elevated plus maze as controls (Medvedeva et al., 2018).

These studies indicate roles for cortical *Foxp2* in motor-skill learning and social behavior, but they do not address its contribution to other behaviors relevant to neurodevelopmental disorders, such as neonatal USVs, hyperactivity, executive function.

Thus, experiments in this thesis were conducted to clarify roles of cortical *Foxp2* in these behaviors.

Striatum-specific FoxP2 manipulations

To assess the role of striatal *Foxp2* in motor-skill learning, striatal *Foxp2* cKO mice were generated using *Rgs9*-Cre, which is expressed at postnatal day (P) 8 in most SPNs (French et al., 2018). These cKO mice show some remaining Foxp2 expression in the striatum and have no changes in striatal neuron density (French et al., 2018). Like cortical cKO mice, striatal cKO mice developed normally, performed normally on the rotarod, and made more missteps during perturbed ErasmusLadder sessions than controls (French et al., 2018). However, in addition, they made fewer lever presses during high-speed operant lever-pressing, and they executed lever presses more variably (French et al., 2018). This variability was not seen in cortical or cerebellar *Foxp2* cKO mice, indicating a particular role for striatal Foxp2 in controlling motor variability (French et al., 2018).

Another study performed *Foxp2* knockdown in the adult striatum to assess its roles in Huntington's disease-related phenotypes, which include motor impairments (Hachigian et al., 2017). Injection of adeno-associated virus (AAV) with a *Foxp2* shRNA construct into the striatum decreased latency to fall off the rotarod; this effect may have been caused by the severely decreased grip strength also present in these mice (Hachigian et al., 2017). They also showed decreased vertical activity, rearing, and climbing in an open field (Hachigian et al., 2017). While grip strength and open field activity were not assessed in striatal *Foxp2* cKO mice, their normal rotarod performance highly contrasts the rotarod impairment after viral *Foxp2* knockdown in adult striatum. This may again highlight

molecular differences between gene knockouts and knockdowns, or it may indicate circuit-level developmental compensation after postnatal *Foxp2* deletion that does not occur with adult *Foxp2* knockdown. Nonetheless, both of these studies indicate that striatal Foxp2 is important for motor function.

Several studies have also demonstrated the requirement for proper FoxP2 expression in zebra finch Area X for song learning and production. Lentiviral delivery of *FoxP2* shRNA constructs into juvenile Area X results in incomplete and inaccurate copying of tutor songs and high vocal variability over development (Haesler et al., 2007; Murugan et al., 2013). This effect may be mediated through decreased spine density on SPNs in Area X, rather than changes in proliferation or incorporation of postembryonic newborn neurons (Schulz et al., 2010). In adult zebra finches, *FoxP2* knockdown abolishes social-context-dependent changes in song variability, namely the decrease in variability that normally occurs during directed singing to a female (Murugan et al., 2013). As previously described, *FoxP2* knockdown decreases dopamine D1R and DARPP-32 expression in Area X, and also slows signal propagation through the cortico-striato-thalamo-cortical circuit of the anterior forebrain pathway (Murugan et al., 2013). Similar to *FoxP2* knockdown, *FoxP2* overexpression in juvenile Area X results in inaccurate tutor song copying, although adult song variability is unaffected (Heston and White, 2015). *FoxP2* overexpression in adult Area X also does not affect vocal variability, but upon deafening, overexpression hastens song deterioration and alters song variability and sequencing, indicating a role for FoxP2 in song stability (Day et al., 2019).

In summary, these studies show a critical role for striatal FoxP2 in motor-skill learning and motor variability in both mice and zebra finches. FoxP2 also regulates striatal SPN spine density in both species, as shown in *Foxp2* whole-body mutant mice and juvenile zebra finches with Area X *FoxP2* knockdown. Further work is needed to clarify the role of striatal Foxp2 in mouse vocalizations and other neurodevelopmental disorder-relevant behaviors. Additionally, given that *Rgs9*-Cre acts postnatally, studies of the effects of embryonic striatal *Foxp2* deletion are ongoing in our laboratory to fully understand its functions in striatal development.

Thalamus-specific Foxp2 manipulations

As previously mentioned, whole-body homozygous *Foxp2*-R552H-KI mice show altered thalamic patterning, with reduced posterior nuclei and expanded intermediate nuclei (Ebisu et al., 2016). To prove a cell-autonomous origin for this phenotype, the authors also performed IUE knockdown of *Foxp2* in the thalamic primordium at E11, and they found a similar result of decreased expression of posterior nuclei markers (*Epha8*, *Cdh6*) and increased expression of intermediate nuclei markers (*Gbx2*, *Lhx2*), confirming the role of thalamic Foxp2 in development of this region (Ebisu et al., 2016). No other published studies have performed thalamus-specific manipulations of Foxp2; therefore, much remains to be explored regarding Foxp2 function in this core region of vocalization and sensorimotor learning circuitry.

Cerebellum-specific Foxp2 manipulations

To assess the contribution of *Foxp2* in Purkinje cells to motor-skill learning, Purkinje *Foxp2* cKO mice were generated using *Pcp2*/*L7*-Cre, which is expressed by P9

in all Purkinje cells of the cerebellum (French et al., 2018). This resulted in complete loss of Foxp2 from these cells without affecting expression in deep cerebellar nuclei (French et al., 2018). While Purkinje cKO mice showed normal performance on the rotarod, they had worse impairments than cortical or striatal cKO mice in other motor-skill learning tests, with fewer presses during both normal and high-speed sessions of lever-pressing, and more missteps during both unperturbed and perturbed sessions of the ErasmusLadder (French et al., 2018). Extracellular recordings of Purkinje cells in head-fixed mice walking on a wheel revealed increased intrinsic activity and decreased correlation of activity with phases of walking (French et al., 2018). These results indicate a larger role for cerebellar Foxp2 in motor learning than cortical or striatal Foxp2.

Another cerebellar manipulation of Foxp2 highlights its importance for mouse USV production. To perform Purkinje cell-specific Foxp2 rescue in whole-body *Foxp2* mutant mice, transgenic mice expressing human FOXP2-myc under the *Pcp2/L7* promoter were generated and crossed to *Foxp2-R552H-KI* heterozygotes (Fujita-Jimbo and Momoi, 2014). The presence of this Purkinje-expressed transgene in heterozygotes restored the relative proportions of whistle-, short-, and click-type calls to wild-type levels, but it did not rescue USVs of homozygotes (Fujita-Jimbo and Momoi, 2014). Thus, cerebellar *Foxp2* expression may be sufficient for rescuing USV deficits in heterozygous *Foxp2* mutant mice.

These Purkinje cell-specific experiments point to the cerebellum as a key site in the brain for Foxp2 function in mice, consistent with the striking reduction in cerebellar

size seen in *Foxp2* mutant homozygotes. Further work exploring cell-autonomous roles of FoxP2 in cerebellar development and USV production is included within this thesis.

Humanized Foxp2 mice

To characterize the functional consequences of the two human-specific *FOXP2* mutations at an organism level, these substitutions were introduced into mice via homologous recombination to generate “humanized” *Foxp2* mice (*Foxp2*^{hum}) (Enard et al., 2009). This resulted in a number of phenotypic alterations, including decreased cortico-basal ganglia dopamine levels, longer neuronal dendrites, increased striatal plasticity, altered pup vocalization, and altered exploratory and learning behaviors (Enard et al., 2009; Reimers-Kipping et al., 2011; Schreiweis et al., 2014). The changes in dopamine levels are especially intriguing given the expression of *FoxP2* in dopaminergic (SNc and VTA) and dopaminoceptive (striatal direct pathway) regions in the brain, as previously noted. Furthermore, the increased neuronal dendrite lengths occur specifically in cortical L6, striatal, and thalamic neurons, implicating human FOXP2 in the evolution of cortico-striato-thalamo-cortical circuits (Reimers-Kipping et al., 2011). Interestingly, *Foxp2*^{hum} mice show no alterations of adult USVs, suggesting that “humanization” of corticostriatal circuits may not affect the innate vocalizations of adult mice, but may play roles in other behaviors relevant to sensorimotor learning and cognitive aspects of language (Hammerschmidt et al., 2015a). Indeed, *Foxp2*^{hum} mice show enhanced strategy set-shifting in a T-maze, a cognitive behavior dependent on corticostriatal function (Schreiweis et al., 2014). More work is needed to understand how humanized Foxp2 impacts brain development to mediate these behaviors.

As a whole, studies of FoxP2 using animal models have identified important roles for this transcription factor in the development and function of corticostriatal circuits and the cerebellum, with regards to vocalization and motor-skill learning behaviors. They also have provided insights into the role of FOXP2 in the evolution of corticostriatal circuits as they pertain to language-relevant behaviors. Further work on cortical and cerebellar *Foxp2* functions is presented in this thesis and contributes to our understanding of molecular pathways and behaviors regulated by Foxp2 in these critical brain regions.

Animal models of Foxp1 function

Whole-body Foxp1 loss-of-function mouse models

Foxp1 mutant mice have also been generated and studied to understand the functions of this gene throughout the body. A study of *Foxp1* in heart function used homologous recombination to replace the forkhead domain with a neomycin cassette, resulting in loss of Foxp1 protein expression in homozygotes (*Foxp1-FH-KO*) (Wang et al., 2004). A study of immune B cell development generated a second *Foxp1* mutant line by targeting the N-terminal two-thirds of the protein, including the forkhead domain, and again saw total loss of Foxp1 protein in homozygotes (*Foxp1*$^{-/-}$) (Hu et al., 2006). Unlike homozygous *Foxp2* mutant mice, homozygous *Foxp1-FH-KO* mice die at E14.5 due to impaired cardiac development, precluding study of the effects of whole-body *Foxp1* loss on postnatal development and behavior. Thus, whole-body heterozygous deletions and tissue-specific manipulations of *Foxp1* have been conducted to investigate its role in brain development and function.

Our laboratory pioneered the study of heterozygous *Foxp1* knockout mice for understanding its functions in the etiology of ASD. Neonatal *Foxp1*$^{+/-}$ mice gain weight and perform gross motor functions normally, but they show abnormalities in USV production and acoustic features (Araujo et al., 2015). In adulthood they exhibit hyperactivity and impaired grip strength, but unlike heterozygous *Foxp2* mutants they perform normally on the rotarod (Araujo et al., 2015). *Foxp1* was thus shown to play a role in motor functions related to USVs, activity levels, and grip strength. Brain region-specific Western blotting and RNA-seq conducted on adult *Foxp1*$^{+/-}$ mice revealed Foxp1 reductions and subsequent gene dysregulation in the hippocampus and striatum; curiously, Foxp1 levels and gene expression were unaffected in the cortex, indicating compensatory *Foxp1* upregulation and suggesting an especially vital role in this brain region (Araujo et al., 2015). In contrast with the unaffected cortex, the striatum of these mice exhibited physiological alterations, most notably an increase in the excitability of D2R SPNs as mentioned previously (Araujo et al., 2015). Thus, similar to Foxp2, the striatum is an important site in the brain for Foxp1 activity, and ongoing work in our laboratory is uncovering the developmental, physiological, and behavioral consequences of deletion one or both of these proteins in a cell type-specific manner.

Brain- and region-specific Foxp1 manipulations

To conduct temporal- and/or tissue-specific deletions of *Foxp1*, mice with a conditional allele were generated using homologous recombination to flank exons 11-12 with loxP sites for Cre-mediated deletion (*Foxp1*$^{flox/flox}$) (Feng et al., 2010). Brain-specific deletion of *Foxp1* was performed by crossing these mice with *Nestin*-Cre mice, resulting

in loss of *Foxp1* from neuronal and glial precursors throughout the brain (Bacon et al., 2015; Frohlich et al., 2017; Tronche et al., 1999). These mice are viable but gain weight more slowly than controls, and like *Foxp2* mutant mice and *Foxp1*$^{+/-}$ mice, they exhibit reduced neonatal USV production and altered USV structure (Bacon et al., 2015; Frohlich et al., 2017). In adulthood they demonstrate severe behavioral deficits, including hyperactivity, repetitive rearing and jumping, impaired learning and memory, social retreat, absent nestbuilding, and reduced sensorimotor integration (Bacon et al., 2015). Morphologically, their brains show large reductions in striatal area and dispersed neuronal organization in hippocampal CA1, and the neurons within these regions have altered dendritic branching (Bacon et al., 2015). Hippocampal CA1 neurons of these mice also have decreased excitability and larger excitatory postsynaptic current amplitudes (Bacon et al., 2015). These analyses prove a requirement for Foxp1 for normal striatal and hippocampal development and CA1 function, but evaluations of the cortex were absent despite high expression of Foxp1 in this brain region.

Knockdown and overexpression studies of *Foxp1* in the cortex have offered some insight into its functions in this region. IUE of *Foxp1* shRNA at E14.5 impairs migration of cortical cells, as evidenced by accumulation of cells in the intermediate zone (IZ) and fewer cells in the CP above (Braccioli et al., 2017; Li et al., 2015). These studies conflicted on whether *Foxp1* knockdown impairs neuronal differentiation, as one study claimed no change in pH3+ dividing cells or TBR2+ intermediate progenitors, while the other saw more TBR2+ progenitors and fewer SATB2+ neurons (Braccioli et al., 2017; Li et al., 2015). Analysis of mature cortex after *Foxp1* knockdown supported cortical migration

impairment via presence of cells expressing upper-layer markers in the lower layers (Li et al., 2015). Additionally, neuronal morphology analyses after knockdown suggested impairments in multipolar-to-bipolar transition and dendritic outgrowth (Li et al., 2015). A recent study has also modeled the effects of *FOXP1* patient mutations on cortical development, with overexpression of Foxp1-R521X phenocopying *Foxp1* knockdown in cortical migration and neuronal morphology deficits (Li et al., 2018).

The cortex-specific upregulation of Foxp1 in *Foxp1*$^{+/-}$ mice, combined with the cortical development defects seen after *Foxp1* knockdown, indicate that this transcription factor has critical functions within this brain region. Prior studies had yet to address Foxp1 roles in cortical development using a genetic mouse model, nor do we know its functions in other animal models with high pallial expression, such as the zebra finch. Studies included in this thesis were conducted to answer these questions and elucidate mechanisms of *FoxP1* function in cortical neurons of mice and zebra finches. Parallel studies were conducted in the same cortico-hippocampal *Foxp1* cKO mouse model to identify its roles in adult hippocampal function and behaviors (Araujo et al., 2017).

Introduction

FOXP2 and FOXP1 are transcription factors implicated in neurodevelopmental disorders and are highly expressed in brain regions involved in vocalization and cognition. They homo- and heterodimerize to bind DNA, and they also interact with numerous other transcriptional regulators. Their gene targets identified thus far are involved in neuronal development, activity, and plasticity, and these functions are reflected by the phenotypes seen in animal models of FoxP2 and FoxP1 function. Despite the wealth of information

provided by published studies on these transcription factors, much remains unknown about their brain region- and cell type-specific contributions to neuronal development and function and downstream behaviors. The molecular mechanisms by which they regulate gene expression, such as cofactor interactions and posttranslational modifications, also require elucidation. Furthermore, current studies in mice cannot resolve their roles in vocal learning versus vocal production, but our poor understanding of molecular cell types in vocal-learning zebra finches limits our ability to interpret phenotypes induced by FoxP2 or FoxP1 manipulation.

For this thesis, I have worked to elucidate the roles of FoxP2 and FoxP1 in the brain as they relate to vocalization and cognition. I characterized and performed cell type-specific molecular analyses in mice lacking *Foxp2* in the cortex, a critical brain region for these abilities. I focused on a particular cortical FoxP2 cofactor, TBR1, to elucidate their interaction dynamics and coregulated genes. I also contributed to studies of cortico-hippocampal Foxp1 and cerebellar Foxp2 to understand their roles in these brain regions and how their modification by sumoylation affects these functions. Finally, I optimized tools and techniques facilitating the study of cell type-specific roles for FoxP2 and FoxP1 in zebra finch song nuclei. Together these studies expand our knowledge of FoxP2 and FoxP1 functions in the brain, and they provide hypotheses and directions for future research on the neurobiology of vocalization and cognition.

Figures

Figure 1.1 *Structural and functional brain abnormalities in affected KE family members.*

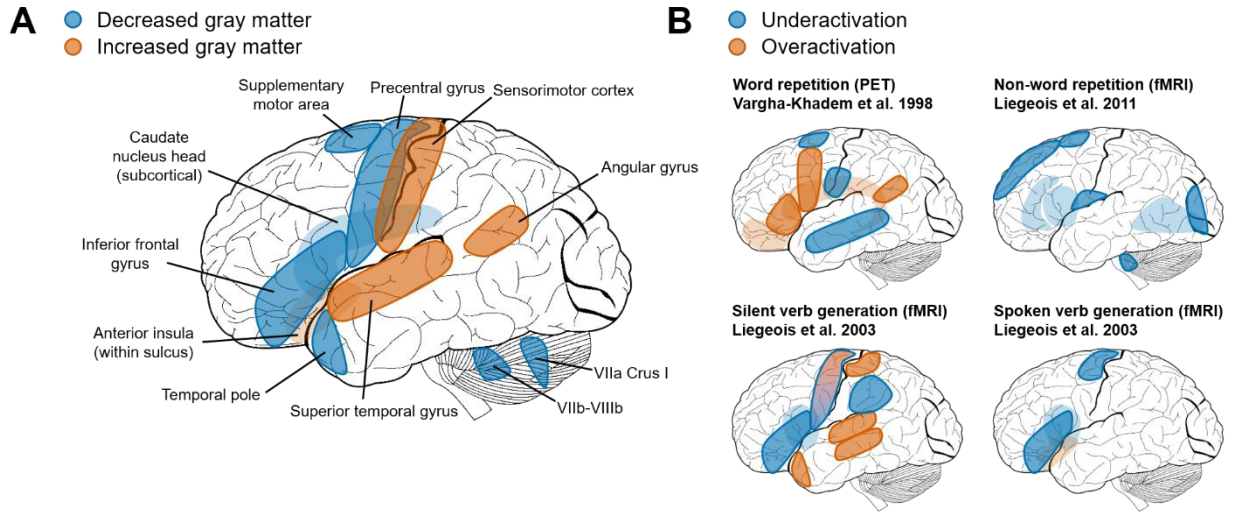

(A) Brain regions containing sites of altered gray matter in KE family members affected by FOXP2 mutation. Regions altered in two or more structural MRI studies are shown. (B) Brain regions containing sites of altered neural activation in PET or fMRI studies of affected KE family members.

Figure 1.2 *FoxP2 and FoxP1 expression patterns in mammalian and zebra finch brain.*

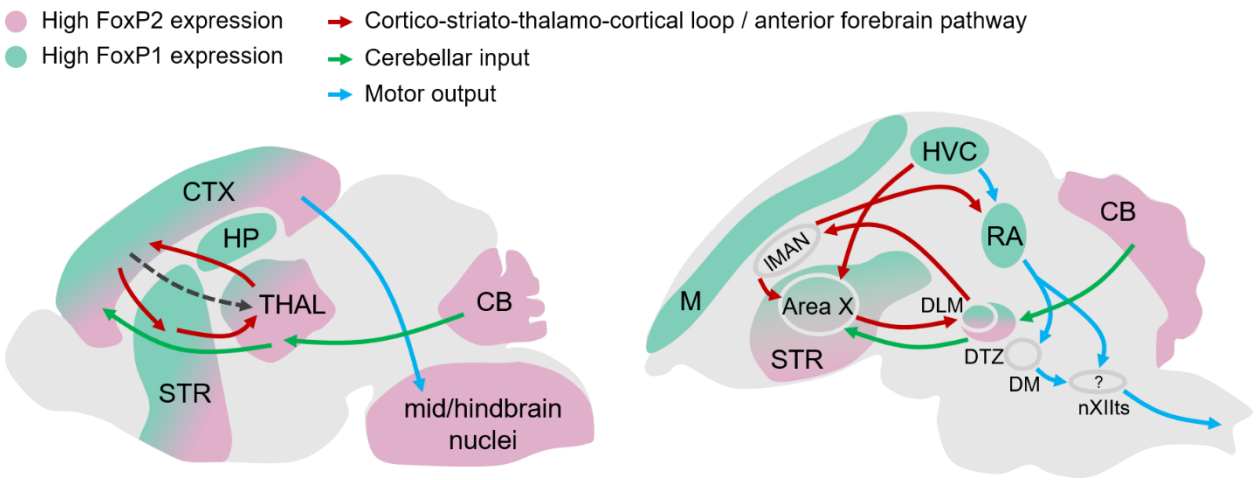

Expression patterns of *FoxP2* and *FoxP1* in mammalian brain (left) and zebra finch brain (right) with relevant vocalization-related circuits highlighted. CB: cerebellum, CTX: cortex, DLM: medial nucleus of dorsolateral thalamus, DM: dorsomedial nucleus of midbrain, DTZ: dorsal thalamic zone, HP: hippocampus, lMAN: lateral magnocellular nucleus of anterior nidopallium, M: mesopallium, nXIIts: tracheosyringeal subdivision of the hypoglossal nucleus, RA: arcopallial vocal nucleus, STR: striatum, THAL: thalamus.

Figure 1.3 *Putative molecular pathways regulated by FoxP2 and FoxP1 in the cortex.*

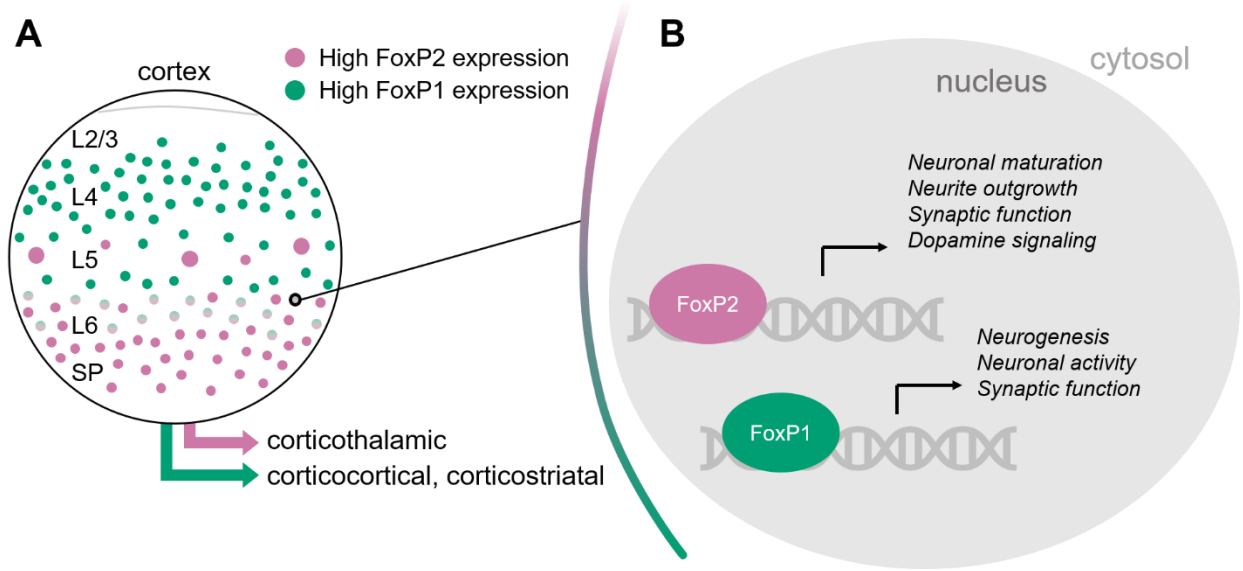

(A) Expression patterns of FoxP2 and FoxP1 across mammalian cortical layers (L) 2-6 and the subplate (SP). (B) Summarized molecular pathways regulated by FoxP2 and FoxP1 in neuronal cells.

Figure 1.4 *FoxP2 and FoxP1 protein interactors.*

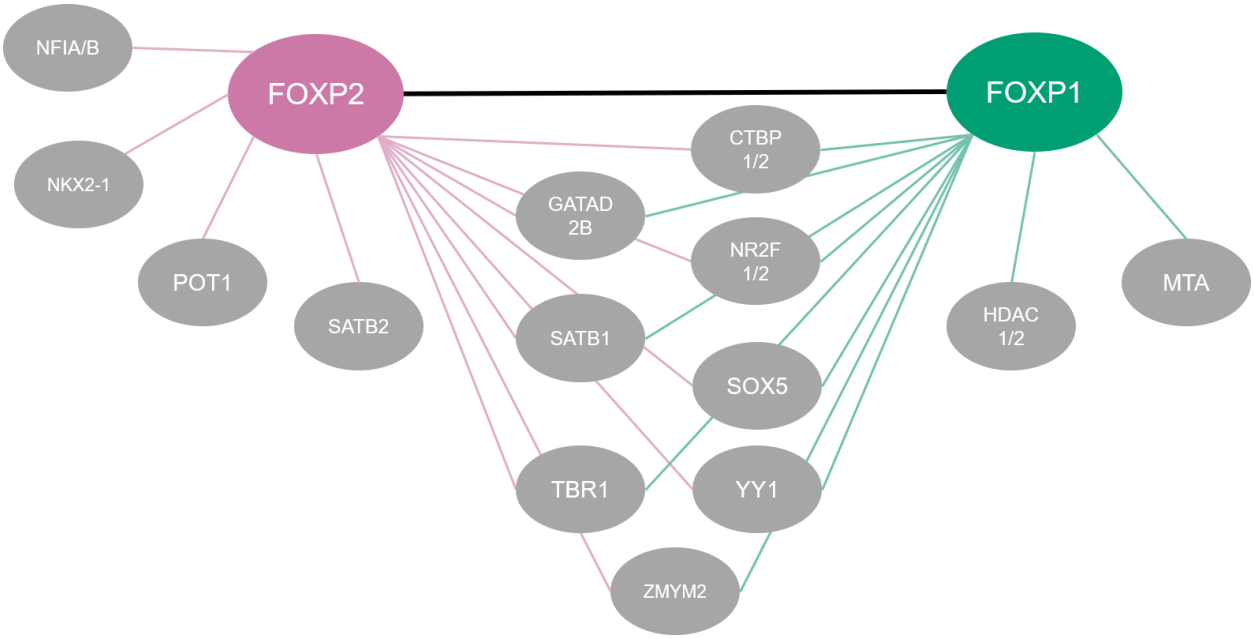

Summary of known protein binding partners of FOXP2 and FOXP1 based on in vitro assays and in vivo coimmunoprecipitations.

CHAPTER TWO: Decoding the molecular evolution of human cognition using comparative genomics

Published as: Usui, N., **Co, M.**, and Konopka, G. (2014). Decoding the molecular evolution of human cognition using comparative genomics. Brain, behavior and evolution *84*, 103-116.

CHAPTER THREE: Cortical *Foxp2* supports behavioral flexibility and developmental dopamine D1 receptor expression

Adapted from: **Co, M.**, Hickey, S.L., Kulkarni, A., Harper, M., and Konopka, G. (2019). Cortical Foxp2 supports behavioral flexibility and developmental dopamine D1 receptor expression. **Under revision at *Cerebral Cortex*.**

Abstract

Genetic studies have associated *FOXP2* variation with speech and language disorders and other neurodevelopmental disorders involving pathology of the cortex. In this brain region, *FoxP2* is expressed from development into adulthood, but little is known about its downstream molecular and behavioral functions. Here, we characterized cortex-specific *Foxp2* conditional knockout mice and found a major deficit in reversal learning, a form of behavioral flexibility. In contrast, they showed normal activity levels, anxiety, and vocalizations, save for a slight decrease in neonatal call loudness. These behavioral phenotypes were accompanied by decreased cortical dopamine D1 receptor (D1R) expression at neonatal and adult stages, while general cortical development remained unaffected. Finally, using single-cell transcriptomics, we identified at least five excitatory and three inhibitory D1R-expressing cell types in neonatal frontal cortex, and we found changes in D1R cell type composition and gene expression upon cortical *Foxp2* deletion. Strikingly, these alterations included non-cell-autonomous changes in upper-layer neurons and interneurons. Together these data support a role for *Foxp2* in the

development of dopamine-modulated cortical circuits and behaviors relevant to neurodevelopmental disorders.

Introduction

FoxP2 encodes a forkhead box transcription factor required for proper brain development and function across species, particularly in neural circuits underlying vocalization and motor-skill learning (French and Fisher, 2014; Konopka and Roberts, 2016b). In humans, *FOXP2* mutations cause a speech and language disorder characterized by childhood apraxia of speech and additional oral motor, linguistic, and/or cognitive deficits (Morgan et al., 2017; Schulze et al., 2017). Recent studies have broadened the clinical spectrum of *FOXP2* by identifying variants associated with autism spectrum disorder (ASD) and attention deficit/hyperactivity disorder (ADHD) (Demontis et al., 2019; Reuter et al., 2017; Satterstrom et al., 2019). Thus, *FOXP2* may subserve general neural functions impaired across neurodevelopmental disorders (NDDs).

FoxP2 is expressed in the developing and mature cerebral cortex, a site of pathology in *FOXP2*-related speech and language disorders as well as in ASD (van Rooij et al., 2018; Vargha-Khadem et al., 2005). Here, *Foxp2* expression is specific to layer 6 corticothalamic projection neurons (CThPNs) and some layer 5 pyramidal tract neurons but excluded from intratelencephalic projection neurons (ITPNs) (Kast et al., 2019; Sorensen et al., 2015; Tasic et al., 2016). Acute manipulations of *Foxp2* expression in embryonic cortex have implicated this gene in cortical neurogenesis and neuronal migration (Garcia-Calero et al., 2016; Tsui et al., 2013). However, mice with cortical

Foxp2 deletion show overtly normal cortical histoarchitecture, suggesting that *Foxp2* may be dispensable for gross corticogenesis (French et al., 2018; Kast et al., 2019; Medvedeva et al., 2018). Nonetheless, these mice show abnormalities in social behavior and motor-skill learning, warranting further investigation into molecular and cellular processes disrupted by cortical *Foxp2* deletion (French et al., 2018; Medvedeva et al., 2018). Foxp2 has been shown to act upstream of two synaptic genes, *Srpx2* and *Mint2*, in cortical neurons, but little else is known about molecular networks regulated by Foxp2 specifically in the cortex (Medvedeva et al., 2018; Sia et al., 2013). Furthermore, it is unknown whether loss of cortical *Foxp2* causes additional NDD-relevant behavioral deficits, such as cognitive impairment or hyperactivity.

In this study, we characterized NDD-relevant behaviors and their potential underlying cellular and molecular mechanisms in cortex-specific *Foxp2* conditional knockout mice (*Emx1-Cre; Foxp2*$^{flox/flox}$). We show that this deletion impaired reversal learning, a form of behavioral flexibility, while sparing other NDD-associated behaviors, such as vocal communication and hyperactivity. Using immunohistochemistry and genetic reporter mice, we confirmed grossly normal cortical development upon *Foxp2* deletion but found decreased expression of cortical dopamine D1 receptors at neonatal and adult stages. Last, using single-cell transcriptomics, we characterized neonatal dopamine D1 receptor-expressing neuronal subtypes, and we identified non-cell-autonomous effects of *Foxp2* deletion on interneuron development and upper-layer gene expression. Together these data support a role for *Foxp2* in specific aspects of cortical development potentially relevant to cognitive impairments seen in NDDs.

Results

Cortical Foxp2 deletion impairs reversal learning

We generated cortex-specific *Foxp2* conditional knockout (cKO) mice and control littermates by crossing *Foxp2*$^{flox/flox}$ mice (French et al., 2007) with mice expressing *Emx1*-Cre, which induces recombination embryonically in progenitors and projection neurons derived from dorsal telencephalon (Gorski et al., 2002). In adult *Foxp2* cKO mice, we confirmed the absence of Foxp2 protein in the cortex and normal expression in other brain regions (**Fig. 3.1A**). Consistent with known expression patterns of *Foxp2* in wild-type mouse brain, Foxp2 protein was absent from control hippocampus, where *Emx1*-Cre is also expressed (Ferland et al., 2003; Gorski et al., 2002) (**Fig. 3.1A**). We observed no gross abnormalities in overall brain morphology of cKO mice (**Fig. 3.1A**), consistent with a previous study utilizing the same conditional knockout strategy (French et al., 2018). In neonatal frontal cortex, we quantified a >90% reduction in Foxp2 protein content, confirming the efficiency of knockout in developing cortex (**Fig. 3.1B**).

We evaluated the contribution of cortical *Foxp2* to neurodevelopmental disorder (NDD)-relevant behaviors, such as behavioral flexibility, hyperactivity, anxiety, and social communication. To assess behavioral flexibility in *Foxp2* cKO mice, we utilized a water Y-maze assay and found significant deficits in reversal learning, but not initial acquisition, of escape platform location (**Fig. 3.2A-B**, statistics for behavioral testing are provided **Table 3.2**). As an additional assay of frontal cortical function, we assessed spontaneous alternation in a dry T-maze (Lalonde, 2002). While there were no significant differences

between genotypes in alternation rate or latency to arm, control mice alternated significantly above chance levels while cKO mice did not (**Fig. 3.2C-D**, **Table 3.2**). We then tested short-term memory using the novel object recognition test with a 5 min delay between training and testing, but we found no differences between genotypes (**Fig. 3.2E**, **Table 3.2**). We also assessed extinction to contextual and cued fear memory, another measure of behavioral flexibility dependent on the frontal cortex (Hamilton and Brigman, 2015). During training, cKO mice exhibited increased freezing over the training period in response to tone-shock pairings (**Fig. 3.2F**, **Table 3.2**). However, there were no differences between genotypes on the first day of contextual or cued fear recall testing, indicating no differences in fear learning (**Fig. 3.2G**, **Table 3.2**). When we tested extinction to context or cue, control mice unexpectedly did not extinguish freezing over 5 days, but nonetheless, cKO mice showed significantly increased freezing over the extinction period (**Fig. 3.2H-I**, **Table 3.2**). There were no differences between genotypes in footshock sensitivity, suggesting altered extinction behavior in cKO mice rather than impaired sensory function (**Fig 3.2J**, **Table 3.2**). In summary, Foxp2 cKO mice show behavioral inflexibility in the form of impaired reversal learning, and other tests of frontal cortical function are suggestive of deficits.

Given the altered social behaviors in mice with Neurod6-Cre-mediated cortical Foxp2 deletion (Medvedeva et al., 2018), we assessed sociability and social novelty preference in our Foxp2 cKO mice using the three-chamber social interaction test. Both genotypes spent significantly more time investigating a conspecific mouse than an object, indicating normal sociability in cKO mice (**Fig. 3.3A-B**, **Table 3.2**). Neither genotype spent

more time investigating a novel mouse compared to a familiar mouse, precluding interpretation of social novelty preference in cKO mice (**Fig. 3.3A-B**, **Table 3.2**). We performed additional assays to determine whether locomotor or anxiety phenotypes contributed to Foxp2 cKO impairment in cognitive behaviors. There were no differences in baseline activity levels in a novel cage (**Fig. 3.3C**, **Table 3.2**) or total distance moved in an open field (**Fig. 3.3D**, **Table 3.2**). Likewise, each genotype spent equal amounts of time in the center or open arms of the open field or elevated plus maze, respectively, indicating normal anxiety levels in cKO mice (**Fig. 3.3E-F**, **Table 3.2**). Altogether these data indicate that cortical Foxp2 is required for behavioral flexibility, but not for other forms of learning and memory or social, locomotor, or anxiety-related behaviors.

Cortical Foxp2 deletion decreases sound pressure of neonatal vocalizations

We evaluated the contribution of cortical *Foxp2* to social communication by measuring courtship ultrasonic vocalization (USV) production and spectral features in adult *Emx1*-Cre *Foxp2* cKO mice. Using automated call detection methods (Holy and Guo, 2005), we found no differences between genotypes in measures related to call number, timing, structure, pitch, or intensity (**Fig. 3.4A**, **Table 3.2**). We next used an automated method to cluster calls into 100 call types (repertoire units or RUs) and compare repertoires between genotypes (Van Segbroeck et al., 2017) (**Fig. 3.4B-F**). This yielded a similarity matrix comparable to matrices generated between cohorts of wild-type C57BL/6 mice (Van Segbroeck et al., 2017), with the top 74 of 100 RUs having Pearson correlations greater than 0.8 (**Fig. 3.4C**). Because the similarity matrix does not account for frequency of call types used, we calculated a median (top 50% most used RUs)

similarity score of 0.90 and an overall (top 95%) similarity score of 0.86 between control and cKO repertoires (**Fig. 3.4D**), comparable to the average similarity of 0.91 ± 0.03 between replicate C57BL/6 studies (Van Segbroeck et al., 2017). As another measure of call usage similarity, we constructed a meta-repertoire of 45 syllables and assessed the frequency of each syllable across control and cKO USV recordings (**Fig. 3.4E-F**). Again, there were no major differences between genotypes in syllable usage (**Fig. 3.4F**). Altogether these analyses lead us to conclude that cKO mice do not differ greatly from controls in courtship call structure and usage.

We also investigated the contribution of cortical *Foxp2* to isolation USVs across postnatal development (P4, P7, P10, P14). Again, we found no differences between genotypes in measures related to call number, timing, structure, or pitch (**Fig. 3.5A**, **Table 3.2**). There was, however, a small but significant decrease in the relative sound pressure of calls emitted by *Foxp2* cKO pups across development (**Fig. 3.5A**, **Table 3.2**). This decrease in loudness was not due to somatic weakness, as cKO pups gained weight and performed gross motor functions normally (**Fig. 3.5B-D**, **Table 3.2**). In summary, cortical *Foxp2* plays a specific role in loudness of neonatal vocalizations, but not in production or other acoustic features of neonatal or adult vocalizations.

Foxp2 is dispensable for cortical layering and layer 6 axon targeting

We asked whether abnormalities of corticogenesis could underlie the cognitive deficits in our *Foxp2* cKO mice. Because acute knockdown of *Foxp2* in embryonic cortex was shown to impair neuronal migration (Tsui et al., 2013), we examined cortical layering in cKO mice using DAPI staining of cytoarchitecture and immunohistochemistry for layer

markers CUX1 (L2-4), CTIP2 (L5b) and TBR1 (L6). We found no gross abnormalities in layer formation or relative thickness at P7 (**Fig. 3.6A-B**, statistics for immunohistochemistry are provided **Table 3.3**). Next, because Foxp2 regulates genes involved in axon outgrowth and guidance in embryonic brain (Vernes et al., 2011), we examined the formation of cortical L6 axon tracts labeled with *golli*-τ-eGFP in P14 cKO mice (Jacobs et al., 2007). We observed normal formation of L6 axon tracts (including the internal capsule, which contains corticothalamic axons), innervation of thalamic nuclei, and intra-cortical axon and dendrite projections to L4 (**Fig. 3.6C**). These results confirm other recent findings that *Foxp2* deletion from cortical progenitors and/or neurons does not affect gross cortical layering or targeting of L6 axons (Kast et al., 2019; Medvedeva et al., 2018).

Cortical Foxp2 deletion reduces dopamine signaling gene expression

FoxP2 has been shown to regulate expression of the dopamine D1 receptor (D1R) and its downstream effector DARPP-32 in zebra finch striatum (Murugan et al., 2013). Given the long-established link between prefrontal cortical dopamine and behavioral flexibility (Ott and Nieder, 2019), we explored the possibility that *Foxp2* deletion impairs reversal learning through dysregulation of cortical dopamine signaling. In cortical L6, Foxp2-expressing corticothalamic projection neurons (CThPNs) are all reported to express DARPP-32, and Foxp2 directly binds the promoter of its gene *Ppp1r1b* in embryonic brain (Hisaoka et al., 2010; Vernes et al., 2011). Retrograde labeling has shown that L6 CThPNs express D1R (Gaspar et al., 1995), and while no studies to date have shown colocalization of Foxp2 and D1R in the cortex, these proteins are highly

coexpressed in striatonigral spiny projection neurons (Vernes et al., 2011). Thus, we hypothesized that Foxp2 activates D1R and DARPP-32 expression in mouse L6 CThPNs.

To visualize D1R and DARPP-32 expression, we crossed our *Foxp2* cKO mice with *Drd1a*-tdTomato BAC reporter mice, which replicate endogenous D1R expression patterns in the cortex, and performed immunohistochemistry at adult and neonatal stages (Ade et al., 2011; Anastasiades et al., 2018). In adult control frontal cortex, DARPP-32 expression closely followed that of Foxp2 in layer 6, but D1R was almost exclusively expressed in Foxp2-negative neurons (**Fig. 3.7A**). In agreement with recent studies in *Drd1a*-tdTomato mouse cortex (Anastasiades et al., 2018), this indicates that mature D1R-expressing neurons are predominantly ITPNs rather than Foxp2/DARPP-32-expressing CThPNs. Unexpectedly, however, cortical *Foxp2* deletion caused a large reduction in D1R-positive cells throughout the adult cortex (**Fig. 3.7A**). Thus, cortical Foxp2 is required for proper D1R expression in mature ITPNs.

In the prefrontal cortex, expression of D1/D1-like receptors is developmentally regulated, with higher expression during earlier stages of development (Andersen et al., 2000; Cullity et al., 2018). Thus, we examined expression of D1R, DARPP-32, and Foxp2 in early postnatal frontal cortex of control and *Foxp2* cKO mice. In contrast with adult control cortex, postnatal control cortex showed a high density of D1R-expressing cells and extensive coexpression of D1R, DARPP-32, and Foxp2 in L6 neurons (**Fig. 3.7B**). Again, upon cortical *Foxp2* deletion, we saw a vast reduction of D1R+ cells throughout the frontal cortex (**Fig. 3.7B**). Quantification of D1R+ cells by layer in the medial prefrontal cortex (mPFC) revealed significant reductions in L5 (33±3.2% vs. 14±2.8%) and L6

(66±3.9% vs. 25±1.5%), layers where Foxp2 expression normally occurs (**Fig. 3.7C**, **Table 3.3**). In addition, there was a 40% reduction in DARPP-32 protein content in postnatal *Foxp2* cKO cortex (**Fig. 3.7D**). These results indicate that in developing cortex, Foxp2 is required for normal expression of dopamine signaling molecules.

To determine whether the decrease in D1R expression in *Foxp2* cKO cortex was due to decreased CThPN density or downregulation of D1R in CThPNs, we examined the CThPN marker TLE4 (Molyneaux et al., 2015) and its coexpression with Foxp2 and D1R in mPFC. In control mice, we found a high degree of overlap among the three proteins in L6 and a moderate degree of overlap in L5 (**Fig. 3.7E**, **Table 3.4**). In *Foxp2* cKO mice, we saw no change in the percentage of TLE4-positive cells in L5 or L6, but there were significant reductions in TLE4/D1R-positive cells in these layers (**Fig. 3.7E**, **Table 3.4**). These results agree with recent findings of unaltered neuronal density in L5-6 of mice lacking *Foxp2* through the same conditional knockout strategy (French et al., 2018; Kast et al., 2019). Interestingly, although nearly all (~92%) control TLE4-expressing neurons were Foxp2/D1R-positive, 41% of TLE4+ neurons maintained D1R expression after *Foxp2* deletion (**Fig. 3.7E**, **Table 3.4**), suggesting that D1R expression is regulated by Foxp2 in only a subset of CThPNs. In summary, we found that postnatal but not adult CThPNs express D1R, and that cortical *Foxp2* is required for proper D1R expression in postnatal CThPNs and adult ITPNs.

Identification of D1R-expressing cell types in developing frontal cortex

Studies using retrograde labeling and genetic markers have identified excitatory and inhibitory neuronal subtypes expressing D1R in adult mouse mPFC (Anastasiades

et al., 2018; Han et al., 2017), but less is known about cell types expressing D1R in developing cortex. To identify these cell types and understand cell type-specific effects of *Foxp2* deletion, we used fluorescence-activated cell sorting (FACS) followed by single-cell RNA-sequencing (scRNA-seq) to genetically profile *Drd1a*-tdTomato+ frontal cortical neurons from P7 control and *Foxp2* cKO mice (**Fig. 3.9A**). Using the 10x Genomics Chromium platform (Zheng et al., 2017), we profiled a total of 7282 cells from 2 mice per genotype, detecting similar numbers of transcripts (median UMI/cell: control=8484, cKO=6832) and genes (median genes/cell: control=2678, cKO=2546) between genotypes (**Fig. 3.8A**). Using Seurat (Butler et al., 2018) we identified 21 clusters containing cells from all mice examined (**Fig. 3.8B-C**), and we annotated cell types by overlapping our cluster marker genes with cluster markers from a published neonatal cortical scRNA-seq dataset (Loo et al., 2019) (**Fig. 3.8D**). We identified multiple projection neuron, interneuron, and, unexpectedly, non-neuronal clusters from our *Drd1a*-tdTomato FACS-scRNA-seq (**Fig. 3.8B, D**). While *Drd1* was not expressed in every cell, it was expressed in every cluster, and re-clustering *Drd1*+ cells resulted in similar cell types as the full dataset (**Fig. 3.8E-F**). As *tdTomato* transcripts are roughly double that of *Drd1* in individual cells of *Drd1a*-tdTomato mouse cortex (Anastasiades et al., 2018), we posited that FACS isolated tdTomato+ cells for which we could not detect *Drd1* transcripts by scRNA-seq. Indeed, using sequence information from the BAC used to generate the *Drd1a*-tdTomato mice (Ade et al., 2011), we found that *Drd1a*-tdTomato BAC expression is enhanced relative to endogenous *Drd1* expression (**Fig. 3.8G**). Thus, *Drd1* transcripts appear to be present in both neurons and glia of the developing frontal cortex.

To refine our D1R neuronal subtype classification, we reclustered the neuronal clusters and identified 11 clusters comprised of 2758 cells (**Fig. 3.9B**). Two low-quality clusters (Clusters 2, 7) were excluded from further assessments, and annotation of the remaining clusters based on P0 data revealed multiple subclasses of upper- and lower-layer projection neurons and interneurons (Loo et al., 2019) (**Fig. 3.9C**). To delineate projection neuron clusters by their projection specificity, we also examined expression of marker genes from a scRNA-seq dataset with retrograde labeling in adult frontal motor cortex (Tasic et al., 2018) (**Fig. 3.9D**). We were able to distinguish L6 CThPNs by *Foxp2, Tle4,* and *Ephb1* (Cluster 4), L5 near-projecting neurons (NPNs) by *Trhr* and *Tshz2* (Cluster 9), L6 ITPNs by *Oprk1* (Cluster 10), and L2/3 ITPNs by *Mdga1* and *Pou3f1* (Cluster 3). Cluster 0 may contain a mix of L2/3 and L5 ITPNs as indicated by expression of both *Pou3f1* and the L5 ITPN marker *Rorb*. Among projection neurons, *Foxp2* expression was restricted to L6 CThPNs and the newly described L5 NPNs, which do not have long-range projections (Tasic et al., 2018) (**Fig. 3.9D**). We also distinguished interneuron subtypes in our scRNA-seq data by expression of *Htr3a* (Cluster 1), *Lamp5* (Cluster 6), and *Sst* (Cluster 8). These results reveal an unprecedented diversity of D1R-expressing neuronal subtypes in the developing frontal cortex, and they identify L5 NPNs as *Foxp2*-expressing cell types in addition to L6 CThPNs.

Foxp2 deletion increases SP9+ interneurons in postnatal cortex

Given that postnatal *Foxp2* cKO mice show reduced D1R expression in CThPNs, but by adulthood show reduced D1R expression in ITPNs, we asked if this potential non-cell-autonomous effect was occurring during development. By examining the proportion

of cKO cells in each D1R neuronal cluster, we found significant underrepresentation of cKO cells in L6 CThPN and L2/3 ITPN clusters, and overrepresentation in interneuron Cluster 5 (**Fig. 3.9E**). Cluster 5 overlapped significantly with a P0 cluster annotated as migrating cortical interneurons, and these cells expressed high levels of *Cdca7* and *Sp9* while expressing lower levels of mature interneuron subtype markers (Loo et al., 2019) (**Fig. 3.9C-D**). Cluster 5 also expressed *Foxp2*, suggesting it arises from an *Emx1*-negative lineage such as basal forebrain-derived cortical interneurons (Gorski et al., 2002) (**Fig. 3.9D**). Immunohistochemistry for SP9 in *Foxp2* cKO mPFC confirmed this increase in total SP9+ cells as well as SP9+D1R+ cells upon *Foxp2* deletion, suggesting the presence of an ectopic population of interneurons in cKO mice (**Fig. 3.9F-G**, **Table 3.3**). Thus, in postnatal frontal cortex, loss of *Foxp2* in *Emx1*-positive cells causes non-cell-autonomous effects on ITPN D1R expression and cortical interneuron numbers.

Foxp2 deletion induces non-cell-autonomous effects on cortical gene expression

To elucidate molecular pathways in cortical D1R neurons affected by *Foxp2* deletion, we performed “pseudo-bulk RNA-seq” differential gene expression analyses between genotypes in our scRNA-seq data. First, we identified differentially expressed genes (DEGs) between all control neurons and all *Foxp2* cKO neurons and found 48 downregulated and 35 upregulated DEGs in cKO neurons (**Fig. 3.10A-B**, **Table 3.5**). In agreement with our immunohistochemistry data, we saw decreased expression of *Foxp2*, *Drd1*, and *Ppp1r1b* (which encodes DARPP-32) in cKO neurons. Overlap of these DEGs with our neuronal cluster markers revealed enrichment of downregulated genes in projection neurons and enrichment of upregulated genes in interneurons (**Fig. 3.10C**).

Summarized gene ontology (GO) terms associated with downregulated DEGs indicated abnormal synaptic plasticity, dopamine signaling, projection organization, and microtubule-based processes in cKO neurons (**Fig. 3.10D**). Summarized GO terms for upregulated DEGs were consistent with and likely driven by the ectopic immature interneuron Cluster 5, which was comprised of more cKO neurons than control neurons (**Fig. 3.10D**).

In a differential gene expression approach less driven by imbalanced cell type proportions between genotypes, we also identified DEGs within each neuronal cluster (**Fig. 3.10E**, **Table 3.6**). L6 CThPNs and L5 NPNs in cKO mice showed surprisingly few gene expression changes, but we confirmed *Ppp1r1b* as a CThPN-specific downregulated DEG (**Fig. 3.10F**). This relatively small number of DEGs in *Foxp2*-expressing neurons was not due to upregulation of related genes *Foxp1* or *Foxp4* (**Fig. 3.10G**). In contrast, L2-5 ITPN clusters showed a greater number of DEGs, including downregulation of genes encoding the cytoskeletal proteins β-actin (*Actb*) and β-tubulin (*Tubb5*) (**Fig. 3.10F**). To confirm these decreases, we performed immunohistochemistry for β-actin and β-tubulin in P7 control and *Foxp2* cKO cortex and saw decreased expression of both proteins across the cortical mantle (**Fig. 3.10H**, **Table 3.3**). Thus, while *Foxp2* expression is restricted to deep-layer non-ITPNs, its deletion causes non-cell-autonomous changes including cytoskeletal gene downregulation in upper-layer ITPNs.

Next, to overcome the differential sampling of cell types between genotypes due to Foxp2 regulation of *Drd1a*-tdTomato, we generated an independent FACS-scRNA-seq dataset from mice expressing the *golli*-τ-eGFP (GTE) reporter, which is expressed in

control Foxp2-positive CThPNs but not decreased in cKO cortex (**Fig. 3.11A-B**). Using similar analysis methods as with the *Drd1a*-tdTomato dataset, we identified projection neuron clusters and calculated pseudo-bulk RNA-seq DEGs between genotypes, 24 of which were downregulated in cKO and 23 upregulated (**Fig. 3.11C-F**, **Table 3.7**). Summarized GO terms associated with downregulated DEGs were related to neuronal projection organization and synaptic signaling, similar to the downregulated GO terms in the *Drd1a*-tdTomato dataset (**Fig. 3.11G**). Notably, *Actb* appeared among the downregulated DEGs in both datasets (**Fig. 3.11H**). In summary, cortical *Foxp2* deletion induces both cell-autonomous and non-cell-autonomous decreases in dopamine-related, synaptic, and projection-related gene expression.

Putative direct targets of Foxp2 in postnatal cortex

In another approach to identify Foxp2 targets in a manner uninfluenced by altered *Drd1a*-tdTomato expression in *Foxp2* cKO cortex, we searched for genes correlated (i.e. activated targets) or anticorrelated (i.e. repressed targets) with *Foxp2* expression across control neurons in the *Drd1a*-tdTomato dataset (**Fig. 3.12A**). To identify potential direct targets, we overlapped these genes with targets from a Foxp2 promoter-binding assay performed in embryonic mouse brain (Vernes et al., 2011). Then, to determine their cell type-specificity, we overlapped these putative direct Foxp2 targets with the *Drd1a*-tdTomato neuronal cluster markers (**Fig. 3.12B**). We found shared and distinct Foxp2-activated targets between CThPNs and NPNs, several of which may exert non-cell-autonomous effects through extracellular matrix organization (*Col23a1, P4ha1*), cell-cell signaling (*Islr2, Plxna2, Sdk1*), or synaptic activity (*Cacna1a, Calm2, Cbln1, Grm3,*

Lrrtm2) (**Fig. 3.12B**). We also identified Foxp2-repressed targets, which were markers for ITPNs, interneurons, and CR cells, suggesting that Foxp2 plays a role in repressing these identities in CThPNs and NPNs (**Fig. 3.12B**). These results provide potential mechanisms by which Foxp2 may exert non-cell-autonomous effects and contribute to the maintenance of deep-layer cortical projection neuron identity.

Efforts toward identification of genome-wide direct Foxp2 targets in postnatal cortex

Last, to identify genome-wide targets of Foxp2 in the cortex, ChIP-seq was performed in postnatal control and *Foxp2* cKO mice. We verified that our antibody could bind and immunoprecipitate Foxp2 under crosslinking conditions, and after ChIP we obtained a suitable quantity of DNA to generate libraries (**Fig. 3.13A-C**). However, upon analysis of the ChIP-seq data, we found that most of the peaks enriched over input conditions were common to both control and cKO samples, whereas we expected to see more peaks in the control samples (**Fig. 3.13D**). Furthermore, manual inspection of track files for control-specific peaks indicated negligible enrichment over cKO or input peaks (**Fig. 3.13E**). Therefore, we concluded that the ChIP-seq experiment was not able to identify Foxp2-bound genomic regions.

In recent years, newer techniques have emerged for identifying protein-bound regions of DNA, such as cleavage under targets and release using nuclease (CUT&RUN) (Skene et al., 2018). This method claims higher resolution and signal-to-noise ratio than ChIP-seq, and it does not require cross-linking and thus avoids epitope and DNA accessibility artefacts. In a preliminary test of this method, we were able to isolate DNA fragments bound to histone H3K27me3 in both postnatal mouse cortex and 293T cells

(**Fig. 3.13F**). Thus, CUT&RUN combined with more recent KO-verified Foxp2 antibodies (rabbit α-Foxp2 D55H9, Cell Signaling Technologies, #5337S; goat α-Foxp2, Abcam, #ab1307) may be a promising alternative to ChIP-seq for identifying direct Foxp2 targets in the cortex.

Discussion

Foxp2-regulated cortical dopamine signaling and behavioral flexibility

We have demonstrated specific roles for cortical *Foxp2* in reversal learning, a form of behavioral flexibility, and cortical dopamine D1R signaling throughout the postnatal lifespan (**Fig. 3.14**). Cortical dopamine signaling regulates many cognitive functions, including behavioral flexibility (Floresco, 2013; Ott and Nieder, 2019), and specific manipulations of cortical D1R signaling or D1R-D2R interactions can modulate reversal learning ability (Calaminus and Hauber, 2008; Mizoguchi et al., 2010; Thompson et al., 2016). Thus, we suggest that the reversal learning deficits in *Foxp2* cKO mice arise from their decreased expression of cortical dopamine D1 receptors. Other studies linking *Foxp2* to cognitive function and dopamine signaling found that humanized *Foxp2* mice demonstrate enhanced strategy set-shifting, another form of behavioral flexibility, and altered frontal cortical dopamine concentrations (Enard et al., 2009; Schreiweis et al., 2014). Furthermore, specific knockdown of *Drd1* in the prefrontal cortex impairs strategy set-shifting (Cui et al., 2018). Interestingly, we only observed significant deficits in cognitive function in the water Y-maze but not in the dry T-maze. Given that dopamine release in the frontal cortex is influenced by acute stress (Arnsten, 2009), the potential

D1R-mediated cognitive impairments in *Foxp2* cKO mice could be exacerbated in aversive tasks such as the water Y-maze.

Cortical *Foxp2* may mediate flexible behaviors through multiple circuit pathways in the brain. Recent optogenetic experiments have demonstrated involvement of both corticothalamic and corticostriatal neurons in probabilistic reversal learning (Nakayama et al., 2018). Thus, the reversal learning deficits in *Foxp2* cKO mice may be due to dysregulation of *Drd1* or other genes in CThPNs and ITPNs, the latter of which encompass corticostriatal neurons. In addition, the hippocampus is known to have a prominent role in reversal learning in rodents and humans (Mala et al., 2015; Vila-Ballo et al., 2017). While Foxp2 protein has limited expression in the hippocampus, we cannot rule out the possibility that loss of *Foxp2* in the cortex might ultimately affect hippocampal function through disruption to brain circuitry.

Genetic diversity of dopaminoceptive cell types in developing cortex

Studies spanning over two decades, reviewed in (Anastasiades et al., 2018), have identified diverse neuronal subtypes expressing dopamine D1 receptors in the adult cortex. However, much less is known about cell types expressing D1R in the developing cortex, despite reports of postnatal regulation of D1R expression in this region (Andersen et al., 2000; Brenhouse et al., 2008; Cullity et al., 2018; Tarazi et al., 1999). To better understand the effects of *Foxp2* deletion on developing D1R neuronal subtypes, we conducted the first cell type characterizations of *Drd1a*-tdTomato postnatal frontal cortex (Ade et al., 2011). A recent study of these mice in adulthood found extensive expression of D1R in ITPNs but limited expression in CThPNs (Anastasiades et al., 2018), a finding

corroborated by the absence of D1R in adult Foxp2-expressing CThPNs. In stark contrast, we found a high degree of D1R expression in both CThPNs and ITPNs of postnatal frontal cortex via immunostaining and single-cell transcriptomics. Similarly, both adult and postnatal cortex show D1R expression in 5HT3R and calretinin-expressing (L1 CR) interneuron subtypes, but only postnatal cortex shows D1R expression in somatostatin (SST)-positive interneurons (Anastasiades et al., 2018). These results suggest transient expression of D1R in certain cell types of postnatal frontal cortex, such as CThPNs and SST interneurons. Additionally, we identified glial expression of *Drd1* in our scRNA-seq data, supporting evidence for the presence of D1-like receptors in prefrontal cortical astrocytes (Liu et al., 2009; Vincent et al., 1993). The developmental functions of these early D1R expression patterns in neurons and potentially glia remain an interesting area of study to be elucidated.

Limited roles of cortical Foxp2 in mouse vocalization

Mice with *Foxp2* mutations commonly exhibit USV abnormalities (Castellucci et al., 2016; Chabout et al., 2016; French and Fisher, 2014; Gaub et al., 2016), which have been attributed to its functions in the striatum (Chen et al., 2016), cerebellum (Fujita-Jimbo and Momoi, 2014; Usui et al., 2017b), and laryngeal cartilage (Xu et al., 2018). Cortical *Foxp2* deletion using *Nex*-Cre was previously shown to alter adult USVs in a social context-dependent manner (Medvedeva et al., 2018), but in our study, *Emx1*-Cre-mediated deletion did not appear to impact adult courtship USVs. Several methodological differences may account for these discrepancies. *Nex*-Cre causes recombination around embryonic day (E) 11.5 in postmitotic projection neurons, whereas *Emx1*-Cre acts by

E10.5 in both projection neurons and their progenitors (Goebbels et al., 2006; Gorski et al., 2002). Thus, perhaps earlier deletion of *Foxp2* from the cortex induces developmental compensation in vocalization circuitry that cannot occur after postmitotic neuronal deletion. Another possibility is that the superovulated females used to elicit courtship calls in the previous study exposed differences between genotypes that we could not detect using females in a natural ovulation state. Furthermore, our analysis did not parse calls based on duration, direction, or size of pitch jumps as did the previous study, but our call repertoire analysis suggested high overall similarity between control and cKO vocalizations.

Neonatal isolation USVs were also largely unaffected by loss of cortical *Foxp2*, contrasting with the USV reductions in pups with cortical *Foxp1* deletion or cerebellar *Foxp2* knockdown (Usui et al., 2017a; Usui et al., 2017b). Whereas Foxp2 is expressed in CThPNs, Foxp1 is likely expressed in callosal and corticostriatal neurons based on its coexpression with Satb2 (Hisaoka et al., 2010; Sohur et al., 2014; Sorensen et al., 2015). Furthermore, cortical layering is altered in *Foxp1* cKO but not *Foxp2* cKO mice (Usui et al., 2017a). Thus, proper positioning and function of ITPNs and cerebellar output neurons may be more essential to USV production than CThPNs.

Cortical *Foxp2* deletion did decrease the sound pressure of USVs across postnatal development. Homozygous *Foxp2-R552H* mutant pups also emit quieter ultrasonic distress calls, which correlates with overall developmental delay of mutants (Gaub et al., 2010; Groszer et al., 2008). However, cortical *Foxp2* alone at least partly contributes to modulation of call loudness, as our cKO pups showed grossly normal development. By

adulthood, heterozygous *Foxp2-R552H* mutants emit abnormally loud courtship USVs and show ectopic positioning of L5 laryngeal motor cortex neurons (Chabout et al., 2016; Gaub et al., 2016). Whether this neuronal population is altered in *Foxp2* cKO pups and contributes to call loudness remains to be explored. As to the possible contribution of dopamine D1 signaling to call loudness, very few studies have explored this area. Systemic D1-like receptor blockade during rat development has been shown to increase USV sound pressure at later postnatal ages, while blockade in adult rats recapitulates the abnormal laryngeal neurophysiology seen in Parkinson's-related hypophonia (Cuomo et al., 1987; Feng et al., 2009). Whether USV loudness is modulated specifically by cortical D1Rs remains to be determined and would clarify the mechanisms by which *Foxp2* cKO pups emit quieter calls.

Neurodevelopmental disorder gene regulation by Foxp2 in the cortex

Foxp2 regulation of cortical dopamine signaling may inform our understanding and treatment of NDDs. FOXP2 variation has recently been associated with ASD and ADHD (Demontis et al. 2019; Reuter et al. 2017; Satterstrom et al. 2019), and genetic perturbations of dopamine signaling have also been implicated in NDDs (Money and Stanwood 2013). Foxp2 cKO mice phenocopy the decreased cortical dopamine gene expression (Drd1, Ppp1r1b) and reversal learning impairments seen in 16p11.2 and Tbr1 mouse models of ASD (Huang et al. 2014; Portmann et al. 2014; Yang et al. 2015), suggesting a possible convergent phenotype of dysregulated cortical dopamine signaling in NDDs affecting behavioral flexibility.

Several other Foxp2-regulated genes are of interest due to their connection with NDDs. Overlap of direct Foxp2 targets with DEGs from Tbr1 models of ASD reveals potential co-activated (Adcy1, Cbln1, Grm3, Lrrtm2, Nfe2l3, Nfia, Nin, Sdk1, Ppp1r1b, Sox5) and co-repressed (Inhba) genes by Foxp2-TBR1 interaction in the cortex (Bedogni et al. 2010; Deriziotis et al. 2014; Fazel Darbandi et al. 2018; Vernes et al. 2011). In addition, Foxp2 expression was anticorrelated with the ASD gene Mef2c, which is directly repressed by Foxp2 in the striatum to control wiring of cortical synaptic inputs (Chen et al. 2016). Furthermore, recently identified ADHD-associated loci include Foxp2 as well as the Foxp2-correlated genes Dusp6, Pcdh7, and Sema6d, the last of which is a direct Foxp2 target in the brain (Demontis et al. 2019; Vernes et al. 2011). We note that our direct target analysis is limited to Foxp2-bound promoters in embryonic brain (Vernes et al. 2011), and recent evidence indicates that FOXP2 promotes chromatin accessibility at enhancers to regulate gene expression (Hickey et al. 2019). Thus, genome-wide targets of Foxp2 must be identified at various developmental stages for a full understanding of its functions in the cortex, including the molecular mechanism of its regulation of D1R expression.

In summary, our work on cortical Foxp2 represents a step forward in elucidating neural mechanisms underlying cognition and vocal communication. Importantly, we identified dysregulated molecular pathways upon cortical Foxp2 deletion in the absence of general cortical development abnormalities. Moreover, these findings provide insights into the etiology and treatment of FOXP2-related and other neurodevelopmental disorders affecting behavioral flexibility.

Materials and Methods

Mice

All procedures were approved by the Institutional Animal Care and Use Committee of UT Southwestern. *Emx1-Cre* (Gorski et al., 2002) (#005628, Jackson Laboratory), *Foxp2*$^{flox/flox}$ (French et al., 2007) (#026259, Jackson Laboratory), *Drd1a-tdTomato* line 6 (Ade et al., 2011) (#016204, Jackson Laboratory, provided by Dr. Craig Powell), and *golli-τ-eGFP* mice (Jacobs et al., 2007) were backcrossed with C57BL/6J mice for at least 10 generations. Genotyping primers can be found in **Table 3.1**. Experimental mice (*Foxp2* cKO) and control littermates were generated by crossing male *Emx1-Cre*; *Foxp2*$^{flox/flox}$ mice with female *Foxp2*$^{flox/flox}$ mice. When used, the *Drd1a*-tdTomato or *golli*-τ-eGFP reporter was present in mice of either sex for breeding. Mice were group-housed under a 12 h light/dark cycle and given *ad libitum* access to food and water. Mice of both sexes were used for all experiments except adult USVs, which were measured in male mice.

Behavioral analyses

Adult *Foxp2* cKO and control littermates were tested at age 10-20 weeks, and pups were tested at postnatal days 4, 7, 10, and 14. Behavioral studies were performed in the following cohorts in the following order: Cohort 1 (neonatal USVs and motor tests, adult USVs), Cohort 2 (three-chamber social interaction, novel cage activity, open field, elevated plus maze), Cohort 3 (three-chamber social interaction, water Y-maze), Cohort 4 (novel object recognition, spontaneous alternation), Cohort 5 (spontaneous alternation, fear conditioning). Mice in Cohorts 2-5 were habituated to handling for 5 min per day for 5 days the week prior to testing. All behavioral experiments were performed during the

light cycle in the afternoon by an experimenter blinded to genotype. Full *n* numbers and statistical information can be found in **Table 3.2**.

Reversal learning in water Y-maze

Mice were tested according to (Stoodley et al., 2017) using a Y-shaped apparatus filled with 20-22°C water up to 0.5 cm above a clear movable platform. On day 1, mice were habituated to the maze for 1 min without the platform. On days 2-4 (Training 1-3), mice were given 15 trials/day, up to 30 s each, to learn the platform location in one of the maze arms. Platform location was counter-balanced by cage to control for side biases. On days 4-6 (Reversal 1-3), the platform was moved to the opposite arm and mice were given 15 trials/day to learn the new location. The fraction of correct trials per day was calculated, as well as number of trials to reach a criterion of 5 consecutive correct trials. Differences between genotypes were assessed using a two-way ANOVA with Bonferroni's multiple comparisons test.

Spontaneous alternation in T-maze

Mice were tested according to (Deacon and Rawlins, 2006). After habituation to a dimly lit testing room for 15 min, the test mouse was placed in the start arm of the T-maze and allowed to enter a goal arm, where it was confined by a guillotine door for 30 s. The mouse was transferred to a holding cage for 15 s while the maze was wiped clean with diluted Process NPD (Steris Life Sciences) to remove odor cues. The mouse was then placed back in the start arm of the maze and allowed to choose a goal arm. Failure to choose a goal arm within 2 min resulted in a failed trial and confinement to the previously chosen arm for 30 s. Mice were tested for 11 consecutive trials. Spontaneous alternation

rate was calculated as number of alternations divided by number of opportunities to alternate (e.g. 10 if no failed trials) and multiplied by 100. Latency to goal arm was also measured. Comparisons of alternation rates between genotypes, and between each genotype and chance levels (50%), were performed using unpaired t-tests. Differences in latency to goal arm between genotypes were assessed using a two-way ANOVA with Bonferroni's multiple comparisons test.

Novel object recognition

Mice were habituated to a 16×16 chamber for 10 min/day for 3 days. During the training phase, two identical objects (sand-filled scintillation vials or empty black-capped nail polish bottles) were placed in the chamber 5 cm away from the back wall and 22 cm apart from each other. Then the test mouse was placed in the chamber and allowed to explore the objects until 30 s of exploration time had been reached. Exploration was scored whenever the mouse sniffed (<2 cm) or touched the object while looking at it, but not when the mouse climbed the object without sniffing it. Mice that did not reach the exploration criterion within 15 min were excluded. After training, the test mouse was placed in a holding cage for 5 min while the chamber was cleaned and one of the objects was replaced with a novel object. Then for the testing phase, the test mouse was placed back in the chamber and time spent sniffing the familiar and novel objects was measured for 10 min. A discrimination index was calculated as the difference between time spent sniffing novel versus familiar object, divided by total sniffing time. Differences between genotypes were assessed using an unpaired t-test.

Cued and contextual fear conditioning with extinction

Mice were tested according to (Araujo et al., 2017). On the training day, mice were placed in a box containing a grid metal floor attached to a scrambled shock generator, allowed to explore for 2 min, then given 3 separate tone-shock pairings (30 s white noise, followed by a 2-second 0.5 mA shock, with 1 min intervals between pairings). Cue recall and extinction were tested once a day for 5 consecutive days after training by placing the mice in boxes that were altered with a plastic floor, an inverted roof, and a vanilla scent. Freezing was then measured for 3 min, followed by the presentation of the white noise cue and measuring freezing for an additional 3 min with Video Freeze software (Med Associates). Context recall and extinction were tested 3 weeks after training for 5 consecutive days by placing the mice back into the original box and recording freezing for 5 min. After all testing was completed, footshock sensitivity was assessed by delivering footshocks every 15 s starting at 0.05 mA and increasing by 0.05 mA at each interval; the minimum current required to elicit flinching, vocalizing, and jumping was recorded for each mouse. Differences between genotypes were assessed using a two-way ANOVA with Bonferroni's multiple comparisons test.

Three-chamber social interaction

Mice were tested according to (Yang et al., 2011). Mice were placed in the center chamber of a three-chambered box with removable doorways and given 10 min to habituate to the apparatus. For the sociability phase, mice were briefly removed from the box and placed in a holding cage, and then a cup containing an object (a 2.5-in screw and bolt) (novel object, NO) was placed in one outer chamber and a cup containing a conspecific C57BL/6J mouse (novel animal, NA) was placed in the opposite outer

chamber. Subject mice were then placed back in the center chamber and allowed to explore for 10 min. Position of the conspecific mouse was counter-balanced to control for side biases. For the social novelty phase, subject mice were again placed in a holding cage while the object was replaced with a second conspecific C57BL/6J mouse (novel animal, NA), and the first conspecific mouse was termed the familiar animal (FA). Subject mice were then placed back in the center chamber and allowed to explore for 10 min. Time spent sniffing the NO vs. NA and FA vs. NA during each phase was manually scored by an experimenter blinded to genotype. Within each genotype, differences in times spent sniffing NO vs. NA or FA vs. NA were compared using an unpaired t-test. A discrimination index was also calculated for each animal in each phase as the difference between time spent sniffing NA and NO (or NA and FA), divided by total time spent sniffing. The average discrimination indices were compared between genotypes using an unpaired t-test.

Novel cage activity

Mice were tested according to (Araujo et al., 2017). Mice were placed into clean, plastic 18×28 cm cages with minimal bedding, and then each cage was then placed into a dark Plexiglas box. Photobeam Activity System-Home Cage software (San Diego Instruments) was used to record the number of infrared beam breaks for 2 h. Data were binned into 5 min intervals and differences between genotypes were assessed using a two-way ANOVA with Bonferroni's multiple comparisons test.

Open field

Mice were tested according to (Araujo et al., 2015). Mice were placed in a 16×16 in Plexiglass box and allowed to explore the arena for 10 min. Ethovision XT software

(Noldus) was used to calculate the total distance moved and time spent in each zone of the field. Differences between genotypes were assessed using an unpaired t-test.

Elevated plus maze

Mice were tested according to (Walf and Frye, 2007). Mice were placed in the center of a plus-shaped maze with two open arms and two enclosed arms and video recorded for 5 min. Ethovision XT software (Noldus) was used to calculate the total distance moved and time spent in each zone of the maze. Differences between genotypes were assessed using an unpaired t-test.

Adult courtship ultrasonic vocalizations

Mice were tested according to (Araujo et al., 2017). Male test mice were paired with age-matched C57BL/6J females for 1 week, then single-housed for 1 week. On the test day, males were habituated in their home cages to the testing room for 30 min, during which their cage lids were replaced with Styrofoam lids containing UltraSoundGate condenser microphones (Avisoft Bioacoustics) positioned at a fixed height of 20 cm. The microphones were connected to UltraSoundGate 416H hardware (Avisoft Bioacoustics) connected to a computer running RECORDER software (Avisoft Bioacoustics). At the start of testing, an unmated age-matched C57BL/6J female was placed in each cage and resultant male songs were recorded for 3 min. Spectrogram preparation and call detection were performed using MATLAB code developed by (Rieger and Dougherty, 2016) based on methods from (Holy and Guo, 2005). Differences between genotypes were assessed using unpaired t-tests. Call repertoire analysis was performed using the MUPET MATLAB package (Van Segbroeck et al., 2017) with a repertoire size of 100 units.

Neonatal isolation ultrasonic vocalizations

Mice were tested according to (Araujo et al., 2015). After habituation in their home cages to the testing room for 30 min, individual pups were placed in plastic containers within 1 of 4 soundproof Styrofoam boxes with lids containing UltraSoundGate condenser microphones. Pups were randomly assigned to recording boxes at each postnatal time point. Isolation USVs were recorded for 3 min and analyzed using the same MATLAB code used for adult USV analysis. Other than call number, USV features were only computed for pups emitting at least 10 calls during the recording session. Differences between genotypes were assessed using a two-way ANOVA with Bonferroni's multiple comparisons test.

Righting reflex

Mice were tested according to (Araujo et al., 2015). Each pup was placed in a supine position on a clean, unobstructed surface, and the time taken to right onto all fours was measured. If a pup failed to right after 60 s, the time was recorded as 60 s. Each pup received one trial at each postnatal time point. Differences between genotypes were assessed using a two-way ANOVA with Bonferroni's multiple comparisons test.

Negative geotaxis

Mice were tested according to (Usui et al., 2017b). Each pup was oriented facing downward at a 30-degree angle on a sloped rough surface, and the time taken to reorient to face upward was recorded. If a pup took longer than 180 s, the time was recorded as 180 s. Each pup received one trial at each postnatal time point. Differences between

genotypes were assessed using a two-way ANOVA with Bonferroni's multiple comparisons test.

Immunohistochemistry, imaging, and analysis

Neonatal and adult mice were anesthetized (pups by cryoanesthetization, adults by injection with 80-100 mg/kg Euthasol) and transcardially perfused with 4% PFA, and their brains were post-fixed overnight in 4% PFA. After cryoprotection in 30% sucrose overnight, brains were embedded in Tissue-Tek CRYO-OCT Compound (#14-373-65, Thermo Fisher Scientific) and cryosectioned at 20-40 µm. Staining was performed on free-floating sections and all washes were performed with TBS or 0.4% Triton X-100 in TBS (TBS-T) unless otherwise stated. For some antibodies (TLE4, CTIP2), antigen retrieval was performed in citrate buffer (10 mM tri-sodium citrate, 0.05% Tween-20, pH 6) for 10 min at 95°C. Free aldehydes were quenched with 0.3M glycine in TBS for 1 h at room temperature. Sections were incubated overnight at 4°C in primary antibodies diluted in 3% normal donkey serum and 10% bovine serum albumin (BSA) in TBS-T. Secondary antibody incubations were performed for 1 h at room temperature in 10% BSA in TBS-T. Sections were mounted onto slides, incubated in DAPI solution (600 nM in PBS) for 5 min at room temperature, and washed 3X with PBS. Coverslips were mounted using ProLong Diamond Antifade Mountant (#P36970, Thermo Fisher Scientific).

For *Foxp2* cKO confirmation, sagittal 20 µm sections from male mice aged 14 weeks were stained as described above. The following antibodies and dilutions were used: rabbit α-Foxp2 (#5337S, Cell Signaling Technology, 1:250), donkey α-rabbit IgG AF555 (#A31572, Thermo Fisher Scientific, 1:2000). Images were acquired using a Zeiss

Axioscan Z1 slide scanner at the UT Southwestern Whole Brain Microscopy Facility and processed using Zeiss ZEN Lite and FIJI. Images were annotated using the Allen Mouse Brain Atlas.

Cortical layer thickness was analyzed as described in (Usui et al., 2017a). Coronal 30 µm sections from male P7 mice were stained as described above. For CTIP2 staining, citrate antigen retrieval was performed. The following antibodies and dilutions were used: rat α-CTIP2 (#ab18465, Abcam, 1:500), rabbit α-CUX1/CDP (#sc13024, Santa Cruz Biotechnology, 1:500), rabbit α-TBR1 (#ab31940, Abcam, 1:500), species-specific secondary antibodies produced in donkey and conjugated to AF488, AF555, or AF647 (Thermo Fisher Scientific, 1:2000). Images of primary somatosensory cortex (S1) were acquired using a Zeiss LSM 710 confocal laser scanning microscope at the UT Southwestern Neuroscience Microscopy Facility and processed and analyzed using Zeiss ZEN Lite and FIJI. For each animal, cortical thickness was calculated as the average of 3 measurements of S1 thickness. Then each layer thickness was calculated as the average of 3 measurements based on cell architecture (DAPI-based) or layer marker staining (Marker-based). Relative layer thickness was calculated as layer thickness divided by cortical thickness multiplied by 100, and compared between genotypes using an unpaired t-test.

For cortical projection analyses, coronal 40 µm sections from male and female P14 mice with the *golli*-τ-eGFP reporter were stained as described above. The following antibodies and dilutions were used: chicken α-GFP (#GFP-1010, Aves Labs, 1:1000), donkey α-chicken IgY AF488 (#NC0215979, Thermo Fisher Scientific, 1:2000). Images

were acquired using a Zeiss Axioscan Z1 slide scanner at the UT Southwestern Whole Brain Microscopy Facility and processed using Zeiss ZEN Lite and FIJI. Images were annotated using the Allen Mouse Brain Atlas.

For *Drd1a*-tdTomato analyses, coronal sections of 20 µm thickness from male and female P7 mice with the *Drd1a*-tdTomato reporter were stained as described above. For TLE4 staining, citrate antigen retrieval was performed. The following antibodies and dilutions were used: mouse α-DARPP-32 (#sc-271111, Santa Cruz Biotechnology, 1:250), rabbit α-Foxp2 (#5337S, Cell Signaling Technology, 1:250), rabbit α-SP9 (#PA564038, Thermo Fisher Scientific, 1:100), goat α-tdTomato (#LS-C340696, LifeSpan BioSciences, 1:500), mouse α-TLE4 (#sc-365406, Santa Cruz Biotechnology, 1:200), species-specific secondary antibodies produced in donkey and conjugated to AF488, AF555, or AF647 (Thermo Fisher Scientific, 1:2000). Images were acquired using a Zeiss LSM 880 confocal microscope at the UT Southwestern Neuroscience Microscopy Facility and processed and analyzed using Zeiss ZEN Lite and FIJI. For cell counts, tile scan Z-stack images of the region of interest were acquired at 20X magnification from similar coronal sections across 2-3 mice/genotype. Stitched maximum intensity projection images were used for manual cell counting using the FIJI Cell Counter plugin. Layers in mPFC were defined based a combination of DAPI-based cytoarchitecture and TLE4+ cell distribution. For layer distribution analysis, differences between genotypes were assessed using a two-way ANOVA with Bonferroni's multiple comparisons test. For expression overlap analysis, differences between genotypes were assessed using an unpaired t-test.

For cytoskeletal DEG confirmation, coronal sections of 20 µm thickness from male and female P7 mice were stained as described above. The following antibodies and dilutions were used: mouse α-β-actin (#A1978, Millipore Sigma, 10 µg/ml), rabbit α-β-tubulin (#ab6046, Abcam, 1:500), species-specific secondary antibodies produced in donkey and conjugated to AF555 or AF647 (Thermo Fisher Scientific, 1:2000). Images were acquired using a Zeiss LSM 880 confocal microscope at the UT Southwestern Neuroscience Microscopy Facility and processed and analyzed using Zeiss ZEN Lite and FIJI. Tile scan Z-stack images of primary motor cortex were acquired at 20X magnification from similar coronal sections across 3 mice/genotype. Stitched maximum intensity projection images were used for fluorescence intensity quantification using the FIJI Plot Profile function. For each mouse, fluorescence values across the vertical profile (pial surface to white matter) for each channel (β-actin, β-tubulin, DAPI) were divided into 10 equal bins and averaged for each bin. These values were averaged for each genotype, and differences between genotypes were assessed using a two-way ANOVA with Bonferroni's multiple comparisons test.

Protein extractions and Western blotting

Western blotting was performed as previously described (Araujo et al., 2015). For tissue samples, frontal cortex from 3 mice/genotype at P7 was lysed in RIPA buffer containing protease inhibitors, and 50 µg protein/well as determined via Bradford assay were used for Western blots. Proteins were resolved on a 10% SDS-PAGE gel at 80-100 V until the loading dye front ran off the gel, and then they were transferred to an Immun-Blot PVDF Membrane (Bio-Rad Laboratories) at 250 mA for 2 h at 4°C. The membrane was dried at

room temperature for 1 h, reactivated in methanol, and blocked for 1 h in 5% milk in TBS. The membrane was incubated with primary antibodies diluted 5% milk in TBS with 0.1% Tween-20 (TBS-T) overnight at 4°C, washed in TBS-T, incubated with secondary antibodies in 5% milk in TBS-T for 1 hr at room temperature, washed in TBS-T, and imaged on an Odyssey Infrared Imaging System (LI-COR Biosciences). The following antibodies were used: rabbit α-DARPP-32 (#AB10518, Millipore Sigma, 1 µg/ml), mouse α-Foxp2 (#MABE415, Millipore, 1 µg/ml), rabbit α-Foxp2 (#5337S, Cell Signaling Technology, 1:1000), mouse α-GAPDH (#MAB374, Millipore Sigma, 1:10,000), donkey α-mouse IgG IRDye 800 (#926-32212, LI-COR Biosciences, 1:20,000), donkey α-rabbit IgG IRDye 800 (#926-32213, LI-COR Biosciences, 1:20,000), donkey α-mouse IgG IRDye 680 (#926-68072, LI-COR Biosciences, 1:20,000). Blots were imaged using an Odyssey Infrared Imaging System (LI-COR Biosciences).

Single-cell RNA sequencing

Tissue processing and library generation

Tissue was dissociated for scRNA-seq based on (Tasic et al., 2016). P7 mice were sacrificed by rapid decapitation and brains were quickly removed and placed in ice-cold artificial cerebrospinal fluid (ACSF) (126 mM NaCl, 20 mM $NaHCO_3$, 20 mM D-Glucose, 3 mM KCl, 1.25 mM NaH_2PO_4, 2 mM $CaCl_2$, 2 mM $MgCl_2$) bubbled with 95% O_2 and 5% CO_2. 400-µm coronal sections were made in ACSF using a VF-200 Compresstome (Precisionary Instruments) and transferred to a room temperature recovery chamber with ACSF containing channel blockers DL-AP5 sodium salt (50 µM), DNQX (20 µM), and tetrodotoxin (100 nM) (ACSF+). After 5 min, frontal isocortex was separated from olfactory

areas, cut into smaller pieces and incubated in 1 mg/ml pronase (#P6911, Sigma) in ACSF+ for 5 min. Pronase solution was replaced with 1% BSA in ACSF and tissue pieces were gently triturated into single-cell suspension using polished glass Pasteur pipettes with 600 µm, 300 µm, and 150 µm openings. Cells were filtered twice through FLOWMI 40 µm Cell Strainers (#H13680-0040, Bel-Art) and live, single tdTomato+ (for *Drd1a*-tdTomato experiments) or eGFP+ (for *golli*-τ-eGFP experiments) cells were sorted using a BD FACSAria (BD Biosciences) at the UT Southwestern Flow Cytometry Facility. After sorting, cells were centrifuged and resuspended in 0.04% BSA in ACSF to target 1000 cells/sample using the Chromium Single Cell 3' Library & Gel Bead Kit v2 (#120237, 10x Genomics) (Zheng et al., 2017). Tissue and library preparation for *Drd1a*-tdTomato experiments were performed in the following batches: Batch 1 – D1Tom-CTL1 (F), D1Tom-CKO1 (F); Batch 2 – D1Tom-CTL2 (F), D1Tom-CKO2 (M). Tissue and library preparation for *golli*-τ-eGFP experiments were performed on separate days: GTE-CTL1 (M), GTE-CTL2 (M), GTE-CKO1 (M), GTE-CKO2 (F). Libraries were sequenced using an Illumina NextSeq 500 at the McDermott Sequencing Core at UT Southwestern.

Data processing

BCL files were demultiplexed with the i7 index using Illumina's bcl2fastq v2.17.1.14 and *mkfastq* from 10x Genomics CellRanger v2.1.1. Extracted paired-end fastq files, consisting of a 26 bp cell barcode and unique molecular identifier (UMI) (R1) and a 124 bp transcript sequence (R2), were checked for read quality using FASTQC v0.11.5 (Andrews, 2010). R1 reads were used to estimate and identify real cells using *whitelist* from UMI-tools v0.5.4 (Smith et al., 2017). A whitelist of cell barcodes and R2 fastq files

were used to extract reads corresponding to cells using *extract* from UMI-tools v0.5.4. This step also appended the cell barcode and UMI sequence information from R1 to read names in the R2 fastq file. Extracted R2 reads were aligned to the mouse reference genome (MM10/GRCm38p6) from the UCSC genome browser (Kent et al., 2002) and reference annotation (Gencode vM17) using STAR v2.5.2b (Dobin et al., 2013) allowing up to 5 mismatches. Uniquely mapped reads were assigned to exons using *featureCounts* from the Subread package (v1.6.2) (Liao et al., 2014). Assigned reads were sorted and indexed using Samtools v1.6 (Liao et al., 2014) and then used to generate raw expression UMI count tables using *count* from UMI-tools v0.5.4. For libraries sequenced in multiple runs, the commonly identified cell barcodes between runs were used for downstream analysis.

Clustering analysis

Cell clusters were identified using the Seurat R package (Butler et al., 2018). Individual cells were retained in the dataset based on the following criteria: <20,000 UMIs, <10% mitochondrial transcripts, <20% ribosomal protein gene transcripts. Sex chromosome and mitochondrial genes were removed from the analysis after filtering. The filtered data were log normalized with a scale factor of 10,000 using *NormalizeData*, and 1576 variable genes were identified with *FindVariableGenes* using the following parameters: mean.function = ExpMean, dispersion.function = LogVMR, x.low.cutoff = 0.2, x.high.cutoff = 2.5, y.cutoff = 0.5. Cell cycle scores were calculated using *CellCycleScoring* as per the Satija Lab cell cycle vignette (https://satijalab.org/seurat/cell_cycle_vignette.html). UMI number, percent mitochondrial

transcripts, percent ribosomal protein gene transcripts, library, and cell cycle scores were regressed during scaling. For the *Drd1a*-tdTomato dataset, we used JackStraw analysis to select principal components (PCs) 1-47 for clustering, excluding PCs with >1 immediate early gene (IEG) in the top 30 associated genes. We used a resolution of 1.6 for UMAP clustering and *ValidateClusters* with default parameters did not lead to cluster merging. For the *golli*-τ-eGFP dataset, we used a resolution of 1 for UMAP clustering.

Cell type annotation

Cluster marker genes were identified using *FindAllMarkers* with default parameters. Clusters were broadly annotated by enriched expression of canonical marker genes (e.g. Astrocytes: *Aqp4*; Microglia: *P2ry12*; Neurons: *Rbfox1*; Excitatory neurons: *Slc17a7*; Layer 2-4 neurons: *Satb2*; L5-6 neurons: *Tbr1*, *Fezf2*; L1 neurons: *Lhx5*; Interneurons: *Gad1*; Oligodendrocytes: *Sox10*). For the *Drd1a*-tdTomato dataset, we refined these annotations by comparing our cluster markers with markers from a published scRNA-seq dataset from P0 mouse cortex (Loo et al., 2019). Metadata and raw expression values for this dataset were downloaded from https://github.com/jeremymsimon/MouseCortex. Cells were filtered as in the original publication and expression values normalized using Seurat's *NormalizeData* with default parameters. The cluster identity of each cell was imported from the published metadata and cluster marker genes were identified using *FindAllMarkers* in Seurat. Enrichment of significant P0 marker genes (adj $p<0.05$) among our P7 cluster marker genes was analyzed using hypergeometric testing with a background of 2800 genes (the average of

the median number of expressed genes in each cluster). P values were corrected for multiple comparisons using the Benjamini-Hochberg procedure.

Cell re-clustering analyses

For *Drd1*+ cell re-clustering, cells with *Drd1* UMI >1 were pulled from the full *Drd1a*-tdTomato dataset and re-clustered with resolution 1.6, then annotated as described above. For *Drd1a*-tdTomato neuronal re-clustering, cells belonging to neuronal clusters (Clusters 2, 6, 8, 10-12, 14-17) were pulled from the full dataset and re-clustered with resolution 1.2 and PCs 1-59, excluding PCs with >1 IEG in the top 30 associated genes. Cell type annotation was performed as described above and refined using scRNA-seq marker genes identified in adult anterior lateral motor cortex (Tasic et al., 2018) (http://celltypes.brain-map.org/rnaseq/mouse). Two neuronal clusters (Clusters 2, 7) with enrichment of glial, mitochondrial, and/or ribosomal genes among their marker genes were included in analyses but excluded from data visualizations. Contributions of neurons to each cluster by genotype were compared using Fisher's exact test.

Differential gene expression analyses

We used the Wilcoxon rank sum test to calculate pseudo-bulk RNA-seq differentially expressed genes (DEGs) in two approaches: between genotypes for all neurons (*Drd1a*-tdTomato and *golli*-τ-eGFP datasets) or between genotypes within each neuronal cluster (*Drd1a*-tdTomato dataset only). Enrichment of all-neuron DEGs among neuronal cluster markers was analyzed using hypergeometric testing with a background of 2800 genes. Gene ontology (GO) analysis was performed using ToppFun from the ToppGene Suite (Chen et al., 2009), and Biological Process GO categories with

Benjamini-Hochberg (BH) FDR<0.05 were summarized using REVIGO, with allowed similarity=0.5 and GO term database for *Mus musculus* (Supek et al., 2011). To identify putative Foxp2 direct gene targets, we calculated the Spearman correlation coefficients between *Foxp2* and all other genes in control cells from the *Drd1a*-tdTomato dataset, and then overlapped genes with |ρ|>0.1 and BH FDR<0.05 with the E16.5 brain Foxp2 ChIP long list from (Vernes et al., 2011).

Gene Expression Omnibus (GEO) accession information

The National Center for Biotechnology Information GEO accession number for the scRNA-seq data reported in this study is GSE130653.

Chromatin immunoprecipitation (ChIP)

ChIP was performed based on (Cotney and Noonan, 2015) with 3 replicates per genotype. All buffers contained protease inhibitors and PMSF. P7 control and *Foxp2* cKO mice were rapidly decapitated and 50 mg of frontal cortex was harvested in ice-cold PBS. Tissue was minced and incubated in 1X fixation buffer for 20 min RT with rotation (10X fixation buffer: 50 mM HEPES-KOH pH 7.6, 100mM NaCl, 1 mM EDTA, 0.5 mM EGTA; 1X fixation buffer with 1% PFA was prepared fresh). Glycine was added to 150 mM final concentration and samples were rotated 10 min RT. Samples were washed once in PBS and resuspended in 6 volumes of cell lysis buffer (50 mM Tris pH 8.0, 140 mM NaCl, 1 mM EDTA, 10% glycerol, 0.5% IGEPAL CA-630, 0.25% Triton X-100). Samples were rotated at 4°C for 20 min, then dounce homogenized with 30-40 strokes of pestle B on ice. Nuclei were then pelleted, flash frozen, and stored at -80°C. On the day prior to ChIP, antibody-bound beads were prepared by washing 50 µl/sample Dynabeads (#10004D,

Life Technologies) 5 times with bead binding buffer (0.5% BSA, 0.2% Tween-20 in PBS), incubating with 5 µg/sample α-Foxp2 (#MABE415, Millipore) overnight at 4°C, washing 5 times with bead binding buffer, washing 5 times with dilution buffer (16.7 mM Tris pH 8.0, 167 mM NaCl, 1.2 mM EDTA, 0.01% SDS, 1.1% Triton X-100), and resuspending in 50 µl dilution buffer per sample. On the day of ChIP, nuclei were thawed on ice and resuspended in five volumes (based on original cell pellet) of nuclear lysis buffer (10 mM Tris pH 8.0, 1 mM EDTA, 0.5 mM EGTA, 0.2% SDS), incubated on ice for 20 min, and sheared for 7 min at 4°C using a Covaris E220 (PIP 105, Duty Factor 2%, CPB 200). Samples were centrifuged at 16,000 g for 10 min at 4°C, and then the supernatant was diluted with dilution buffer until the SDS concentration was <0.1%. Input (10%) was set aside and IP fractions were incubated with 50 µl antibody-bound beads overnight at 4°C. The next day, samples were washed 8 times with wash buffer (100 mM Tris pH 8.0, 500 nM NaCl, 1% IGEPAL CA-620, 1% deoxycholic acid), washed once with TE buffer (50 mM Tris pH 8.0, 10 mM EDTA), and then eluted in elution buffer (50 mM Tris pH 8.0, 10 mM EDTA, 1% SDS) for 10 min at 65°C with shaking. For ChIP-Western, loading buffer was added to samples and Western blotting was performed as described above. For ChIP-seq, NaCl was added to samples to a concentration of 0.3M, then crosslinks were reversed at 65°C overnight with shaking. Samples were treated with 10 µg RNase A and 200 µg Proteinase K and chromatin was purified using the QIAquick PCR Purification Kit (#28104, Qiagen). Libraries were prepared as described previously (Takahashi et al., 2015) and sequenced at the McDermott Sequencing Core on an Illumina Nextseq 500 to generate single-end 75 bp reads. ChIP-seq data was analyzed as described previously

(Fontenot et al., 2017) with reads aligned to the mouse mm10 reference genome and the common peak set consisting of peaks present in 2 out of 3 replicates per genotype.

Cleavage under targets and release using nuclease (CUT&RUN)

CUT&RUN was performed according to (Skene et al., 2018). P7 cortical tissue from one mouse was dissected and nuclei were extracted using Nuclei EZ Lysis Buffer (#N3408, Sigma) with dounce homogenization. Nuclei were washed twice with CUT&RUN wash buffer, filtered through a FLOWMI 40 µm tip strainer (#H13680-0040, Bel-Art Products), and divided into three aliquots with ~120,000 nuclei each for the following conditions: +ab (α-H3K27me3, #9733T, Cell Signaling Technology), rabbit anti-mouse IgG (#A27022, Thermo Scientific), and -ab to observe nonspecific chromatin fragments cut by free MNase. Nuclei were bound to concanavalin A-coated beads as described, and antibodies were prepared as described at 1:100 dilution and incubated with samples at 4°C overnight. MNase binding, chromatin digestion, and chromatin released were performed as described. DNA was purified using the QIAquick PCR Purification Kit (Qiagen, #28104).

Figures

Figure 3.1 *Cortex-specific deletion of Foxp2 by Emx1-Cre.*

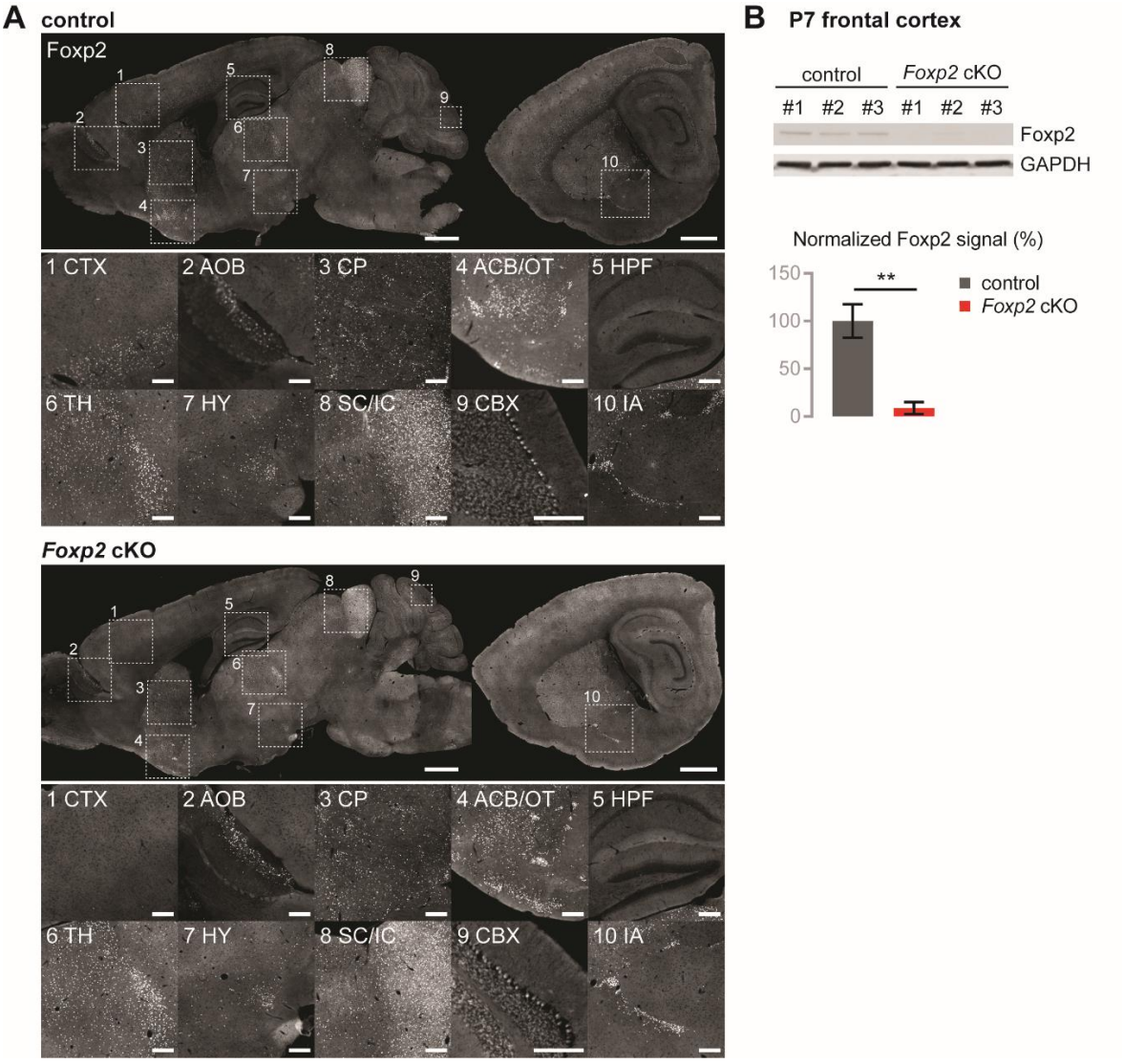

(A) IHC for Foxp2 in sagittal brain sections from adult control (*Foxp2*$^{flox/flox}$) and *Foxp2* cKO (*Emx1-Cre; Foxp2*$^{flox/flox}$) mice. Top scale bar: 1000 µm, bottom scale bars: 200 µm. (B) Top: Western blot for Foxp2 and GAPDH from frontal cortical lysates of P7 control and cKO mice. Bottom: Western blot quantification. Foxp2 signals were normalized to GAPDH signals. Error bars represent ±SEM. (**) $P < 0.01$, t-test. $n = 3$ per condition. ACB: nucleus accumbens, AOB: accessory olfactory bulb, CBX: cerebellar cortex, CP: caudoputamen, CTX: cortex, HPF: hippocampal formation, HY: hypothalamus, IA: interposed amygdalar nucleus, IC: inferior colliculus, OT: olfactory tubercle, SC: superior colliculus, TH: thalamus.

Figure 3.2 *Foxp2 cKO mice show cognitive deficits specific to behavioral flexibility.*

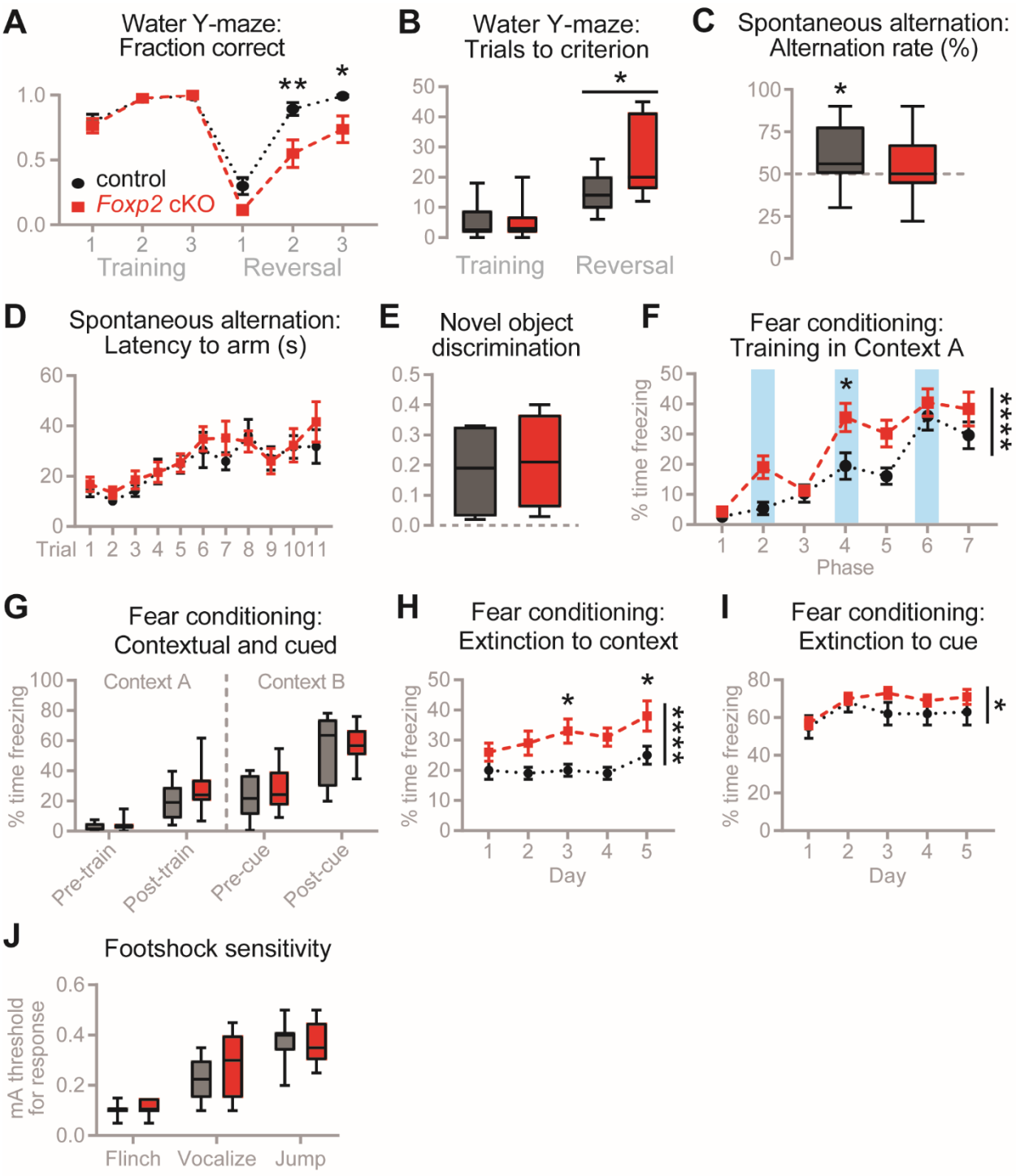

(A-B) Reversal learning in water Y-maze. n = 10-17 per condition. (A) Fraction of correct trials. Data are shown as means (±SEM). (*) $P < 0.05$, (**) $P < 0.01$, two-way ANOVA with Bonferroni's multiple comparisons test. (B) Number of trials to criterion. Box shows 25-75 percentiles, whiskers show min-max. (*) $P < 0.05$, t-test. (C-D) Spontaneous alternation in T-maze. n = 16-19 per condition. (C) Spontaneous alternation rate. Box shows 25-75 percentiles, whiskers show min-max. (*) $P < 0.05$ compared to chance levels (50%), t-test. (D) Latency to arm. Data are represented as means (±SEM). (E) Discrimination index in novel object recognition task, calculated as the difference between time spent sniffing novel versus familiar object, divided by total sniffing time. Box shows 25-75 percentiles, whiskers show min-max. n = 4 per condition. (F-I) Cued and contextual fear conditioning (FC) with extinction. n = 14-15 per condition. (F) FC training to cue in Context A. Blue shaded bars represent tone-shock pairs. Data are represented as means (±SEM). (*) $P < 0.05$, (****) $P < 0.0001$, two-way ANOVA with Bonferroni's multiple comparisons test. (G) Contextual (Context A) and cued (Context B) fear memory on the first test day after training, compared with pre-training or pre-tone freezing levels, respectively. Box shows 25-75 percentiles, whiskers show min-max. (H) Extinction of freezing behavior to Context A. Data are represented as means (±SEM). (*) $P < 0.05$, (****) $P < 0.0001$, two-way ANOVA with Bonferroni's multiple comparisons test. (I) Extinction of freezing behavior to tone in Context B. Y-axis represents time spent freezing during tone. Data are represented as means (±SEM). (*) $P < 0.05$, two-way ANOVA with Bonferroni's multiple comparisons test. (J) Footshock sensitivity as measured by current required to elicit flinching, vocalizing, and/or jumping.

Figure 3.3 *Foxp2 cKO mice show normal social, locomotor, and anxiety-related behaviors.*

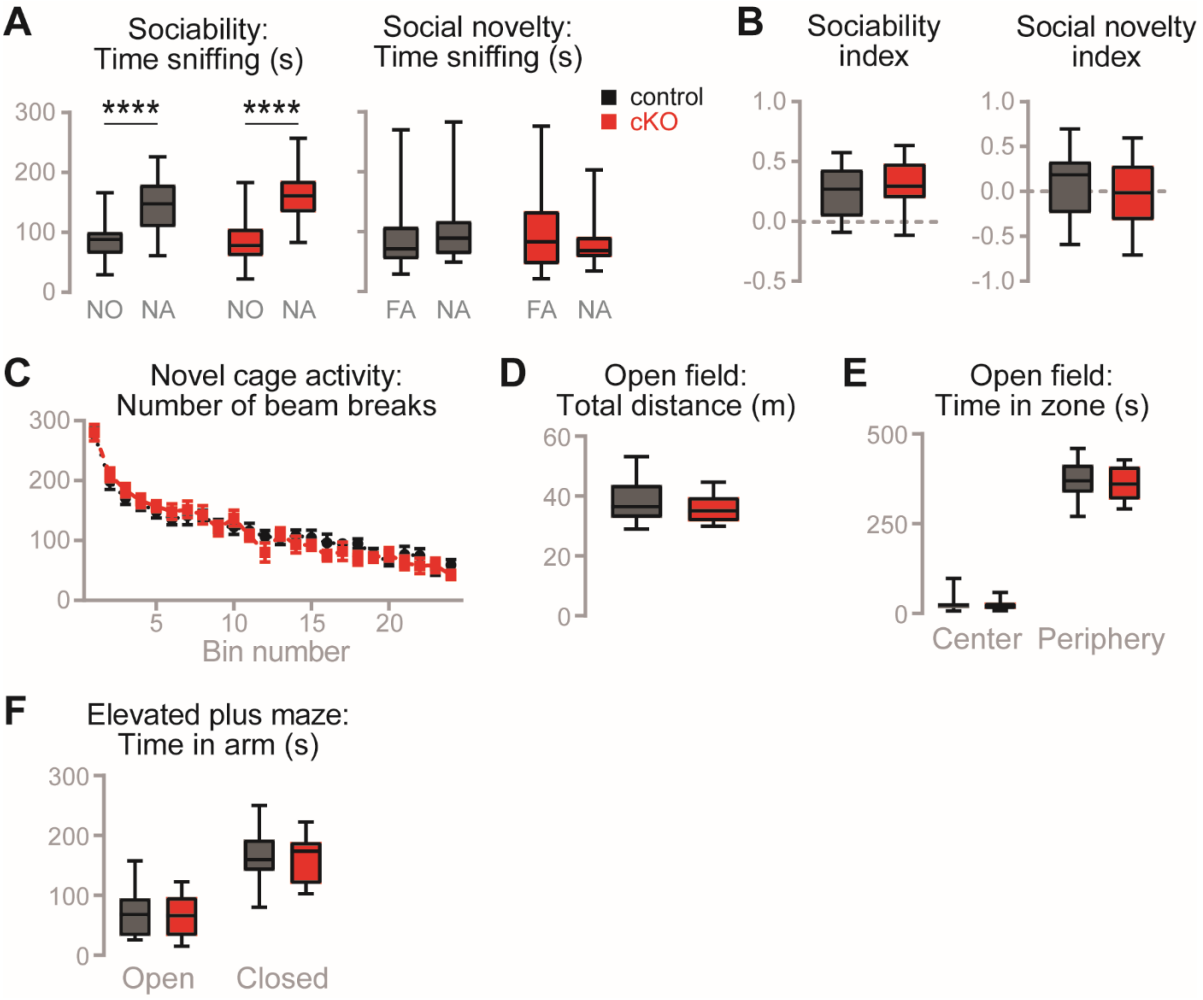

(A-B) Three-chamber social interaction test. *n* = 24-31 per condition. (A) Time spent sniffing novel object (NO) versus novel animal (NA) in the sociability phase, and familiar animal (FA) versus novel animal (NA) in the social novelty phase. Box shows 25-75 percentiles, whiskers show min-max. (****) $P < 0.0001$, t-test. (B) Sociability and social novelty indices, calculated as the difference between time spent sniffing NA versus NO or FA versus NA, respectively, divided by total sniffing time. Box shows 25-75 percentiles, whiskers show min-max. (C-F) Activity and anxiety measures. *n* = 13 per condition. (C) Number of infrared beam breaks in a novel cage per 5-minute bin. Data are represented as means (±SEM). (D) Total distance moved in open field. Box shows 25-75 percentiles, whiskers show min-max. (E) Time in zone in open field. Box shows 25-75 percentiles, whiskers show min-max. (F) Time in zone in elevated plus maze. Box shows 25-75 percentiles, whiskers show min-max.

Figure 3.4 *Foxp2 cKO mice show normal adult courtship vocalizations.*

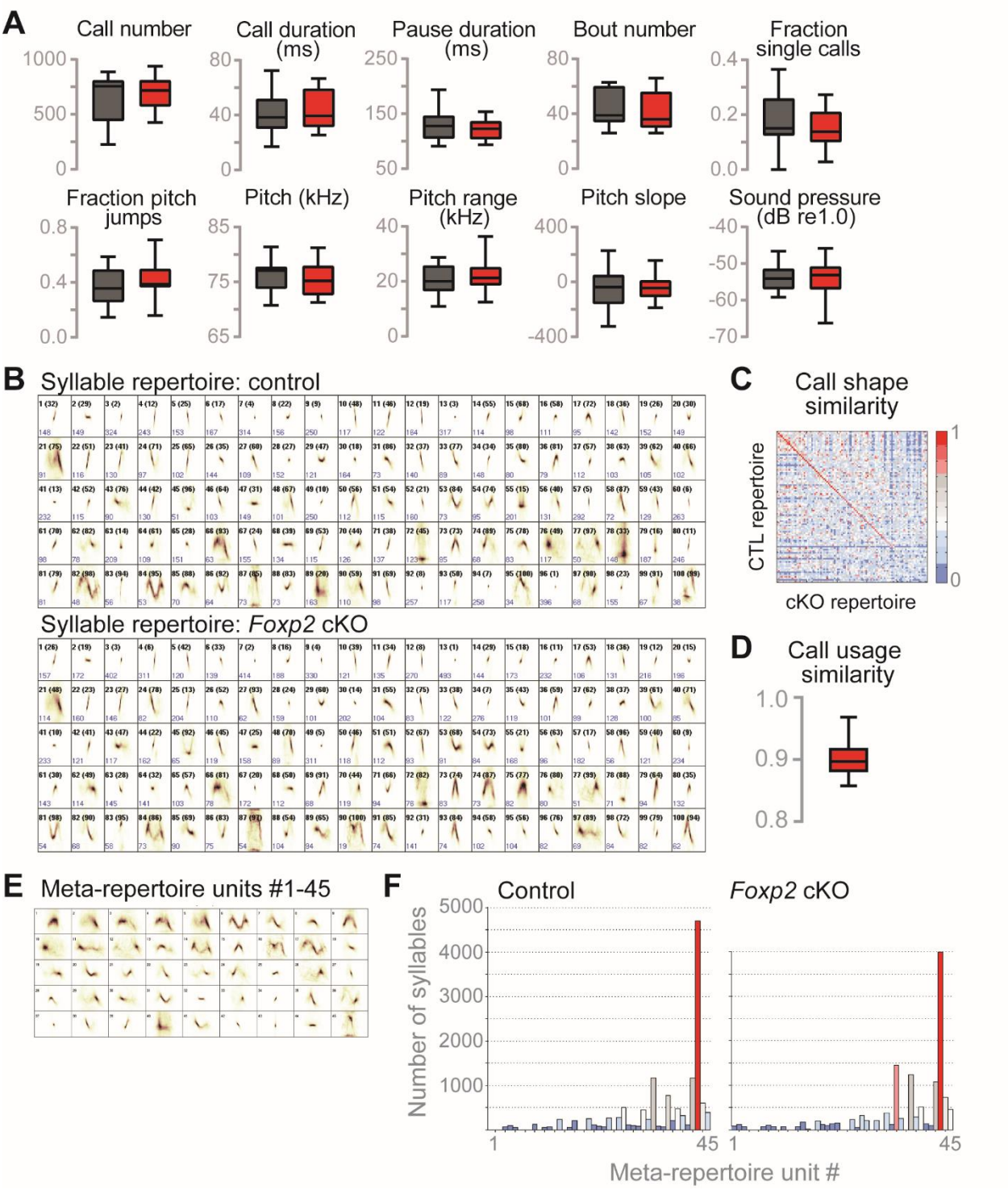

(A) Adult courtship ultrasonic vocalizations (USVs) analyzed according to (Holy and Guo, 2005). Box shows 25-75 percentiles, whiskers show min-max. *n* = 14-15 per condition. (B-F) Adult courtship USVs analyzed according to (Van Segbroeck et al., 2017). *n* = 14-15 per condition. (B) Call shapes for control and *Foxp2* cKO repertoires (size 100). (C) Call shape similarity matrix between adult control and cKO USV repertoires (size 100). Scale represents Pearson correlation coefficient. (D) Call usage similarity of adult cKOs compared to controls. Box shows 25-75 percentiles, whiskers show 5-95 percentiles. (E) Meta-repertoire (size 45) generated from control and cKO call repertoires. (F) Frequency of meta-repertoire syllables across control and cKO USV recordings.

Figure 3.5 *Foxp2 cKO mice show normal postnatal isolation vocalizations, save for decreased loudness.*

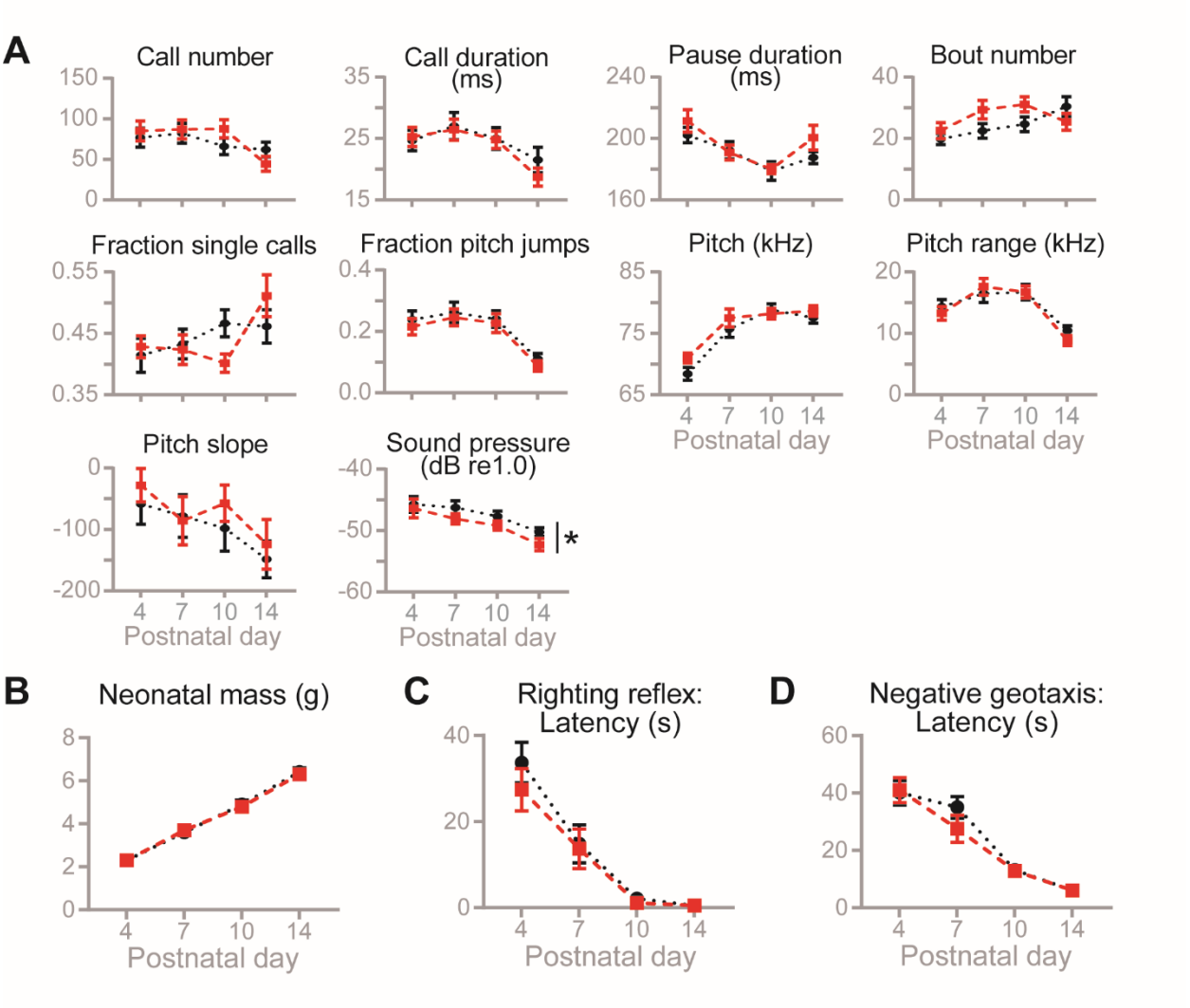

(A) Postnatal isolation USVs analyzed according to (Holy and Guo, 2005). Data are represented as means (±SEM). (*) $P < 0.05$, two-way ANOVA with Bonferroni's multiple comparisons test. n = 34-42 per condition. (B-D) Neonatal development assessments. Data are represented as means (±SEM). n = 18-23 per condition. (B) Neonatal mass in grams. (C) Righting reflex latency. (D) Negative geotaxis latency. Full statistical analyses can be found in Table 3.2.

Figure 3.6 *Foxp2 cKO mice show normal gross cortical development.*

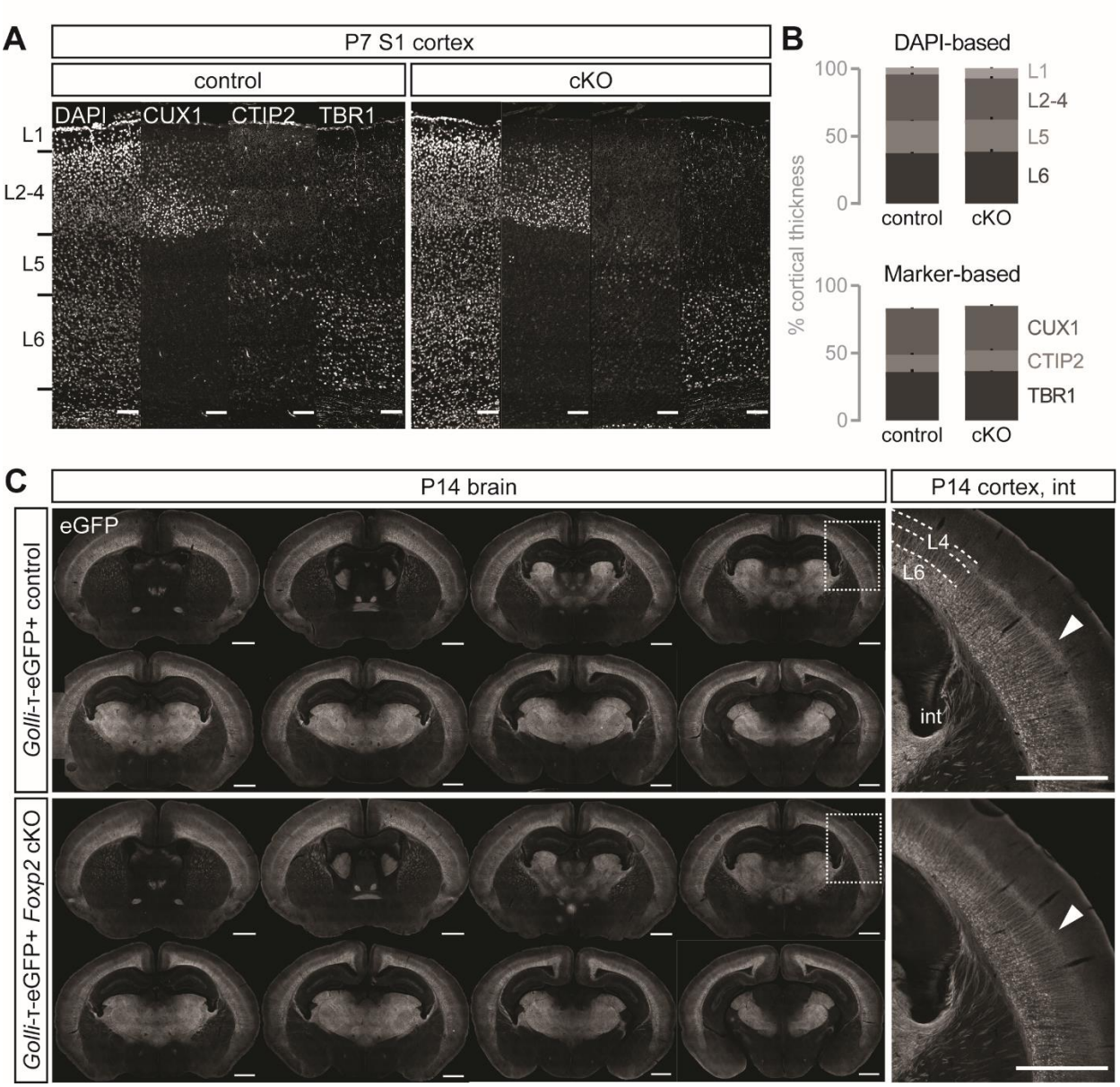

(A) Immunohistochemistry (IHC) for cortical layer markers in P7 control and cKO primary somatosensory (S1) cortex. Scale bar: 100 µm. (B) Quantification of relative layer thickness based on DAPI cytoarchitecture (top) and layer markers (bottom). Data are represented as means (±SEM). *n* = 3 per condition. Full statistical analysis can be found in Table 3.3. (C) IHC for *golli*-τ-eGFP in P14 control and cKO brain sections (left) and corticothalamic axons (right). Arrowhead indicates L6 axon and dendrite terminations in L4. Int: internal capsule. Scale bars: 1000 µm.

Figure 3.7 *Foxp2 cKO mice show decreased dopamine D1 receptor expression in postnatal and adult cortex.*

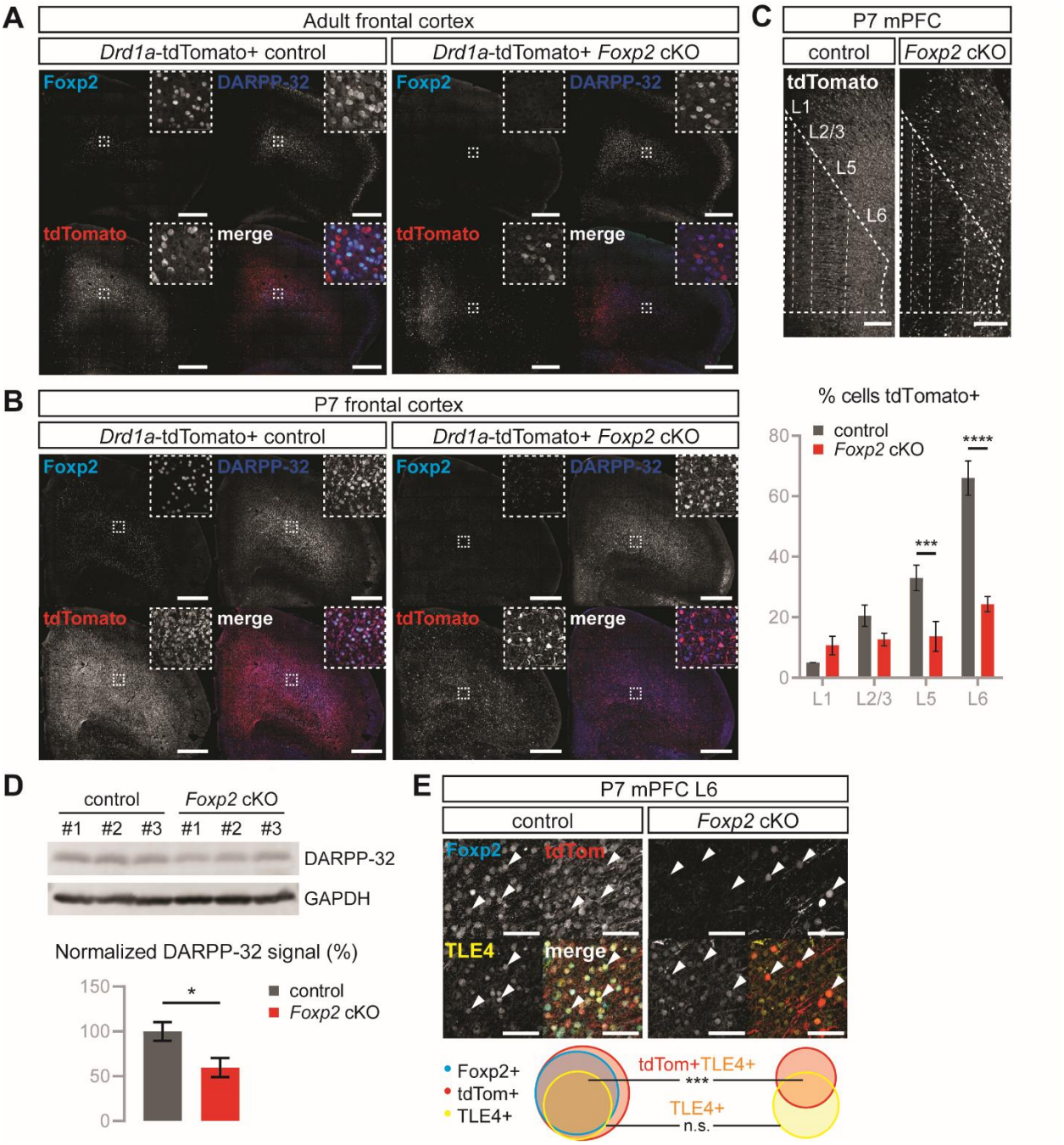

(A) IHC for Foxp2, DARPP-32, and *Drd1a*-tdTomato in adult control and *Foxp2* cKO frontal cortex. Scale bar: 500 µm. (B) IHC for Foxp2, DARPP-32, and *Drd1a*-tdTomato in P7 control and cKO frontal cortex. Scale bar: 500 µm. (C) Top: IHC for *Drd1a*-tdTomato

in P7 control and cKO mPFC. Scale bar: 200 µm. Bottom: Percentage of DAPI+ cells expressing tdTomato per layer in P7 mPFC. Error bars represent ±SEM. (***) $P < 0.001$, (****) $P < 0.0001$, two-way ANOVA with Bonferroni's multiple comparisons test. n = 2-3 per condition. Full statistical analysis can be found in Table 3.3. (D) Top: Western blot for DARPP-32 and GAPDH loading control from frontal cortical lysates of P7 control and cKO mice. Bottom: Western blot quantification. DARPP-32 signals were normalized to GAPDH signals. Error bars represent ±SEM. (*) $P < 0.05$, t-test. n = 3 per condition. (E) Top: IHC for Foxp2, *Drd1a*-tdTomato, and TLE4 in P7 control and cKO mPFC L6. Arrowheads indicate cells with protein coexpression. Scale bar: 50 µm. Bottom: Weighted Venn diagrams summarizing Foxp2, *Drd1a*-tdTomato, and TLE4 coexpression in P7 control and cKO mPFC L6. (***) $P < 0.001$, t-test. n = 2-3 per condition. Full quantification and statistical analysis can be found in Table 3.4.

Figure 3.8 *Dopamine D1 receptors are expressed in multiple cell types in postnatal frontal cortex.*

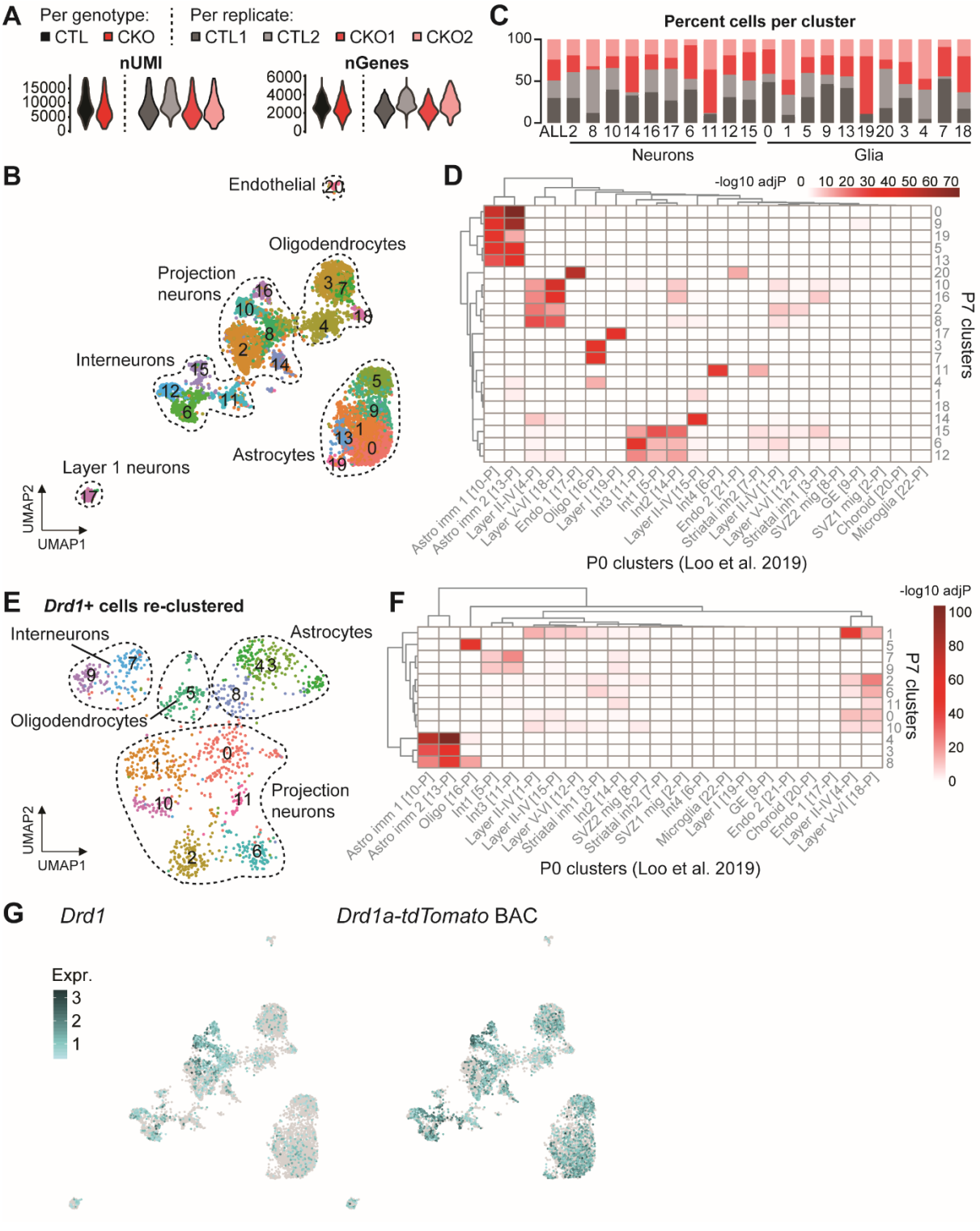

(A) Violin plots showing number of UMIs (left) and number of genes (right) detected per genotype and per replicate. (B) UMAP projection of clusters identified from control and cKO cells combined. (C) Percentage of cells from each replicate per cluster, colored based on (A). (D) Hypergeometric overlaps of marker genes from our P7 *Drd1a*-tdTomato clusters with P0 mouse cortex clusters from (Loo et al., 2019). (E) UMAP projection of re-clustered *Drd1*+ cells from (B). (F) Hypergeometric overlaps of *Drd1*+ cell cluster marker genes with P0 mouse cortex clusters from (Loo et al., 2019). (G) Feature plots of clusters from (B) showing expression levels of *Drd1* (left) and a partial *Drd1a*-tdTomato BAC sequence (right).

Figure 3.9 *Foxp2 cKO mice show altered composition of dopamine D1 receptor-expressing neuronal subtypes.*

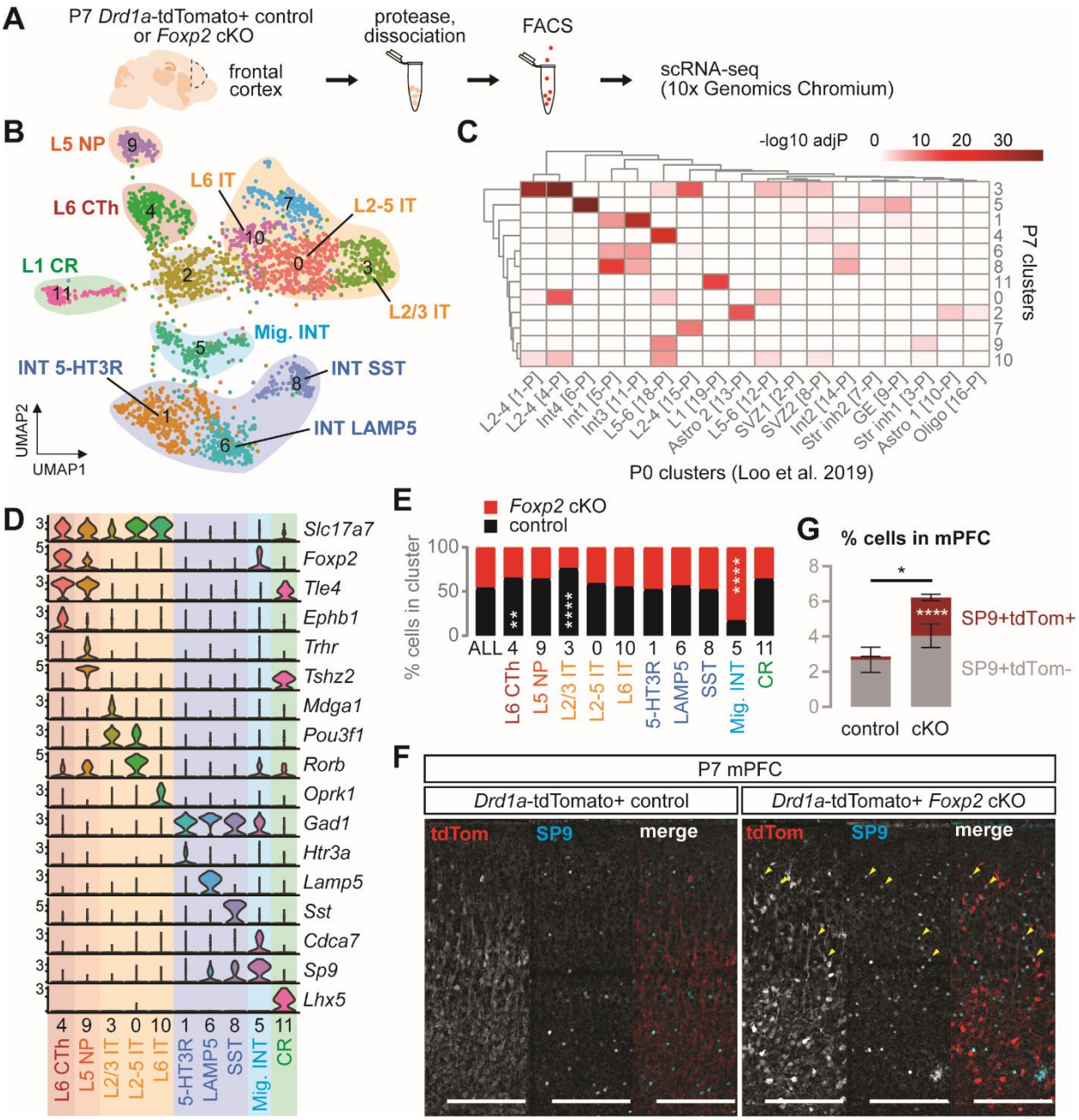

(A) Experimental design for D1R scRNA-seq. *n* = 2 per condition. (B) UMAP projection of clusters with neurons combined from both genotypes. (C) Hypergeometric overlaps of neuronal cluster marker genes with P0 mouse cortex cluster marker genes from Loo et al 2019. (D) Violin plots of selected marker genes. Y-axes show log-scaled expression. (E)

Percentage of control and cKO cells per cluster. (**) $P < 0.01$, (****) $P < 0.0001$, Fisher's exact test with Benjamini-Hochberg post-hoc test. (F) IHC for tdTomato and SP9 in P7 control and cKO mPFC. Pial surface is at the top. Arrowheads indicate cells expressing both proteins. Scale bar: 200 µm. (G) Percentage of cells expressing SP9 ± tdTomato in P7 control and cKO mPFC. Data are represented as means±SEM. (*) $P < 0.05$, (****) $P < 0.0001$, t-test. n = 3-4 per condition. CR: Cajal-Retzius, CTh: corticothalamic, INT: interneuron, IT: intratelencephalic, Mig INT: migrating interneuron, NP: near-projecting.

Figure 3.10 *Cortical Foxp2 deletion induces non-cell-autonomous dysregulation of cytoskeletal genes.*

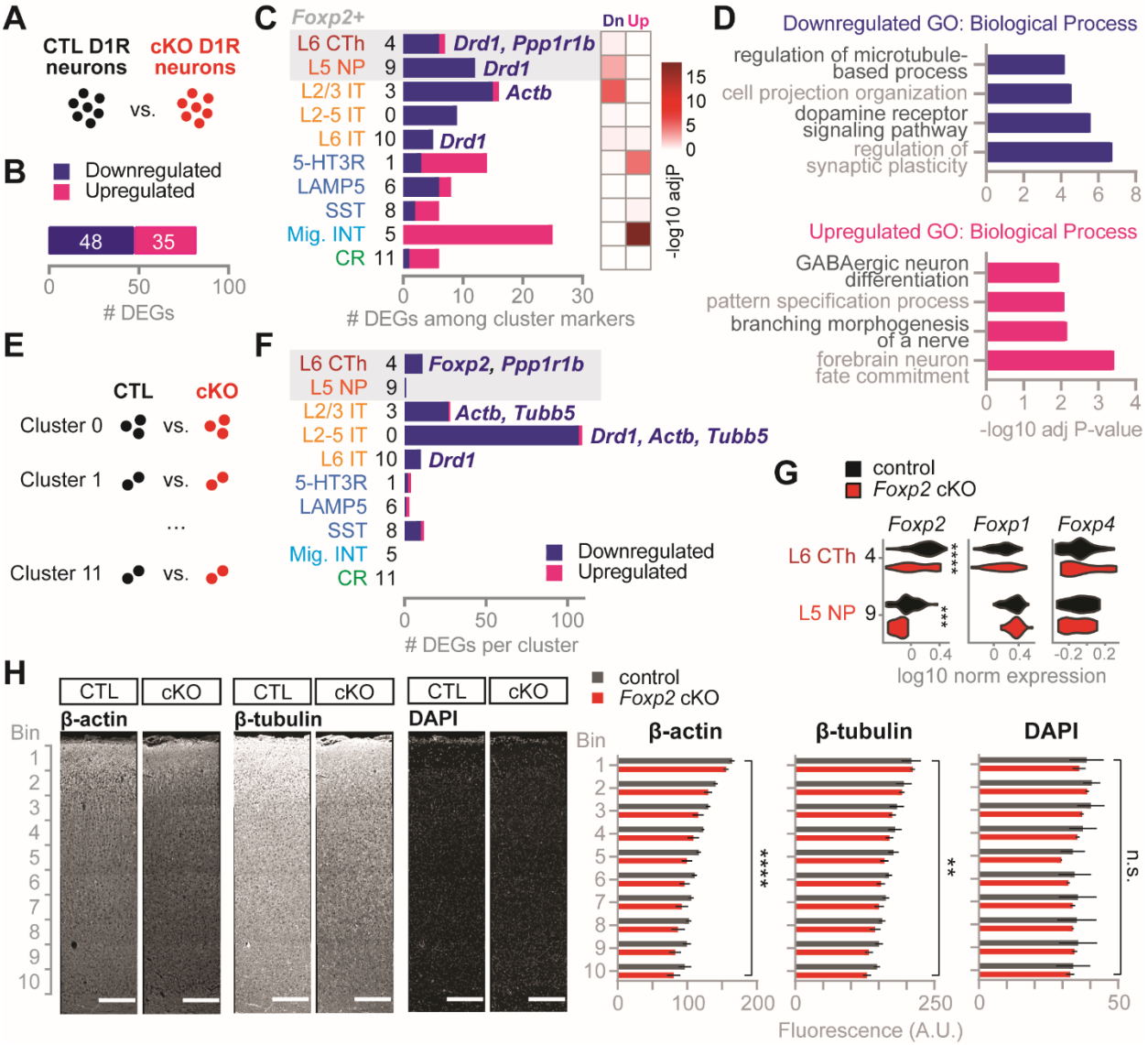

(A) Identification of differentially expressed genes (DEGs) between all control and all *Foxp2* cKO neurons from D1R scRNA-seq. (B) Number of DEGs significantly down- or upregulated in cKO neurons. (C) Number (left) and hypergeometric enrichment (right) of DEGs among neuronal cluster marker genes. Gray shaded area indicates clusters with *Foxp2* enrichment. (D) Summarized gene ontology (GO) Biological Process terms for down- and upregulated DEGs. (E) Analysis of DEGs by cluster between control and cKO neurons. (F) Number of DEGs per cluster with selected genes shown. Gray shaded area indicates clusters with *Foxp2* enrichment. (G) Violin plots of *Foxp* gene expression in clusters with *Foxp2* enrichment. (***) $P < 0.001$, (****) $P < 0.0001$, Wilcoxon rank sum test. (H) Left: IHC for β-actin and β-tubulin in P7 control and cKO motor cortex. Right:

Quantification of fluorescence intensity averaged by cortical bin. Data are represented as means±SEM. (**) $P < 0.01$, (****) $P < 0.0001$, two-way ANOVA with Bonferroni's multiple comparisons test. $n = 3$ per condition.

Figure 3.11 *Identification of genes directly regulated by Foxp2 in the cortex.*

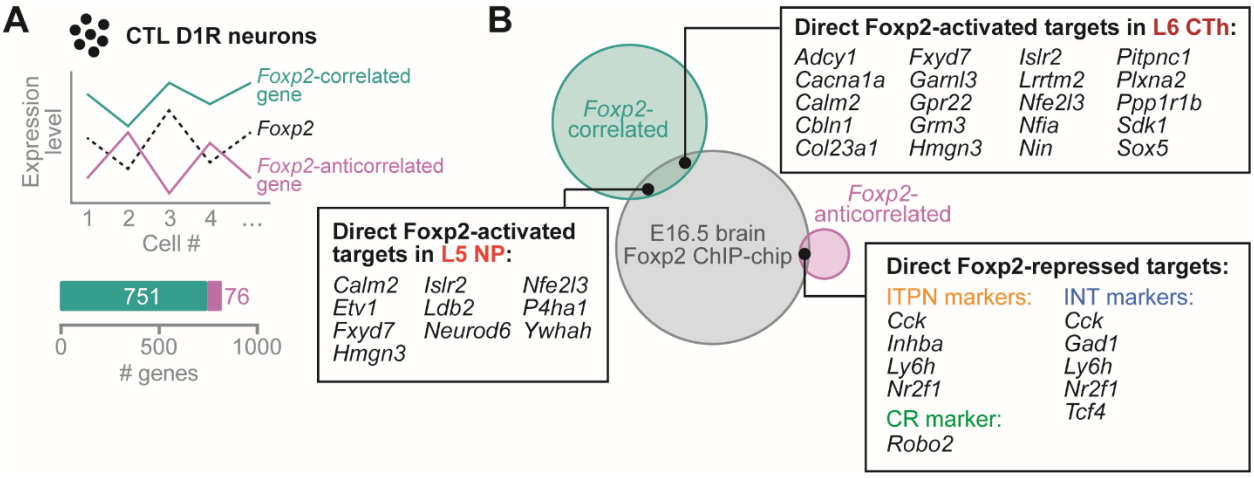

(A) Top: Analysis of genes correlated or anticorrelated with *Foxp2* expression across control neurons from D1R scRNA-seq. Bottom: Number of *Foxp2*-correlated or -anticorrelated genes. (B) Overlap of *Foxp2*-correlated or -anticorrelated genes with embryonic brain Foxp2 ChIP-chip targets from (Vernes et al., 2011) and with neuronal cluster marker genes. CR: Cajal-Retzius, CTh: corticothalamic, INT: interneuron, IT: intratelencephalic, Mig INT: migrating interneuron, NP: near-projecting.

Figure 3.12 *Efforts toward identification of genome-wide direct Foxp2 targets in postnatal cortex*

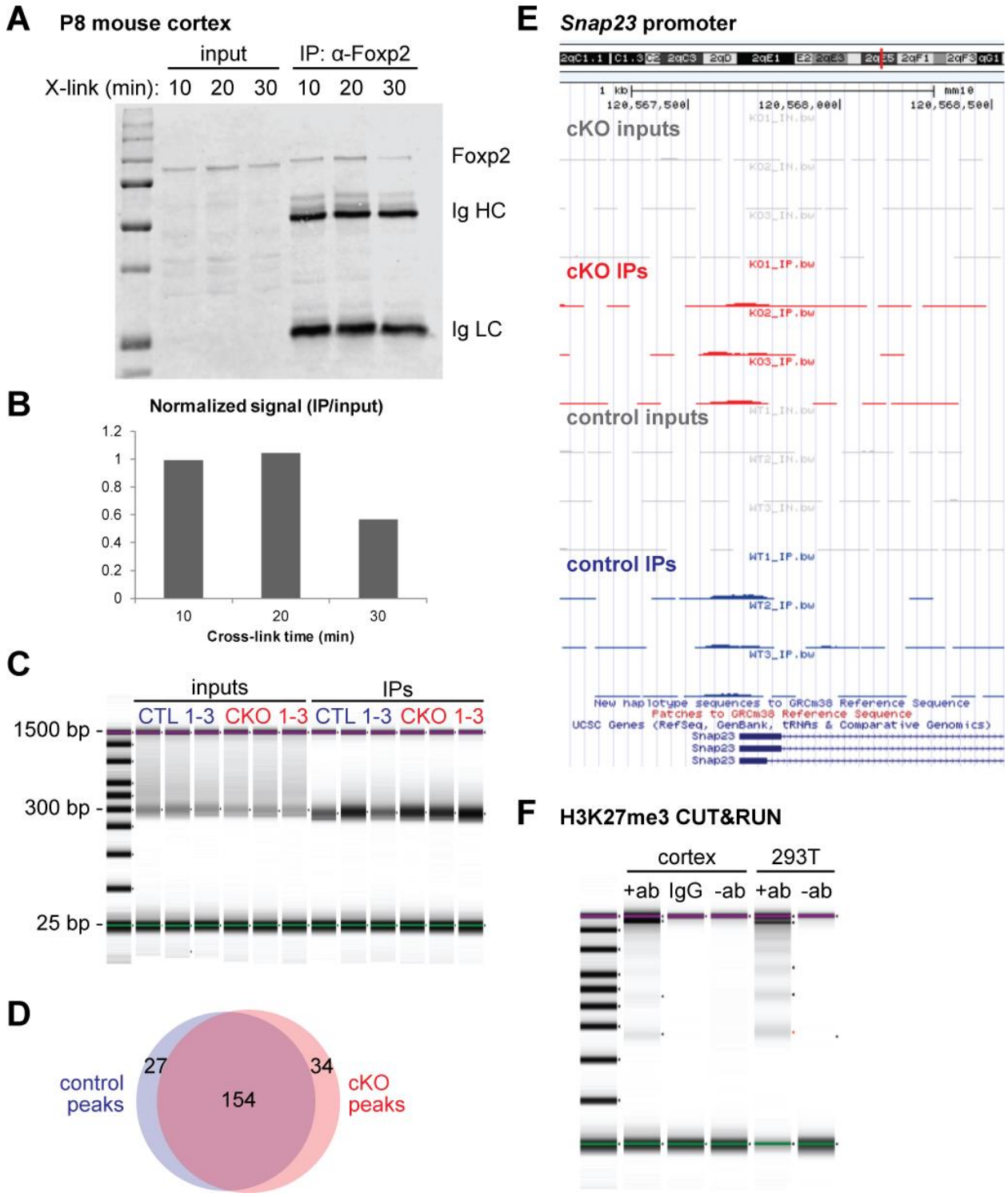

(A) ChIP-Western showing IP of Foxp2 after three different crosslinking durations in P8 mouse cortical tissue. Ig HC: immunoglobin heavy chain, Ig LC: immunoglobin light chain. (B) Quantification of (A). (C) TapeStation analysis of ChIP-seq library sizes. (D) Overlap of control and cKO peaks significantly enriched over input fractions. (E) Representative track file for a control-specific peak at the *Snap23* promoter. (F) TapeStation analysis of released DNA fragments after CUT&RUN for H3K27me3 in P7 mouse cortex and 293T cells (cell experiment performed by Stephanie Lepp Hickey).

Figure 3.13 *Summary of behavioral and molecular findings in Foxp2 cKO mice.*

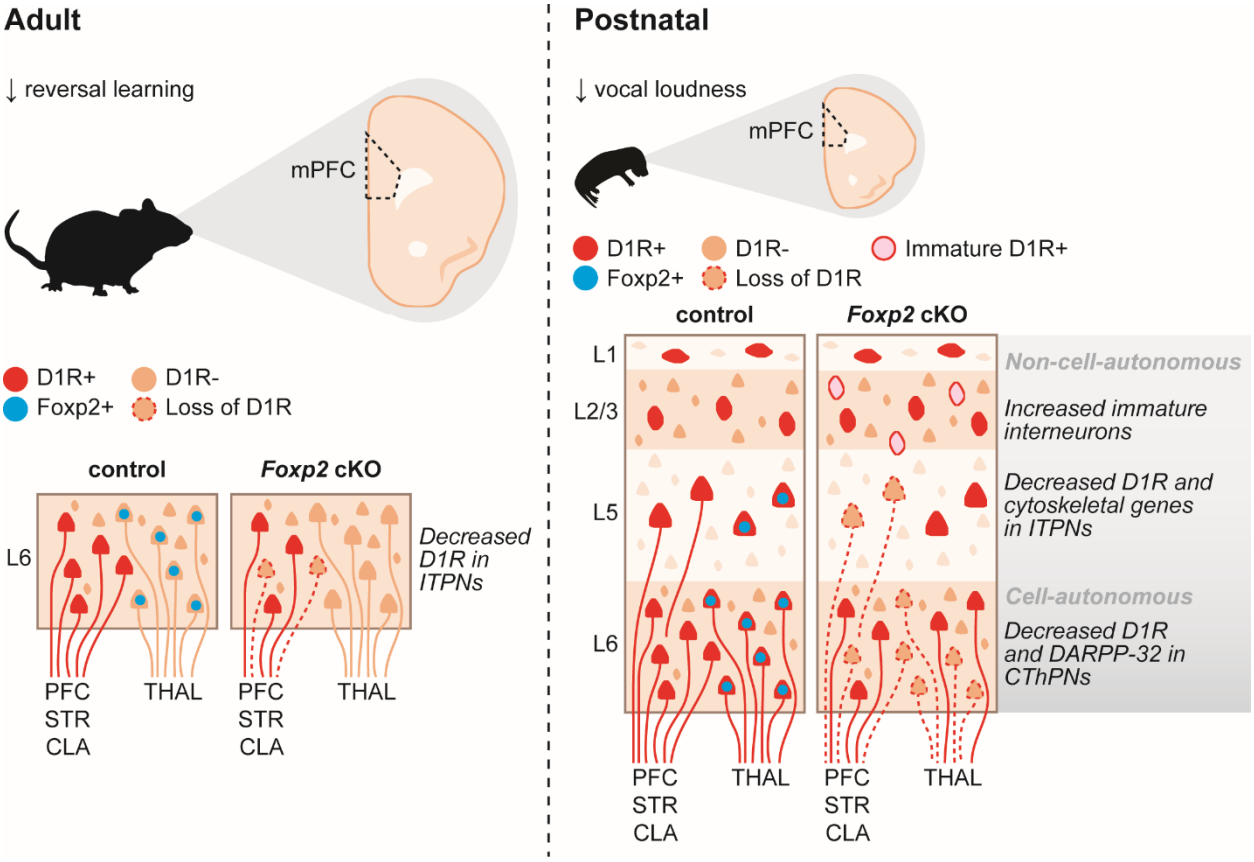

CLA: claustrum, CThPNs: corticothalamic projection neurons, D1R: dopamine D1 receptor, ITPNs: intratelencephalic projection neurons, L: layer, mPFC: medial prefrontal cortex, STR: striatum, THAL: thalamus.

Tables

Table 3.1 *PCR genotyping primers.*

Genotyping	JAX primers	Forward primer (5'-3')	Reverse primer (5'-3')
Emx1-Cre transgene	oIMR1084, oIMR1085	GCGGTCTGGCAGTAAAAACTATC	GTGAAACAGCATTGCTGTCACTT
Emx1 wild-type	oIMR4170, oIMR4171	AAGGTGTGGTTCCAGAATCG	CTCTCCACCAGAAGGCTGAG
Foxp2$^{flox/flox}$	24915, 24916	AATAACAGTCACGCCCCGTA	GGCCATCTAACAAAGGAGGAG
Drd1a-tdTomato	12153, 12154	CTTCTGAGGCGGAAAGAACC	TTTCTGATTGAGAGCATTCG
Golli-τ-eGFP	NA	ACGTAAACGGCCACAAGTTC	TGCTCAGGTAGTGGTTGTCG

Table 3.2 *Results and statistics for behavioral analyses.*

Behavioral Test	n	p-value	F	Multiple Comparisons
WATER Y-MAZE				
Control	10			
Foxp2 cKO	17			
Fraction correct		RM two-way ANOVA		Bonferroni
Control vs. cKO		**0.0286**	F(1,25)=5.397	Training 1/2/3 >0.9999/>0.9999/>0.9999 Reversal 1/2/3 0.2769/**0.0016**/**0.0374**
No. of trials prior to 5 consecutive correct responses				
Control vs. cKO		Unpaired t-test		
Training 1-3		0.7721		
Reversal 1-3		**0.0188**		
SPONTANEOUS ALTERNATION				
Control	19			
Foxp2 cKO	16			
Alternation rate		Unpaired t-test		
Control vs. cKO		0.4317		
Control vs. chance (50%)		**0.0306**		
cKO vs. chance (50%)		0.3009		
Latency to arm		Two-way ANOVA		Bonferroni
Control vs. *Foxp2* cKO		0.1799	F(1,354)=1.806	All trials >0.9999
NOVEL OBJECT DISCRIMINATION				
Control	4			
Foxp2 cKO	4			
Discrimination index		Unpaired t-test		
Control vs. cKO		0.8145		

Behavioral Test	n	p-value	F	Multiple Comparisons
FEAR CONDITIONING WITH EXTINCTION				
Control	14			
Foxp2 cKO	15			
Training		Two-way ANOVA		Bonferroni Phase 1/2/3/4/5/6/7
Control vs. cKO		**<0.0001**	F(1,189)=18.43	>0.9999/0.0707/>0.9999/**0.0181**/ 0.0557/>0.9999/0.6896
Fear learning		Two-way ANOVA		Bonferroni
Control vs. cKO		0.129	F(1,108)=2.34	
Pre-train:control vs. Pre-train:cKO (baseline freezing Context A)				>0.9999
Pre-train:control vs. Post-train:control (contextual fear learning)				**0.0183**
Pre-train:control vs. Pre-cue:control (Context A vs. Context B)				**0.0018**
Pre-train:cKO vs. Post-train:cKO (contextual fear learning)				**0.0002**
Pre-train:cKO vs. Pre-cue:cKO (Context A vs. Context B)				**0.0002**
Post-train:control vs. Post-train:cKO (contextual fear learning)				>0.9999
Pre-cue:control vs. Pre-cue:cKO (baseline freezing Context B)				>0.9999
Pre-cue:control vs. Post-cue:control (cued fear learning)				**<0.0001**
Pre-cue:cKO vs. Post-cue:cKO (cued fear learning)				**<0.0001**
Post-cue:control vs. Post-cue:cKO (cued fear learning)				>0.9999
Extinction to context		Two-way ANOVA		Bonferroni Day 1/2/3/4/5
Control vs. cKO		**<0.0001**	F(1,135)=26.88	0.9995/0.1680/**0.0301**/ 0.0553/0.0301
Extinction to cue		Two-way ANOVA		Bonferroni Day 1/2/3/4/5
Control vs. cKO		**0.0476**	F(1,135)=3.995	>0.9999/>0.9999/0.5179/ >0.9999/>0.9999
Footshock sensitivity		Two-way ANOVA		Bonferroni Flinch/Vocalize/Jump
Control vs. cKO		0.2976	F(1,27)=1.128	>0.9999/0.2342/>0.9999

Behavioral Test	n	p-value	F	Multiple Comparisons
THREE-CHAMBER SOCIAL INTERACTION				
Control	24			
Foxp2 cKO	31			
Sociability		Unpaired t-test		
Control NO vs. NA		**<0.0001**		
cKO NO vs. NA		**<0.0001**		
Control vs. cKO		0.2499		
Social novelty		Unpaired t-test		
Control FA vs. NA		0.3411		
cKO FA vs. NA		0.2339		
Control vs. cKO		0.2715		
NOVEL CAGE ACTIVITY				
Control	13			
cKO	13			
No. of beam breaks		Two-way ANOVA		Bonferroni
Control vs. cKO		0.7669	F(1,24) =0.0899	All trials >0.9999
OPEN FIELD				
Control	13			
Foxp2 cKO	13			
Control vs. cKO		Unpaired t-test		
Total distance		0.2344		
Time in center		0.7080		
Time in periphery		0.6661		
ELEVATED PLUS MAZE				
Control	13			
Foxp2 cKO	13			

Behavioral Test	n	p-value	F	Multiple Comparisons
Control vs. cKO		Unpaired t-test		
Time in open arms		0.8309		
Time in closed arms		0.9800		
ADULT ULTRASONIC VOCALIZATIONS				
Control	14			
Foxp2 cKO	15			
Control vs. cKO		Unpaired t-test		
Call number		0.4717		
Call duration		0.7583		
Pause duration		0.3894		
Bout number		0.7972		
Fraction single calls		0.4013		
Fraction pitch jumps		0.3783		
Pitch		0.6155		
Pitch range		0.5046		
Pitch slope		0.9454		
Sound pressure		0.9379		
NEONATAL ULTRASONIC VOCALIZATIONS				
P4 control	34			
P4 *Foxp2* cKO	35			
P7 control	35			
P7 *Foxp2* cKO	37			
P10 control	36			
P10 *Foxp2* cKO	42			
P14 control	36			
P14 *Foxp2* cKO	42			
Control vs. cKO		Two-way ANOVA		Bonferroni P4/P7/P10/P14
Call number		0.5881	F(1,289)=0.2940	>0.9999/>0.9999/0.6200/0.9698
Call duration		0.5408	F(1,239)=0.365	>0.9999/>0.9999/>0.9999/>0.9999
Pause duration		0.1752	F(1,238*)=1.942	>0.9999/>0.9999/>0.9999/0.4420
Bout number		0.1332	F(1,239)=2.270	>0.9999/0.2127/0.3013/0.8318

Behavioral Test	n	p-value	F	Multiple Comparisons
Fraction single calls		0.8770	F(1,239)=0.0240	>0.9999/>0.9999/0.2020/0.6796
Fraction pitch jumps		0.3286	F(1,239)=0.903	>0.9999/>0.9999/>0.9999/>0.9999
Pitch		0.1213	F(1,239)=2.417	0.3792/0.9402/>0.9999/>0.9999
Pitch range		0.6469	F(1,239)=0.2103	>0.9999/>0.9999/>0.9999/>0.9999
Pitch slope		0.3638	F(1,239)=0.8278	>0.9999/>0.9999/>0.9999/>0.9999
Sound pressure		**0.0444**	F(1,239)=4.083	>0.9999/0.8063/>0.9999/0.8042

Other than call number, USV features were only computed for pups emitting at least 10 calls during the recording session. (*) For one pup at one time point, call number equaled bout number, resulting in a null value for pause duration and decreasing the n for pause duration by 1.

NEONATAL DEVELOPMENT

P4 control	22
P4 *Foxp2* cKO	23
P7 control	21
P7 *Foxp2* cKO	18
P10 control	22
P10 *Foxp2* cKO	23
P14 control	22
P14 *Foxp2* cKO	23

Control vs. cKO	Two-way ANOVA		Bonferroni P4/P7/P10/P14
Neonatal Mass	0.7915	F(1,166)=0.0701	>0.9999/>0.9999/>0.9999/>0.9999
Righting reflex	0.3585	F(1,166)=0.8479	0.6433/>0.9999/>0.9999/>0.9999
Negative geotaxis	0.4198	F(1,166)=0.6541	>0.9999/0.4304/>0.9999/>0.9999

Table 3.3 *Results and statistics for IHC analyses.*

IHC Test	n	p-value	F	Multiple Comparisons
CORTICAL LAYERING ANALYSES				
Control	3			
Foxp2 cKO	3			
Control vs. *Foxp2* cKO		Unpaired t-test		
DAPI-based layer thickness				
L1		0.0939		
L2-4		0.1217		
L5		0.9781		
L6		0.6423		
Marker-based layer thickness				
CUX1 (L2-4)		0.3344		
CTIP2 (L5b)		0.2736		
TBR1 (L6)		0.7221		
TDTOMATO+ CELL COUNTS BY LAYER				
D1Tom control	2			
D1Tom *Foxp2* cKO	3			
Control vs. *Foxp2* cKO		Two-way ANOVA		Bonferroni's multiple comparisons test
				L1/L2-3/L5/L6
Percentage of cells tdTomato+		**<0.0001**	F (1,12) = 95.02	0.4232/0.1298/**0.0003**/**<0.0001**
SP9+TDTOMATO+ CELL COUNTS				
D1Tom control	4			
D1Tom *Foxp2* cKO	3			
Control vs. *Foxp2* cKO		Unpaired t-test		
Percentage of cells SP9+		**0.0230**		
Percentage of cells SP9+tdTomato+		**>0.0001**		
Percentage of cells SP9+tdTomato-		0.2356		
β-ACTIN AND β-TUBULIN FLUORESCENCE				

IHC Test	n	p-value	F	Multiple Comparisons
Control	3			
Foxp2 cKO	3			
Control vs. *Foxp2* cKO		Two-way ANOVA		Bonferroni's multiple comparisons test
				Bin 1/2/3/4/5/6/7/8/9/10
β-actin fluorescence		**<0.0001**	F (1, 40) = 23.07	All bins >0.9999
β-tubulin fluorescence		**0.0092**	F (1, 40) = 7.492	0.9336/0.7854/>0.9999/>0.9999/>0.9999/ 0.7352/>0.9999/>0.9999/>0.9999/>0.9999

Table 3.4 *Foxp2, tdTomato, and TLE4 overlaps in P7 mPFC L5 and L6.*

	Layer 5			**Layer 6**		
	CTL	**CKO**	**Pval**	**CTL**	**CKO**	**Pval**
% cells Foxp2+	14 ± 1.1	-	-	52 ± 3.3	-	-
% cells tdTom+	33 ± 3.2	14 ± 2.8	**0.0213**	66 ± 3.9	25 ± 1.5	**0.0014**
% cells TLE4+	8.8 ± 1.7	8.3 ± 0.7	0.7605	35 ± 1.7	32 ± 2.4	0.4326
% Foxp2+ also tdTom+	63 ± 1.4	-	-	99 ± 1.1	-	-
% Foxp2+ also TLE4+	38 ± 3.5	-	-	62 ± 0.2	-	-
% tdTom+ also Foxp2+	28 ± 5.3	-	-	79 ± 0.7	-	-
% tdTom+ also TLE4+	28 ± 8.0	19 ± 1.8	0.2504	53 ± 1.1	53 ± 3.6	0.9069
% TLE4+ also Foxp2+	62 ± 2.1	-	-	93 ± 1.6	-	-
% TLE4+ also tdTom+	100 ± 0	30 ± 6.4	**0.0034**	99 ± 0.8	41 ± 3.2	**0.0008**
% TLE4+ also Foxp2+tdTom+	62 ± 2.1	-	-	92 ± 0.8	-	-

Data are represented as means±SEM. Genotypes were compared using t-tests. *n* = 2-3 per condition.

Table 3.5 *Pseudo-bulk RNA-seq DEGs between control and cKO Drd1a-tdTomato neurons.*

Gene	Avg_LogFC	Adj_Pval
Abhd2	-0.4558	6.25E-23
Actb	-0.9371	1.70E-17
Actr2	-0.2650	9.58E-17
Atp1a2	0.3126	0.0251
Bend6	-0.2712	2.28E-21
Bhlhe22	-0.2828	1.61E-08
Btg1	0.6583	4.19E-07
Ccdc85c	-0.3320	1.44E-29
Ccnd2	0.6580	0.0079
Cdca7	0.2634	6.13E-16
Clasp2	-0.4104	1.04E-18
Cnih2	-0.2937	8.63E-27
Cpe	0.2745	1.44E-08
Cplx2	-0.2935	1.45E-13
Crmp1	-0.2607	6.30E-20
Dbi	0.2857	8.67E-06
Dlx1	0.3133	8.44E-09
Dlx2	0.4330	1.82E-11
Dlx5	0.3008	1.04E-09
Dpysl2	-0.3689	1.39E-24
Drd1	-0.3119	6.17E-22
Eif1b	-0.3331	9.06E-10
Enc1	-0.3396	7.69E-15
Fam81a	-0.2650	3.48E-16
Fos	-0.3205	7.55E-10
Gap43	-0.2546	5.26E-20
Gas7	-0.3159	1.42E-18
Gatad1	-0.3094	3.63E-15
Gm17669	0.2554	1.79E-10
Gnb1	-0.4722	3.68E-18
Gng2	-0.2661	1.89E-19
Gsk3b	-0.2573	6.80E-09
H2afv	0.4376	1.77E-05
Hist1h2ap	0.6927	0.0036
Hmgb2	0.5186	0.0045
Id4	0.3675	1.42E-10
Igfbpl1	0.7819	2.26E-15
Insig1	-0.3458	4.07E-19
Kdelr2	-0.3130	1.65E-15
Kdm6b	-0.2858	2.39E-12
Map1b	-0.2601	9.88E-27
Mdk	0.2639	0.0028

Gene	Avg_LogFC	Adj_Pval
Mllt11	-0.2603	2.44E-24
Mt1	0.3111	0.0069
Mt3	0.3850	5.67E-06
Ncam1	-0.4619	8.00E-28
Neurod2	-0.3570	5.28E-23
Neurod6	-0.4121	1.92E-18
Nrgn	-0.2813	1.70E-06
Nrxn3	0.2956	3.39E-11
Paip1	-0.3219	1.00E-12
Pam	-0.3057	2.64E-13
Pax6	0.3051	4.31E-15
Pbx3	0.4423	1.96E-16
Pclaf	0.3802	0.0007
Plpp3	0.2756	0.0022
Pnisr	0.2778	2.02E-06
Ppp1r14c	-0.2746	3.25E-16
Ppp1r1b	-0.2604	1.11E-07
Ppp6r2	-0.3356	5.05E-17
Qk	0.3933	3.74E-12
RP23-35N23.2	-0.3144	5.26E-17
RP24-158L15.1	-0.2916	6.46E-27
Rpgrip1	-0.4623	3.23E-28
Rprm	-0.3533	8.70E-13
S100a16	0.2659	3.25E-05
Sfxn1	-0.5041	5.35E-94
Slc1a3	0.5095	0.0184
Slc22a15	0.4495	6.49E-24
Slc24a5	-0.2605	1.72E-11
Slc39a1	-0.2560	5.85E-10
Snca	-0.3193	3.09E-21
Sp8	0.2702	9.63E-08
Sp9	0.3548	4.29E-14
Spry2	-0.3366	5.65E-08
Srpk1	0.4567	2.37E-27
St13	-0.3112	1.61E-16
Supt16	-0.2894	1.67E-12
Synpr	0.3205	0.0215
Tmpo	0.2722	1.48E-07
Tshz1	0.3872	8.30E-10
Wtap	-0.3002	1.38E-12
Zbtb20	0.2712	0.0171

Table 3.6 *Pseudo-bulk RNA-seq DEGs by cell type between control and cKO Drd1a-tdTomato neurons.*

Gene	Avg LogFC	Adj Pval	Cell Type
Bcas2	-0.9117	5.63E-17	L6 CTh
Eef1a1	-0.4239	2.74E-05	L6 CTh
Eif1	-0.5897	0.0002	L6 CTh
Fam177a	-0.5215	0.0010	L6 CTh
Foxp2	-0.4464	0.0041	L6 CTh
Hmgb1	-0.4162	0.0086	L6 CTh
Isca1	-0.5083	0.0139	L6 CTh
Marcksl1	-0.7087	0.0214	L6 CTh
Mrfap1	-0.4912	0.0293	L6 CTh
Ppp1r1b	-0.3984	0.0322	L6 CTh
Sfxn1	-0.4481	0.0372	L6 CTh
Sfxn1	-0.7653	7.49E-09	L5 NP
Actb	-1.2528	3.69E-20	L2/3 IT
Actr2	-0.5225	7.70E-06	L2/3 IT
Cd24a	-0.6636	1.62E-05	L2/3 IT
Cnih2	-0.4018	6.38E-05	L2/3 IT
Cpe	-0.3996	0.0002	L2/3 IT
Dpysl2	-0.5910	0.0004	L2/3 IT
Eef1a1	-0.5557	0.0008	L2/3 IT
Enc1	-0.8880	0.0009	L2/3 IT
Ftl1	-0.5333	0.0012	L2/3 IT
Gas7	0.6414	0.0017	L2/3 IT
Gnb1	-1.3803	0.0027	L2/3 IT
Gprin1	-0.4185	0.0056	L2/3 IT
Hnrnpa1	-0.4145	0.0072	L2/3 IT
Map1b	-0.4477	0.0076	L2/3 IT
Marcksl1	-0.4525	0.0090	L2/3 IT
Mllt11	-0.4657	0.0111	L2/3 IT
Mtss1	-0.4549	0.0143	L2/3 IT
Pabpc1	-0.3600	0.0152	L2/3 IT
Ralyl	-0.4817	0.0195	L2/3 IT
RP24-158L15.1	-0.4420	0.0198	L2/3 IT
Rpl9	-0.4051	0.0225	L2/3 IT
Rps2	-0.2964	0.0262	L2/3 IT
Rps27a	-0.4576	0.0285	L2/3 IT
Sfxn1	-0.4161	0.0308	L2/3 IT
Shtn1	-0.4590	0.0346	L2/3 IT
Sox11	-0.3800	0.0463	L2/3 IT

Gene	Avg LogFC	Adj Pval	Cell Type
Nrgn	-0.3267	0.0014	L2-5 IT
Nudt4	-0.3837	0.0017	L2-5 IT
Pafah1b1	-0.3008	0.0019	L2-5 IT
Paip1	-0.3456	0.0021	L2-5 IT
Pgm2l1	-0.4324	0.0022	L2-5 IT
Pkig	-0.4103	0.0023	L2-5 IT
Polr1d	-0.3767	0.0025	L2-5 IT
Ppp1r14b	-0.4203	0.0030	L2-5 IT
Ppp1r14c	-0.3658	0.0035	L2-5 IT
Ppp1r1a	-0.4071	0.0038	L2-5 IT
Ppp6r2	-0.2985	0.0039	L2-5 IT
Prr7	-0.4103	0.0039	L2-5 IT
Prrxl1	-0.4955	0.0039	L2-5 IT
Ptges3	-0.3349	0.0040	L2-5 IT
Rala	-0.3425	0.0041	L2-5 IT
Rap2b	-0.3400	0.0041	L2-5 IT
RP23-35N23.2	-0.3227	0.0042	L2-5 IT
RP23-440D19.2	-0.2980	0.0045	L2-5 IT
RP24-158L15.1	-0.4302	0.0057	L2-5 IT
Rpl12	-0.3410	0.0064	L2-5 IT
Rpl14	-0.2616	0.0065	L2-5 IT
Rpl17	0.5726	0.0067	L2-5 IT
Rpl21	-0.3143	0.0075	L2-5 IT
Rpl3	-0.3930	0.0091	L2-5 IT
Rpl4	-0.3417	0.0093	L2-5 IT
Rpl6	-0.3158	0.0096	L2-5 IT
Rpl8	-0.3038	0.0097	L2-5 IT
Rpl9	-0.3056	0.0101	L2-5 IT
Rplp0	-0.2818	0.0107	L2-5 IT
Rprm	-0.3361	0.0113	L2-5 IT
Rps14	-0.3991	0.0118	L2-5 IT
Rps19	-0.3158	0.0132	L2-5 IT
Rps2	-0.3153	0.0140	L2-5 IT
Rps3a1	-0.3687	0.0144	L2-5 IT
Rps7	-0.4192	0.0146	L2-5 IT
Rpsa	-0.3201	0.0146	L2-5 IT
Sepw1	-0.3755	0.0155	L2-5 IT
Serf1	-0.3735	0.0168	L2-5 IT

Gene	Avg LogFC	Adj Pval	Cell Type
Srrm2	-0.4252	0.0485	L2/3 IT
Tubb5	-0.4630	0.0490	L2/3 IT
Abhd2	-0.9501	1.85E-27	L2-5 IT
Actb	-0.5092	1.80E-11	L2-5 IT
Actr2	-0.5149	5.59E-10	L2-5 IT
Arhgap35	-0.4255	9.02E-10	L2-5 IT
Atxn7l3b	-0.4479	3.69E-09	L2-5 IT
Basp1	-0.7240	1.94E-08	L2-5 IT
Bend6	-0.4628	2.59E-07	L2-5 IT
Calm1	-0.4459	7.31E-07	L2-5 IT
Camk2n2	-0.5409	1.26E-06	L2-5 IT
Ccdc85c	-0.5829	2.19E-06	L2-5 IT
Cdk5r1	-0.5190	2.39E-06	L2-5 IT
Cdv3	-0.4739	2.92E-06	L2-5 IT
Cib2	-0.8555	3.25E-06	L2-5 IT
Clasp2	-1.3261	4.59E-06	L2-5 IT
Cnih2	-0.5011	4.60E-06	L2-5 IT
Cops9	-0.3886	4.66E-06	L2-5 IT
Crmp1	-0.5828	7.64E-06	L2-5 IT
Csnk2a1	-0.5083	8.91E-06	L2-5 IT
Ctxn1	-0.3860	1.18E-05	L2-5 IT
Dctn4	-0.4095	2.20E-05	L2-5 IT
Dpf1	-0.3956	2.45E-05	L2-5 IT
Dpysl2	0.3436	3.02E-05	L2-5 IT
Dpysl3	-0.4420	3.39E-05	L2-5 IT
Drd1	-0.6084	6.01E-05	L2-5 IT
Eef1a1	-0.4555	7.30E-05	L2-5 IT
Enc1	-0.4476	9.08E-05	L2-5 IT
Fam174a	-0.3988	9.56E-05	L2-5 IT
Fam81a	-0.4003	9.57E-05	L2-5 IT
Fth1	-0.3632	0.0001	L2-5 IT
Ftl1	-0.4203	0.0001	L2-5 IT
Gatad1	-0.3895	0.0002	L2-5 IT
Gnb1	-0.5688	0.0002	L2-5 IT
Gnb2l1	-0.4463	0.0002	L2-5 IT
Gng2	-0.3512	0.0002	L2-5 IT
Gsk3b	-0.3844	0.0002	L2-5 IT
Hmgcs1	-0.5733	0.0002	L2-5 IT
Hsp90ab1	-0.4355	0.0003	L2-5 IT
Klhl9	-0.3371	0.0003	L2-5 IT
Map1b	-0.3323	0.0004	L2-5 IT
Mapre2	-0.4363	0.0004	L2-5 IT
Mapt	-0.4203	0.0004	L2-5 IT

Gene	Avg LogFC	Adj Pval	Cell Type
Serp2	-0.3258	0.0175	L2-5 IT
Set	-0.2875	0.0176	L2-5 IT
Sfxn1	-0.3555	0.0184	L2-5 IT
Skil	-0.3357	0.0201	L2-5 IT
Skp1a	-0.2723	0.0213	L2-5 IT
Slc24a5	-0.3741	0.0219	L2-5 IT
Smap1	-0.3385	0.0221	L2-5 IT
Snca	-0.4246	0.0251	L2-5 IT
Snn	-0.3403	0.0277	L2-5 IT
Spin1	-0.3160	0.0329	L2-5 IT
Sprn	-0.2544	0.0343	L2-5 IT
Srpk1	-0.3766	0.0349	L2-5 IT
St13	-0.3017	0.0357	L2-5 IT
Suds3	-0.3744	0.0364	L2-5 IT
Svbp	-0.2943	0.0366	L2-5 IT
Taok3	-0.2841	0.0366	L2-5 IT
Tmsb10	-0.3361	0.0391	L2-5 IT
Tubb5	-0.3611	0.0420	L2-5 IT
Tusc2	-0.2818	0.0422	L2-5 IT
Ybx1	-0.3017	0.0430	L2-5 IT
Ythdf2	-0.4054	0.0461	L2-5 IT
Ywhaz	-0.2650	0.0471	L2-5 IT
Drd1	-1.0379	2.51E-08	L6 IT
Dynlt1a	-0.7675	0.0011	L6 IT
Fth1	-0.7450	0.0039	L6 IT
Ftl1	-0.5341	0.0079	L6 IT
Ptms	-0.7145	0.0101	L6 IT
RP24-158L15.1	-0.5271	0.0107	L6 IT
Sfxn1	-0.5948	0.0110	L6 IT
Svbp	-0.7443	0.0125	L6 IT
Taok3	-0.6603	0.0238	L6 IT
Yaf2	-0.5819	0.0278	L6 IT
Fam177a	0.3546	1.51E-05	5HT3R INT
Fos	0.4495	0.0003	5HT3R INT
Prrxl1	-0.2954	0.0010	5HT3R INT
Slc22a15	-0.5504	0.0034	5HT3R INT
Fos	0.7396	3.29E-06	LAMP5 INT
Slc22a15	-0.9139	0.0036	LAMP5 INT
Srpk1	0.5025	0.0470	LAMP5 INT
Cnih2	0.9231	0.0025	SST INT
Cwc15	-0.7406	0.0026	SST INT
Dda1	-0.5317	0.0027	SST INT
Eapp	1.1095	0.0055	SST INT

Gene	Avg LogFC	Adj Pval	Cell Type
Marcksl1	-0.5184	0.0004	L2-5 IT
Mettl9	-0.4308	0.0004	L2-5 IT
Mllt11	-0.3565	0.0006	L2-5 IT
Mmd	-0.3867	0.0009	L2-5 IT
Mrpl30	-0.4360	0.0010	L2-5 IT
Mtpn	-0.3382	0.0011	L2-5 IT
Ncam1	-0.3851	0.0011	L2-5 IT
Neurod6	-0.2722	0.0013	L2-5 IT

Gene	Avg LogFC	Adj Pval	Cell Type
Gap43	-1.3410	0.0086	SST INT
Gng3	-0.5682	0.0089	SST INT
Mien1	-0.4985	0.0149	SST INT
Npy	-0.5018	0.0163	SST INT
Rsrp1	-0.6074	0.0190	SST INT
Sepw1	-0.4355	0.0252	SST INT
Srpk1	-0.5740	0.0332	SST INT
Tmsb10	-0.5281	0.0469	SST INT

CTh: corticothalamic, INT: interneuron, IT: intratelencephalic, L: layer, NP: near-projecting.

Table 3.7 *Pseudo-bulk RNA-seq DEGs between control and cKO golli-τ-eGFP neurons.*

Gene	Avg LogFC	Adj Pval
Actb	-0.6382	0.0002
Adcy1	-0.3723	0.0004
Adgrl1	-0.4172	0.0229
Ank2	-0.3636	0.0139
Apoe	0.3895	0.0011
Arf3	-0.3607	2.82E-05
Atp2a2	-0.5065	0.0223
Camk2a	-0.4312	0.0020
Camk4	-0.3857	0.0032
Cfl1	0.2729	2.27E-05
Cirbp	0.4558	0.0331
Clasp2	-0.6944	0.0002
Cox5a	0.3672	0.0002
Cst3	0.4632	6.58E-05
Dbi	0.3544	7.25E-05
Dclk1	-0.3690	0.0018
Dlg4	-0.4288	3.29E-05
Dynlrb1	0.2989	0.0194
Erh	0.3950	9.05E-06
Fabp5	0.5228	1.72E-10
Fabp7	0.5613	2.20E-12
Gm9493	-0.4205	1.53E-10
Gnb1	-0.5672	1.92E-06
Gpm6a	-0.3387	0.0001
H3f3a	0.4253	3.25E-05
Hint1	0.2927	0.0041
Iqsec1	-0.3124	0.0230
Map2	-0.3132	0.0188
Mif	0.3552	8.44E-06
Mt2	0.4523	4.73E-05
Ndufs7	0.3989	0.0459
Ndufs8	0.3888	0.0457
Nipsnap3b	0.4837	0.0031
Pcp4	-0.7507	1.56E-06
Pfn1	0.4119	0.0010
Pgm2l1	-0.4116	0.0001
Ppia	0.4663	1.35E-15
Prkcb	-0.4181	0.0028
Psmb6	0.4060	0.0249
Scd2	-0.3202	0.0318
Sdhb	0.4452	8.34E-05
Slc1a2	-0.3901	0.0002
Stmn1	0.3781	1.38E-08
Sv2b	-0.3139	0.0412
Syt1	-0.4749	0.0010
Tle4	-0.4799	0.0356
Ubb	0.2660	0.0025

CHAPTER FOUR: Molecular characterizations of FoxP2-TBR1 interaction

Abstract

Mutations of the forkhead transcription factor FOXP2 are associated with neurodevelopmental disorders, including speech and language disorder and autism spectrum disorder (ASD). In vitro studies have shown that FOXP2 interacts with TBR1, a high-confidence ASD transcription factor, and they colocalize in cortical layer 6, suggesting that they may coregulate gene expression within this brain region. However, their interaction has not been confirmed in vivo, nor have any of their coregulated gene targets been identified. Here, I confirm their interaction in mouse cortex using nanoscale-resolution microscopy, and I identify genes synergistically regulated by FOXP2 and TBR1 in neural cell lines. I also characterize TBR1-interacting residues of FOXP2 through deletion mutagenesis studies. These results highlight candidate gene targets of FOXP2-TBR1 interaction and further our understanding of its roles in cortical development.

Introduction

Mutations of the forkhead transcription factor FOXP2 have long been known to cause a severe developmental speech and language disorder (Lai et al., 2001; Morgan et al., 2017). Recently, *FOXP2* has also been associated with autism spectrum disorder (ASD) in the largest exome sequencing study of this disorder to date (Satterstrom et al., 2019). Given the core phenotype of communication deficits in ASD, study of molecular

and cellular functions of FOXP2 can inform our understanding of the etiology of neurodevelopmental disorders affecting language.

Protein interactors, gene targets, and neural expression patterns of FoxP2 strengthen its ties to ASD. For example, FOXP2 directly interacts with several proteins associated with syndromic forms of ASD, including NR2F1, NR2F2, SATB2, SOX5, YY1, and its paralog FOXP1 (Estruch et al., 2018). FOXP2 has also been shown to directly regulate ASD risk genes *CNTNAP2*, *MET*, *DISC1*, and *MEF2C* (Chen et al., 2016; Mukamel et al., 2011; Vernes et al., 2008; Walker et al., 2012). In the brain, Foxp2 is highly expressed in select cell types that show enrichment of ASD-associated genes, including striatal spiny projection neurons, cerebellar Purkinje cells, and cortical deep-layer projection neurons (Chang et al., 2015; Clifford et al., 2019; Coe et al., 2019; Ferland et al., 2003; Takata et al., 2018; Willsey et al., 2013). Thus, within these cell types, FOXP2 and its cofactors may be driving gene expression networks vulnerable to disruption in ASD.

Within one of these cell types, layer 6 corticothalamic projection neurons, FOXP2 colocalizes with TBR1, one of the most recurrently mutated transcription factors in ASD (De Rubeis et al., 2014; Hisaoka et al., 2010; Iossifov et al., 2014; O'Roak et al., 2012; Sanders et al., 2015; Satterstrom et al., 2019). Their colocalization has been observed during human mid-fetal cortical development, a critical time point for the etiology of ASD (Willsey et al., 2013). Additionally, FOXP2 and TBR1 have been shown to directly interact in cultured cells overexpressing these factors (Deriziotis et al., 2014). Together these studies suggest that FOXP2 and TBR1 may interact in the developing cortex to coregulate

gene expression. In this chapter, I describe efforts to confirm their interaction in vivo and identify their coregulated gene targets in neural cells. Furthermore, I characterized a potential TBR1-interacting region of the FOXP2 protein. These studies of FoxP2-TBR1 interaction represent steps forward in disentangling the molecular networks underlying ASD and other language-disrupting disorders.

Results and Discussion

Foxp2 and TBR1 follow similar expression patterns over mouse cortical development

To compare the developmental trajectories of Foxp2 and TBR1 in the mouse cortex, I immunoblotted for the two proteins from embryonic day (E) 15 to postnatal day (P) 21 (**Fig. 4.1A**). I found a peak of expression for both proteins at E17 and a progressive decrease into postnatal development (**Fig. 4.1B**). This decline in expression may be reflective of the expansion of the cortex over development, and thus a decreasing proportion of Foxp2+TBR1+ neurons relative to other cells in the cortex. Nonetheless, this result shows that both of these transcription factors are abundant in embryonic cortex. Next, I examined their colocalization in deep-layer lateral prefrontal cortex (lPFC) from embryonic to postnatal time points (**Fig. 4.1C**). At all stages I observed Foxp2+TBR1+ and Foxp2-TBR1+ populations in layer (L) 6, and the proportion of TBR1+ neurons expressing Foxp2 was highest at E15 (**Fig. 4.1D**). Taken together these results show similar developmental trajectories and high coexpression of Foxp2 and TBR1 in the cortex, particularly during embryonic development.

Nuclear colocalization of Foxp2 and TBR1 in cortical layer 6

To examine nuclear distribution of Foxp2 and TBR1 proteins in vivo, I used multicolor stimulated emission depletion (STED) microscopy to take high-resolution images of Foxp2 and TBR1 in P7 cortical L6. Using this technique, I was able to visualize clear Foxp2 and TBR1 puncta in the nucleus that cannot be resolved using traditional confocal microscopy (**Fig. 4.1E**). These puncta varied in size, perhaps representing homomers and heteromers of these proteins (**Fig. 4.1E**). The majority of Foxp2 and TBR1 puncta did not overlap, but some colocalized puncta could be observed, suggesting sparse heteromeric Foxp2-TBR1 interactions (**Fig. 4.1E**). This result thus supports in vivo interaction between Foxp2 and TBR1 in cortical L6, and it also reveals the powerful approach of STED microscopy for examining endogenous protein-protein interactions.

Mixed results for endogenous Foxp2-TBR1 interaction by coimmunoprecipitation

Another approach to assess endogenous protein interactions is the coimmunoprecipitation (co-IP) assay. A previous co-IP experiment performed by a former postdoctoral researcher in our laboratory found that Foxp2 could pull down TBR1 in P4 mouse cortical tissue (**Fig. 4.1F**). However, my attempts to replicate this result were unable to show pulldown in either direction, even in lower-layer cortical dissections pooled from multiple P7 mice (**Fig. 4.1G**). One major difference between these experiments is the method of protein detection, where the initial experiment used chemiluminescence while I used fluorescence. While fluorescent methods boast more stable signals, two-color detection, and greater dynamic range for protein quantification, personal communications and this Western blotting guide claim that chemiluminescent methods are more sensitive. Thus, my co-IP Western blots may have lacked the sensitivity to

detect endogenous Foxp2-TBR1 interaction. Moreover, the STED data suggest that at P7, Foxp2-TBR1 interaction events are infrequent, further limiting my ability to detect them by co-IP. It may be informative to perform STED and co-IP experiments at different time points in developing and mature cortex, as Foxp2-TBR1 interaction may occur more frequently in a specific developmental context.

Synergistic gene regulation by FoxP2 and TBR1 in neural cells

To identify candidate coregulated targets of Foxp2 and TBR1, I overlapped lists of their targets identified from chromatin immunoprecipitation (ChIP) assays and knockout (KO) mouse gene expression studies (Bedogni et al., 2010; Han et al., 2011; Huang et al., 2014; Notwell et al., 2016; Vernes et al., 2011) (**Table 4.1**). Interestingly, the gene appearing most often in these lists is *Ppp1r1b*, which encodes the dopamine D1 receptor effector DARPP-32. This gene is downregulated in both *Foxp2* KO and *Tbr1* KO brains and is coexpressed in L6 corticothalamic neurons with Foxp2 (Hisaoka et al., 2010). Other robust targets include membrane and extracellular proteins (*Cck, Cdh8, Flrt3, Nrgn, Nrn1, Ntng1*) and transcription factors (*Nfe2l3, Nfia, Sox5*), suggesting roles for Foxp2-TBR1 interaction in cell-cell signaling and regulation of transcription.

To test coregulation of these gene targets by Foxp2-TBR1 interaction, I overexpressed FOXP2, TBR1, or both proteins in neural cell lines and performed quantitative reverse transcription PCR (qRT-PCR) for selected candidate targets. Among mouse Neuro2a neuroblastoma cells and two lines of human neural progenitors (hNPs), endogenous expression of these candidate gene targets varied, as would be expected given their differences in cell type and cell state (**Fig. 4.2A-C**). Furthermore, depending

on the cell line, FOXP2 and FOXP2-TBR1 overexpression produced different effects, such as >2-fold activation of *Cnot* and *Flrt3* in Neuro2a cells but negligible effects in hNP line 062409 (**Fig. 4.2A-B**). This could reflect differences in chromatin state and cofactors among these cell lines that would affect gene regulation by FOXP2 and/or TBR1. In Neuro2a cells, some genes (*Bach1*, *Cnot4*, *Kcnh3*, *Rhobtb3*) showed synergistic coactivation by FOXP2-TBR1 (**Fig. 4.2A**). Between the two hNP lines, OF4106 showed more instances of synergistic gene regulation by FOXP2-TBR1, such as coactivation of *FLRT3* and *PPP1R1B* (**Fig. 4.2B-C**). Two genes (*CDH8* and *SYT6*) were repressed by FOXP2 and TBR1 separately but showed no expression changes in the presence of both transcription factors (**Fig. 4.2C**). This could indicate that FOXP2 homodimers and TBR1 homodimers separately repress these genes, but when coexpressed they form FOXP2-TBR1 heteromers and regulate a separate set of genes. Taken together these results suggest cell line-specific gene coregulation by FOXP2-TBR1 interaction. Performing these studies in cortical progenitors, which have chromatin states and cofactors relevant to FOXP2-TBR1 molecular functions, would facilitate identification of their endogenous coregulated targets.

To elucidate the molecular mechanism by which FOXP2 and TBR1 could coregulate gene expression, I performed dual-luciferase assays to determine whether TBR1 alters FOXP2's ability to repress transactivation of a luciferase reporter containing a canonical FOXP2 motif. Overexpression of FOXP2 alone caused repression of the reporter, while overexpression of a non-homodimerizing mutant FOXP2ΔE400 had no effect, as expected (Li et al., 2004) (**Fig. 4.2D**). However, there was no effect of

coexpression with TBR1 or TBR1-Q418R, a mutant lacking ability to bind FOXP2 (Deriziotis et al., 2014). This result rules out a mechanism of FOXP2-TBR1 gene coregulation where FOXP2 binds to a canonical DNA motif while TBR1 binds to FOXP2 but not DNA.

Reduced pulldown of TBR1 by FOXP2 deletion mutants

To identify the TBR1-interacting residue(s) of FOXP2, I performed deletion mutagenesis on *FOXP2* based on previous studies of its interaction domain. A yeast two-hybrid screen using amino acids 122-382 of FOXP2 as bait found interaction with TBR1, and a later study using FOXP2 truncation mutants further narrowed this interaction domain to amino acids 122-258 (Deriziotis et al., 2014; Sakai et al., 2011). This region contains two polyglutamine tracts, but deletion of these did not affect interaction with TBR1 (Deriziotis et al., 2014). Thus, I generated five deletion mutants of FOXP2 to further narrow down the TBR1-interacting residue(s): Δ122-258, Δ122-149 (ΔA), 215-236 (ΔB), 237-258 (ΔC), and 259-382 (ΔD) (**Fig. 4.3A**).

I next performed co-IPs from 293T cells overexpressing TBR1 and each of these FOXP2 deletion mutants. Surprisingly, none of the FOXP2 deletions appeared to ablate interaction with TBR1 (**Fig. 4.3B**). Mutants ΔB and Δ122-258 did show a ~40% reduction in binding to TBR1 based on this assay (**Fig. 4.3B**). To test if these co-IP signals could be artefacts of protein overexpression, I overexpressed Foxp2-V5 with FOXP2ΔE400-FLAG, a non-homodimerizing mutant, and performed co-IPs (Li et al., 2004). Again, I saw an unanticipated interaction between wild-type Foxp2 and its non-homodimerizing form, contrary to published co-IPs between these proteins (**Fig. 4.3C**). This suggests that

protein overexpression in 293T cells may introduce artificial interactions between proteins because of their overabundance. Even so, this would not preclude the possibility that FOXP2-TBR1 binding occurs through multiple contacts distributed across FOXP2, and that deletion of one region is not sufficient to disrupt their interaction. Nonetheless, these experiments show that amino acids 215-236 of FOXP2 at least partially mediate interaction with TBR1.

Altered subcellular localization of TBR1 by FOXP2 deletion mutants

Another approach for testing interaction between proteins is examining their subcellular localization, which can reveal whether a mutant with altered localization also changes the localization of its predicted binding partner. To test this, I overexpressed TBR1 with FOXP2 mutants Δ122-258, ΔA, ΔB, and ΔC, as well as a GFP negative control and FOXP2 WT positive control (**Fig. 4.4A**). In control conditions, TBR1 localized to the nucleus as expected, as did FOXP2 WT (**Fig. 4.4B**). FOXP2 mutants Δ122-258 and ΔA showed some cytoplasmic localization, and this appeared to promote cytoplasmic localization of TBR1 as well, suggesting that this mutant retains binding capability to TBR1 (**Fig. 4.4B**). FOXP2 mutants ΔB and ΔC occasionally showed a punctate staining pattern, which also promoted punctate TBR1 staining, again suggesting that these mutants can bind TBR1 (**Fig. 4.4B**). Thus, similar to the co-IP assays, these results suggest that deletions of residues within 122-258 do not interfere with the ability of FOXP2 to bind TBR1. Interestingly, they also show a role for residues 122-149 in nuclear localization of FOXP2, which is unexpected given that its nuclear localization sequences flank the forkhead domain far from this region (Mizutani et al., 2007). Deletion of these

residues could disrupt protein folding in a manner affecting these distant nuclear localization signals, or it could interfere with binding to a protein that regulates FOXP2 trafficking within the cell. Given that the full FOXP2 protein structure remains to be solved, much remains unknown about the effects of protein deletions on its structure and function.

In this chapter, I have shown evidence for in vivo Foxp2-TBR1 interaction, their gene coregulation in neural cells, and the necessity of certain FOXP2 residues for their proper interaction. While a few experiments were confounded by technical artefacts, overall these results increase our knowledge of molecular properties of FOXP2-TBR1 interaction and inform future studies of their cooperative role in cortical development.

Materials and Methods

Mice

All procedures were approved by the Institutional Animal Care and Use Committee of UT Southwestern. Wild-type C57BL/6J mice were used for all mouse experiments.

Cell cultures and lentivirus production

293T and Neuro2a cells were cultured in high-glucose DMEM containing 4 mM L-glutamine, 10% fetal bovine serum (#10437028, Invitrogen), and 1% antibiotic-antimycotic (#15240-062, Invitrogen) at 37°C under 5% CO_2. Human neural progenitors (hNPs) were cultured as previously described (Konopka et al., 2009) in Neurobasal A medium (#10888-022, Invitrogen) supplemented with 10% BIT (#9500, Stemcell Technologies), 2% antibiotic-antimycotic (#15240-062, Invitrogen), 1% Glutamax (#35050-061, Invitrogen), 10 ng/ml FGF (#100-18B, PeproTech) and 10 ng/ml EGF (#100-15, PeproTech) on polyornithine- (#P3655, Sigma-Aldrich) and fibronectin- (#F1141, Sigma-Aldrich) coated plates incubated at 37°C under 5% CO_2. Cells were half-fed every other day to maintain concentrations of growth factors.

For lentivirus production, lentiviral (4 µg), VSV-G (2 µg), and psPAX2 (2 µg) vectors were transfected into 293T cells using FuGENE 6 Transfection Reagent (#E2691, Promega) according to the manufacturer's instructions. Twenty-four hours after transfection, medium was changed to hNP proliferation media (Neurobasal A with 10% BIT, 2% antibiotic-antimycotic, 1% Glutamax). Forty-eight hours after transfection, viral supernatants were centrifuged, filtered through a 0.45 µm filter, and stored at -80°C in aliquots.

Constructs

The following published constructs were used: pLUGIP-GFP, pLUGIP-FOXP2-3xFLAG (Konopka et al., 2009). The following constructs were generated using the Invitrogen Gateway system from pENTRD (Open Biosystems): pLenti6.4-TBR1-V5, pLenti6.4-Foxp2-V5, pLenti6.4-GFP-V5. The following constructs were generated for this study by site-directed mutagenesis as described below: pLUGIP-FOXP2ΔE400-3xFLAG, pLUGIP-FOXP2Δ122-258-3xFLAG, pLUGIP-FOXP2Δ122-149-3xFLAG, pLUGIP-FOXP2Δ215-236-3xFLAG, pLUGIP-FOXP2Δ237-258-3xFLAG, FOXP2Δ259-382-3xFLAG, pLenti6.4-TBR1-Q418R-V5.

Site-directed mutagenesis was performed with the megaprimer method using PrimeSTAR Max DNA Polymerase (#R045A, TaKaRa Bio). Briefly, primers containing the deletion or substitution were used to generate a megaprimer from a parent template using the following PCR program: 98°C 2 min, 30 x (98°C 10 s, 55°C 5 s, 72°C 10 s), 72°C 7 min. Then the megaprimer was purified and used to mutagenize the parent template using the following PCR program: 98°C 2 min, 30 x (98°C 10 s, 55°C 5 s, 72°C 1 min/kb), 72°C 7 min. Parent templates were digested using DpnI and the remaining mutagenized constructs were used to transform competent cells and proceed with standard plasmid preparations.

Protein extractions, coimmunoprecipitations, Western blotting

For protein extractions from tissue, mouse brain tissue was minced on ice, dounce homogenized in cold RIPA buffer (20 mM Tris–HCl pH 7.4, 150 mM NaCl, 2 mM EDTA, 1% Nonidet P-40, 0.1% sodium deoxycholate, 0.1% SDS, protease inhibitor cocktail,

PMSF), incubated at 4°C for 1 h with rotation, and sonicated in ice water using a Diagenode Bioruptor (high, 10 s ON, 20 s OFF, 5 min × 2). Samples were centrifuged and the supernatant was kept and quantified using a Bradford assay. For the Foxp2-TBR1 cortical expression time course, loading buffer was added, samples were boiled at 95°C for 5 min, and Western blotting was performed as described in Chapter 3 using the following antibodies: goat α-Foxp2 N-16 (#sc-21069, Santa Cruz Biotechnologies, 1:100), mouse α-GAPDH (#MAB374, Millipore, 1:10,000), rabbit α-TBR1 (#ab31940, Abcam, 1:500), species-specific secondary antibodies produced in donkey and conjugated to IRDye 680 or 800 (LI-COR Biosciences, 1:20,000).

For tissue coimmunoprecipitations (co-IPs), lower-layer cortex was dissected from 5 P7 mice and pooled for protein extraction as described above. Dynabeads (#10004D, Life Technologies) were prepared by washes in RIPA buffer. After sonication and centrifugation, the supernatant was pre-cleared with washed Dynabeads for 30 min at 4°C. A 5% input was taken and the sample was divided equally into IgG and antibody IP fractions, which were incubated overnight at 4°C with washed Dynabeads and 4 µg goat IgG (#sc-2028, Santa Cruz Biotechnologies) or 4 µg goat α-Foxp2 N-16 (#sc-21069, Santa Cruz Biotechnologies). The following day, IP fractions were washed in RIPA buffer and eluted in loading buffer. Loading buffer was added to the input fraction, and all samples were boiled at 95°C for 5 min. Western blotting was performed as described in Chapter 3 with the following antibodies: goat α-Foxp2 N-16 (#sc-21069, Santa Cruz Biotechnologies, 1:1000), rabbit α-TBR1 (#ab31940, Abcam, 1:1000), species-specific

secondary antibodies produced in donkey and conjugated to IRDye 680 or 800 (LI-COR Biosciences, 1:20,000).

For 293T co-IPs, cells were transfected with 2.5-3.5 µg of each plasmid (5-7 µg total DNA) using FuGENE 6 Transfection Reagent (#E2691, Promega) according to the manufacturer's instructions. The following combinations were transfected: pLUGIP-FOXP2-3xFLAG + pLenti6.4-GFP-V5, pLUGIP-FOXP2-3xFLAG + pLenti6.4-TBR1-V5, pLUGIP-FOXP2Δ122-258-3xFLAG + pLenti6.4-TBR1-V5, pLUGIP-FOXP2Δ122-149-3xFLAG + pLenti6.4-TBR1-V5, pLUGIP-FOXP2Δ215-236-3xFLAG + pLenti6.4-TBR1-V5, pLUGIP-FOXP2Δ237-258-3xFLAG + pLenti6.4-TBR1-V5, pLUGIP-FOXP2Δ259-382-3xFLAG + pLenti6.4-TBR1-V5. After 48 h, cells were washed and harvested in PBS, centrifuged, resuspended in IP buffer (20 mM Tris pH8.0, 1 mM EDTA pH8.0, 0.1% Triton X-100, 150 mM NaCl, protease inhibitor cocktail), and sonicated in ice water using a Diagenode Bioruptor (medium, 10 s ON, 20 s OFF, 5 min × 2). Dynabeads were prepared by washes in IP buffer. After sonication and centrifugation, the supernatants were pre-cleared with washed Dynabeads for 30 min at 4°C. Then a Bradford assay was performed and equal amounts of protein were used for subsequent IPs. Input fractions of 80 µg were taken, and IP fractions were incubated overnight at 4°C with washed Dynabeads and mouse IgG (#5415S, Cell Signaling Technologies) or mouse α-V5 (#R960-25, Life Technologies). The following day, IP fractions were washed in IP buffer and eluted in loading buffer. Loading buffer was added to the input fractions, and all samples were boiled at 95°C for 5 min. Western blotting was performed as described in Chapter 3 with

the following antibodies: mouse α-FLAG (#F1804, Sigma, 1:10,000), donkey α-mouse IgG IRDye 800 (#926-32212, LI-COR Biosciences, 1:20,000).

Immunostaining and imaging

For examining Foxp2-TBR1 overlaps in mouse cortex with confocal microscopy, immunohistochemistry (IHC) was performed as described in Chapter 3 using the following antibodies: goat α-Foxp2 N-16 (#sc-21069, Santa Cruz Biotechnologies, 1:500), rabbit α-TBR1 (#ab31940, Abcam, 1:1000), donkey α-goat IgG AF488 (#A-11055, Thermo Fisher Scientific, 1:2000), donkey α-rabbit IgG AF555 (#A31572, Thermo Fisher Scientific, 1:2000). Images of lateral prefrontal cortex (lPFC) were acquired using a Zeiss LSM 510 confocal laser scanning microscope at the UT Southwestern Neuroscience Microscopy Facility and processed and analyzed using Zeiss ZEN Lite and FIJI. Cells were counted manually using the FIJI Cell Counter plugin.

For examining Foxp2-TBR1 overlaps with stimulated emission depletion (STED) microscopy, IHC was performed as described in Chapter 3, except that sections were mounted on coverslips, which were then added to slides using Abberior Mount Solid. The following antibodies were used: mouse α-Foxp2 (#MABE415, Millipore, 1:200), rabbit α-TBR1 (#ab31940, Abcam, 1:500), goat α-mouse IgG Abberior STAR 580 (#52403, Sigma, 1:100), goat α-rabbit IgG Abberior STAR RED (#41699, Sigma, 1:100). Frontal cortex nuclei images were acquired during the Abberior Instruments STED Demo at the UT Southwestern Live Cell Imaging Facility. The microscope used was an Olympus IX83 with a 100X 1.4 NA oil immersion objective. The STED excitation wavelengths were 595 nm (1W at 40 MHz) and 775 nm (1.25W at 40 MHz).

For examining FOXP2 mutants and TBR1 in 293T cells, cells were grown on glass coverslips in 24-well plates and transfected with 0.6 µg of each plasmid (1.2 µg total DNA) using FuGENE 6 Transfection Reagent (#E2691, Promega) according to the manufacturer's instructions. The following combinations were transfected: pLUGIP-GFP + pLenti6.4-TBR1-V5, pLUGIP-FOXP2-3xFLAG + pLenti6.4-TBR1-V5, pLUGIP-FOXP2Δ122-258-3xFLAG + pLenti6.4-TBR1-V5, pLUGIP-FOXP2Δ122-149-3xFLAG + pLenti6.4-TBR1-V5, pLUGIP-FOXP2Δ215-236-3xFLAG + pLenti6.4-TBR1-V5, pLUGIP-FOXP2Δ237-258-3xFLAG + pLenti6.4-TBR1-V5. After 24h, PFA was added to the media to a final concentration of 4% and incubated 15 min at room temperature. Coverslips were washed in TBS, permeabilized in 0.4% Triton X-100 in TBS, washed in TBS, blocked in 3% normal donkey serum and 0.2% Triton X-100 in TBS, and incubated in primary antibodies diluted in 1% NDS, 0.2% Triton X-100 in TBS overnight at 4°C. The next day, coverslips were washed in TBS, incubated in secondary antibodies diluted in 0.2% Triton X-100 in TBS with TO-PRO-3 Iodide (#T3605, Thermo Fisher Scientific, 1:1000), washed in TBS, rinsed in ddH_2O, and mounted onto slides using Prolong Gold (#P36931, Thermo Fisher Scientific). The following antibodies were used: mouse α-FLAG (#F1804, Sigma, 1:1000), rabbit α-TBR1 (#ab31940, Abcam, 1:500), donkey α-mouse IgG AF488 (#A21202, Thermo Fisher Scientific, 1:2000), donkey α-rabbit IgG AF555 (#A31572, Thermo Fisher Scientific, 1:2000). Slides were imaged using a Zeiss Observer.Z1 inverted microscope and processed using ZEN 2011 software.

Quantitative reverse transcription PCR

Quantitative reverse transcription PCR (qRT-PCR) was performed as previously described (Araujo et al., 2015). Neuro2a cells were transfected with 2 µg of each plasmid (4 µg total DNA) using Lipofectamine 2000 Transfection Reagent (#11668027, Thermo Fisher Scientific) according to the manufacturer's instructions. hNPs were transduced with lentiviruses. The following combinations were used: pLUGIP-GFP + pLenti6.4-GFP-V5, pLUGIP-FOXP2-3xFLAG + pLenti6.4-GFP-V5, pLenti6.4-TBR1-V5 + pLUGIP-GFP, pLUGIP-FOXP2-3xFLAG + pLenti6.4-TBR1-V5. After 48 h, RNA was extracted using the miRNeasy Mini kit (#217004, Qiagen) according to the manufacturer's instructions. Single-stranded cDNAs were made using DNaseI, Amplification grade (#18068015, Invitrogen) and SuperScript III First-Strand Synthesis SuperMix (#18080400, Invitrogen) and amplified by PCR according to the manufacturer's instructions. qRT-PCR was performed using iTaq Universal SYBR Green Supermix (#172-5121, Bio-Rad Laboratories) and a Touch Real-Time PCR Detection System (CFX384, Bio-Rad Laboratories). Each biological sample had 4 technical replicates for qRT-PCR and each experiment had 3 biological replicates. *18S* rRNA was used as the reference gene for normalization. Data analysis was performed by the ΔΔCq method using CFX Manager software. Conditions were compared using a two-way ANOVA with Tukey's multiple comparisons test.

Dual-luciferase assays

Dual-luciferase assays were performed as previously described (Konopka et al., 2009). 293T cells grown in 96-well plates were transfected with 50 ng of reporter construct expressing *Photinus pyralis* (firefly) luciferase, 1 ng of *Renilla* luciferase plasmid (pRL-

EF), and 25 ng of each expression plasmid (50 ng total) using FuGENE 6 Transfection Reagent (#E2691, Promega) according to the manufacturer's instructions. The canonical FOXP2 binding site (AATTTG in triplicate into pGL4) driving luciferase vector was used (Konopka et al., 2009). The following combinations were transfected: pLUGIP-GFP + pLenti6.4-GFP-V5, pLUGIP-FOXP2-3xFLAG + pLenti6.4-GFP-V5, pLUGIP-FOXP2ΔE400-3xFLAG + pLenti6.4-GFP-V5, pLUGIP-FOXP2-3xFLAG + pLenti6.4-TBR1-V5, pLUGIP-FOXP2-3xFLAG + pLenti6.4-TBR1-Q418R-V5. Forty-eight hours later, cells were lysed and analyzed using the Dual-Luciferase Reporter Assay System (#E1910, Promega) according to the manufacturer's instructions. Co-transfection of *Renilla* luciferase was used for transfection normalization, and values were additionally normalized to GFP-transfected cells. Conditions were compared using a one-way ANOVA with Tukey's multiple comparisons test.

Figures

Figure 4.1 *Foxp2 and TBR1 colocalize and interact in cortical layer 6*

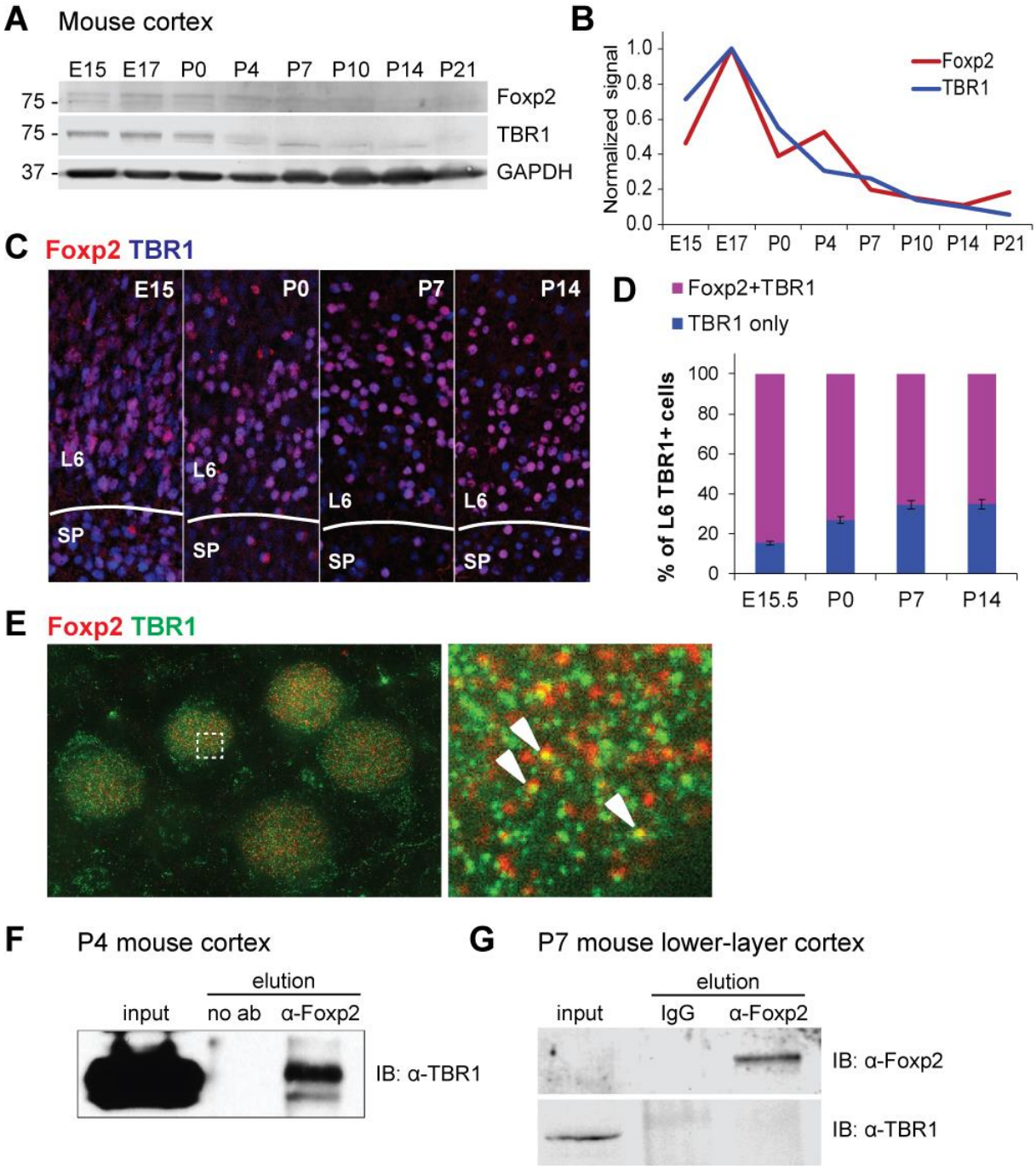

(A) Western blot showing Foxp2 and TBR1 expression over mouse cortical development. (B) Quantification of (A). (C) IHC for Foxp2 and TBR1 in lateral prefrontal cortex (lPFC) over development. L6: layer 6, SP: subplate. (D) Quantification of Foxp2/TBR1 overlaps in lPFC. Data are represented as means (±SEM). n = 3 per condition. (E) Stimulated emission depletion (STED) microscopy of Foxp2 and TBR1 in P7 cortical L6 nuclei. Arrowheads show colocalized puncta. (F) Chemiluminescence-imaged Western blot of co-IP assay from P4 mouse cortical lysate (performed by Noriyoshi Usui). Ab: antibody, IB: immunoblot. (G) Fluorescence-imaged Western blot of co-IP assay from P7 lower-layer cortical lysates pooled from 5 mice.

Figure 4.2 *Synergistic gene regulation by FoxP2 and TBR1 in neural cells at a non-canonical FoxP2 motif*

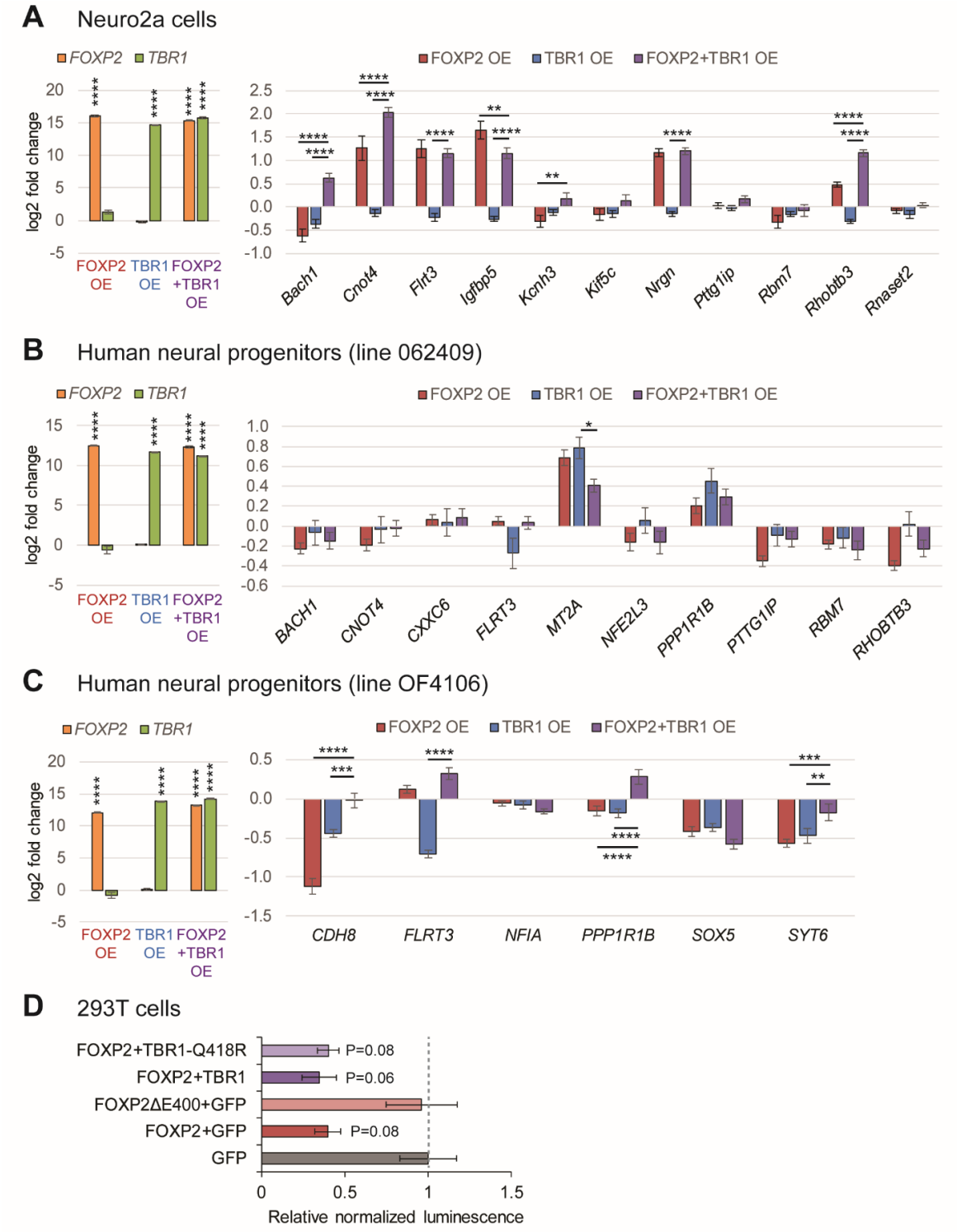

(A-C) Expression of *FoxP2* and *TBR1* (left) and predicted coregulated targets (right) by qRT-PCR in cell lines overexpressing FOXP2, TBR1, or both. Gene expression was normalized to control GFP-overexpressing cells. Data are represented as means (±SEM). Left: (****) $P < 0.0001$ compared to GFP control, t-test. Right: (*) $P < 0.05$, (**) $P < 0.01$, (***) $P < 0.001$, (****) $P < 0.0001$, two-way ANOVA with Tukey's multiple comparisons test. $n = 3$ biological replicates per condition. (A) Gene expression in mouse Neuro2a cells. The following genes were tested but not expressed in these cells: *Bbc3, Cck, Cdh8, Cntnap2, Efnb2, Gad1, Mt2, Neurod6, Nfe2l3, Ntng1, Ppp1r1b, Tcfap2c, Tet1 / Cxxc6, Thy1*. (B) Gene expression in human neural progenitor line 062409. The following genes were tested but not expressed in these cells: *BBC3, CALB, CCK, CDH8, FEZF2, KCNH3, NEUROD6, NRGN, NTNG1*. (C) Gene expression in human neural progenitor line OF4106. The following genes were tested but not expressed in these cells: *CCK, DHRS3, NTNG1*. (D) Dual-luciferase assay for canonical FOXP2 motif transactivation by GFP, FOXP2, FOXP2ΔE400 (non-homodimerizing), TBR1, and/or TBR1-Q418R (non-FOXP2-interacting (Deriziotis et al., 2014)). Data are represented as means (±SEM). One-way ANOVA with Tukey's multiple comparisons test. $n = 2$ per condition.

Figure 4.3 *Reduced pulldown of TBR1 by FOXP2 deletion mutants*

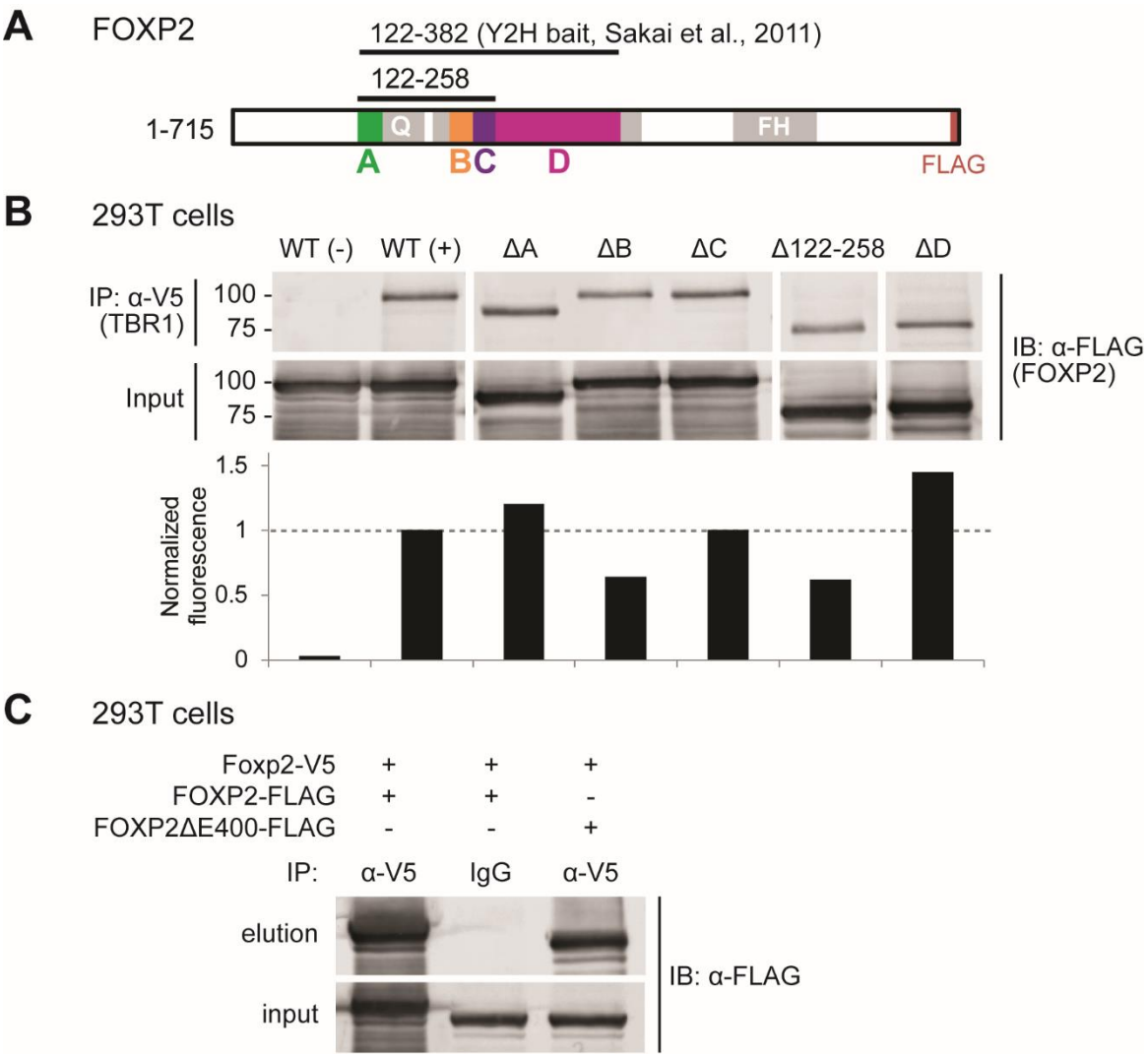

(A) Schematic of FOXP2 protein showing regions deleted by site-directed mutagenesis. FH: forkhead domain, Q: polyglutamine tract, Y2H, yeast two-hybrid. (B) Western blot (top) and quantification (bottom) of co-IP assays between TBR1 and FOXP2 deletion mutants in 293T cells. (-) IgG negative control, (+) positive control. (C) Western blot of co-IP assay between Foxp2 and FOXP2ΔE400, a non-homodimerizing mutant.

Figure 4.4 *Altered subcellular localization of TBR1 by FOXP2 deletion mutants*

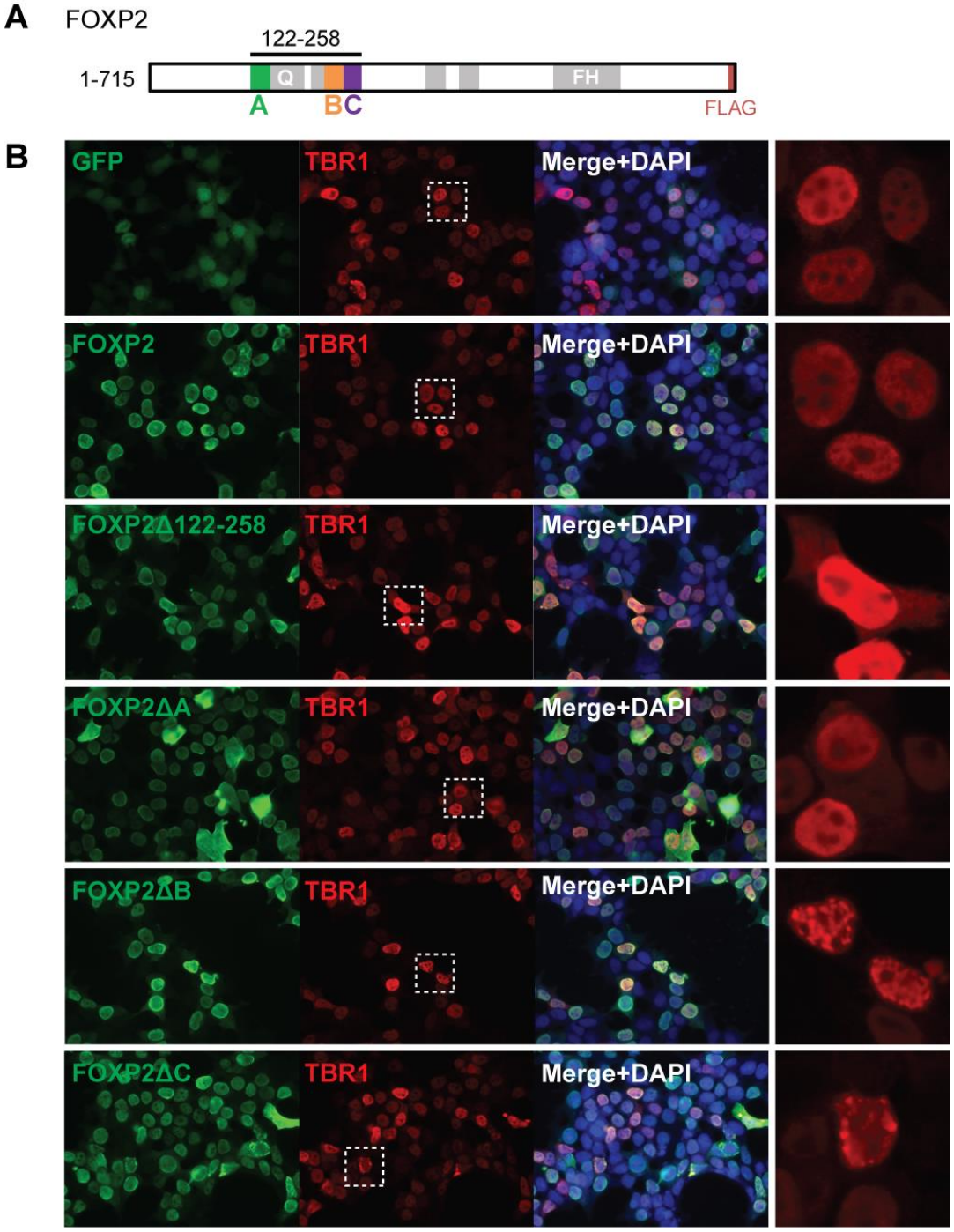

(A) Schematic of FOXP2 protein showing regions deleted by site-directed mutagenesis. FH: forkhead domain, Q: polyglutamine tract. (B) ICC of control GFP, TBR1, and FOXP2 deletion mutants overexpressed in 293T cells.

Tables

Table 4.1 *Candidate Foxp2-TBR1 targets.*

Gene	Refs	Gene	Refs	Gene	Refs
1700037C18Rik	4,5	*Gnai1*	4,5	*Plk2*	4,5
1810032O08Rik	4,5	*Gnal*	4,5	*Plxna2*	1,4,5
1810041L15Rik	4,5	*Gpc6*	4,5	*Pmch*	4,5
2310028H24Rik	1,5	*Gphn*	4,5	*Pou3f4*	1,5
2310044G17Rik	4,5	*Gpm6a*	4,5	*Ppap2b*	4,5
2810403A07Rik	4,5	*Gpr113*	4,5	*Ppp1r1b*	1,2,3,4,5
4930506M07Rik	4,5	*Gpr176*	4,5	*Ppp1r7*	4,5
4930544G11Rik	4,5	*Gpr50*	4,5	*Prcp*	4,5
4933405O20Rik	4,5	*Gpr65*	4,5	*Prdm2*	4,5
6430548M08Rik	4,5	*Grm3*	4,5	*Prdm8*	4,5
Aak1	4,5	*Gsk3b*	4,5	*Prdx1*	1,5
Abca6	1,5	*Gtf3c4*	4,5	*Prickle2*	4,5
Acvr2a	4,5	*Habp2*	4,5	*Prkab1*	4,5
Adamts19	4,5	*Hfe2*	4,5	*Prkce*	4,5
Adcy1	3,4,5	*Hpcal1*	4,5	*Prkrir*	4,5
Akap10	4,5	*Hsd17b3*	4,5	*Prokr2*	1,4,5
Alcam	4,5	*Hsfy2*	4,5	*Prss2*	4,5
Alox12e	4,5	*Htr1a*	4,5	*Psma3*	1,5
Ampd3	4,5	*Igf2bp3*	4,5	*Psmd1*	1,5
Anapc10	4,5	*Igfbp5*	2,4,5	*Psmd12*	1,5
Ap3b1	4,5	*Il12b*	4,5	*Psmd6*	4,5
Arg1	4,5	*Impdh1*	4,5	*Psmd7*	1,4,5
Arhgap28	1,5	*Ina*	4,5	*Ptch1*	4,5
Arid5b	4,5	*Inhba*	4,5	*Ptgfrn*	4,5
Arl11	4,5	*Inhbb*	4,5	*Qk*	4,5
Armc1	4,5	*Insig2*	4,5	*Rab28*	4,5
Arrdc2	4,5	*Irx3*	4,5	*Rab3c*	4,5
Arx	4,5	*Isl1*	4,5	*Rapgef4*	4,5
Ass1	4,5	*Islr2*	4,5	*Rapgef5*	4,5
Atg7	4,5	*Jph3*	4,5	*Rasal1*	4,5
Atpbd4	4,5	*Kbtbd2*	4,5	*Rasgrf1*	1,4,5
Bach1	4,5	*Kcna4*	4,5	*Rasgrp3*	4,5
Baz2b	4,5	*Kcnc4*	2,4,5	*Rbbp6*	4,5
BC043934	4,5	*Kcnh3*	4,5	*Rbm28*	4,5
Bcl2l11	4,5	*Kcnip4*	4,5	*Rbm7*	2,5
Bcl9	4,5	*Kcnmb4*	4,5	*Reps2*	4,5
Blmh	4,5	*Kcnq5*	4,5	*Rgs4*	4,5
Bmp7	4,5	*Kcnu1*	4,5	*Rhof*	4,5

Gene	Refs
Boc	1,4,5
Brd2	4,5
Brd4	4,5
C1qtnf7	4,5
C78339	4,5
Cacna1a	4,5
Cacna2d1	4,5
Cacnb3	4,5
Cald1	4,5
Calm2	4,5
Capza2	4,5
Casq2	4,5
Cbln2	4,5
Cbx6	4,5
Ccdc80	4,5
Ccdc91	4,5
Cck	1,3,4,5
Ccnd2	4,5
Cdh12	4,5
Cdh8	2,3,4,5
Cdk8	4,5
Cdyl2	4,5
Celsr2	4,5
Chaf1a	4,5
Chrna1	4,5
Cit	4,5
Cited2	4,5
Clasp2	4,5
Clcc1	1,5
Clic4	4,5
Cnksr2	4,5
Cnot3	4,5
Cnot4	4,5
Cnr2	1,5
Cobl	4,5
Col23a1	4,5
Col24a1	4,5
Cox7c	4,5
Csmd1	4,5
Cstf2t	4,5
Ctdsp1	4,5
Cul1	4,5

Gene	Refs
Kctd4	4,5
Kctd8	4,5
Klf6	4,5
Large	4,5
Ldb2	4,5
Ldhb	1,5
Lep	4,5
Leprotl1	4,5
Lgals3	4,5
Lipc	4,5
Lmnb1	4,5
Lmo4	4,5
Lnpep	4,5
Lpl	4,5
Lpp	4,5
Lrba	4,5
Lrp6	4,5
Lrrc6	4,5
Lrrn1	4,5
Lrrtm2	1,4,5
Lsg1	4,5
Lsm11	4,5
Ly6h	4,5
Magoh	4,5
Malt1	4,5
Maml3	4,5
Mapk4	4,5
Mapk8	4,5
Mark2	4,5
Mat2b	4,5
Mcph1	4,5
Mllt3	4,5
Mmaa	4,5
Moap1	4,5
Moxd1	4,5
Mpp2	4,5
Mrgprb1	4,5
Mrpl38	4,5
Msrb3	4,5
Mt2	1,2,5
Mtmr2	4,5
Mtpn	4,5

Gene	Refs
Riok1	4,5
Robo2	4,5
Rpe	4,5
Rpl27	4,5
Rpl31	4,5
Rprml	4,5
Rps6ka4	4,5
Rras2	4,5
Rwdd3	4,5
Scfd1	4,5
Scgn	4,5
Scml2	4,5
Scn3b	4,5
Sdccag8	4,5
Sdk1	1,4,5
Sema3a	4,5
Sema4g	4,5
Sema6a	4,5
Sema6d	4,5
Serpina12	4,5
Sfxn4	1,5
Sgol2	4,5
Sh3gl1	4,5
Siae	4,5
Siah2	4,5
Slc12a2	4,5
Slc14a1	4,5
Slc25a36	4,5
Slc2a3	4,5
Slc33a1	4,5
Slc39a10	4,5
Slc41a1	4,5
Slc45a1	1,4,5
Slc4a3	4,5
Slc5a12	4,5
Slc6a7	2,5
Smarcd3	4,5
Sncb	2,4,5
Sox17	4,5
Sox5	1,3,4,5
Spata13	4,5
Spata17	4,5

Gene	Refs
Cwf19l2	4,5
Cxxc4	4,5
Dach1	4,5
Dact1	4,5
Dcun1d4	4,5
Ddhd1	4,5
Ddit4l	4,5
Depdc1a	4,5
Dgat2	4,5
Dhrs3	1,5
Diap2	4,5
Diap3	4,5
Dicer1	4,5
Dlgap1	4,5
Dmrta1	4,5
Dnajc7	4,5
Dnmbp	4,5
Dock8	4,5
Dolpp1	1,5
Dtna	4,5
Ebf2	4,5
Edil3	4,5
Ednrb	4,5
Eef2k	4,5
Efnb2	4,5
Egr1	4,5
Elk3	4,5
Elmod1	4,5
Elovl6	4,5
Elp3	4,5
Emx2	4,5
Epb4.1l5	4,5
Epha6	1,4,5
Epsti1	4,5
Esr1	1,4,5
Etv1	1,4,5
Etv5	4,5
Eya1	4,5
Ezh2	4,5
Fbxl13	4,5
Fbxl4	4,5
Fchsd2	4,5

Gene	Refs
Mtus1	4,5
Mynn	4,5
Myom2	4,5
Myrip	4,5
Nap1l2	1,5
Nap1l5	4,5
Ncald	4,5
Ncam1	4,5
Ndufa8	4,5
Nedd1	4,5
Negr1	4,5
Nell2	4,5
Neurod6	3,4,5
Nfe2l3	1,2,3,4,5
Nfia	1,3,4,5
Nfil3	2,4,5
Ngrn	4,5
Nhp2l1	2,5
Nid1	4,5
Nin	1,4,5
Nnmt	4,5
Noc4l	4,5
Notch2	4,5
Npffr2	4,5
Nploc4	1,5
Nr2f1	4,5
Nrgn	1,3,4,5
Nrn1	1,3,4,5
Nrp2	4,5
Ntn4	4,5
Ntng1	1,3,4,5
Ntrk2	4,5
Ntrk3	4,5
Nuak1	4,5
Nup210	4,5
Olfm4	4,5
Olfr1359	4,5
Olfr1370	4,5
Osbpl5	4,5
Osbpl6	4,5
Oxgr1	4,5
P4ha1	4,5

Gene	Refs
Spesp1	4,5
Sri	4,5
Srl	4,5
Ssu72	4,5
Stam	4,5
Stard4	4,5
Stau2	4,5
Steap1	4,5
Stx7	4,5
Stxbp3a	4,5
Sumf1	4,5
Syt6	1,4,5
Tac1	4,5
Tank	4,5
Tbc1d19	4,5
Tcf12	4,5
Tcf4	4,5
Tcfap2c	3,5
Tdrd3	4,5
Tex21	4,5
Tgfbi	4,5
Tgfbr3	4,5
Thbs2	1,4,5
Thy1	2,4,5
Tlk1	4,5
Tm2d1	4,5
Tm9sf4	4,5
Tmed2	2,5
Tmem104	4,5
Tmem38b	4,5
Tmem55a	4,5
Tnks	4,5
Tpk1	4,5
Tram1l1	4,5
Trex1	4,5
Trib2	4,5
Tssc1	4,5
Twist1	4,5
Twistnb	4,5
Tyrobp	4,5
Ube3a	4,5
Ubl7	4,5

Gene	Refs
Fech	4,5
Fgf1	4,5
Flrt3	1,2,3,4,5
Fnbp1l	4,5
Foxk1	4,5
Foxn2	4,5
Foxo1	4,5
Foxp2	4,5
Fut8	1,4,5
Gabrg1	4,5
Gad1	3,5
Galc	4,5
Ganc	4,5
Gata6	4,5
Gcsh	4,5
Gem	4,5
Gjb6	4,5
Glg1	4,5

Gene	Refs
Pak3	1,5
Palm	4,5
Paqr3	4,5
Paqr7	4,5
Pask	4,5
Pcdh20	4,5
Pclo	4,5
Pdcd10	4,5
Pdhx	4,5
Pdia4	4,5
Pgc	4,5
Pik3r1	1,2,4,5
Pitpnc1	4,5
Pitpnm2	4,5
Pitx2	4,5
Pla2g4a	4,5
Plch2	4,5

Gene	Refs
Ufm1	4,5
Ugt2b35	4,5
Umps	4,5
Unc5c	4,5
Vapb	4,5
Vps37b	4,5
Whrn	1,4,5
Wnt5a	4,5
Ywhah	4,5
Zcchc14	4,5
Zfp148	4,5
Zfp366	4,5
Zfp36l1	4,5
Zfp521	1,4,5
Znrd1	4,5
Znrf2	4,5
Zswim2	4,5

References:

1. (Bedogni et al., 2010)
2. (Han et al., 2011)
3. (Huang et al., 2014)
4. (Notwell et al., 2016)
5. (Vernes et al., 2011)

CHAPTER FIVE: Foxp1 regulation of neonatal vocalizations via cortical development

Published as: Usui, N., Araujo, D.J., Kulkarni, A., **Co, M.**, Ellegood, J., Harper, M., Toriumi, K., Lerch, J.P., and Konopka, G. (2017). Foxp1 regulation of neonatal vocalizations via cortical development. Genes & development *31*, 2039-2055.

Contributions as co-author:

- Microscopy and protein lysate preparation for confirmation of *Foxp1* conditional knockout by *Emx1*-Cre (Figure 1)
- Cortical layering analysis in *Foxp1* conditional knockout mice (Figure 2, Figure S1, Table S1)

CHAPTER SIX: Sumoylation of FOXP2 regulates motor function and vocal communication through Purkinje cell development

Published as: Usui, N., **Co, M.**, Harper, M., Rieger, M.A., Dougherty, J.D., and Konopka, G. (2017). Sumoylation of FOXP2 Regulates Motor Function and Vocal Communication Through Purkinje Cell Development. Biological psychiatry *81*, 220-230.

Contributions as co-author:

- Quantification of neurite outgrowth in mouse neural progenitors after overexpression of FOXP2 WT or KR (Figure S3)
- Quantification of proportion of Purkinje cells electroporated by in utero electroporation (Figure S4)
- Co-immunoprecipitation assays between FOXP2 WT or KR and other FOXP proteins or CTBP (Figure S6)
- Scoring of in vivo subcellular localization of FOXP2 WT and KR (Figure S8)
- Analysis of sex differences in postnatal behaviors after FOXP2 manipulations (Table S2)

CHAPTER SEVEN: Tools and techniques for understanding FoxP function in zebra finch song nuclei

Abstract

As vocal learners, zebra finches are an optimal model system for studying genes involved in language, such as *FoxP2* and *FoxP1*. Corticostriatal regions highly express these genes, making them key sites for studying roles of *FoxP2* and *FoxP1* in vocal learning. While it is known that *FoxP2* knockdown in Area X disrupts song learning and production, the molecular mechanisms underlying this effect are largely unknown. No studies have been carried out on *FoxP1* function in the pallial nucleus HVC, nor are the basic cell types in Area X or HVC well-defined. In this chapter, I describe development and optimization of tools and methods for studying *FoxP2* function in Area X and *FoxP1* function in HVC in a cell type-specific manner. Combining viral knockdown of these genes with single-cell transcriptomics in the zebra finch will greatly advance our understanding of molecular mechanisms important for language.

Introduction

Zebra finches learn their vocalizations during development through a sensorimotor process similar to speech learning, making them an important model system for studying genes involved in speech and language disorders. The autism spectrum disorder (ASD)-associated gene *FoxP1* is highly expressed in the pallial nucleus HVC, while both *FoxP1* and its language-associated paralog *FoxP2* are highly expressed in the striatal nucleus Area X (Mendoza et al., 2015). Projections from HVC to Area X form the corticostriatal

component of the anterior forebrain pathway mediating song learning. Thus, these regions are key sites for studying the roles of FoxP2 and FoxP1 in vocal learning.

FoxP2 knockdown in Area X has been shown to disrupt both vocal learning and production, but the molecular mechanisms by which this occurs are largely unknown (Haesler et al., 2007; Murugan et al., 2013). Even less is known about *FoxP1* functions in the zebra finch brain, but the vocalization deficits in mice lacking cortical *Foxp1* predict a critical role for *FoxP1* in HVC (Araujo et al., 2017; Usui et al., 2017a). Additionally, the cell type compositions of these song nuclei are poorly understood, further inhibiting our understanding of FoxP2 and FoxP1 molecular functions in these regions. To answer these questions, I optimized protocols for generating single-cell transcriptomic datasets from zebra finch brain tissue, and I have collected data from birds with viral knockdown of *FoxP2* in Area X. I also generated viral constructs for knockdown and rescue of *FoxP1*, and experiments using these tools are ongoing to uncover *FoxP1* functions in HVC.

Results and Discussion

Optimization of Area X tissue processing for single-nucleus RNA-seq

High-quality single-cell transcriptomic datasets require optimization of methods for generating single-cell or single-nuclei suspensions. First, we tested a published tissue dissociation method for generating single-cell suspensions on Area X tissue from an adult (~150 days post hatch or DPH) zebra finch (Tasic et al., 2016). Despite trituration and filtering, we saw a high degree of clumping and cellular debris (**Fig. 7.1A**). Also, based

on trypan blue staining, over half of the single cells observed were dead. Thus, this was not a suitable method for generating a single-cell suspension for scRNA-seq.

Next, we turned to nuclei extraction and tested two methods for generating nuclear suspensions: one involving hypotonic lysis and filtering (quick) and the other involving hypotonic lysis, sucrose gradient purification, and filtering (sucrose). Both methods produced clean nuclear suspensions from juvenile Area X tissue, particularly the sucrose method (**Fig. 7.1B**). We proceeded with snRNA-seq of one sample per extraction method and found that while both methods produced usable data, the sucrose method produced higher-quality data (data not shown). This result is consistent with other snRNA-seq tests performed on mouse and human tissue in our laboratory.

Preliminary analysis of FoxP2 expression in juvenile Area X cell types

We proceeded with a preliminary analysis of cell types in juvenile Area X. We identified 9 cell clusters defined by gene expression, and our annotations suggested the presence of pallidal neurons (Clusters 2, 4, 6, 7), interneurons (Clusters 0, 5), spiny projection neurons (SPNs) (Cluster 1), and non-neurons (Clusters 3, 9) (**Fig. 7.1C**). Cluster 8 could not be assigned to any cell type (**Fig. 7.1C**). We next examined expression of *FoxP2* in these cell types to assess the feasibility of detecting *FoxP2* knockdown at the single-cell level. We found FoxP2 expression in ~40% of Area X nuclei, and highest enrichment was seen in SPNs (~63%), followed by interneurons and non-neurons (~52-55%) (**Fig. 7.1D-E**). Few pallidal neurons expressed FoxP2 (<20%). We concluded that this was a suitable degree of FoxP2 expression to be able to detect knockdown, and we proceeded with snRNA-seq of adult Area X injected with control and *shFoxP2* viruses, as

well as a non-injected adult Area X sample. Information on samples collected for this project can be found in **Table 7.1**. Data analyses are ongoing and will greatly enhance our understanding of Area X cell types and FoxP2 functions within them.

Antibody test for FoxP2 ChIP

Direct FoxP2 targets have not yet been identified in Area X, so we attempted chromatin immunoprecipitation (ChIP) for FoxP2 from Area X tissue. We used a protocol and antibody resulting in Foxp2 pulldown from mouse cortical tissue (**Fig. 3.12A**) and performed ChIP from Area X and nidopallium, a negative control region with reportedly low FoxP2 expression. We did not see pulldown of FoxP2 with this method, and unexpectedly the input samples showed higher FoxP2 expression in nidopallium than in Area X (**Fig. 7.2A**). We also saw a band near 40 kilodaltons that might correspond to FoxP2 isoform 10+ (Vernes et al., 2006). We probed our ChIP-Western blot with a second FOXP2 antibody but again did not see any FoxP2 bands in the IP fractions (**Fig. 7.2B**). Thus, further work is needed to identify a suitable antibody and protocol for identifying direct FoxP2 targets. As with mouse Foxp2, perhaps newer methods such as CUT&RUN and other FoxP2 antibodies will prove more successful.

Viral constructs for FoxP1 knockdown and rescue in HVC

For viral knockdown of *FoxP1* in HVC, I subcloned a DNA fragment encoding a FoxP1 short hairpin RNA under control of the U6 promoter into a self-complementary AAV vector containing GFP under control of the CBh promoter (pscAAV-GFP-shFoxP1). I also generated a scrambled hairpin construct as a control, but this virus later showed an effect on behavior when injected into HVC. I tested pscAAV-GFP-shFoxP1 in 293T cells by

overexpressing zebra finch FoxP1 cDNA with this construct and the scrambled control. I found that overexpression of FoxP1 cDNA produced at least two isoforms of FoxP1 corresponding in size to mouse Foxp1A and Foxp1D (Wang et al., 2003) (Araujo et al., 2017) (**Fig. 7.3A**). A third product may be a posttranslationally modified form of FoxP1D (**Fig. 7.3A**). Expression of shFoxP1 reduced expression of all FoxP1 products by more than half in 293T cells (**Fig. 7.3B**). Next, we tested shFoxP1 in vivo by examining FoxP1 expression after injection of pscAAV-GFP or pscAAV-GFP-shFoxP1 into HVC. We confirmed endogenous expression of FoxP1 proteins corresponding to mouse Foxp1A, Foxp1D, and a modified form of Foxp1D (**Fig. 7.3C**). We also saw reductions of these proteins upon expression of shFoxP1, with a stronger effect on FoxP1D (**Fig. 7.3D**). These results show the efficacy of our viral tools for reducing FoxP1 expression in HVC.

I also generated a hairpin-resistant form of FoxP1 for in vivo rescue experiments by introducing synonymous mutations into the hairpin-targeting region of FoxP1 (pCMV-FoxP1^{RES}). To test hairpin-resistance of FoxP1^{RES}, I transfected 293T cells with pCMV-FoxP1^{RES} or the original construct (pCMV-FoxP1^{WT}) along with shFoxP1 or control AAV constructs. I confirmed knockdown of FoxP1^{WT} and found that both isoforms of FoxP1^{RES} were expressed at comparable levels as FoxP1^{WT} and unaffected by shFoxP1 (**Fig. 7.4A-B**). Having confirmed its hairpin resistance, I proceeded to subclone FoxP1^{RES} into the scAAV plasmid under the control of the CBh promoter (pscAAV-FoxP1^{RES}). Testing of this viral rescue construct in 293T cells with shFoxP1 showed its hairpin resistance as well (**Fig. 7.4C-D**). Interestingly, there was a significant and specific increase in expression of isoform D of FoxP1^{RES} upon coexpression with shFoxP1 (**Fig. 7.4D**).

Whether this is a technical artefact or a biological effect remains to be determined, but nonetheless these results show the potential utility of pscAAV-FoxP1^{RES} for in vivo rescue experiments.

Materials and Methods

Area X single-cell dissociation

Testing of single-cell dissociation on ~150 DPH Area X tissue was performed largely as described in Chapter 3. Coronal 500 µm sections were made in cold, oxygenated ACSF using a VF-200 Compresstome (Precisionary Instruments) and allowed to recover in ACSF with channel blockers for 5 min. Six punches of Area X were incubated in pronase for 30 min, washed in ACSF with 0.04% BSA, and triturated with polished glass pipettes of 600, 300, and 150 µm diameters. Cells were washed twice more with ACSF/BSA and filtered twice through FLOWMI 40 µm tip strainers. Cells were stained for viability using Trypan blue and counted using a hemocytometer.

Area X nuclear extractions and single-nucleus RNA sequencing

Two methods of nuclei extraction were tested on juvenile Area X tissue: hypotonic lysis with filtering (quick) (Habib et al., 2017) and hypotonic lysis with sucrose gradient and filtering (sucrose). The quick method (sample MCX15) was performed as follows: Area X was dissected from one juvenile female bird and dounce homogenized in 2 ml ice-cold Nuclei EZ Lysis Buffer (#NUC101-1KT, Sigma). Nuclei were incubated on ice for 5 min, pelleted at 500 × *g* for 5 min at 4°C, and again incubated in 2 ml Nuclei EZ Lysis Buffer on ice for 5 min and pelleted. Nuclei were then washed in 500 µl PBS with 0.2% RNase inhibitors (#2313A, Clontech) and resuspended in 200 µl nuclei suspension buffer (NSB) consisting of 1% UltraPure BSA (#AM2618, Thermo Fisher Scientific) and 0.2% RNase inhibitors in PBS. Nuclei were filtered through a FLOWMI 40 µm tip strainer

(#H13680-0040, Bel-Art), counted under a microscope, and diluted with NSB to target 5000 nuclei for single-nucleus RNA sequencing (snRNA-seq) as described below.

The sucrose nuclei extraction method (sample MCX16) was performed as follows: Area X was dissected from one juvenile female bird and dounce homogenized in 500 µl ice-cold Lysis Buffer (10 mM Tris pH 7.4, 10 mM NaCl, 3 mM $MgCl_2$, 0.1% IGEPAL CA-630). Nuclei were pipette-mixed 10 times with 900 µl of 1.8 M Sucrose Cushion Solution (#NUC201-1KT, Sigma). To a clean 2ml tube, 500 µl of 1.8 M Sucrose Cushion Solution was added, and the nuclei sample was layered on top of the cushion without mixing. The sample was centrifuged at 13,000 × g for 45 min at 4°C and all but ~100 µl of supernatant was discarded to preserve the pellet. The pellet was washed in 300 µl NSB (~400 µl total volume) and centrifuged at 550 × g for 5 min at 4°C. All but ~50 µl of supernatant was discarded and the pellet was resuspended in the remaining liquid and filtered through a FLOWMI 40 µm tip strainer (#H13680-0040, Bel-Art). Nuclei were counted under a microscope and 3000 nuclei were targeted for snRNA-seq as described below.

For adult non-injected Area X (sample MCX17), shScramble-injected Area X (sample MCX20), and shFoxP2-injected Area X (sample MCX21), tissue was prepared from 2 birds per condition for snRNA-seq as follows: Each bird was rapidly decapitated and its brain was placed in ice-cold ACSF (126 mM NaCl, 3 mM KCl, 1.25 mM NaH_2PO_4, 26 mM $NaHCO_3$, 10 mM D-(+)-glucose, 2 mM $MgSO_4$, 2 mM $CaCl_2$) bubbled with carbogen gas (95% O_2, 5% CO_2). The cerebellum was removed with a razor and the cerebrum was glued to a specimen tube for sectioning with a VF-200 Compresstome (Precisionary Instruments). Coronal 500 µm sections were made in ice-cold ACSF and

allowed to recover in room temperature ACSF for 5 min. Area X punches were collected into a tube containing ACSF on ice until all punches were collected and pooled from 2 birds per condition. ACSF was removed with a pipette and replaced with 500 µl Lysis Buffer, and sucrose nuclei extraction proceeded as described above. Samples were diluted to 1000 nuclei/µl with NSB for targeting 10,000 nuclei for snRNA-seq as described below.

Libraries were prepared using the Chromium Single Cell 3' Library & Gel Bead Kit v2 for samples MCX15-17 (#120237, 10x Genomics) or v3 for samples MCX20-21 (#1000075, 10x Genomics) (Zheng et al., 2017) according to the manufacturer's instructions and sequenced using an Illumina NextSeq 500 at the McDermott Sequencing Core at UT Southwestern (MCX15-17) or an Illumina NovaSeq 6000 at the North Texas Genome Center at UT Arlington (MCX20-21). Bioinformatic analysis was performed by Ashwinikumar Kulkarni.

Area X chromatin immunoprecipitation

Chromatin immunoprecipitation followed by Western blotting (ChIP-Western) was performed as described in Chapter 3 from 30 mg nidopallium or Area X tissue. IP fractions were incubated with 5 µg of α-Foxp2 (#MABE415, Millipore) overnight at 4°C. Western blotting was performed with the following antibodies: mouse α-Foxp2 (#MABE415, Millipore, 1 µg/ml), goat α-Foxp2 N-16 (#sc-21069, Santa Cruz Biotechnologies, 1:200), donkey α-mouse IgG IRDye 800 (#926-32212, LI-COR Biosciences, 1:20,000), donkey α-goat IgG IRDye 680 (#926-68074, LI-COR Biosciences, 1:20,000).

Constructs

pscAAV-GFP-shFoxP1 was generated by PCR-amplifying U6-shFoxp1 from pLKO.1 (TRCN0000072005, Broad Institute) while adding NotI and BamHI sites, then ligating into pscAAV9-CBh-GFP (Xiao et al., 2018) digested with these enzymes. pCMV-FoxP1^{WT} was generated by subcloning FoxP1 cDNA from pGEMTeasy (Haesler et al., 2004) into pCMV-Tag4a using EcoRI. pCMV-FoxP1^{RES} was generated by introducing 5 synonymous mutations into the hairpin-targeting site of FoxP1 using site-directed mutagenesis as described below. pscAAV-FoxP1^{RES} was generated by PCR-amplifying FoxP1^{RES} while adding AgeI and BamHI sites and then ligating into pscAAV-GFP-shFoxP1 digested with these enzymes.

Site-directed mutagenesis was performed with the megaprimer method using PrimeSTAR Max DNA Polymerase (#R045A, TaKaRa Bio). Briefly, primers containing the substitutions were used to generate a megaprimer from a parent template using the following PCR program: 98°C 2 min, 30 x (98°C 10 s, 55°C 5 s, 72°C 10 s), 72°C 7 min. Then the megaprimer was purified and used to mutagenize the parent template using the following PCR program: 98°C 2 min, 30 x (98°C 10 s, 55°C 5 s, 72°C 1 min/kb), 72°C 7 min. Parent templates were digested using DpnI and the remaining mutagenized constructs were used to transform competent cells and proceed with standard plasmid preparations.

Hairpin tests in 293T cells

293T cells were cultured in high-glucose DMEM containing 4 mM L-glutamine, 10% fetal bovine serum (#10437028, Invitrogen), and 1% antibiotic-antimycotic (#15240-062, Invitrogen) at 37°C under 5% CO_2. Cells were plated in 6-well plates and transfected

with 0.1 pmol/well of overexpression constructs and 0.4 pmol/well of hairpin constructs using FuGENE 6 Transfection Reagent (#E2691, Promega) according to the manufacturer's instructions. After 24-48h, cells were washed twice with PBS and collected into tubes by scraping in Lysis Buffer (50 mM Tris pH 8.0, 0.1 mM EDTA, 250 mM NaCl, 50 mM NaF, 0.1 mM $NaVO_4$, 10% glycerol, 0.5% IGEPAL CA-630, 1 mM DTT, 0.7 mM PMSF). Samples were incubated for 10 min at 4°C with rotation and centrifuged at 15,000 rpm for 10 min at 4°C. The supernatant was quantified using a Bradford assay, mixed with loading buffer, incubated at 95°C for 5 min, and stored at -20°C. Western blotting was performed as described in Chapter 3 with the following antibodies: rabbit α-FOXP1 (Spiteri et al., 2007) (1:5000), mouse α-GAPDH (#MAB374, Millipore, 1:10,000), donkey α-rabbit IgG IRDye 800 (#926-32213, LI-COR Biosciences, 1:20,000), donkey α-mouse IgG IRDye 680 (#926-68072, LI-COR Biosciences, 1:20,000).

Figures

Figure 7.1 *Optimization of snRNA-seq for Area X FoxP2 knockdown.*

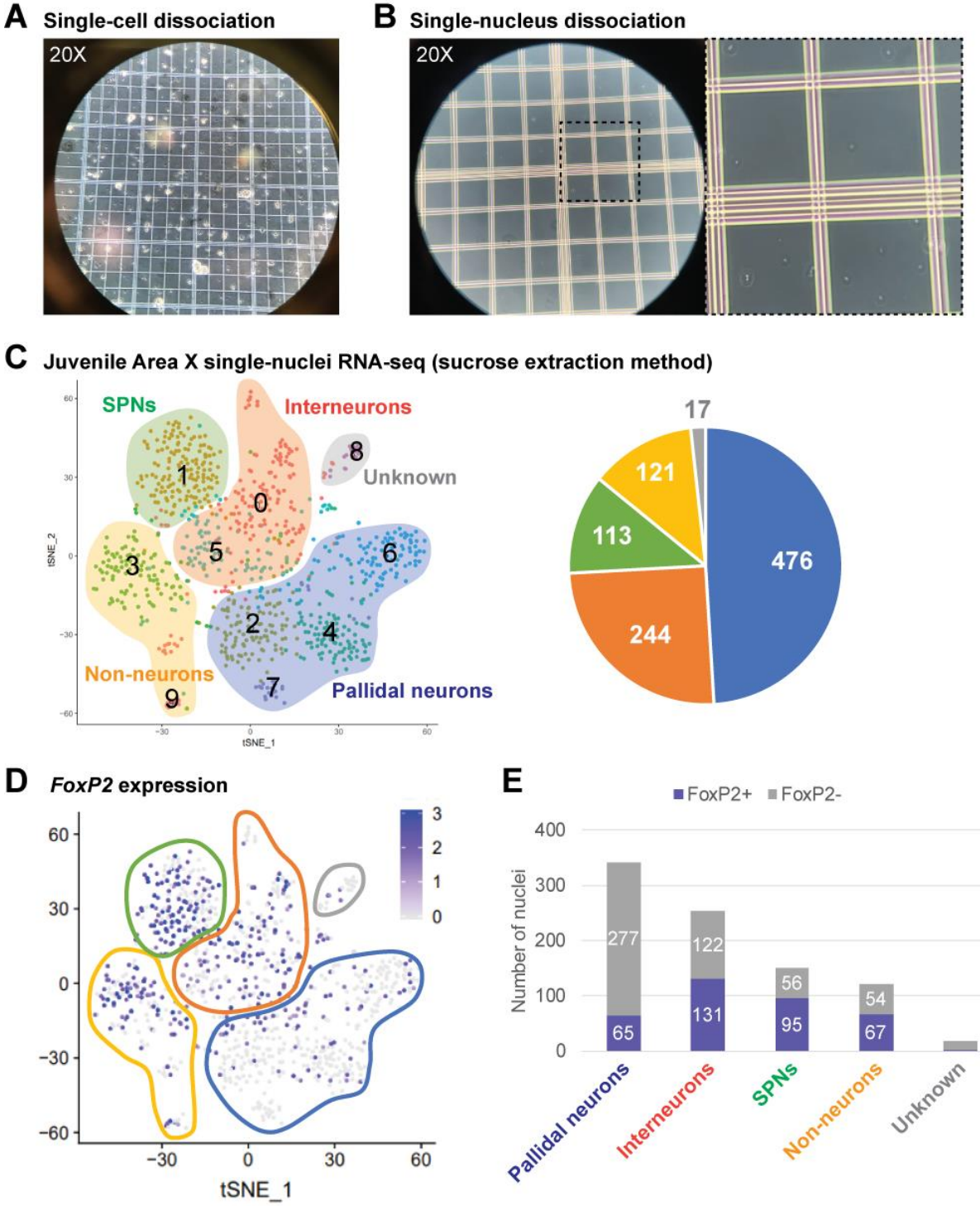

(A) Cell suspension from pronase digestion of Area X from a ~150 DPH zebra finch. (B) Nuclei suspension from sucrose gradient purification method performed on Area X from a juvenile zebra finch. (C) Preliminary snRNA-seq analysis of sucrose gradient-purified nuclei from Area X of a juvenile zebra finch. Left: tSNE clustering of nuclei. Right: Number of nuclei per annotated cell type. SPNs: spiny projection neurons. (D) Feature plot of *FoxP2* expression in clusters from C. (E) Numbers and proportions of *FoxP2*+ nuclei per cell type.

Figure 7.2 *Antibody test for Area X FoxP2 chromatin immunoprecipitation.*

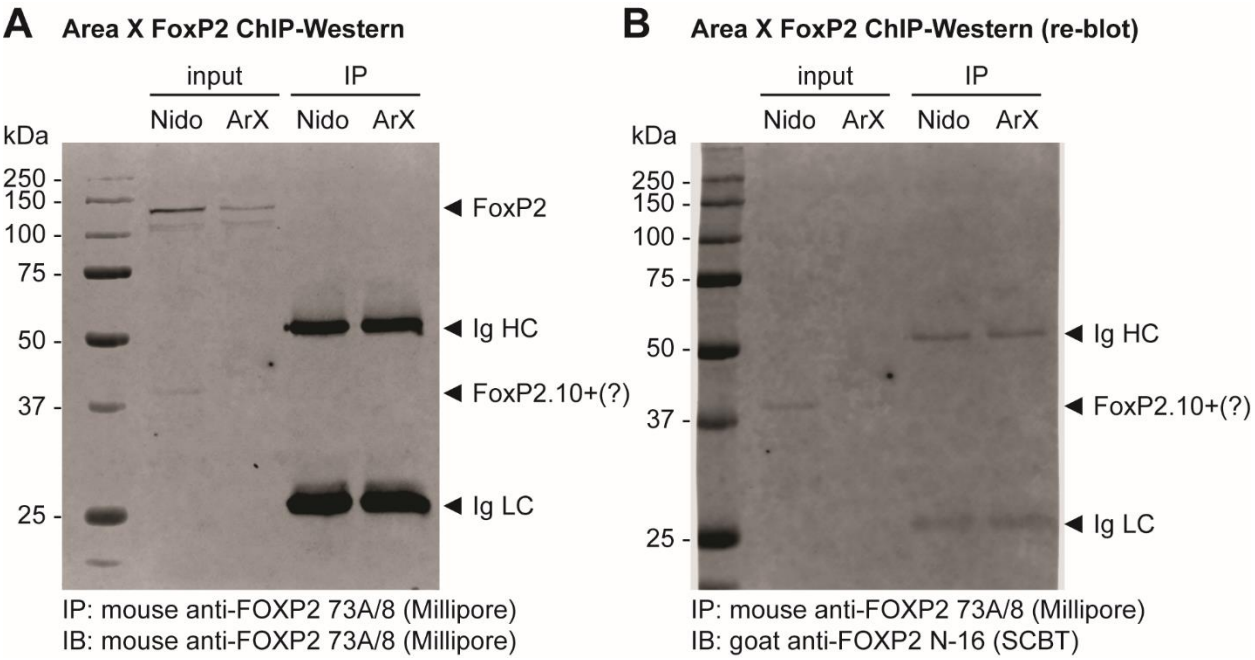

(A) FoxP2 ChIP-Western performed on nidopallium (Nido) and Area X (ArX) tissue. (B) Membrane from A re-blotted with a second FOXP2 antibody. IB: immunoblot, Ig HC: immunoglobin heavy chain, Ig LC: immunoglobin light chain.

Figure 7.3 *In vitro and in vivo tests of a viral FoxP1 knockdown construct.*

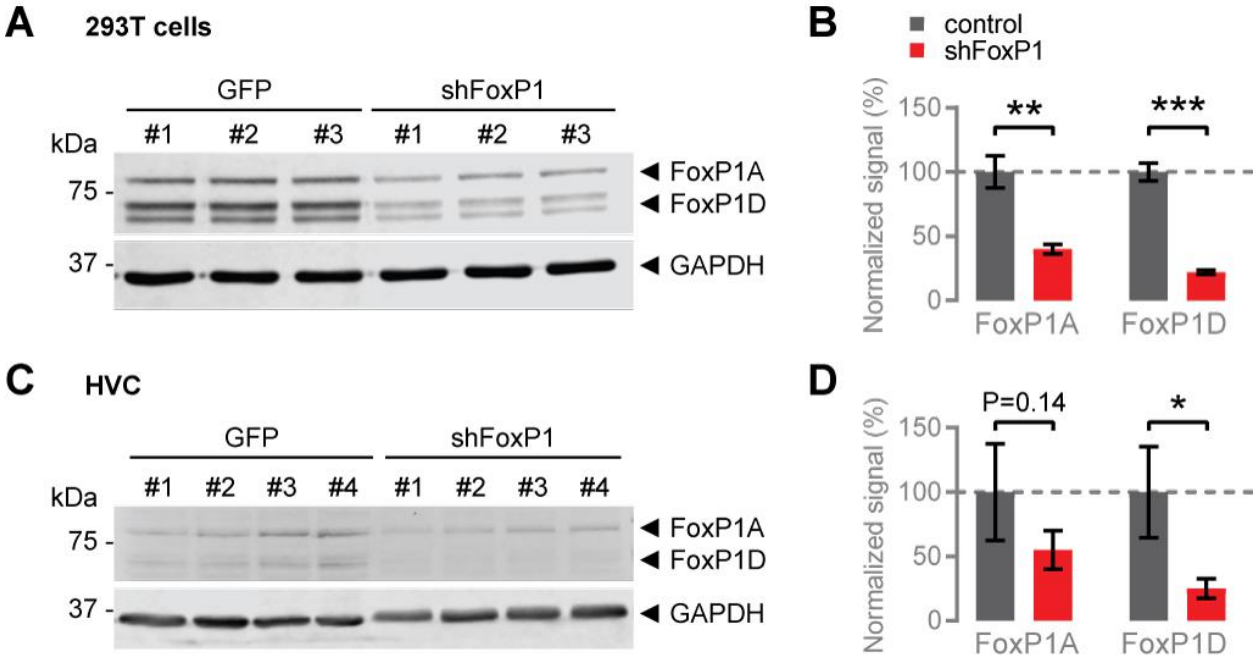

(A) Western blot of lysates from 293T cells overexpressing pCMV-FoxP1 and either control or FoxP1 short hairpin (shFoxP1) AAV constructs. (B) Quantification of A. Data are represented as means (±SEM). (**) $P < 0.01$, (***) $P < 0.001$, t-test. $n = 3$ per condition. (C) Western blot of lysates from HVC (90-92 DPH) injected with control or shFoxP1 AAV. (D) Quantification of C. Data are represented as means (±SEM). (*) $P < 0.05$, t-test. $n = 4$ per condition.

Figure 7.4 *In vitro tests of hairpin-resistant FoxP1 rescue constructs.*

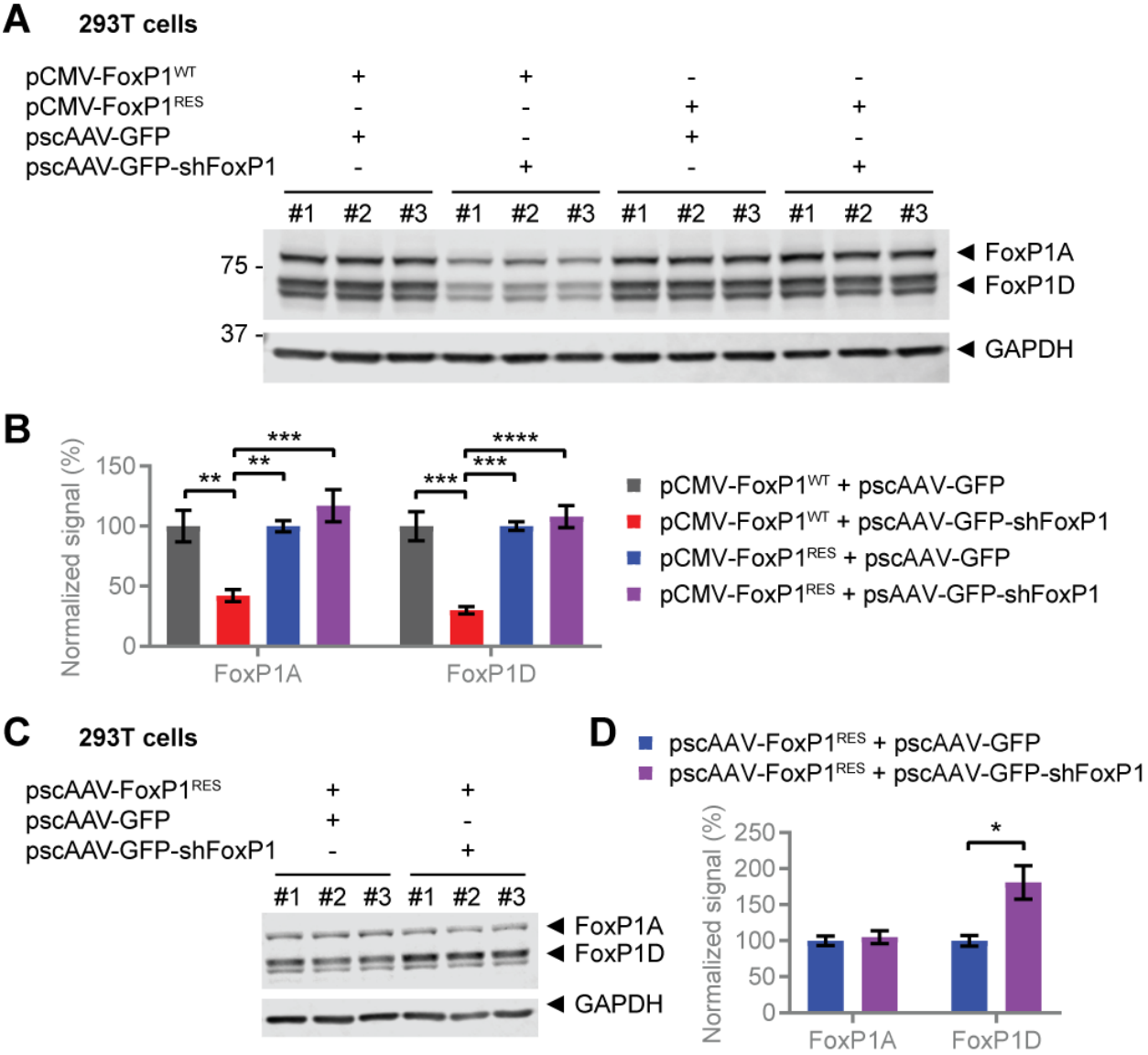

(A) Western blot of lysates from 293T cells overexpressing combinations of wild-type FoxP1 ($FoxP1^{WT}$), hairpin-resistant FoxP1 ($FoxP1^{RES}$), control GFP, and FoxP1 short hairpin (shFoxP1) constructs. (B) Quantification of A. Data are represented as means (±SEM). (**) $P < 0.01$, (***) $P < 0.001$, (****) $P < 0.0001$, two-way ANOVA with Tukey's multiple comparisons test. $n = 3$ per condition. (C) Western blot of lysates from 293T cells overexpressing pscAAV-$FoxP1^{RES}$ with control GFP or shFoxP1 constructs. (D) Quantification of C. Data are represented as means (±SEM). (*) $P < 0.05$, t-test. $n = 3$ per condition.

Tables

Table 7.1 *Samples collected for Area X snRNA-seq.*

Sample ID	Age	Sex	Injection	# birds	Nuclei method	Target cell recovery	Chemistry	Sequencer
MCX15	juvenile	F	none	1	quick	5000	v2	NextSeq 500
MCX16	juvenile	F	none	1	sucrose	3000	v2	NextSeq 500
MCX17	adult	M	none	2	sucrose	10000	v2	NextSeq 500
MCX20	adult	M	shScramble	2	sucrose	10000	v3	NovaSeq 6000
MCX21	adult	M	shFoxP2	2	sucrose	10000	v3	NovaSeq 6000

Table 7.2 *Primers used to generate constructs.*

Reaction	Template	Forward (5'-3')	Reverse (5'-3')
NotI-U6-shFoxP1-BamHI PCR	pLKO.1-shFoxP1	ATAAGAATGCGGCCGCTTTCCCATGATTCCTTC	CGCGGATCCAAAAAGCTAACACTAAACG
FoxP1^{RES} megaprimer	pCMV-FoxP1	CATCCTGGAATCTCCTGAAAAACAGCTGACGCTGAATGAGATCTACAACTGGTTCACACGAATGTTC	TGTGGTTGGCTGTTGTCACT
AgeI-FoxP1^{RES}-BamHI PCR	pCMV-FoxP1^{RES}	TAAGCAACCGGTATGATGACACCTCAAGTG	CGCGGATCCTCATTCTATGTCCTCATT

CHAPTER EIGHT: Discussion and Future Directions

In this thesis, I have described my work toward understanding how these genes modulate behavior and exert their molecular functions in various cell types throughout the brain. These results carry broader implications for the neurobiology of vocal and cognitive behaviors, and here I hope to impart further recommendations for the study of FoxP2 and FoxP1 in the brain.

***Foxp2* and *Foxp1* have distinct cortical functions**

Comparison of *Foxp2* cKO and *Foxp1* cKO mice with gene deletion through the same *Emx1*-Cre driver has offered valuable insights into the roles of these respective genes in cortical development and function. Cortical morphology analyses by our laboratory and others have revealed stark disparities between the cKO lines: while *Foxp1* cKO mice have an overall thinner cortex and abnormal layer distributions across the cortex, *Foxp2* cKO mice have overtly normal cortical size and layering, despite early experiments suggesting Foxp2 control over cortical neurogenesis and migration (Co et al., 2019; Kast et al., 2019; Medvedeva et al., 2018; Tsui et al., 2013; Usui et al., 2017a). It has not yet been investigated whether these proteins are coexpressed in the same cells early in cortical development, and it remains unclear if either protein is truly expressed in proliferative zones. Answering these questions may lend insight into whether Foxp1 can compensate for loss of Foxp2 in early cortical development. Additionally, there are multiple molecular pathways by which *Foxp1* deletion could lead to a smaller cortex, such as decreased cell proliferation or increased cell death. While our RNA-seq analysis of P0

Foxp1 cKO cortex suggests downregulation of cell proliferation genes (Usui et al., 2017a), functional studies such as Ki67 staining for proliferating cells are needed to confirm this mechanism.

These differences in cortical development between the two cKO lines are reflected at the behavioral level, although it is important to remember that *Emx1*-Cre affects hippocampal *Foxp1* as well. *Foxp1* deletion reduces postnatal and adult USV production and alters their acoustic features, while *Foxp2* deletion has no effect on USVs save for a slight decrease in postnatal call loudness (Araujo et al., 2017; Co et al., 2019; Usui et al., 2017a). The effect of *Foxp1* cKO on USV loudness has not been assessed, but nonetheless their vocalization deficits are more severe. As discussed in our *Foxp1* cKO study, this is particularly intriguing given that mice with developmental ablation of the cortex still emit somewhat normal USVs (Hammerschmidt et al., 2015b). It may be the case that *Foxp1* deletion causes abnormal sensory integration and/or corticostriatal activity in a manner that inhibits the production of USVs, an effect that does not occur with the mere absence of corticostriatal neurons. Because *Foxp2* cKO mice have largely normal USVs, we conclude that corticothalamic neurons do not play a major role in the production and spectral features of USVs. They do appear to modulate call loudness over development, and given that the onset of hearing in mice is not until P10-12 (Wang and Bergles, 2015), they may function to control motor systems governing call amplitude independent of auditory feedback (Co et al., 2019).

Other divergent behavioral phenotypes between *Foxp2* cKO and *Foxp1* cKO mice are their activity and anxiety levels. *Foxp1* cKO mice show hyperactivity and increased

anxiety while *Foxp2* cKO mice are normal in these measures (Araujo et al., 2017; Co et al., 2019). The altered activity levels may again reflect dysfunction of cortical inputs to the basal ganglia, which regulate the activation of movement, while the increased anxiety could be due to dysfunction of L3-5 mPFC inputs to the basolateral amygdala (Anastasiades et al., 2018). However, it is important to note that *Foxp1* cKO mice do not show alterations in fear learning, suggesting differential regulation of anxiety versus fear by cortical *Foxp1*. The lack of activity or anxiety phenotypes in *Foxp2* cKO mice indicates that corticothalamic neurons may not play a large role in modulating these behaviors.

One behavioral domain potentially impaired only in *Foxp2* cKO mice is cognitive flexibility. Cortical *Foxp2* deletion impairs reversal learning in the water Y-maze, while *Foxp1* deletion has no effect on performance in a set-shifting task (Araujo et al., 2017; Co et al., 2019). Recent work dissecting cortical cell type contributions to cognitive flexibility found that both corticostriatal and corticothalamic neurons contribute to flexible behaviors in a food reward-based reversal learning task (Nakayama et al., 2018). This supports the importance of *Foxp2* in corticothalamic neurons for reversal learning, but it is also somewhat surprising that *Foxp1* deletion did not impair corticostriatal neurons in a manner producing this type of cognitive deficit. Perhaps a more stressful assay such as the water Y-maze is required to elicit cognitive flexibility deficits in *Foxp1* cKO mice. It would be interesting to test the two cKO lines in the same assays, whether aversive or appetitive, to more directly compare how *Foxp2* and *Foxp1* regulate cognitive flexibility and frontal cortical function.

Altogether these studies have revealed major differences between *Foxp2* cKO and *Foxp1* cKO mice in cortical development and behavioral phenotypes, reflecting their largely non-overlapping cortical expression patterns described nearly a decade ago (Hisaoka et al., 2010). Furthermore, they provide insights into the distinct etiologies of *FOXP2*-related speech and language disorders and *FOXP1* syndrome. Still, further work is needed to fully understand *Foxp2* and *Foxp1* functions in the cortex. One main task is identification of genome-wide direct targets of Foxp2 and Foxp1 in this region, as studies thus far have used promoter ChIP-chip in tissue or ChIP-seq in cultured cells to identify targets. Finding suitable antibodies and/or protocols for ChIP-seq has proven challenging, but newer methodologies such as CUT&RUN may be promising avenues for achieving this goal.

A second major gap in our knowledge of *Foxp2* and *Foxp1* function is their role in cortical neuronal activity and plasticity. Prior studies have not examined this but have shown *Foxp2* involvement in striatal and cerebellar physiology and *Foxp1* involvement in striatal and hippocampal physiology (Araujo et al., 2015; Araujo et al., 2017; French et al., 2012; French et al., 2018; Groszer et al., 2008; van Rhijn et al., 2018). Thus, I would predict an effect of *Foxp2* or *Foxp1* deletion on cortical physiology as well. Given the absence of major cortical morphological abnormalities in *Foxp2* cKO mice, Foxp2 might instead function to modulate neuronal activity or synaptic signaling. A related feature to examine in cortical neurons of both *Foxp2* cKO and *Foxp1* cKO mice is dendritic spine density, especially given the spine abnormalities seen after previous *FoxP2*

manipulations in rodent neurons and zebra finch Area X (Chen et al., 2016; Schulz et al., 2010; Sia et al., 2013).

Other unexplored avenues of *Foxp2* and *Foxp1* function in the cortex are related to axon outgrowth and targeting. Gene ontology analysis of FOXP1 targets in human neural progenitors found enrichment of genes related to axon guidance, and cortical neurons cultured after *Foxp1* knockdown show decreased axon lengths (Araujo et al., 2015; Li et al., 2015). Further support for abnormal projections in *Foxp1* cKO mice is their decreased corpus callosum volumes at both postnatal and adult stages (Araujo et al., 2017; Usui et al., 2017a). Whether this is due to failure of axon outgrowth, misguided targeting, or another factor is unknown. A simple way to test this would be to cross *Foxp1* cKO mice to a Cre-dependent Rosa-tdTomato reporter line and then examine labeling of the corpus callosum and other cortical axon tracts throughout the brain. With this approach, it may be possible to visualize mistargeted axons in *Foxp1* cKO mice. Although *Foxp2* cKO mice do not have cortical axon abnormalities, their thalamocortical axons have not yet been examined, and these afferents are dependent upon corticothalamic axons and signaling within the cortex to reach their final destinations (Deck et al., 2013). These axons can be examined by immunohistochemistry using α-L1CAM at an embryonic time point, or by performing retrograde labeling from the cortex.

Finally, an interesting topic of study would be gene expression and behavioral coregulation by Foxp2 and Foxp1 in L6a corticothalamic neurons. This is one of the few cell types in the brain coexpressing these heterodimerizing transcription factors, another major site being striatal direct pathway SPNs. Their coexpression patterns in L6a neurons

follow an interesting trajectory: no colabeling occurs in early postnatal cortex, but by adulthood, 31-64% of Foxp1+ L6a neurons express Foxp2 (Hisaoka et al., 2010). This suggests a mature-onset upregulation of Foxp1 in corticothalamic neurons, as Foxp2 is specific to corticothalamic neurons in mature cortex (Kast et al., 2019). One strategy for studying functional compensation or coregulated pathways between Foxp2 and Foxp1 could be deletion of one or both using *Ntsr1*-Cre, which is expressed in L6 corticothalamic neurons reportedly starting around E16.5 (Fazel Darbandi et al., 2018). The Cre-dependent Rosa-tdTomato reporter could also be useful for electrophysiology and neuronal morphology experiments, or for FACS isolation of corticothalamic neurons for genomics studies. In summary, the next major steps for understanding roles of *Foxp2* and *Foxp1* in the cortex include direct target identification, neurophysiological studies, examination of efferent and afferent axons, and exploration of Foxp2-Foxp1 interaction in corticothalamic neurons.

FoxP2 regulation of dopamine signaling in the brain

Previous studies of FoxP2 expression patterns and functions have suggested associations with dopamine signaling, more so than other neurotransmitter systems. FoxP2 is expressed in the SNc and VTA, two major sources of dopamine in the brain, and *Foxp2* mutation in mice affects dopamine levels in the cortex and basal ganglia (Campbell et al., 2009; Enard et al., 2009). Foxp2 is also enriched in D1R+ striatal SPNs and DARPP-32+ corticothalamic projection neurons, and knockdown of *FoxP2* in zebra finch Area X reduces expression of these proteins (Hisaoka et al., 2010; Murugan et al., 2013; Vernes et al., 2011). Our work has supported this link to dopamine signaling by

showing that in mouse cortex, Foxp2 is coexpressed with D1R in postnatal corticothalamic neurons (Co et al., 2019). Furthermore, *Foxp2* deletion decreases D1R expression in these and other projection neurons throughout the cortex, suggesting both cell-autonomous and non-cell-autonomous mechanisms of downregulation (Co et al., 2019).

Several questions remain about the cellular and molecular mechanisms underlying this cortex-wide D1R downregulation in *Foxp2* cKO mice. One possibility is that D1R loss in corticothalamic neurons induces circuit-level downregulation of D1R expression in intratelencephalic neurons to preserve some optimal ratio of D1R+ excitatory neuron subclasses in the cortex. This could be achieved through altered electrical or chemical signaling from corticothalamic neurons to other neurons in the cortex. Another possibility is that Foxp2 is indeed expressed in radial glia of the developing cortex, as one study has suggested, and that loss of *Foxp2* from these cortical precursors using *Emx1*-Cre affects D1R expression across multiple excitatory neuron subclasses (Tsui et al., 2013). One could test the former possibility by generating *Drd1a-tdTomato;Ntsr1-Cre;Drd1*$^{flox/flox}$ mice to examine cortex-wide D1R expression after selective deletion of Drd1 from corticothalamic neurons (Sarinana et al., 2014). The latter hypothesis could be tested using *Drd1a-tdTomato;Neurod6-Cre;Foxp2*$^{flox/flox}$ mice, as *Neurod6*-Cre is exclusive to postmitotic excitatory neurons (Goebbels et al., 2006).

Also unknown is the impact of cortical *Foxp2* deletion on dopaminergic innervation or release from the VTA. The altered dopamine levels in previous *Foxp2* mutant mice could simply be due to *Foxp2* mutation within the VTA, but if that were the only contributor,

we would expect to a single brain-wide effect on dopamine concentration. Instead, the altered dopamine levels are specific to the cortex and basal ganglia, where *Foxp2* is also mutated, suggesting Foxp2-mediated regulation of VTA innervation and/or dopamine release in these target brain regions. Thus, it may be possible that D1R downregulation in *Foxp2* cKO mice could be altering cortical dopamine levels as well. This could be tested by immunohistochemistry for VTA terminals in the cortex of these mice using α-DAT, as well as assays to measure dopamine concentrations or release.

Another question is how Foxp2 regulates *Drd1* expression at the molecular level. To my knowledge, ChIP studies of FoxP2 to date have not identified binding near *Drd1*, but embryonic whole-brain ChIP-chip indicates binding at the *Ppp1r1b* promoter (Vernes et al., 2011). A possible scenario could be that intracellular DARPP-32 can act in a feedback loop to regulate expression levels of its upstream D1R receptor in order to achieve a molecular homeostasis of the D1R signaling pathway. Therefore, if Foxp2 is unable to directly activate *Ppp1r1b* expression, D1R levels are indirectly decreased. This could easily be tested by examining *Drd1* or *Drd1a*-tdTomato expression in a *Ppp1r1b* KO mouse. Another indirect mechanism could simply be Foxp2 regulation of other transcription factors affecting D1R expression. It is important to keep in mind that published Foxp2 ChIP studies are not comprehensive, so Foxp2 may still directly regulate *Drd1* through an as-yet unidentified binding site.

While these mechanisms remain to be elucidated, it is clear that FoxP2 is required for proper D1R expression in the cortex and striatum (Co et al., 2019; Murugan et al., 2013). Cerebellar Purkinje cells also express D1R, raising the possibility that Foxp2

regulates *Drd1* expression in this cell type as well (Barili et al., 2000). If so, then a major function for FoxP2 in the brain would be to promote receptiveness of vocalization and learning circuits to modulation by dopamine through the D1 receptor. Dopamine has long been studied in the brain for its roles in learning, motivation, and motor control, and manipulation of dopamine signaling in songbirds and rodents has begun to resolve these functions in vocal behavior (Rippberger et al., 2015; Woolley, 2019). Thus, for *FOXP2*-related and other speech and language disorders, dopamine signaling and especially D1 signaling could be an entry point for designing and testing therapeutics.

Relating mouse behavioral phenotypes to human *FOXP2* and *FOXP1* disorders

The brain region-specific mouse models of *Foxp* function described in this thesis show varying degrees of similarity to patients with *FOXP* mutations. Cortico-hippocampal *Foxp1* cKO mice show impaired vocal communication, spatial learning deficits, decreased social behavior, hyperactivity, and anxiety (Araujo et al., 2017; Usui et al., 2017a). Likewise, patients with *FOXP1* syndrome show language deficits, intellectual disability, ASD and ADHD symptoms, and anxiety (Siper et al., 2017). These similarities suggest that FOXP1 dysfunction in the cortex and hippocampus contributes to these symptoms, and ongoing work in our laboratory is finding roles for Foxp1 in striatal direct and indirect circuits in these phenotypes as well (Anderson et al., 2019).

Embryonic cerebellar *Foxp2* knockdown produces drastic vocalization and gross motor impairments in mice, while postnatal deletion in Purkinje cells produces greater motor-skill learning deficits than cortical or striatal *Foxp2* deletion (French et al., 2018; Usui et al., 2017b). Imaging studies of the KE family show structural and functional

abnormalities of the cerebellum, indicating that FOXP2 within this region controls the development and function of circuits needed for proper speech learning and production (Argyropoulos et al., 2018; Belton et al., 2003). It appears then that the cerebellum is a key site for FOXP2 function in the motor aspects of language, but further studies using covert or silent language tasks are needed to observe cerebellar function in the cognitive aspects of language.

In contrast with cerebellum-specific *Foxp2* manipulations, cortex-specific *Foxp2* deletion produces behavioral deficits less related to innate vocalization and motor functions. *Foxp2* cKO mice show almost no USV alterations, and their motor-skill learning impairments are the least severe of the three *Foxp2* cKO lines studied in motor-skill tasks (Co et al., 2019; French et al., 2018). Instead, they show deficits specific to behavioral flexibility and social interactions (Medvedeva et al., 2018). These results are challenging to interpret with respect to language, especially given the cortical morphological and functional abnormalities commonly found in the KE family (Belton et al., 2003; Liegeois et al., 2003; Liegeois et al., 2011; Vargha-Khadem et al., 1998; Watkins et al., 2002b). One possibility is that these cortical differences arise as a response to abnormal signaling from subcortical structures affected by *FOXP2* mutation, rather than originating in the cortex itself. This scenario seems unlikely, however, considering the similar impairments seen in affected KE members and patients with acquired lesions of the opercular region of the cortex (Watkins et al., 2002a). Another hypothesis is that the role of cortical *FOXP2* is highly linked to vocal learning and/or human-specific features of cortical development, and thus cannot be adequately studied in a mouse model. Even so, cortical *FoxP2* might

still play conserved roles in cognition that were appropriated during human evolution to subserve the cognitive aspects of language, as could be suggested by the behavioral inflexibility in *Foxp2* cKO mice. One might speculate that the grammatical impairments seen in affected KE family members, such as failure to derive “sunny” from “sun” or “walked” from “walk”, could be a defect in cognitive flexibility specific to language. It is also important to note the link between *FOXP2* and other neurodevelopmental disorders such as ASD, and it could be the case that cortical FOXP2 underlies the behavioral rigidity and social impairments seen in *FOXP2* patients outside the KE family that are diagnosed with these disorders.

In summary, the work conducted in this thesis provides novel insights into the roles of *FoxP2* and *FoxP1* in the brain as they relate to vocalization and cognition. For the first time we linked *Foxp2* to mammalian cortical dopamine signaling and showed a requirement for cortical *Foxp2* in PFC-mediated cognitive behaviors. We also conducted the first cell type-specific molecular analyses in *Foxp2* mutant mice and found both cell-autonomous and non-cell-autonomous developmental effects of *Foxp2* deletion. We conducted further work to elucidate binding dynamics and coregulated targets between FoxP2 and its cortical cofactor TBR1. We also compared mice with brain region-specific *Foxp2* or *Foxp1* manipulations and found distinct roles for these genes in the development and function of these regions, leading to different outcomes in vocal and cognitive behaviors. Furthermore, we identified important roles for sumoylation of FOXP2 and FOXP1 in their molecular, cellular, and behavioral functions. Finally, we generated tools and methods for elucidating the functions of these genes in the zebra finch, which

will advance our understanding of cell types and molecular mechanisms involved in vocal learning. Altogether these findings highlight the power of single-gene approaches, molecular techniques, and animal models for understanding brain circuits involved in vocalization and cognition.

BIBLIOGRAPHY

Adam, I., Mendoza, E., Kobalz, U., Wohlgemuth, S., and Scharff, C. (2016). FoxP2 directly regulates the reelin receptor VLDLR developmentally and by singing. Molecular and cellular neurosciences *74*, 96-105.

Adam, I., Mendoza, E., Kobalz, U., Wohlgemuth, S., and Scharff, C. (2017). CNTNAP2 is a direct FoxP2 target in vitro and in vivo in zebra finches: complex regulation by age and activity. Genes, brain, and behavior *16*, 635-642.

Ade, K.K., Wan, Y., Chen, M., Gloss, B., and Calakos, N. (2011). An Improved BAC Transgenic Fluorescent Reporter Line for Sensitive and Specific Identification of Striatonigral Medium Spiny Neurons. Frontiers in systems neuroscience *5*, 32.

Alcamo, E.A., Chirivella, L., Dautzenberg, M., Dobreva, G., Farinas, I., Grosschedl, R., and McConnell, S.K. (2008). Satb2 regulates callosal projection neuron identity in the developing cerebral cortex. Neuron *57*, 364-377.

Alcock, K.J., Passingham, R.E., Watkins, K., and Vargha-Khadem, F. (2000a). Pitch and timing abilities in inherited speech and language impairment. Brain and language *75*, 34-46.

Alcock, K.J., Passingham, R.E., Watkins, K.E., and Vargha-Khadem, F. (2000b). Oral dyspraxia in inherited speech and language impairment and acquired dysphasia. Brain and language *75*, 17-33.

Anastasiades, P.G., Boada, C., and Carter, A.G. (2018). Cell-Type-Specific D1 Dopamine Receptor Modulation of Projection Neurons and Interneurons in the Prefrontal Cortex. Cerebral cortex (New York, NY : 1991).

Andersen, S.L., Thompson, A.T., Rutstein, M., Hostetter, J.C., and Teicher, M.H. (2000). Dopamine receptor pruning in prefrontal cortex during the periadolescent period in rats. Synapse (New York, NY) *37*, 167-169.

Anderson, A., Trivedi, K., and Konopka, G. (unpublished). Expression of Foxp1 in corticostriatal projection neurons.

Anderson, A.G., Kulkarni, A., Harper, M., and Konopka, G. (2019). Single-cell analysis of Foxp1-driven mechanisms essential for striatal development. bioRxiv, 611780.

Anderson, G.R., Galfin, T., Xu, W., Aoto, J., Malenka, R.C., and Sudhof, T.C. (2012). Candidate autism gene screen identifies critical role for cell-adhesion molecule CASPR2 in dendritic arborization and spine development. Proceedings of the National Academy of Sciences of the United States of America *109*, 18120-18125.

Andrews, S. (2010). FastQC: a quality control tool for high throughput sequence data.

Araujo, D.J., Anderson, A.G., Berto, S., Runnels, W., Harper, M., Ammanuel, S., Rieger, M.A., Huang, H.C., Rajkovich, K., Loerwald, K.W.*, et al.* (2015). FoxP1 orchestration of ASD-relevant signaling pathways in the striatum. Genes & development *29*, 2081-2096.

Araujo, D.J., Toriumi, K., Escamilla, C.O., Kulkarni, A., Anderson, A.G., Harper, M., Usui, N., Ellegood, J., Lerch, J.P., Birnbaum, S.G.*, et al.* (2017). Foxp1 in Forebrain Pyramidal Neurons Controls Gene Expression Required for Spatial Learning and Synaptic Plasticity. The Journal of neuroscience : the official journal of the Society for Neuroscience *37*, 10917-10931.

Argyropoulos, G.P.D., Watkins, K.E., Belton-Pagnamenta, E., Liégeois, F., Saleem, K.S., Mishkin, M., and Vargha-Khadem, F. (2018). Neocerebellar Crus I Abnormalities Associated with a Speech and Language Disorder Due to a Mutation in FOXP2. The Cerebellum.

Arnsten, A.F.T. (2009). Stress signalling pathways that impair prefrontal cortex structure and function. Nature reviews Neuroscience *10*, 410-422.

Arriaga, G., Zhou, E.P., and Jarvis, E.D. (2012). Of mice, birds, and men: the mouse ultrasonic song system has some features similar to humans and song-learning birds. PloS one *7*, e46610.

Atkinson, E.G., Audesse, A.J., Palacios, J.A., Bobo, D.M., Webb, A.E., Ramachandran, S., and Henn, B.M. (2018). No Evidence for Recent Selection at FOXP2 among Diverse Human Populations. Cell *174*, 1424-1435.e1415.

Bacon, C., Schneider, M., Le Magueresse, C., Froehlich, H., Sticht, C., Gluch, C., Monyer, H., and Rappold, G.A. (2015). Brain-specific Foxp1 deletion impairs neuronal development and causes autistic-like behaviour. Molecular psychiatry *20*, 632-639.

Barili, P., Bronzetti, E., Ricci, A., Zaccheo, D., and Amenta, F. (2000). Microanatomical localization of dopamine receptor protein immunoreactivity in the rat cerebellar cortex. Brain research *854*, 130-138.

Bedogni, F., Hodge, R.D., Elsen, G.E., Nelson, B.R., Daza, R.A., Beyer, R.P., Bammler, T.K., Rubenstein, J.L., and Hevner, R.F. (2010). Tbr1 regulates regional and laminar identity of postmitotic neurons in developing neocortex. Proceedings of the National Academy of Sciences of the United States of America *107*, 13129-13134.

Belton, E., Salmond, C.H., Watkins, K.E., Vargha-Khadem, F., and Gadian, D.G. (2003). Bilateral brain abnormalities associated with dominantly inherited verbal and orofacial dyspraxia. Human brain mapping *18*, 194-200.

Braccioli, L., Vervoort, S.J., Adolfs, Y., Heijnen, C.J., Basak, O., Pasterkamp, R.J., Nijboer, C.H., and Coffer, P.J. (2017). FOXP1 Promotes Embryonic Neural Stem Cell Differentiation by Repressing Jagged1 Expression. Stem cell reports *9*, 1530-1545.

Bray, S.J. (2016). Notch signalling in context. Nature Reviews Molecular Cell Biology *17*, 722.

Brenhouse, H.C., Sonntag, K.C., and Andersen, S.L. (2008). Transient D1 dopamine receptor expression on prefrontal cortex projection neurons: relationship to enhanced motivational salience of drug cues in adolescence. The Journal of neuroscience : the official journal of the Society for Neuroscience *28*, 2375-2382.

Briscoe, S.D., Albertin, C.B., Rowell, J.J., and Ragsdale, C.W. (2018). Neocortical Association Cell Types in the Forebrain of Birds and Alligators. Current biology : CB *28*, 686-696.e686.

Briscoe, S.D., and Ragsdale, C.W. (2018). Molecular anatomy of the alligator dorsal telencephalon. The Journal of comparative neurology *526*, 1613-1646.

Britanova, O., de Juan Romero, C., Cheung, A., Kwan, K.Y., Schwark, M., Gyorgy, A., Vogel, T., Akopov, S., Mitkovski, M., Agoston, D.*, et al.* (2008). Satb2 is a

postmitotic determinant for upper-layer neuron specification in the neocortex. Neuron *57*, 378-392.

Bulfone, A., Smiga, S.M., Shimamura, K., Peterson, A., Puelles, L., and Rubenstein, J.L. (1995). T-brain-1: a homolog of Brachyury whose expression defines molecularly distinct domains within the cerebral cortex. Neuron *15*, 63-78.

Butler, A., Hoffman, P., Smibert, P., Papalexi, E., and Satija, R. (2018). Integrating single-cell transcriptomic data across different conditions, technologies, and species. Nature biotechnology *36*, 411-420.

Calaminus, C., and Hauber, W. (2008). Guidance of instrumental behavior under reversal conditions requires dopamine D1 and D2 receptor activation in the orbitofrontal cortex. Neuroscience *154*, 1195-1204.

Campbell, P., Reep, R.L., Stoll, M.L., Ophir, A.G., and Phelps, S.M. (2009). Conservation and diversity of Foxp2 expression in muroid rodents: functional implications. The Journal of comparative neurology *512*, 84-100.

Casey, J.P., Magalhaes, T., Conroy, J.M., Regan, R., Shah, N., Anney, R., Shields, D.C., Abrahams, B.S., Almeida, J., Bacchelli, E.*, et al.* (2012). A novel approach of homozygous haplotype sharing identifies candidate genes in autism spectrum disorder. Human genetics *131*, 565-579.

Castellucci, G.A., McGinley, M.J., and McCormick, D.A. (2016). Knockout of Foxp2 disrupts vocal development in mice. Scientific reports *6*, 23305.

Chabout, J., Sarkar, A., Patel, S.R., Radden, T., Dunson, D.B., Fisher, S.E., and Jarvis, E.D. (2016). A Foxp2 Mutation Implicated in Human Speech Deficits Alters Sequencing of Ultrasonic Vocalizations in Adult Male Mice. Frontiers in behavioral neuroscience *10*, 197.

Chang, J., Gilman, S.R., Chiang, A.H., Sanders, S.J., and Vitkup, D. (2015). Genotype to phenotype relationships in autism spectrum disorders. Nature neuroscience *18*, 191-198.

Chen, J., Bardes, E.E., Aronow, B.J., and Jegga, A.G. (2009). ToppGene Suite for gene list enrichment analysis and candidate gene prioritization. Nucleic acids research *37*, W305-311.

Chen, Y.C., Kuo, H.Y., Bornschein, U., Takahashi, H., Chen, S.Y., Lu, K.M., Yang, H.Y., Chen, G.M., Lin, J.R., Lee, Y.H.*, et al.* (2016). Foxp2 controls synaptic wiring of corticostriatal circuits and vocal communication by opposing Mef2c. Nature neuroscience *19*, 1513-1522.

Chien, Y.L., Wu, Y.Y., Chiu, Y.N., Liu, S.K., Tsai, W.C., Lin, P.I., Chen, C.H., Gau, S.S., and Chien, W.H. (2011). Association study of the CNS patterning genes and autism in Han Chinese in Taiwan. Progress in neuro-psychopharmacology & biological psychiatry *35*, 1512-1517.

Chiu, Y.-C., Li, M.-Y., Liu, Y.-H., Ding, J.-Y., Yu, J.-Y., and Wang, T.-W. (2014). Foxp2 regulates neuronal differentiation and neuronal subtype specification. Developmental neurobiology *74*, 723-738.

Chokas, A.L., Trivedi, C.M., Lu, M.M., Tucker, P.W., Li, S., Epstein, J.A., and Morrisey, E.E. (2010). Foxp1/2/4-NuRD interactions regulate gene expression and epithelial

injury response in the lung via regulation of interleukin-6. The Journal of biological chemistry *285*, 13304-13313.

Clifford, H., Dulneva, A., Ponting, C.P., Haerty, W., and Becker, E.B.E. (2019). A gene expression signature in developing Purkinje cells predicts autism and intellectual disability co-morbidity status. Scientific reports *9*, 485.

Co, M., Hickey, S.L., Kulkarni, A., Harper, M., and Konopka, G. (2019). Cortical Foxp2 supports executive functions and developmental dopamine D1 receptor expression.

Coe, B.P., Stessman, H.A.F., Sulovari, A., Geisheker, M.R., Bakken, T.E., Lake, A.M., Dougherty, J.D., Lein, E.S., Hormozdiari, F., Bernier, R.A.*, et al.* (2019). Neurodevelopmental disease genes implicated by de novo mutation and copy number variation morbidity. Nature genetics *51*, 106-116.

Coop, G., Bullaughey, K., Luca, F., and Przeworski, M. (2008). The timing of selection at the human FOXP2 gene. Molecular biology and evolution *25*, 1257-1259.

Cotney, J.L., and Noonan, J.P. (2015). Chromatin immunoprecipitation with fixed animal tissues and preparation for high-throughput sequencing. Cold Spring Harbor protocols *2015*, 191-199.

Cui, Q., Li, Q., Geng, H., Chen, L., Ip, N.Y., Ke, Y., and Yung, W.H. (2018). Dopamine receptors mediate strategy abandoning via modulation of a specific prelimbic cortex-nucleus accumbens pathway in mice. Proceedings of the National Academy of Sciences of the United States of America *115*, E4890-e4899.

Cullity, E.R., Madsen, H.B., Perry, C.J., and Kim, J.H. (2018). Postnatal developmental trajectory of dopamine receptor 1 and 2 expression in cortical and striatal brain regions. The Journal of comparative neurology.

Cuomo, V., Cagiano, R., Renna, G., De Salvia, M.A., and Racagni, G. (1987). Ultrasonic vocalization in rat pups: effects of early postnatal exposure to SCH 23390 (a DA1-receptor antagonist) and sulpiride (a DA2-receptor antagonist). Neuropharmacology *26*, 701-705.

Dahoun, T., Trossbach, S.V., Brandon, N.J., Korth, C., and Howes, O.D. (2017). The impact of Disrupted-in-Schizophrenia 1 (DISC1) on the dopaminergic system: a systematic review. Translational Psychiatry *7*, e1015.

Day, N.F., Hobbs, T.G., Heston, J.B., and White, S.A. (2019). Beyond Critical Period Learning: Striatal FoxP2 Affects the Active Maintenance of Learned Vocalizations in Adulthood. eNeuro *6*.

De Rienzo, G., Bishop, J.A., Mao, Y., Pan, L., Ma, T.P., Moens, C.B., Tsai, L.H., and Sive, H. (2011). Disc1 regulates both beta-catenin-mediated and noncanonical Wnt signaling during vertebrate embryogenesis. FASEB journal : official publication of the Federation of American Societies for Experimental Biology *25*, 4184-4197.

De Rubeis, S., He, X., Goldberg, A.P., Poultney, C.S., Samocha, K., Cicek, A.E., Kou, Y., Liu, L., Fromer, M., Walker, S.*, et al.* (2014). Synaptic, transcriptional and chromatin genes disrupted in autism. Nature *515*, 209-215.

Deacon, R.M.J., and Rawlins, J.N.P. (2006). T-maze alternation in the rodent. Nature protocols *1*, 7.

Deciphering Developmental Disorders, S. (2015). Large-scale discovery of novel genetic causes of developmental disorders. Nature *519*, 223-228.

Deck, M., Lokmane, L., Chauvet, S., Mailhes, C., Keita, M., Niquille, M., Yoshida, M., Yoshida, Y., Lebrand, C., Mann, F.*, et al.* (2013). Pathfinding of corticothalamic axons relies on a rendezvous with thalamic projections. Neuron *77*, 472-484.

Demontis, D., Walters, R.K., Martin, J., Mattheisen, M., Als, T.D., Agerbo, E., Baldursson, G., Belliveau, R., Bybjerg-Grauholm, J., Baekvad-Hansen, M.*, et al.* (2019). Discovery of the first genome-wide significant risk loci for attention deficit/hyperactivity disorder. Nature genetics *51*, 63-75.

Deriziotis, P., O'Roak, B.J., Graham, S.A., Estruch, S.B., Dimitropoulou, D., Bernier, R.A., Gerdts, J., Shendure, J., Eichler, E.E., and Fisher, S.E. (2014). De novo TBR1 mutations in sporadic autism disrupt protein functions. Nature communications *5*, 4954.

Devanna, P., Middelbeek, J., and Vernes, S.C. (2014). FOXP2 drives neuronal differentiation by interacting with retinoic acid signaling pathways. Frontiers in cellular neuroscience *8*, 305.

Dobin, A., Davis, C.A., Schlesinger, F., Drenkow, J., Zaleski, C., Jha, S., Batut, P., Chaisson, M., and Gingeras, T.R. (2013). STAR: ultrafast universal RNA-seq aligner. Bioinformatics (Oxford, England) *29*, 15-21.

Ebisu, H., Iwai-Takekoshi, L., Fujita-Jimbo, E., Momoi, T., and Kawasaki, H. (2016). Foxp2 Regulates Identities and Projection Patterns of Thalamic Nuclei During Development. Cerebral cortex (New York, NY : 1991).

El-Brolosy, M.A., Kontarakis, Z., Rossi, A., Kuenne, C., Günther, S., Fukuda, N., Kikhi, K., Boezio, G.L.M., Takacs, C.M., Lai, S.-L.*, et al.* (2019). Genetic compensation triggered by mutant mRNA degradation. Nature *568*, 193-197.

Enard, W., Gehre, S., Hammerschmidt, K., Holter, S.M., Blass, T., Somel, M., Bruckner, M.K., Schreiweis, C., Winter, C., Sohr, R.*, et al.* (2009). A humanized version of Foxp2 affects cortico-basal ganglia circuits in mice. Cell *137*, 961-971.

Enard, W., Przeworski, M., Fisher, S.E., Lai, C.S., Wiebe, V., Kitano, T., Monaco, A.P., and Paabo, S. (2002). Molecular evolution of FOXP2, a gene involved in speech and language. Nature *418*, 869-872.

Estruch, S.B., Graham, S.A., Quevedo, M., Vino, A., Dekkers, D.H.W., Deriziotis, P., Sollis, E., Demmers, J., Poot, R.A., and Fisher, S.E. (2018). Proteomic analysis of FOXP proteins reveals interactions between cortical transcription factors associated with neurodevelopmental disorders. Human molecular genetics.

Fazel Darbandi, S., Robinson Schwartz, S.E., Qi, Q., Catta-Preta, R., Pai, E.L., Mandell, J.D., Everitt, A., Rubin, A., Krasnoff, R.A., Katzman, S.*, et al.* (2018). Neonatal Tbr1 Dosage Controls Cortical Layer 6 Connectivity. Neuron *100*, 831-845.e837.

Feng, X., Henriquez, V.M., Walters, J.R., and Ludlow, C.L. (2009). Effects of dopamine D1 and D2 receptor antagonists on laryngeal neurophysiology in the rat. Journal of neurophysiology *102*, 1193-1205.

Feng, X., Ippolito, G.C., Tian, L., Wiehagen, K., Oh, S., Sambandam, A., Willen, J., Bunte, R.M., Maika, S.D., Harriss, J.V.*, et al.* (2010). Foxp1 is an essential transcriptional

regulator for the generation of quiescent naive T cells during thymocyte development. Blood *115*, 510-518.

Ferland, R.J., Cherry, T.J., Preware, P.O., Morrisey, E.E., and Walsh, C.A. (2003). Characterization of Foxp2 and Foxp1 mRNA and protein in the developing and mature brain. The Journal of comparative neurology *460*, 266-279.

Fisher, S.E., Vargha-Khadem, F., Watkins, K.E., Monaco, A.P., and Pembrey, M.E. (1998). Localisation of a gene implicated in a severe speech and language disorder. Nature genetics *18*, 168-170.

Floresco, S.B. (2013). Prefrontal dopamine and behavioral flexibility: shifting from an "inverted-U" toward a family of functions. Front Neurosci *7*, 62.

Fong, W.L., Kuo, H.Y., Wu, H.L., Chen, S.Y., and Liu, F.C. (2018). Differential and Overlapping Pattern of Foxp1 and Foxp2 Expression in the Striatum of Adult Mouse Brain. Neuroscience *388*, 214-223.

Fontenot, M.R., Berto, S., Liu, Y., Werthmann, G., Douglas, C., Usui, N., Gleason, K., Tamminga, C.A., Takahashi, J.S., and Konopka, G. (2017). Novel transcriptional networks regulated by CLOCK in human neurons. Genes & development *31*, 2121-2135.

French, C.A., and Fisher, S.E. (2014). What can mice tell us about Foxp2 function? Current opinion in neurobiology *28*, 72-79.

French, C.A., Groszer, M., Preece, C., Coupe, A.M., Rajewsky, K., and Fisher, S.E. (2007). Generation of mice with a conditional Foxp2 null allele. Genesis (New York, NY : 2000) *45*, 440-446.

French, C.A., Jin, X., Campbell, T.G., Gerfen, E., Groszer, M., Fisher, S.E., and Costa, R.M. (2012). An aetiological Foxp2 mutation causes aberrant striatal activity and alters plasticity during skill learning. Molecular psychiatry *17*, 1077-1085.

French, C.A., Vinueza Veloz, M.F., Zhou, K., Peter, S., Fisher, S.E., Costa, R.M., and De Zeeuw, C.I. (2018). Differential effects of Foxp2 disruption in distinct motor circuits. Molecular psychiatry *24*, 447-462.

Frohlich, H., Rafiullah, R., Schmitt, N., Abele, S., and Rappold, G.A. (2017). Foxp1 expression is essential for sex-specific murine neonatal ultrasonic vocalization. Human molecular genetics *26*, 1511-1521.

Fujita-Jimbo, E., and Momoi, T. (2014). Specific expression of FOXP2 in cerebellum improves ultrasonic vocalization in heterozygous but not in homozygous Foxp2 (R552H) knock-in pups. Neuroscience letters *566*, 162-166.

Fujita, E., Tanabe, Y., Shiota, A., Ueda, M., Suwa, K., Momoi, M.Y., and Momoi, T. (2008). Ultrasonic vocalization impairment of Foxp2 (R552H) knockin mice related to speech-language disorder and abnormality of Purkinje cells. Proceedings of the National Academy of Sciences of the United States of America *105*, 3117-3122.

Fujita, H., and Sugihara, I. (2012). FoxP2 expression in the cerebellum and inferior olive: development of the transverse stripe-shaped expression pattern in the mouse cerebellar cortex. The Journal of comparative neurology *520*, 656-677.

Gandal, M.J., Haney, J.R., Parikshak, N.N., Leppa, V., Ramaswami, G., Hartl, C., Schork, A.J., Appadurai, V., Buil, A., Werge, T.M.*, et al.* (2018). Shared molecular

neuropathology across major psychiatric disorders parallels polygenic overlap. Science (New York, NY) *359*, 693-697.

Garcia-Calero, E., Botella-Lopez, A., Bahamonde, O., Perez-Balaguer, A., and Martinez, S. (2016). FoxP2 protein levels regulate cell morphology changes and migration patterns in the vertebrate developing telencephalon. Brain Struct Funct *221*, 2905-2917.

Gaspar, P., Bloch, B., and Le Moine, C. (1995). D1 and D2 receptor gene expression in the rat frontal cortex: cellular localization in different classes of efferent neurons. The European journal of neuroscience *7*, 1050-1063.

Gaub, S., Fisher, S.E., and Ehret, G. (2016). Ultrasonic vocalizations of adult male Foxp2-mutant mice: behavioral contexts of arousal and emotion. Genes, brain, and behavior *15*, 243-259.

Gaub, S., Groszer, M., Fisher, S.E., and Ehret, G. (2010). The structure of innate vocalizations in Foxp2-deficient mouse pups. Genes, brain, and behavior *9*, 390-401.

Gauthier, J., Joober, R., Mottron, L., Laurent, S., Fuchs, M., De Kimpe, V., and Rouleau, G.A. (2003). Mutation screening of FOXP2 in individuals diagnosed with autistic disorder. American journal of medical genetics Part A *118a*, 172-175.

Ghirardi, L., Brikell, I., Kuja-Halkola, R., Freitag, C.M., Franke, B., Asherson, P., Lichtenstein, P., and Larsson, H. (2017). The familial co-aggregation of ASD and ADHD: a register-based cohort study. Molecular psychiatry *23*, 257.

Goebbels, S., Bormuth, I., Bode, U., Hermanson, O., Schwab, M.H., and Nave, K.A. (2006). Genetic targeting of principal neurons in neocortex and hippocampus of NEX-Cre mice. Genesis (New York, NY : 2000) *44*, 611-621.

Gong, X., Jia, M., Ruan, Y., Shuang, M., Liu, J., Wu, S., Guo, Y., Yang, J., Ling, Y., Yang, X.*, et al.* (2004). Association between the FOXP2 gene and autistic disorder in Chinese population. American journal of medical genetics Part B, Neuropsychiatric genetics : the official publication of the International Society of Psychiatric Genetics *127b*, 113-116.

Gopnik, M., and Crago, M.B. (1991). Familial aggregation of a developmental language disorder. Cognition *39*, 1-50.

Gorski, J.A., Talley, T., Qiu, M., Puelles, L., Rubenstein, J.L., and Jones, K.R. (2002). Cortical excitatory neurons and glia, but not GABAergic neurons, are produced in the Emx1-expressing lineage. The Journal of neuroscience : the official journal of the Society for Neuroscience *22*, 6309-6314.

Groszer, M., Keays, D.A., Deacon, R.M., de Bono, J.P., Prasad-Mulcare, S., Gaub, S., Baum, M.G., French, C.A., Nicod, J., Coventry, J.A.*, et al.* (2008). Impaired synaptic plasticity and motor learning in mice with a point mutation implicated in human speech deficits. Current biology : CB *18*, 354-362.

Habib, N., Avraham-Davidi, I., Basu, A., Burks, T., Shekhar, K., Hofree, M., Choudhury, S.R., Aguet, F., Gelfand, E., Ardlie, K.*, et al.* (2017). Massively parallel single-nucleus RNA-seq with DroNc-seq. Nature methods *14*, 955-958.

Hachigian, L.J., Carmona, V., Fenster, R.J., Kulicke, R., Heilbut, A., Sittler, A., Pereira de Almeida, L., Mesirov, J.P., Gao, F., Kolaczyk, E.D.*, et al.* (2017). Control of

Huntington's Disease-Associated Phenotypes by the Striatum-Enriched Transcription Factor Foxp2. Cell reports *21*, 2688-2695.

Haesler, S., Rochefort, C., Georgi, B., Licznerski, P., Osten, P., and Scharff, C. (2007). Incomplete and inaccurate vocal imitation after knockdown of FoxP2 in songbird basal ganglia nucleus Area X. PLoS biology *5*, e321.

Haesler, S., Wada, K., Nshdejan, A., Morrisey, E.E., Lints, T., Jarvis, E.D., and Scharff, C. (2004). FoxP2 expression in avian vocal learners and non-learners. The Journal of neuroscience : the official journal of the Society for Neuroscience *24*, 3164-3175.

Hamdan, F.F., Daoud, H., Rochefort, D., Piton, A., Gauthier, J., Langlois, M., Foomani, G., Dobrzeniecka, S., Krebs, M.O., Joober, R.*, et al.* (2010). De novo mutations in FOXP1 in cases with intellectual disability, autism, and language impairment. American journal of human genetics *87*, 671-678.

Hamilton, D.A., and Brigman, J.L. (2015). Behavioral flexibility in rats and mice: contributions of distinct frontocortical regions. Genes, brain, and behavior *14*, 4-21.

Hammerschmidt, K., Reisinger, E., Westekemper, K., Ehrenreich, L., Strenzke, N., and Fischer, J. (2012). Mice do not require auditory input for the normal development of their ultrasonic vocalizations. BMC neuroscience *13*, 40.

Hammerschmidt, K., Schreiweis, C., Minge, C., Paabo, S., Fischer, J., and Enard, W. (2015a). A humanized version of Foxp2 does not affect ultrasonic vocalization in adult mice. Genes, brain, and behavior *14*, 583-590.

Hammerschmidt, K., Whelan, G., Eichele, G., and Fischer, J. (2015b). Mice lacking the cerebral cortex develop normal song: insights into the foundations of vocal learning. Scientific reports *5*, 8808.

Han, S.W., Kim, Y.C., and Narayanan, N.S. (2017). Projection targets of medial frontal D1DR-expressing neurons. Neuroscience letters *655*, 166-171.

Han, W., Kwan, K.Y., Shim, S., Lam, M.M., Shin, Y., Xu, X., Zhu, Y., Li, M., and Sestan, N. (2011). TBR1 directly represses Fezf2 to control the laminar origin and development of the corticospinal tract. Proceedings of the National Academy of Sciences of the United States of America *108*, 3041-3046.

Heston, J.B., and White, S.A. (2015). Behavior-linked FoxP2 regulation enables zebra finch vocal learning. The Journal of neuroscience : the official journal of the Society for Neuroscience *35*, 2885-2894.

Hickey, S.L., Berto, S., and Konopka, G. (2019). Chromatin Decondensation by FOXP2 Promotes Human Neuron Maturation and Expression of Neurodevelopmental Disease Genes. Cell reports *27*, 1699-1711.e1699.

Hisaoka, T., Nakamura, Y., Senba, E., and Morikawa, Y. (2010). The forkhead transcription factors, Foxp1 and Foxp2, identify different subpopulations of projection neurons in the mouse cerebral cortex. Neuroscience *166*, 551-563.

Hoerder-Suabedissen, A., and Molnar, Z. (2015). Development, evolution and pathology of neocortical subplate neurons. Nature reviews Neuroscience *16*, 133-146.

Holy, T.E., and Guo, Z. (2005). Ultrasonic songs of male mice. PLoS biology *3*, e386.

Hu, H., Wang, B., Borde, M., Nardone, J., Maika, S., Allred, L., Tucker, P.W., and Rao, A. (2006). Foxp1 is an essential transcriptional regulator of B cell development. Nature immunology *7*, 819-826.

Huang, T.N., Chuang, H.C., Chou, W.H., Chen, C.Y., Wang, H.F., Chou, S.J., and Hsueh, Y.P. (2014). Tbr1 haploinsufficiency impairs amygdalar axonal projections and results in cognitive abnormality. Nature neuroscience *17*, 240-247.

Hurst, J.A., Baraitser, M., Auger, E., Graham, F., and Norell, S. (1990). An extended family with a dominantly inherited speech disorder. Developmental medicine and child neurology *32*, 352-355.

Iossifov, I., O'Roak, B.J., Sanders, S.J., Ronemus, M., Krumm, N., Levy, D., Stessman, H.A., Witherspoon, K.T., Vives, L., Patterson, K.E.*, et al.* (2014). The contribution of de novo coding mutations to autism spectrum disorder. Nature *515*, 216-221.

Jacobs, E.C., Campagnoni, C., Kampf, K., Reyes, S.D., Kalra, V., Handley, V., Xie, Y.Y., Hong-Hu, Y., Spreur, V., Fisher, R.S.*, et al.* (2007). Visualization of corticofugal projections during early cortical development in a tau-GFP-transgenic mouse. The European journal of neuroscience *25*, 17-30.

Jamadar, S., Powers, N.R., Meda, S.A., Gelernter, J., Gruen, J.R., and Pearlson, G.D. (2011). Genetic influences of cortical gray matter in language-related regions in healthy controls and schizophrenia. Schizophrenia research *129*, 141-148.

Kast, R.J., Lanjewar, A.L., Smith, C.D., and Levitt, P. (2019). FOXP2 exhibits neuron class specific expression, but is not required for multiple aspects of cortical histogenesis. eLife *8*.

Kast, R.J., Wu, H.H., and Levitt, P. (2017). Developmental Connectivity and Molecular Phenotypes of Unique Cortical Projection Neurons that Express a Synapse-Associated Receptor Tyrosine Kinase. Cerebral cortex (New York, NY : 1991), 1-13.

Kent, W.J., Sugnet, C.W., Furey, T.S., Roskin, K.M., Pringle, T.H., Zahler, A.M., and Haussler, D. (2002). The human genome browser at UCSC. Genome research *12*, 996-1006.

Konopka, G., Bomar, J.M., Winden, K., Coppola, G., Jonsson, Z.O., Gao, F., Peng, S., Preuss, T.M., Wohlschlegel, J.A., and Geschwind, D.H. (2009). Human-specific transcriptional regulation of CNS development genes by FOXP2. Nature *462*, 213-217.

Konopka, G., and Roberts, T.F. (2016a). Animal Models of Speech and Vocal Communication Deficits Associated With Psychiatric Disorders. Biological psychiatry *79*, 53-61.

Konopka, G., and Roberts, T.F. (2016b). Insights into the Neural and Genetic Basis of Vocal Communication. Cell *164*, 1269-1276.

Krause, J., Lalueza-Fox, C., Orlando, L., Enard, W., Green, R.E., Burbano, H.A., Hublin, J.J., Hanni, C., Fortea, J., de la Rasilla, M.*, et al.* (2007). The derived FOXP2 variant of modern humans was shared with Neandertals. Current biology : CB *17*, 1908-1912.

Kuerbitz, J., Arnett, M.G., Ehrman, S., Williams, M.T., Vorhees, C.V., Fisher, S.E., Garratt, A.N., Muglia, L.J., Waclaw, R.R., and Campbell, K. (2017). Loss of

intercalated cells (ITCs) in the mouse amygdala of Tshz1 mutants correlates with fear, depression and social interaction phenotypes. The Journal of neuroscience : the official journal of the Society for Neuroscience.

Kurt, S., Fisher, S.E., and Ehret, G. (2012). Foxp2 mutations impair auditory-motor association learning. PloS one *7*, e33130.

Kurt, S., Groszer, M., Fisher, S.E., and Ehret, G. (2009). Modified sound-evoked brainstem potentials in Foxp2 mutant mice. Brain research *1289*, 30-36.

Lai, C.S., Fisher, S.E., Hurst, J.A., Levy, E.R., Hodgson, S., Fox, M., Jeremiah, S., Povey, S., Jamison, D.C., Green, E.D.*, et al.* (2000). The SPCH1 region on human 7q31: genomic characterization of the critical interval and localization of translocations associated with speech and language disorder. American journal of human genetics *67*, 357-368.

Lai, C.S., Fisher, S.E., Hurst, J.A., Vargha-Khadem, F., and Monaco, A.P. (2001). A forkhead-domain gene is mutated in a severe speech and language disorder. Nature *413*, 519-523.

Lai, C.S., Gerrelli, D., Monaco, A.P., Fisher, S.E., and Copp, A.J. (2003). FOXP2 expression during brain development coincides with adult sites of pathology in a severe speech and language disorder. Brain : a journal of neurology *126*, 2455-2462.

Lalonde, R. (2002). The neurobiological basis of spontaneous alternation. Neuroscience and biobehavioral reviews *26*, 91-104.

Laroche, F., Ramoz, N., Leroy, S., Fortin, C., Rousselot-Paillet, B., Philippe, A., Colleaux, L., Bresson, J.L., Mogenet, A., Golse, B.*, et al.* (2008). Polymorphisms of coding trinucleotide repeats of homeogenes in neurodevelopmental psychiatric disorders. Psychiatric genetics *18*, 295-301.

Lee, G.H., and D'Arcangelo, G. (2016). New Insights into Reelin-Mediated Signaling Pathways. Frontiers in cellular neuroscience *10*, 122-122.

Li, H., Yamagata, T., Mori, M., and Momoi, M.Y. (2005). Absence of causative mutations and presence of autism-related allele in FOXP2 in Japanese autistic patients. Brain & development *27*, 207-210.

Li, S., Weidenfeld, J., and Morrisey, E.E. (2004). Transcriptional and DNA binding activity of the Foxp1/2/4 family is modulated by heterotypic and homotypic protein interactions. Molecular and cellular biology *24*, 809-822.

Li, T., Zeng, Z., Zhao, Q., Wang, T., Huang, K., Li, J., Li, Y., Liu, J., Wei, Z., Wang, Y.*, et al.* (2013). FoxP2 is significantly associated with schizophrenia and major depression in the Chinese Han population. The world journal of biological psychiatry : the official journal of the World Federation of Societies of Biological Psychiatry *14*, 146-150.

Li, X., Han, X., Tu, X., Zhu, D., Feng, Y., Jiang, T., Yang, Y., Qu, J., and Chen, J.G. (2018). An Autism-Related, Nonsense Foxp1 Mutant Induces Autophagy and Delays Radial Migration of the Cortical Neurons. Cerebral cortex (New York, NY : 1991).

Li, X., Xiao, J., Fröhlich, H., Tu, X., Li, L., Xu, Y., Cao, H., Qu, J., Rappold, G.A., and Chen, J.-G. (2015). Foxp1 Regulates Cortical Radial Migration and Neuronal Morphogenesis in Developing Cerebral Cortex. PloS one *10*, e0127671.

Li, Z., Chen, J., Yu, H., He, L., Xu, Y., Zhang, D., Yi, Q., Li, C., Li, X., Shen, J.*, et al.* (2017). Genome-wide association analysis identifies 30 new susceptibility loci for schizophrenia. Nature genetics *49*, 1576.

Liao, Y., Smyth, G.K., and Shi, W. (2014). featureCounts: an efficient general purpose program for assigning sequence reads to genomic features. Bioinformatics (Oxford, England) *30*, 923-930.

Liegeois, F., Baldeweg, T., Connelly, A., Gadian, D.G., Mishkin, M., and Vargha-Khadem, F. (2003). Language fMRI abnormalities associated with FOXP2 gene mutation. Nature neuroscience *6*, 1230-1237.

Liegeois, F., Morgan, A.T., Connelly, A., and Vargha-Khadem, F. (2011). Endophenotypes of FOXP2: dysfunction within the human articulatory network. European journal of paediatric neurology : EJPN : official journal of the European Paediatric Neurology Society *15*, 283-288.

Liegeois, F.J., Hildebrand, M.S., Bonthrone, A., Turner, S.J., Scheffer, I.E., Bahlo, M., Connelly, A., and Morgan, A.T. (2016). Early neuroimaging markers of FOXP2 intragenic deletion. Scientific reports *6*, 35192.

Lim, L., Mi, D., Llorca, A., and Marin, O. (2018). Development and Functional Diversification of Cortical Interneurons. Neuron *100*, 294-313.

Liu, J., Wang, F., Huang, C., Long, L.H., Wu, W.N., Cai, F., Wang, J.H., Ma, L.Q., and Chen, J.G. (2009). Activation of phosphatidylinositol-linked novel D1 dopamine receptor contributes to the calcium mobilization in cultured rat prefrontal cortical astrocytes. Cellular and molecular neurobiology *29*, 317-328.

Loo, L., Simon, J.M., Xing, L., McCoy, E.S., Niehaus, J.K., Guo, J., Anton, E.S., and Zylka, M.J. (2019). Single-cell transcriptomic analysis of mouse neocortical development. Nature communications *10*, 134.

Lui, J.H., Hansen, D.V., and Kriegstein, A.R. (2011). Development and evolution of the human neocortex. Cell *146*, 18-36.

Mahrt, E.J., Perkel, D.J., Tong, L., Rubel, E.W., and Portfors, C.V. (2013). Engineered deafness reveals that mouse courtship vocalizations do not require auditory experience. The Journal of neuroscience : the official journal of the Society for Neuroscience *33*, 5573-5583.

Mala, H., Andersen, L.G., Christensen, R.F., Felbinger, A., Hagstrom, J., Meder, D., Pearce, H., and Mogensen, J. (2015). Prefrontal cortex and hippocampus in behavioural flexibility and posttraumatic functional recovery: reversal learning and set-shifting in rats. Brain research bulletin *116*, 34-44.

Marui, T., Koishi, S., Funatogawa, I., Yamamoto, K., Matsumoto, H., Hashimoto, O., Nanba, E., Kato, C., Ishijima, M., Watanabe, K.*, et al.* (2005). No association of FOXP2 and PTPRZ1 on 7q31 with autism from the Japanese population. Neuroscience research *53*, 91-94.

McCarthy, N.S., Clark, M.L., Jablensky, A., and Badcock, J.C. (2018). No association between common genetic variation in FOXP2 and language impairment in schizophrenia. Psychiatry research *271*, 590-597.

Medina, L., Abellán, A., Vicario, A., and Desfilis, E. (2014). Evolutionary and Developmental Contributions for Understanding the Organization of the Basal Ganglia. Brain, behavior and evolution *83*, 112-125.

Medvedeva, V.P., Rieger, M.A., Vieth, B., Mombereau, C., Ziegenhain, C., Ghosh, T., Cressant, A., Enard, W., Granon, S., Dougherty, J.D.*, et al.* (2018). Altered social behavior in mice carrying a cortical Foxp2 deletion. Human molecular genetics.

Mendoza, E., and Scharff, C. (2017). Protein-Protein Interaction Among the FoxP Family Members and their Regulation of Two Target Genes, VLDLR and CNTNAP2 in the Zebra Finch Song System. Frontiers in molecular neuroscience *10*, 112.

Mendoza, E., Tokarev, K., During, D.N., Retamosa, E.C., Weiss, M., Arpenik, N., and Scharff, C. (2015). Differential coexpression of FoxP1, FoxP2, and FoxP4 in the Zebra Finch (Taeniopygia guttata) song system. The Journal of comparative neurology *523*, 1318-1340.

Miller, J.E., Spiteri, E., Condro, M.C., Dosumu-Johnson, R.T., Geschwind, D.H., and White, S.A. (2008). Birdsong decreases protein levels of FoxP2, a molecule required for human speech. Journal of neurophysiology *100*, 2015-2025.

Mizoguchi, K., Shoji, H., Tanaka, Y., and Tabira, T. (2010). Orbitofrontal dopaminergic dysfunction causes age-related impairment of reversal learning in rats. Neuroscience *170*, 1110-1119.

Mizutani, A., Matsuzaki, A., Momoi, M.Y., Fujita, E., Tanabe, Y., and Momoi, T. (2007). Intracellular distribution of a speech/language disorder associated FOXP2 mutant. Biochemical and biophysical research communications *353*, 869-874.

Molyneaux, B.J., Goff, L.A., Brettler, A.C., Chen, H.H., Hrvatin, S., Rinn, J.L., and Arlotta, P. (2015). DeCoN: genome-wide analysis of in vivo transcriptional dynamics during pyramidal neuron fate selection in neocortex. Neuron *85*, 275-288.

Morgan, A., Fisher, S.E., Scheffer, I., and Hildebrand, M. (2017). FOXP2-Related Speech and Language Disorders. In GeneReviews((R)), M.P. Adam, H.H. Ardinger, R.A. Pagon, S.E. Wallace, L.J.H. Bean, K. Stephens, and A. Amemiya, eds. (Seattle (WA): University of Washington, Seattle

University of Washington, Seattle. GeneReviews is a registered trademark of the University of Washington, Seattle. All rights reserved.).

Morikawa, Y., Hisaoka, T., and Senba, E. (2009). Characterization of Foxp2-expressing cells in the developing spinal cord. Neuroscience *162*, 1150-1162.

Mukamel, Z., Konopka, G., Wexler, E., Osborn, G.E., Dong, H., Bergman, M.Y., Levitt, P., and Geschwind, D.H. (2011). Regulation of MET by FOXP2, genes implicated in higher cognitive dysfunction and autism risk. The Journal of neuroscience : the official journal of the Society for Neuroscience *31*, 11437-11442.

Murugan, M., Harward, S., Scharff, C., and Mooney, R. (2013). Diminished FoxP2 levels affect dopaminergic modulation of corticostriatal signaling important to song variability. Neuron *80*, 1464-1476.

Nakayama, H., Ibanez-Tallon, I., and Heintz, N. (2018). Cell-Type-Specific Contributions of Medial Prefrontal Neurons to Flexible Behaviors. The Journal of neuroscience : the official journal of the Society for Neuroscience *38*, 4490-4504.

Newbury, D.F., Bonora, E., Lamb, J.A., Fisher, S.E., Lai, C.S., Baird, G., Jannoun, L., Slonims, V., Stott, C.M., Merricks, M.J.*, et al.* (2002). FOXP2 is not a major susceptibility gene for autism or specific language impairment. American journal of human genetics *70*, 1318-1327.

Noelanders, R., and Vleminckx, K. (2016). How Wnt Signaling Builds the Brain: Bridging Development and Disease. The Neuroscientist *23*, 314-329.

Notwell, J.H., Heavner, W.E., Darbandi, S.F., Katzman, S., McKenna, W.L., Ortiz-Londono, C.F., Tastad, D., Eckler, M.J., Rubenstein, J.L., McConnell, S.K.*, et al.* (2016). TBR1 regulates autism risk genes in the developing neocortex. Genome research *26*, 1013-1022.

O'Roak, B.J., Deriziotis, P., Lee, C., Vives, L., Schwartz, J.J., Girirajan, S., Karakoc, E., Mackenzie, A.P., Ng, S.B., Baker, C.*, et al.* (2011). Exome sequencing in sporadic autism spectrum disorders identifies severe de novo mutations. Nature genetics *43*, 585-589.

O'Roak, B.J., Vives, L., Fu, W., Egertson, J.D., Stanaway, I.B., Phelps, I.G., Carvill, G., Kumar, A., Lee, C., Ankenman, K.*, et al.* (2012). Multiplex targeted sequencing identifies recurrently mutated genes in autism spectrum disorders. Science (New York, NY) *338*, 1619-1622.

Oliva, C., Vargas, J., and Inestrosa, N. (2013). Wnts in adult brain: from synaptic plasticity to cognitive deficiencies. Frontiers in cellular neuroscience *7*.

Oswald, F., Kloble, P., Ruland, A., Rosenkranz, D., Hinz, B., Butter, F., Ramljak, S., Zechner, U., and Herlyn, H. (2017). The FOXP2-Driven Network in Developmental Disorders and Neurodegeneration. Frontiers in cellular neuroscience *11*, 212.

Ott, T., and Nieder, A. (2019). Dopamine and Cognitive Control in Prefrontal Cortex. Trends in Cognitive Sciences *23*, 213-234.

Pearson, C.A., Moore, D.M., Tucker, H.O., Dekker, J.D., Hu, H., Miquelajáuregui, A., and Novitch, B.G. (2018). Foxp1 controls neural stem cell competence and bias towards deep layer cortical fates. bioRxiv, 386276.

Pidoux, L., Le Blanc, P., Levenes, C., and Leblois, A. (2018). A subcortical circuit linking the cerebellum to the basal ganglia engaged in vocal learning. eLife *7*, e32167.

Precious, S.V., Kelly, C.M., Reddington, A.E., Vinh, N.N., Stickland, R.C., Pekarik, V., Scherf, C., Jeyasingham, R., Glasbey, J., Holeiter, M.*, et al.* (2016). FoxP1 marks medium spiny neurons from precursors to maturity and is required for their differentiation. Experimental neurology *282*, 9-18.

Rao, W., Du, X., Zhang, Y., Yu, Q., Hui, L., Yu, Y., Kou, C., Yin, G., Zhu, X., Man, L.*, et al.* (2017). Association between forkhead-box P2 gene polymorphism and clinical symptoms in chronic schizophrenia in a Chinese population. Journal of neural transmission (Vienna, Austria : 1996) *124*, 891-897.

Reimers-Kipping, S., Hevers, W., Paabo, S., and Enard, W. (2011). Humanized Foxp2 specifically affects cortico-basal ganglia circuits. Neuroscience *175*, 75-84.

Reuter, M.S., Riess, A., Moog, U., Briggs, T.A., Chandler, K.E., Rauch, A., Stampfer, M., Steindl, K., Glaser, D., Joset, P.*, et al.* (2017). FOXP2 variants in 14 individuals with developmental speech and language disorders broaden the mutational and clinical spectrum. Journal of medical genetics *54*, 64-72.

Richler, E., Reichert, J.G., Buxbaum, J.D., and McInnes, L.A. (2006). Autism and ultraconserved non-coding sequence on chromosome 7q. Psychiatric genetics *16*, 19-23.

Rieger, M.A., and Dougherty, J.D. (2016). Analysis of within Subjects Variability in Mouse Ultrasonic Vocalization: Pups Exhibit Inconsistent, State-Like Patterns of Call Production. Frontiers in behavioral neuroscience *10*, 182.

Rippberger, H., van Gaalen, M.M., Schwarting, R.K., and Wohr, M. (2015). Environmental and Pharmacological Modulation of Amphetamine- Induced 50-kHz Ultrasonic Vocalizations in Rats. Current neuropharmacology *13*, 220-232.

Rochefort, C., He, X., Scotto-Lomassese, S., and Scharff, C. (2007). Recruitment of FoxP2-expressing neurons to area X varies during song development. Developmental neurobiology *67*, 809-817.

Rodenas-Cuadrado, P., Ho, J., and Vernes, S.C. (2013). Shining a light on CNTNAP2: complex functions to complex disorders. European Journal Of Human Genetics *22*, 171.

Rodenas-Cuadrado, P.M., Mengede, J., Baas, L., Devanna, P., Schmid, T.A., Yartsev, M., Firzlaff, U., and Vernes, S.C. (2018). Mapping the distribution of language related genes FoxP1, FoxP2, and CntnaP2 in the brains of vocal learning bat species. The Journal of comparative neurology *526*, 1235-1266.

Roll, P., Vernes, S.C., Bruneau, N., Cillario, J., Ponsole-Lenfant, M., Massacrier, A., Rudolf, G., Khalife, M., Hirsch, E., Fisher, S.E.*, et al.* (2010). Molecular networks implicated in speech-related disorders: FOXP2 regulates the SRPX2/uPAR complex. Human molecular genetics *19*, 4848-4860.

Sakai, Y., Shaw, C.A., Dawson, B.C., Dugas, D.V., Al-Mohtaseb, Z., Hill, D.E., and Zoghbi, H.Y. (2011). Protein interactome reveals converging molecular pathways among autism disorders. Science translational medicine *3*, 86ra49.

Sanders, S.J., He, X., Willsey, A.J., Ercan-Sencicek, A.G., Samocha, K.E., Cicek, A.E., Murtha, M.T., Bal, V.H., Bishop, S.L., Dong, S.*, et al.* (2015). Insights into Autism Spectrum Disorder Genomic Architecture and Biology from 71 Risk Loci. Neuron *87*, 1215-1233.

Sanjuan, J., Tolosa, A., Gonzalez, J.C., Aguilar, E.J., Molto, M.D., Najera, C., and de Frutos, R. (2005). FOXP2 polymorphisms in patients with schizophrenia. Schizophrenia research *73*, 253-256.

Sanjuan, J., Tolosa, A., Gonzalez, J.C., Aguilar, E.J., Perez-Tur, J., Najera, C., Molto, M.D., and de Frutos, R. (2006). Association between FOXP2 polymorphisms and schizophrenia with auditory hallucinations. Psychiatric genetics *16*, 67-72.

Sarinana, J., Kitamura, T., Kunzler, P., Sultzman, L., and Tonegawa, S. (2014). Differential roles of the dopamine 1-class receptors, D1R and D5R, in hippocampal dependent memory. Proceedings of the National Academy of Sciences of the United States of America *111*, 8245-8250.

Satterstrom, F.K., Kosmicki, J.A., Wang, J., Breen, M.S., De Rubeis, S., An, J.-Y., Peng, M., Collins, R.L., Grove, J., Klei, L.*, et al.* (2019). Large-scale exome sequencing study implicates both developmental and functional changes in the neurobiology of autism. bioRxiv, 484113.

Schizophrenia Working Group of the Psychiatric Genomics, C., Ripke, S., Neale, B.M., Corvin, A., Walters, J.T.R., Farh, K.-H., Holmans, P.A., Lee, P., Bulik-Sullivan, B., Collier, D.A.*, et al.* (2014). Biological insights from 108 schizophrenia-associated genetic loci. Nature *511*, 421.

Schreiweis, C., Bornschein, U., Burguiere, E., Kerimoglu, C., Schreiter, S., Dannemann, M., Goyal, S., Rea, E., French, C.A., Puliyadi, R.*, et al.* (2014). Humanized Foxp2 accelerates learning by enhancing transitions from declarative to procedural performance. Proceedings of the National Academy of Sciences of the United States of America *111*, 14253-14258.

Schubert, D., Martens, G.J.M., and Kolk, S.M. (2015). Molecular underpinnings of prefrontal cortex development in rodents provide insights into the etiology of neurodevelopmental disorders. Molecular psychiatry *20*, 795-809.

Schulz, S.B., Haesler, S., Scharff, C., and Rochefort, C. (2010). Knockdown of FoxP2 alters spine density in Area X of the zebra finch. Genes, brain, and behavior *9*, 732-740.

Schulze, K., Vargha-Khadem, F., and Mishkin, M. (2017). Phonological working memory and FOXP2. Neuropsychologia *108*, 147-152.

Shu, W., Cho, J.Y., Jiang, Y., Zhang, M., Weisz, D., Elder, G.A., Schmeidler, J., De Gasperi, R., Sosa, M.A., Rabidou, D.*, et al.* (2005). Altered ultrasonic vocalization in mice with a disruption in the Foxp2 gene. Proceedings of the National Academy of Sciences of the United States of America *102*, 9643-9648.

Shu, W., Yang, H., Zhang, L., Lu, M.M., and Morrisey, E.E. (2001). Characterization of a new subfamily of winged-helix/forkhead (Fox) genes that are expressed in the lung and act as transcriptional repressors. The Journal of biological chemistry *276*, 27488-27497.

Sia, G.M., Clem, R.L., and Huganir, R.L. (2013). The human language-associated gene SRPX2 regulates synapse formation and vocalization in mice. Science (New York, NY) *342*, 987-991.

Sin, C., Li, H., and Crawford, D.A. (2015). Transcriptional regulation by FOXP1, FOXP2, and FOXP4 dimerization. Journal of molecular neuroscience : MN *55*, 437-448.

Siper, P.M., De Rubeis, S., Trelles, M.D.P., Durkin, A., Di Marino, D., Muratet, F., Frank, Y., Lozano, R., Eichler, E.E., Kelly, M.*, et al.* (2017). Prospective investigation of FOXP1 syndrome. Molecular autism *8*, 57.

Skene, P.J., Henikoff, J.G., and Henikoff, S. (2018). Targeted in situ genome-wide profiling with high efficiency for low cell numbers. Nature protocols *13*, 1006.

Smith, T., Heger, A., and Sudbery, I. (2017). UMI-tools: modeling sequencing errors in Unique Molecular Identifiers to improve quantification accuracy. Genome research *27*, 491-499.

Sohur, U.S., Padmanabhan, H.K., Kotchetkov, I.S., Menezes, J.R.L., and Macklis, J.D. (2014). Anatomic and molecular development of corticostriatal projection neurons in mice. Cerebral cortex (New York, NY : 1991) *24*, 293-303.

Sollis, E., Deriziotis, P., Saitsu, H., Miyake, N., Matsumoto, N., Hoffer, M.J.V., Ruivenkamp, C.A.L., Alders, M., Okamoto, N., Bijlsma, E.K.*, et al.* (2017). Equivalent missense variant in the FOXP2 and FOXP1 transcription factors causes distinct neurodevelopmental disorders. Human mutation.

Sorensen, S.A., Bernard, A., Menon, V., Royall, J.J., Glattfelder, K.J., Desta, T., Hirokawa, K., Mortrud, M., Miller, J.A., Zeng, H.*, et al.* (2015). Correlated gene expression and target specificity demonstrate excitatory projection neuron diversity. Cerebral cortex (New York, NY : 1991) *25*, 433-449.

Spiteri, E., Konopka, G., Coppola, G., Bomar, J., Oldham, M., Ou, J., Vernes, S.C., Fisher, S.E., Ren, B., and Geschwind, D.H. (2007). Identification of the transcriptional targets of FOXP2, a gene linked to speech and language, in developing human brain. American journal of human genetics *81*, 1144-1157.

Stoodley, C.J., D'Mello, A.M., Ellegood, J., Jakkamsetti, V., Liu, P., Nebel, M.B., Gibson, J.M., Kelly, E., Meng, F., Cano, C.A.*, et al.* (2017). Altered cerebellar connectivity in autism and cerebellar-mediated rescue of autism-related behaviors in mice. Nature neuroscience *20*, 1744-1751.

Stroud, J.C., Wu, Y., Bates, D.L., Han, A., Nowick, K., Paabo, S., Tong, H., and Chen, L. (2006). Structure of the forkhead domain of FOXP2 bound to DNA. Structure (London, England : 1993) *14*, 159-166.

Supek, F., Bosnjak, M., Skunca, N., and Smuc, T. (2011). REVIGO summarizes and visualizes long lists of gene ontology terms. PloS one *6*, e21800.

Takahashi, J.S., Kumar, V., Nakashe, P., Koike, N., Huang, H.C., Green, C.B., and Kim, T.K. (2015). ChIP-seq and RNA-seq methods to study circadian control of transcription in mammals. Methods in enzymology *551*, 285-321.

Takahashi, K., Liu, F.C., Hirokawa, K., and Takahashi, H. (2003). Expression of Foxp2, a gene involved in speech and language, in the developing and adult striatum. Journal of neuroscience research *73*, 61-72.

Takahashi, K., Liu, F.C., Oishi, T., Mori, T., Higo, N., Hayashi, M., Hirokawa, K., and Takahashi, H. (2008). Expression of FOXP2 in the developing monkey forebrain: comparison with the expression of the genes FOXP1, PBX3, and MEIS2. The Journal of comparative neurology *509*, 180-189.

Takata, A., Miyake, N., Tsurusaki, Y., Fukai, R., Miyatake, S., Koshimizu, E., Kushima, I., Okada, T., Morikawa, M., Uno, Y.*, et al.* (2018). Integrative Analyses of De Novo Mutations Provide Deeper Biological Insights into Autism Spectrum Disorder. Cell reports *22*, 734-747.

Tamura, S., Morikawa, Y., Iwanishi, H., Hisaoka, T., and Senba, E. (2003). Expression pattern of the winged-helix/forkhead transcription factor Foxp1 in the developing central nervous system. Gene expression patterns : GEP *3*, 193-197.

Tanabe, Y., Fujita, E., and Momoi, T. (2011). FOXP2 promotes the nuclear translocation of POT1, but FOXP2(R553H), mutation related to speech-language disorder,

partially prevents it. Biochemical and biophysical research communications *410*, 593-596.

Tarazi, F.I., Tomasini, E.C., and Baldessarini, R.J. (1999). Postnatal development of dopamine D1-like receptors in rat cortical and striatolimbic brain regions: An autoradiographic study. Developmental neuroscience *21*, 43-49.

Tasic, B., Menon, V., Nguyen, T.N., Kim, T.K., Jarsky, T., Yao, Z., Levi, B., Gray, L.T., Sorensen, S.A., Dolbeare, T.*, et al.* (2016). Adult mouse cortical cell taxonomy revealed by single cell transcriptomics. Nature neuroscience *19*, 335-346.

Tasic, B., Yao, Z., Graybuck, L.T., Smith, K.A., Nguyen, T.N., Bertagnolli, D., Goldy, J., Garren, E., Economo, M.N., Viswanathan, S.*, et al.* (2018). Shared and distinct transcriptomic cell types across neocortical areas. Nature *563*, 72-78.

Teramitsu, I., Kudo, L.C., London, S.E., Geschwind, D.H., and White, S.A. (2004). Parallel FoxP1 and FoxP2 expression in songbird and human brain predicts functional interaction. The Journal of neuroscience : the official journal of the Society for Neuroscience *24*, 3152-3163.

Teramitsu, I., and White, S.A. (2006). FoxP2 regulation during undirected singing in adult songbirds. The Journal of neuroscience : the official journal of the Society for Neuroscience *26*, 7390-7394.

Thompson, J.L., Yang, J., Lau, B., Liu, S., Baimel, C., Kerr, L.E., Liu, F., and Borgland, S.L. (2016). Age-Dependent D1-D2 Receptor Coactivation in the Lateral Orbitofrontal Cortex Potentiates NMDA Receptors and Facilitates Cognitive Flexibility. Cerebral cortex (New York, NY : 1991) *26*, 4524-4539.

Tolosa, A., Sanjuan, J., Dagnall, A.M., Molto, M.D., Herrero, N., and de Frutos, R. (2010). FOXP2 gene and language impairment in schizophrenia: association and epigenetic studies. BMC medical genetics *11*, 114.

Toma, C., Hervas, A., Torrico, B., Balmana, N., Salgado, M., Maristany, M., Vilella, E., Martinez-Leal, R., Planelles, M.I., Cusco, I.*, et al.* (2013). Analysis of two language-related genes in autism: a case-control association study of FOXP2 and CNTNAP2. Psychiatric genetics *23*, 82-85.

Tronche, F., Kellendonk, C., Kretz, O., Gass, P., Anlag, K., Orban, P.C., Bock, R., Klein, R., and Schütz, G. (1999). Disruption of the glucocorticoid receptor gene in the nervous system results in reduced anxiety. Nature genetics *23*, 99-103.

Tsui, D., Vessey, J.P., Tomita, H., Kaplan, D.R., and Miller, F.D. (2013). FoxP2 regulates neurogenesis during embryonic cortical development. The Journal of neuroscience : the official journal of the Society for Neuroscience *33*, 244-258.

Usui, N., Araujo, D.J., Kulkarni, A., Co, M., Ellegood, J., Harper, M., Toriumi, K., Lerch, J.P., and Konopka, G. (2017a). Foxp1 regulation of neonatal vocalizations via cortical development. Genes & development *31*, 2039-2055.

Usui, N., Co, M., Harper, M., Rieger, M.A., Dougherty, J.D., and Konopka, G. (2017b). Sumoylation of FOXP2 Regulates Motor Function and Vocal Communication Through Purkinje Cell Development. Biological psychiatry *81*, 220-230.

van Rhijn, J.-R., Fisher, S.E., Vernes, S.C., and Nadif Kasri, N. (2018). Foxp2 loss of function increases striatal direct pathway inhibition via increased GABA release. Brain Structure and Function.

van Rooij, D., Anagnostou, E., Arango, C., Auzias, G., Behrmann, M., Busatto, G.F., Calderoni, S., Daly, E., Deruelle, C., Di Martino, A.*, et al.* (2018). Cortical and Subcortical Brain Morphometry Differences Between Patients With Autism Spectrum Disorder and Healthy Individuals Across the Lifespan: Results From the ENIGMA ASD Working Group. The American journal of psychiatry *175*, 359-369.

Van Segbroeck, M., Knoll, A.T., Levitt, P., and Narayanan, S. (2017). MUPET-Mouse Ultrasonic Profile ExTraction: A Signal Processing Tool for Rapid and Unsupervised Analysis of Ultrasonic Vocalizations. Neuron *94*, 465-485.e465.

Vargha-Khadem, F., Gadian, D.G., Copp, A., and Mishkin, M. (2005). FOXP2 and the neuroanatomy of speech and language. Nature reviews Neuroscience *6*, 131-138.

Vargha-Khadem, F., Watkins, K., Alcock, K., Fletcher, P., and Passingham, R. (1995). Praxic and nonverbal cognitive deficits in a large family with a genetically transmitted speech and language disorder. Proceedings of the National Academy of Sciences of the United States of America *92*, 930-933.

Vargha-Khadem, F., Watkins, K.E., Price, C.J., Ashburner, J., Alcock, K.J., Connelly, A., Frackowiak, R.S., Friston, K.J., Pembrey, M.E., Mishkin, M.*, et al.* (1998). Neural basis of an inherited speech and language disorder. Proceedings of the National Academy of Sciences of the United States of America *95*, 12695-12700.

Vernes, S.C., Newbury, D.F., Abrahams, B.S., Winchester, L., Nicod, J., Groszer, M., Alarcon, M., Oliver, P.L., Davies, K.E., Geschwind, D.H.*, et al.* (2008). A functional genetic link between distinct developmental language disorders. The New England journal of medicine *359*, 2337-2345.

Vernes, S.C., Nicod, J., Elahi, F.M., Coventry, J.A., Kenny, N., Coupe, A.M., Bird, L.E., Davies, K.E., and Fisher, S.E. (2006). Functional genetic analysis of mutations implicated in a human speech and language disorder. Human molecular genetics *15*, 3154-3167.

Vernes, S.C., Oliver, P.L., Spiteri, E., Lockstone, H.E., Puliyadi, R., Taylor, J.M., Ho, J., Mombereau, C., Brewer, A., Lowy, E.*, et al.* (2011). Foxp2 regulates gene networks implicated in neurite outgrowth in the developing brain. PLoS genetics *7*, e1002145.

Vernes, S.C., Spiteri, E., Nicod, J., Groszer, M., Taylor, J.M., Davies, K.E., Geschwind, D.H., and Fisher, S.E. (2007). High-throughput analysis of promoter occupancy reveals direct neural targets of FOXP2, a gene mutated in speech and language disorders. American journal of human genetics *81*, 1232-1250.

Vila-Ballo, A., Mas-Herrero, E., Ripolles, P., Simo, M., Miro, J., Cucurell, D., Lopez-Barroso, D., Juncadella, M., Marco-Pallares, J., Falip, M.*, et al.* (2017). Unraveling the Role of the Hippocampus in Reversal Learning. The Journal of neuroscience : the official journal of the Society for Neuroscience *37*, 6686-6697.

Vincent, S.L., Khan, Y., and Benes, F.M. (1993). Cellular distribution of dopamine D1 and D2 receptors in rat medial prefrontal cortex. The Journal of neuroscience : the official journal of the Society for Neuroscience *13*, 2551-2564.

Walf, A.A., and Frye, C.A. (2007). The use of the elevated plus maze as an assay of anxiety-related behavior in rodents. Nature protocols *2*, 322-328.

Walker, R.M., Hill, A.E., Newman, A.C., Hamilton, G., Torrance, H.S., Anderson, S.M., Ogawa, F., Derizioti, P., Nicod, J., Vernes, S.C.*, et al.* (2012). The DISC1 promoter: characterization and regulation by FOXP2. Human molecular genetics *21*, 2862-2872.

Wang, B., Lin, D., Li, C., and Tucker, P. (2003). Multiple domains define the expression and regulatory properties of Foxp1 forkhead transcriptional repressors. The Journal of biological chemistry *278*, 24259-24268.

Wang, B., Weidenfeld, J., Lu, M.M., Maika, S., Kuziel, W.A., Morrisey, E.E., and Tucker, P.W. (2004). Foxp1 regulates cardiac outflow tract, endocardial cushion morphogenesis and myocyte proliferation and maturation. Development (Cambridge, England) *131*, 4477-4487.

Wang, H.C., and Bergles, D.E. (2015). Spontaneous activity in the developing auditory system. Cell and tissue research *361*, 65-75.

Wassink, T.H., Piven, J., Vieland, V.J., Pietila, J., Goedken, R.J., Folstein, S.E., and Sheffield, V.C. (2002). Evaluation of FOXP2 as an autism susceptibility gene. American journal of medical genetics *114*, 566-569.

Watkins, K.E., Dronkers, N.F., and Vargha-Khadem, F. (2002a). Behavioural analysis of an inherited speech and language disorder: comparison with acquired aphasia. Brain : a journal of neurology *125*, 452-464.

Watkins, K.E., Vargha-Khadem, F., Ashburner, J., Passingham, R.E., Connelly, A., Friston, K.J., Frackowiak, R.S., Mishkin, M., and Gadian, D.G. (2002b). MRI analysis of an inherited speech and language disorder: structural brain abnormalities. Brain : a journal of neurology *125*, 465-478.

Wilcke, A., Ligges, C., Burkhardt, J., Alexander, M., Wolf, C., Quente, E., Ahnert, P., Hoffmann, P., Becker, A., Müller-Myhsok, B.*, et al.* (2011). Imaging genetics of FOXP2 in dyslexia. European Journal Of Human Genetics *20*, 224.

Willsey, A.J., Sanders, S.J., Li, M., Dong, S., Tebbenkamp, A.T., Muhle, R.A., Reilly, S.K., Lin, L., Fertuzinhos, S., Miller, J.A.*, et al.* (2013). Coexpression networks implicate human midfetal deep cortical projection neurons in the pathogenesis of autism. Cell *155*, 997-1007.

Woolley, S.C. (2019). Dopaminergic regulation of vocal-motor plasticity and performance. Current opinion in neurobiology *54*, 127-133.

Xiao, L., Chattree, G., Oscos, F.G., Cao, M., Wanat, M.J., and Roberts, T.F. (2018). A Basal Ganglia Circuit Sufficient to Guide Birdsong Learning. Neuron *98*, 208-221.e205.

Xu, S., Liu, P., Chen, Y., Chen, Y., Zhang, W., Zhao, H., Cao, Y., Wang, F., Jiang, N., Lin, S.*, et al.* (2018). Foxp2 regulates anatomical features that may be relevant for vocal behaviors and bipedal locomotion. Proceedings of the National Academy of Sciences.

Yang, M., Silverman, J.L., and Crawley, J.N. (2011). Automated Three-Chambered Social Approach Task for Mice. Current protocols in neuroscience / editorial board, Jacqueline N Crawley [et al] *Chapter 8*, Unit-8.26.

Yin, J., Jia, N., Liu, Y., Jin, C., Zhang, F., Yu, S., Wang, J., and Yuan, J. (2018). No association between FOXP2 rs10447760 and schizophrenia in a replication study of the Chinese Han population. Psychiatric genetics.

Zhao, H., Zhou, W., Yao, Z., Wan, Y., Cao, J., Zhang, L., Zhao, J., Li, H., Zhou, R., Li, B.*, et al.* (2015). Foxp1/2/4 regulate endochondral ossification as a suppresser complex. Developmental biology *398*, 242-254.

Zheng, G.X., Terry, J.M., Belgrader, P., Ryvkin, P., Bent, Z.W., Wilson, R., Ziraldo, S.B., Wheeler, T.D., McDermott, G.P., Zhu, J.*, et al.* (2017). Massively parallel digital transcriptional profiling of single cells. Nature communications *8*, 14049.

Zhou, B., Zhong, Q., Minoo, P., Li, C., Ann, D.K., Frenkel, B., Morrisey, E.E., Crandall, E.D., and Borok, Z. (2008). Foxp2 inhibits Nkx2.1-mediated transcription of SP-C via interactions with the Nkx2.1 homeodomain. American journal of respiratory cell and molecular biology *38*, 750-758.